Geodynamics III: Integrating geophysical observations into global mantle flow models

Thorsten W. Becker
Jackson School of Geosciences
University of Texas at Austin

CIDER Summer School *Flow In the Deep Earth*
Santa Barbara CA
July 2016

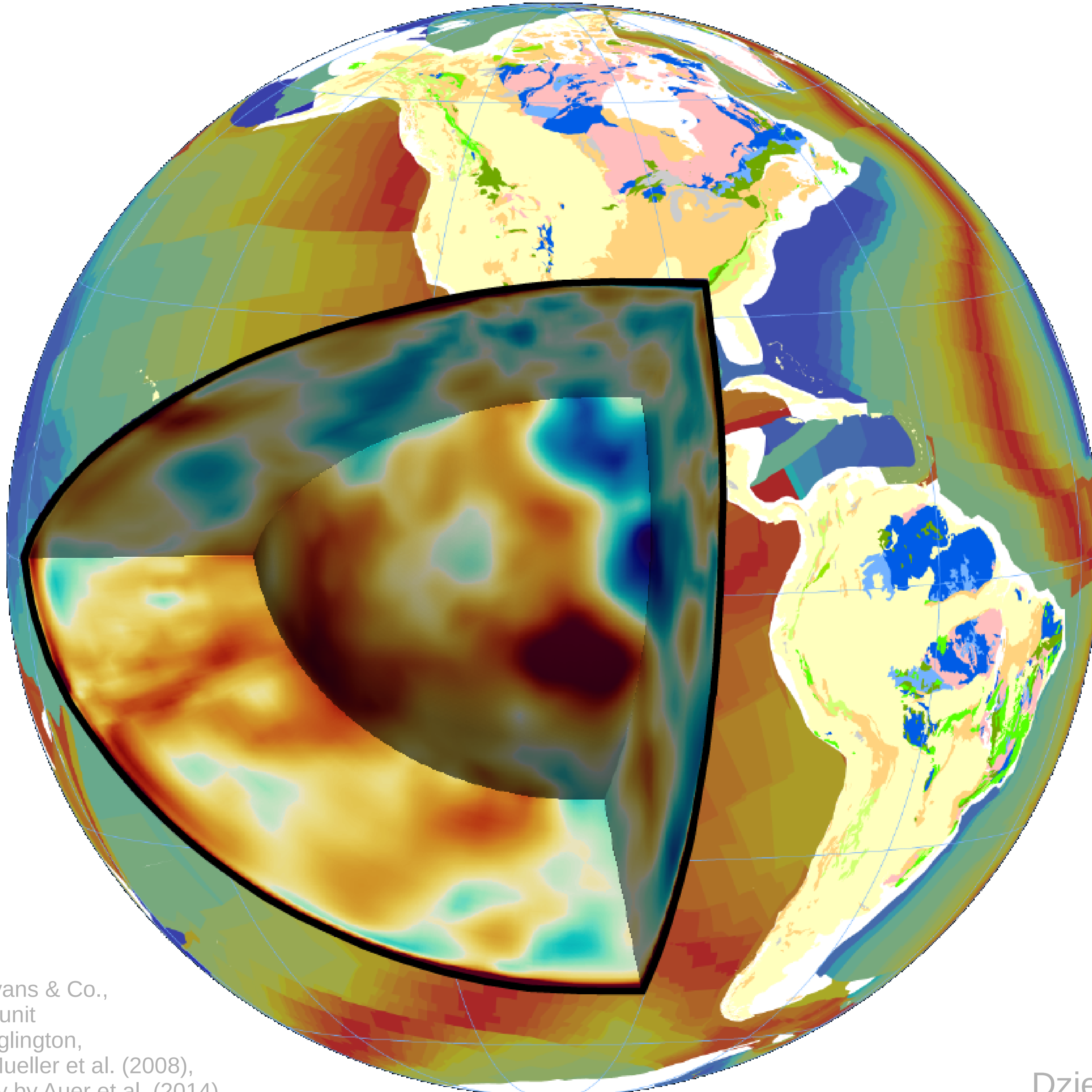

Composite by D. Evans & Co.,
showing geological unit
compilation by D. Eglington,
seafloor age from Mueller et al. (2008),
SAVANI tomography by Auer et al. (2014)

Dziewonski plot

reconstructed seafloor age

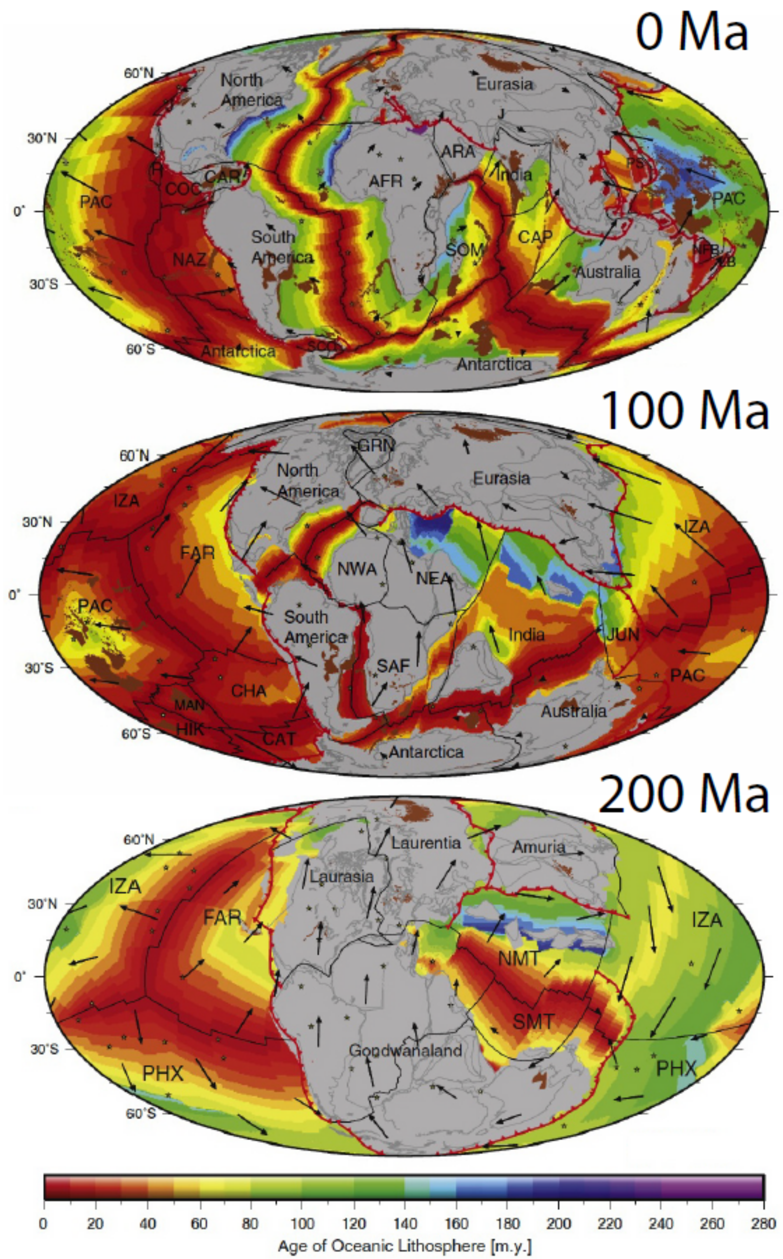

Seton et al. (2012)

hot temperature isosurface

dense chemical piles

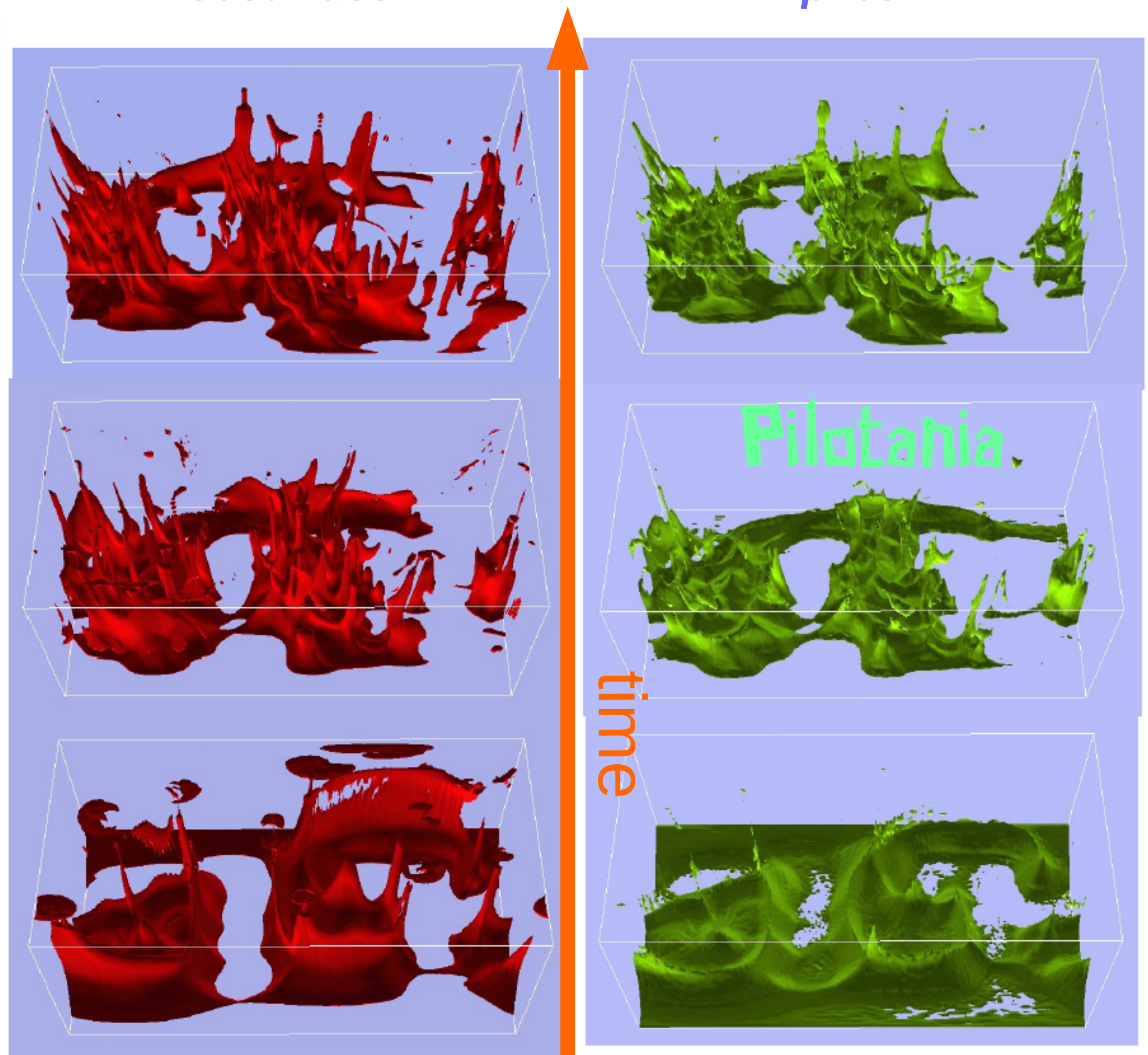

Olson et al. (2016)

cf. McNamara and Zhong (2005) and many others

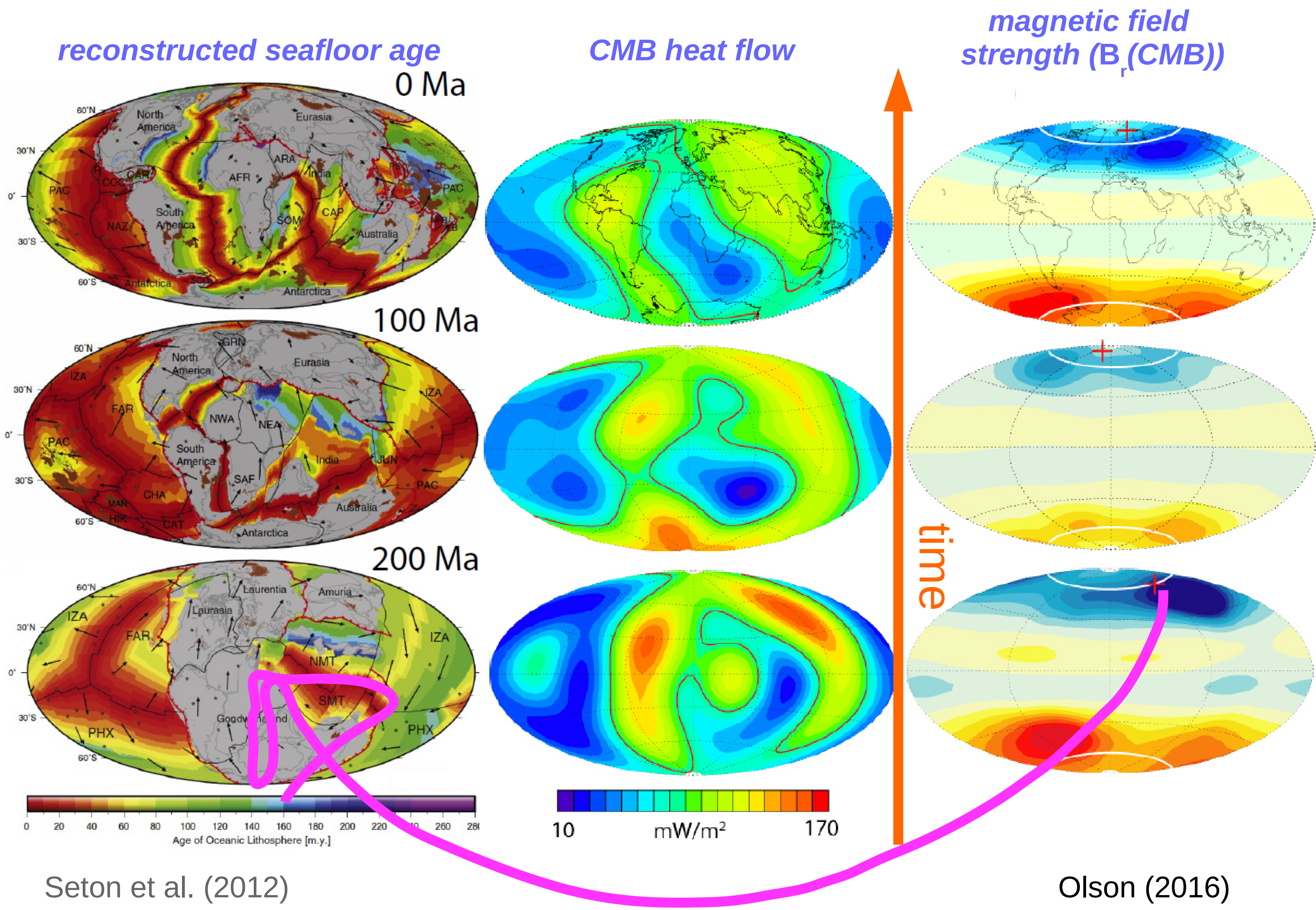

reconstructed seafloor age
CMB heat flow
magnetic field strength (B_r(CMB))
0 Ma
100 Ma
200 Ma
time
0 20 40 60 80 100 120 140 160 180 200 220 240 260 280
Age of Oceanic Lithosphere [m.y.]
10 mW/m² 170
Seton et al. (2012)
Olson (2016)

We know how plate tectonics works

(~true, and often assumed)

Plate tectonics is the top boundary layer of thermo-chemical convection

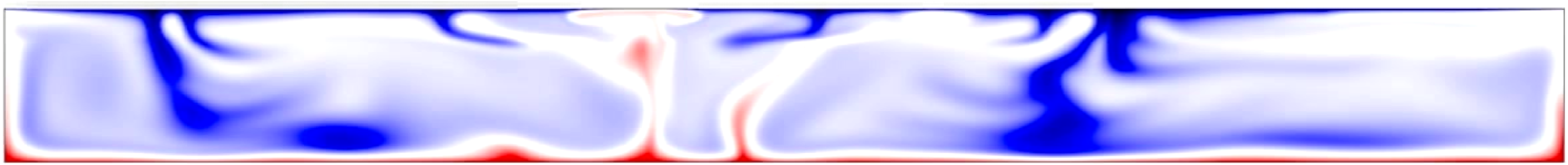

Symmetry of upwellings and downwellings of Rayleigh-Taylor convection is broken by:

- **temperature dependence of viscosity**
- **depth-dependent viscosity**
- internal vs. bottom heating
- fractionation (e.g. continents and thermo-chemical piles)
- ...

Plate driving forces:

Integrals over individual components of thermo-chemical convection

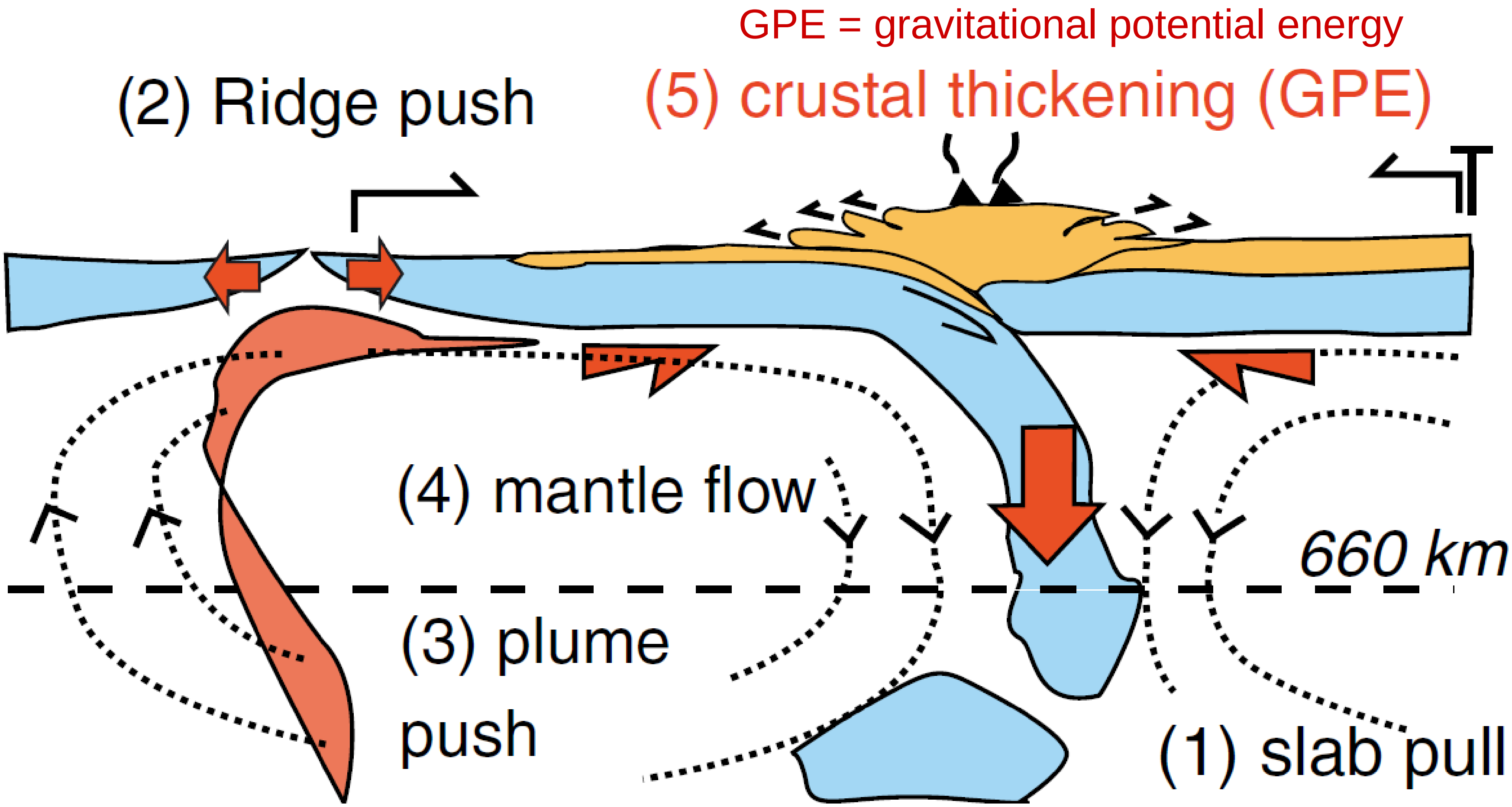

Lithospheric thickening
(AKA ridge push, oceanic GPE)

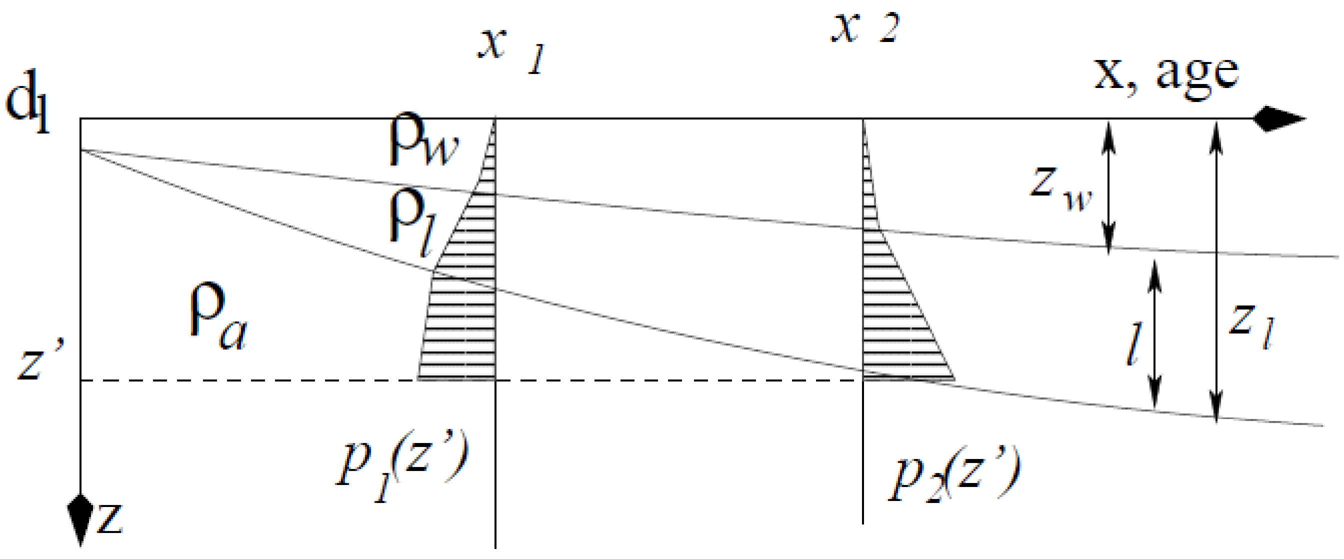

$$l = a(z_w - d_l) = a\Delta z_w \qquad a = \frac{\rho_w - \rho_a}{\rho_a - \rho_l} \qquad z_w(x) = c\sqrt{\frac{x}{u_0}}$$

$$F = \frac{ac^2}{2u_0} g \Delta\rho \Delta x$$

Slab pull
(subducting thermal boundary layer)

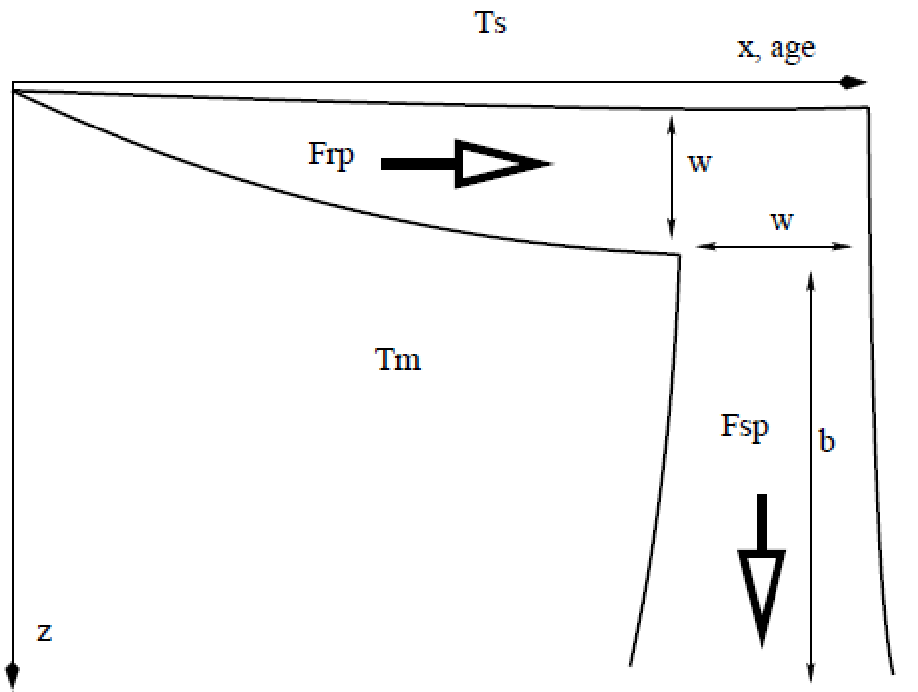

$$F_b = -2\rho_0 g \alpha b (T_m - T_s)\sqrt{\frac{\kappa t_s}{\pi}}$$

Force estimates from half-space cooling

(hugely important reference model and achievement of geodynamics)

- Ridge push (lithospheric thickening) ~ 10^{12} N/m
- Slab pull ~ 10^{13} N/m

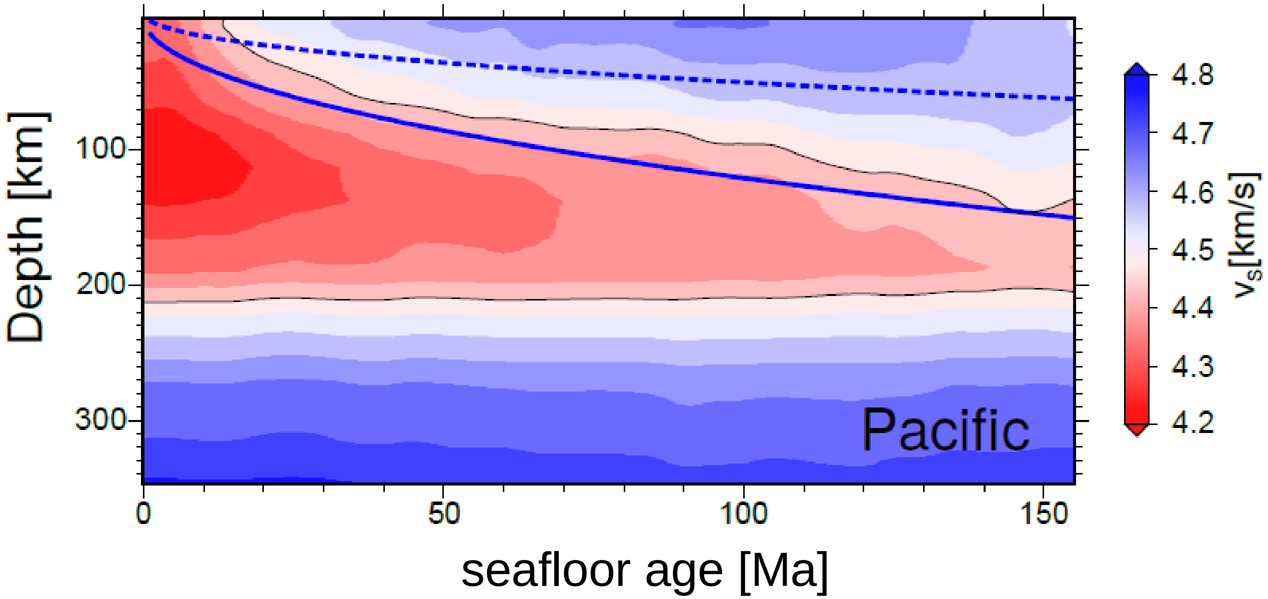

Auer et al. (2015)

Slab pull

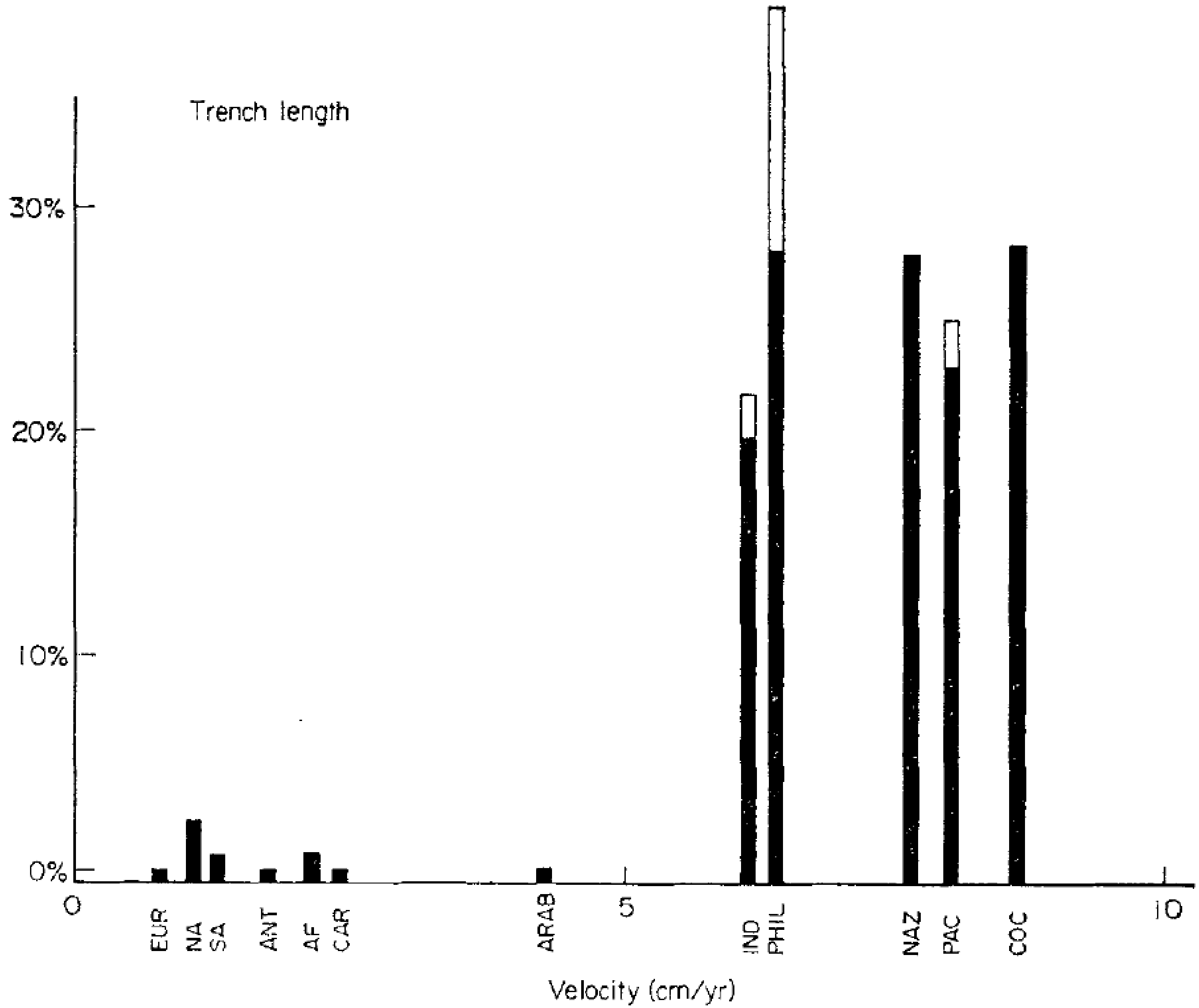

FIG. 8. Percentage of circumference of plate connected to downgoing slab. Open bar is total length, filled bar is effective length.

Forsyth & Uyeda (1975)

How does the mantle drive the plates at present?
Estimate from global circulation modeling

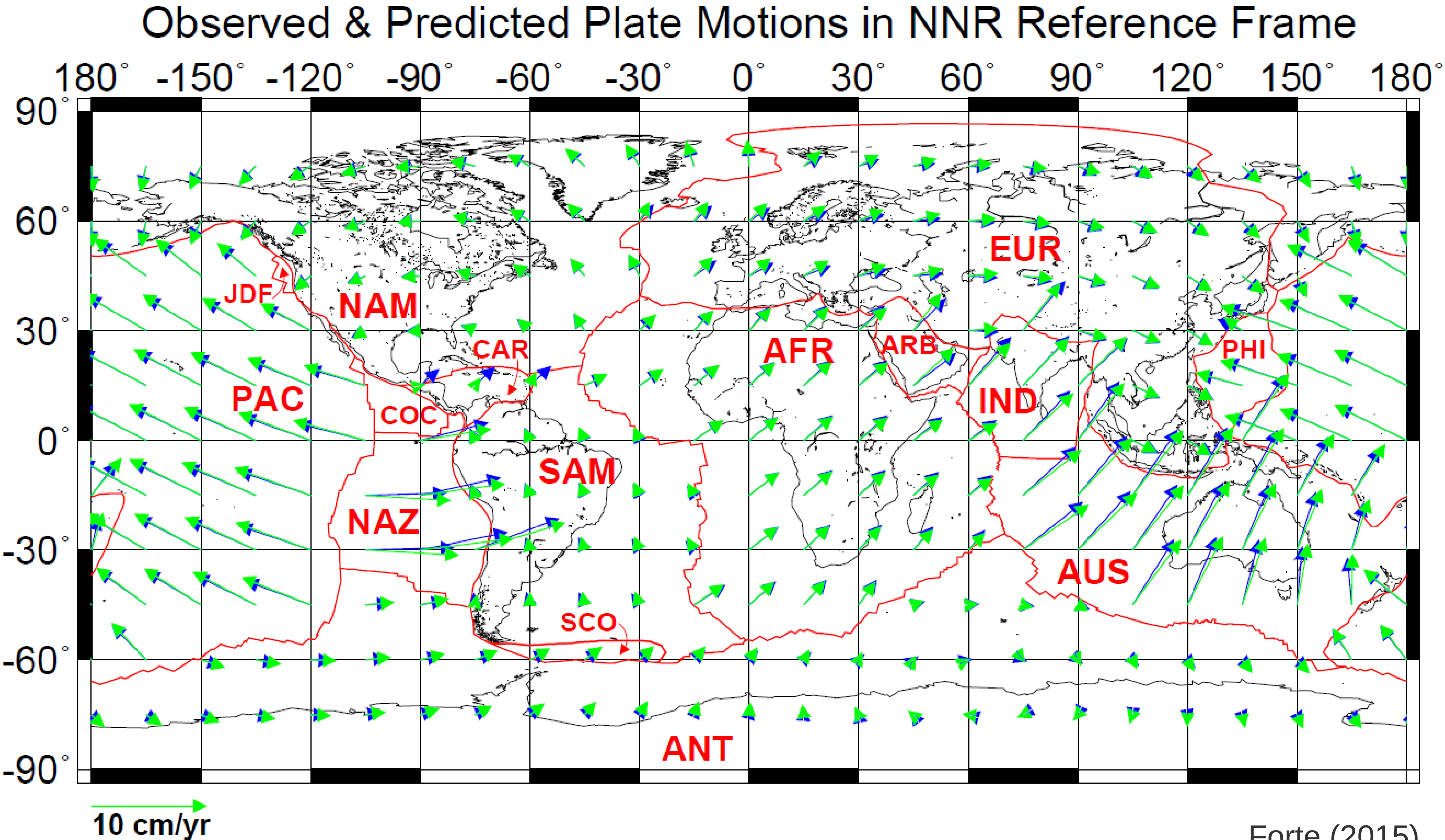

Forte (2015)

Plate boundaries matter...

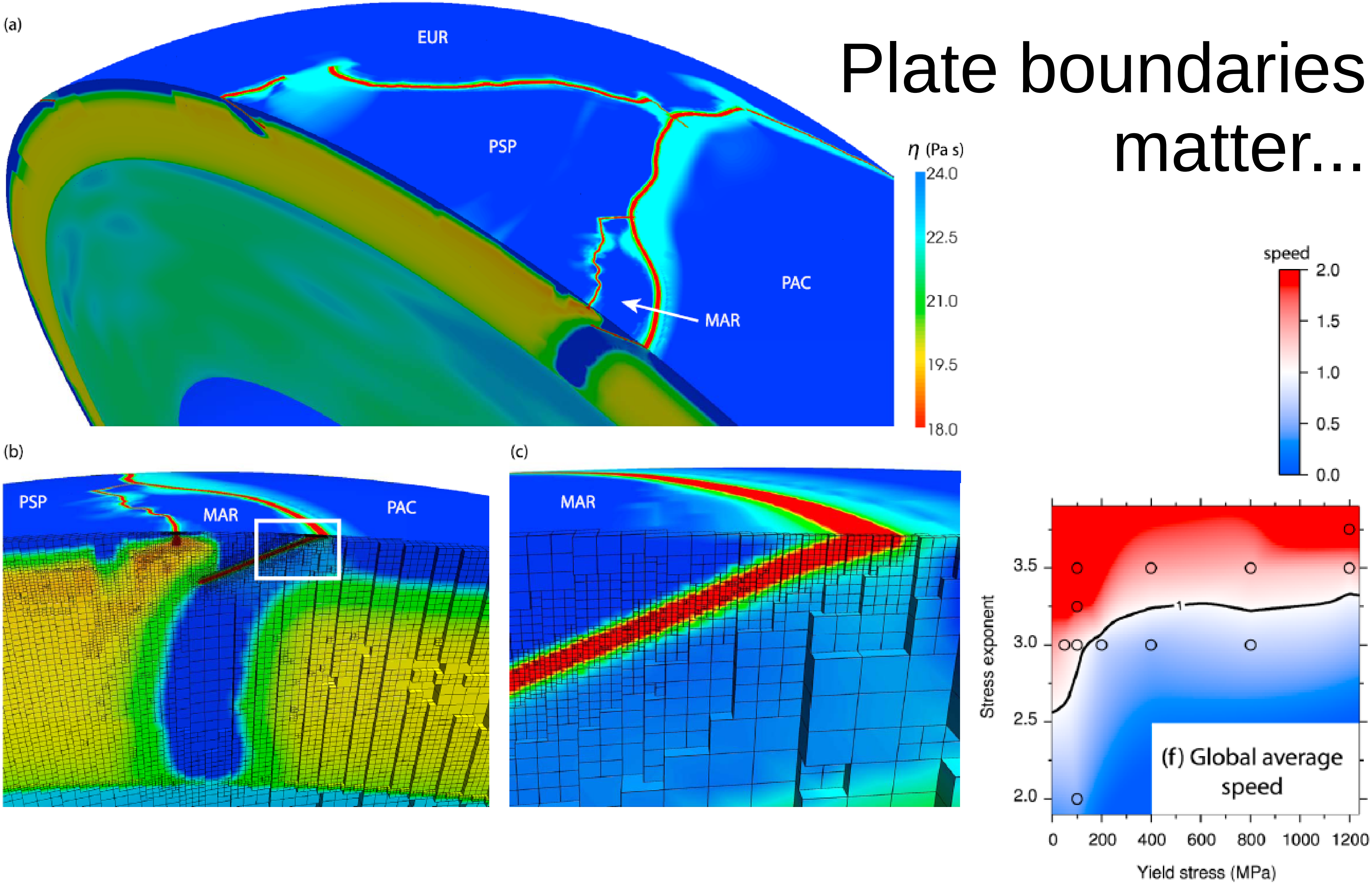

cf. Ricard and Vigny (1989), Forte (1993),
King and Hager (1990), Gable et al. (1991), Han and Gurnis (1999)

Alisic et al. (2012)

Why do we have plate tectonics?

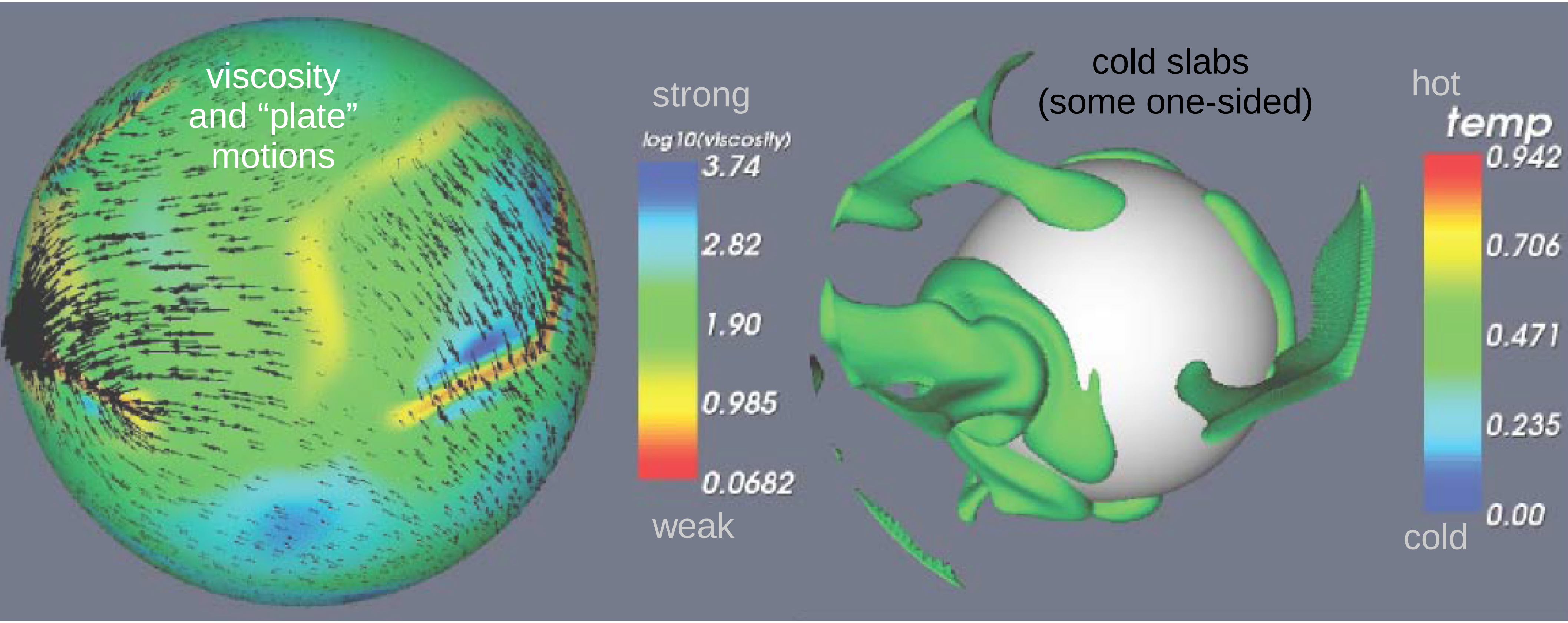

Foley & Becker (2009)

free-slip, global convection computation with temperature-dependent viscosity and yield stress, $Ra > Ra_{Earth}$

van Heck and Tackley (2008); Yoshida (2008); Foley and Becker (2009); Nakagawa et al. (2009); Coltice et al. (2013), Coltice et al. (2016)

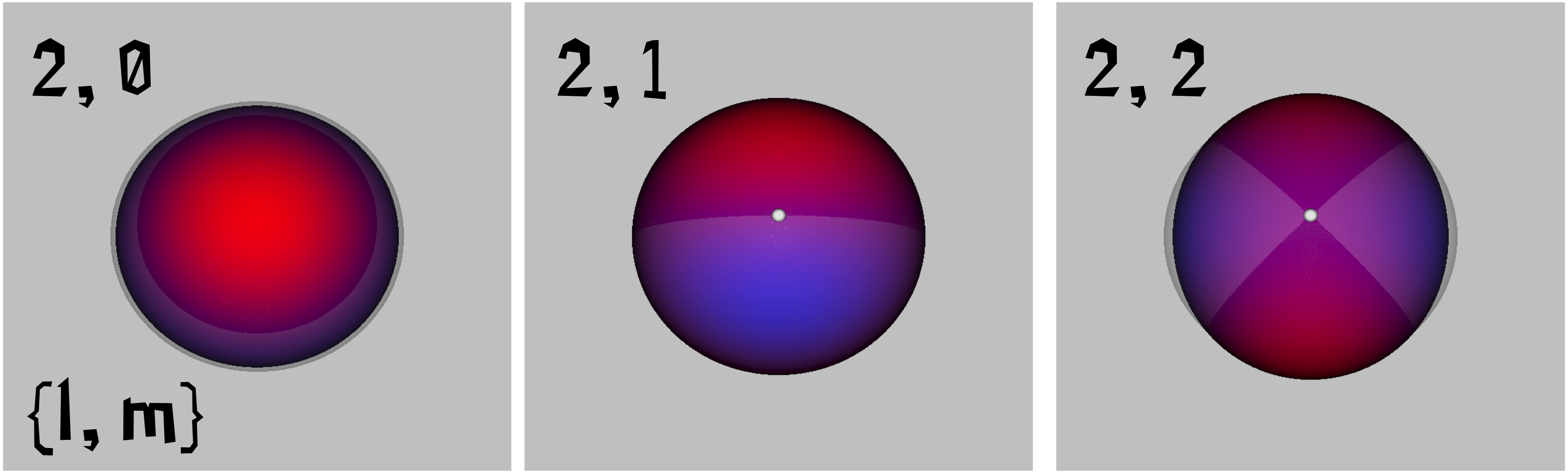

spherical harmonic basis function of degree *l* and order *m*

$$\delta v(\theta,\ \phi) \approx \sum_{l=0}^{\ell_{\max}} \left[a_{\ell 0} X_{\ell 0}(\theta) + \sqrt{2} \sum_{m=1}^{\ell} X_{\ell m}(\theta) \times \left(a_{\ell m}\ \cos\, m\phi + b_{\ell m}\ \sin\, m\phi \right) \right]$$

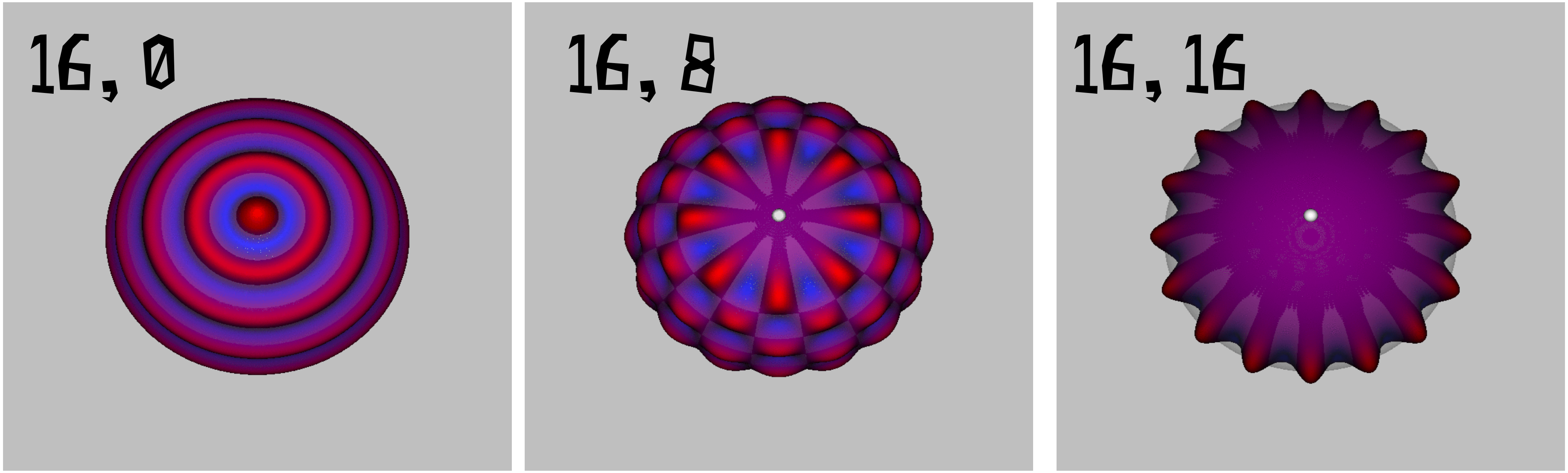

Stochastic constraints:
Mantle tomography shows long wavelength (*l* ~ 2) structure

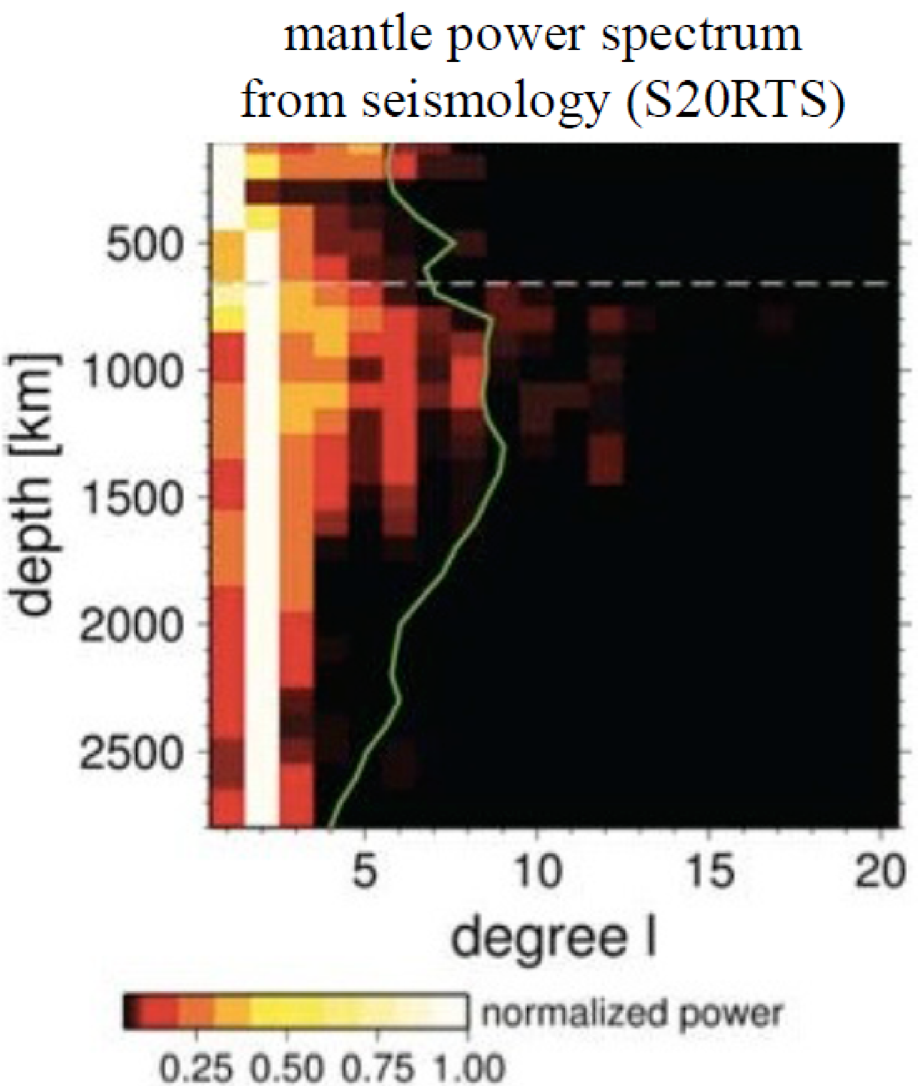

Convection models predict this heterogeneity

(because it has plates and those organize convection)

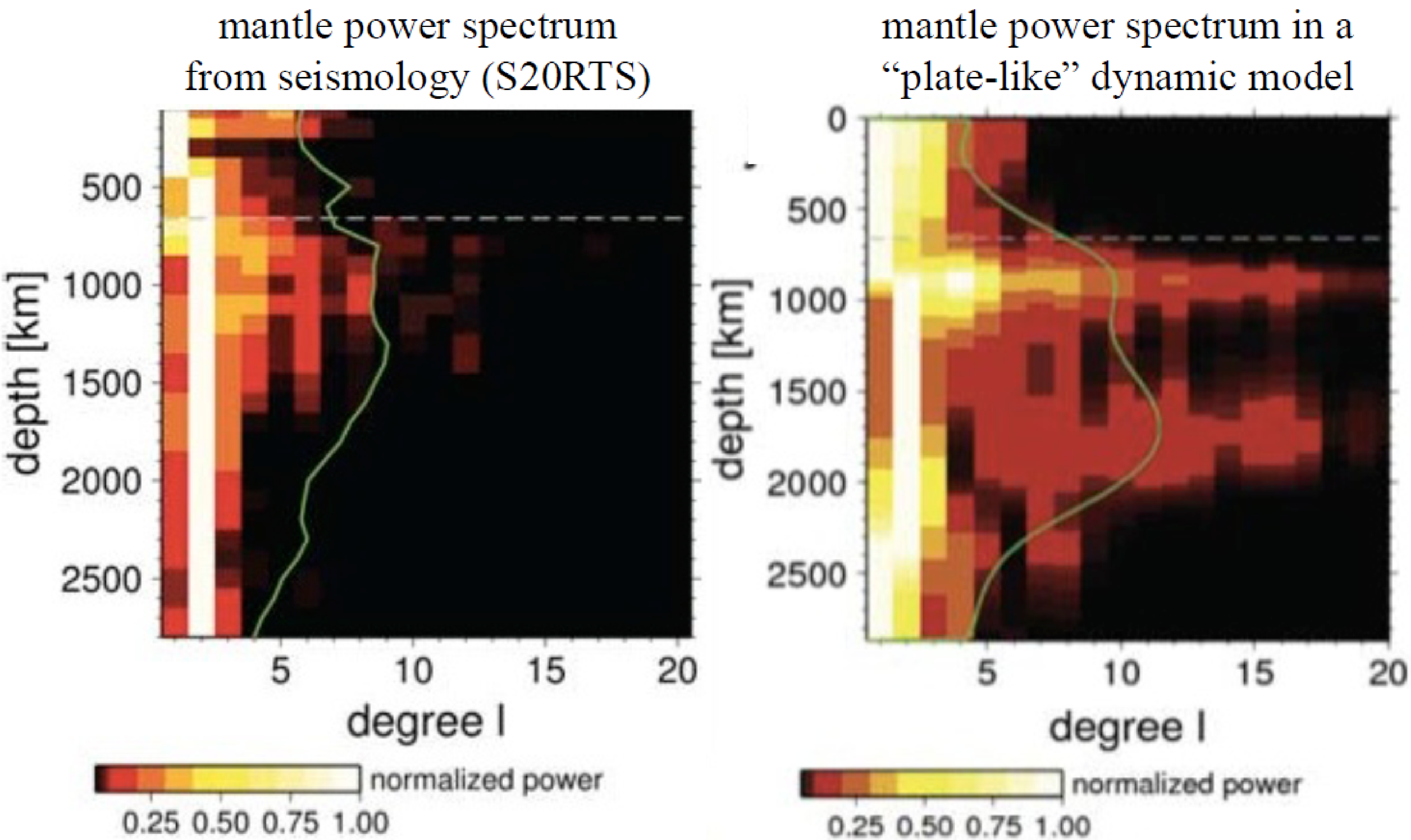

cf. Tackley (2000a,2000), Richards et al. (2001),
van Heck and Tackley (2008), Mallard et al. (2016)

Foley and Becker (2009)

We don't know how plate tectonics works

(questioning models assuming known physics)

Seafloor age distribution vs. boundary layer instability

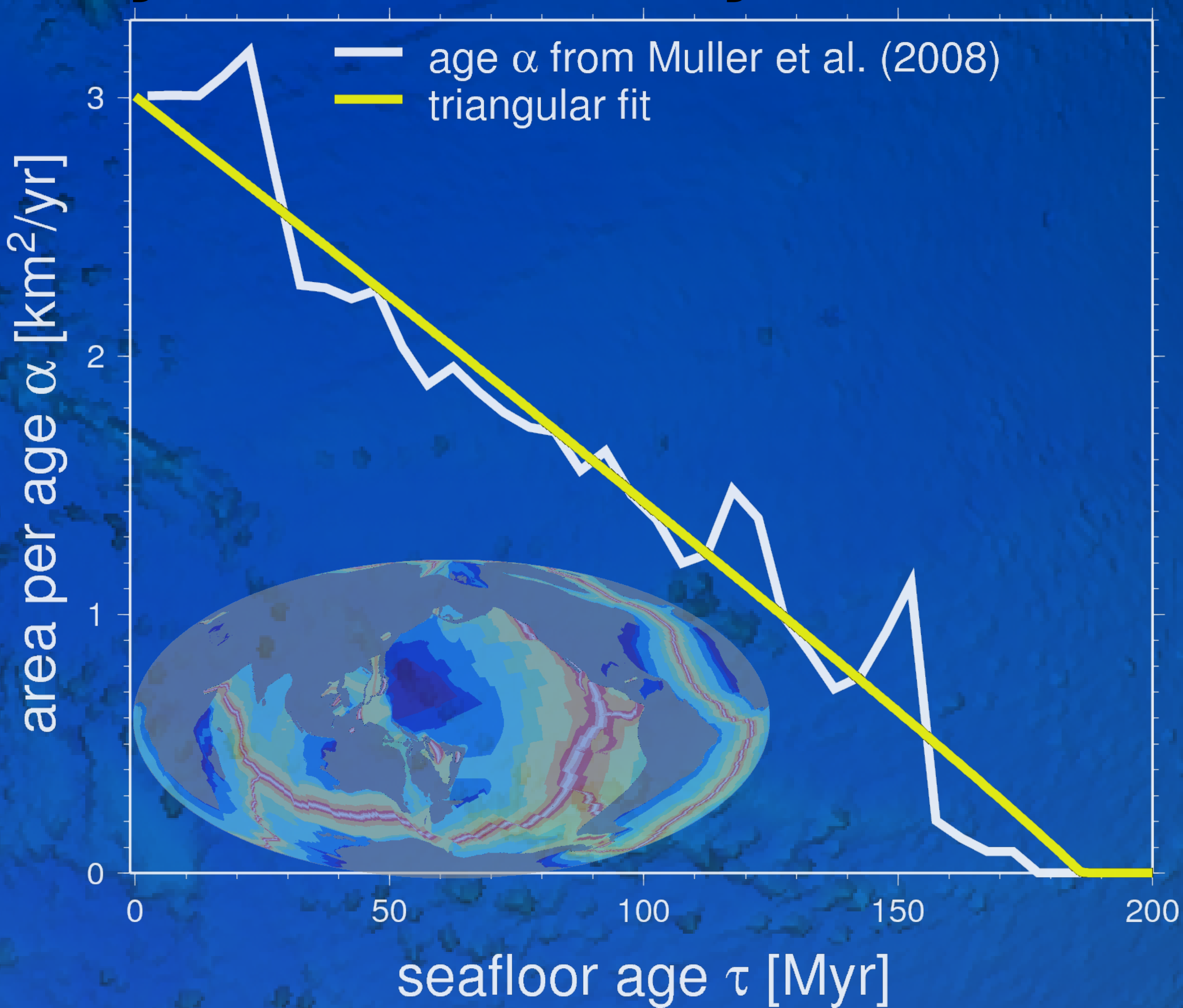

cf. Becker et al. (2009)
Coltice et al. (2013)

Kinematic vs. dynamic models

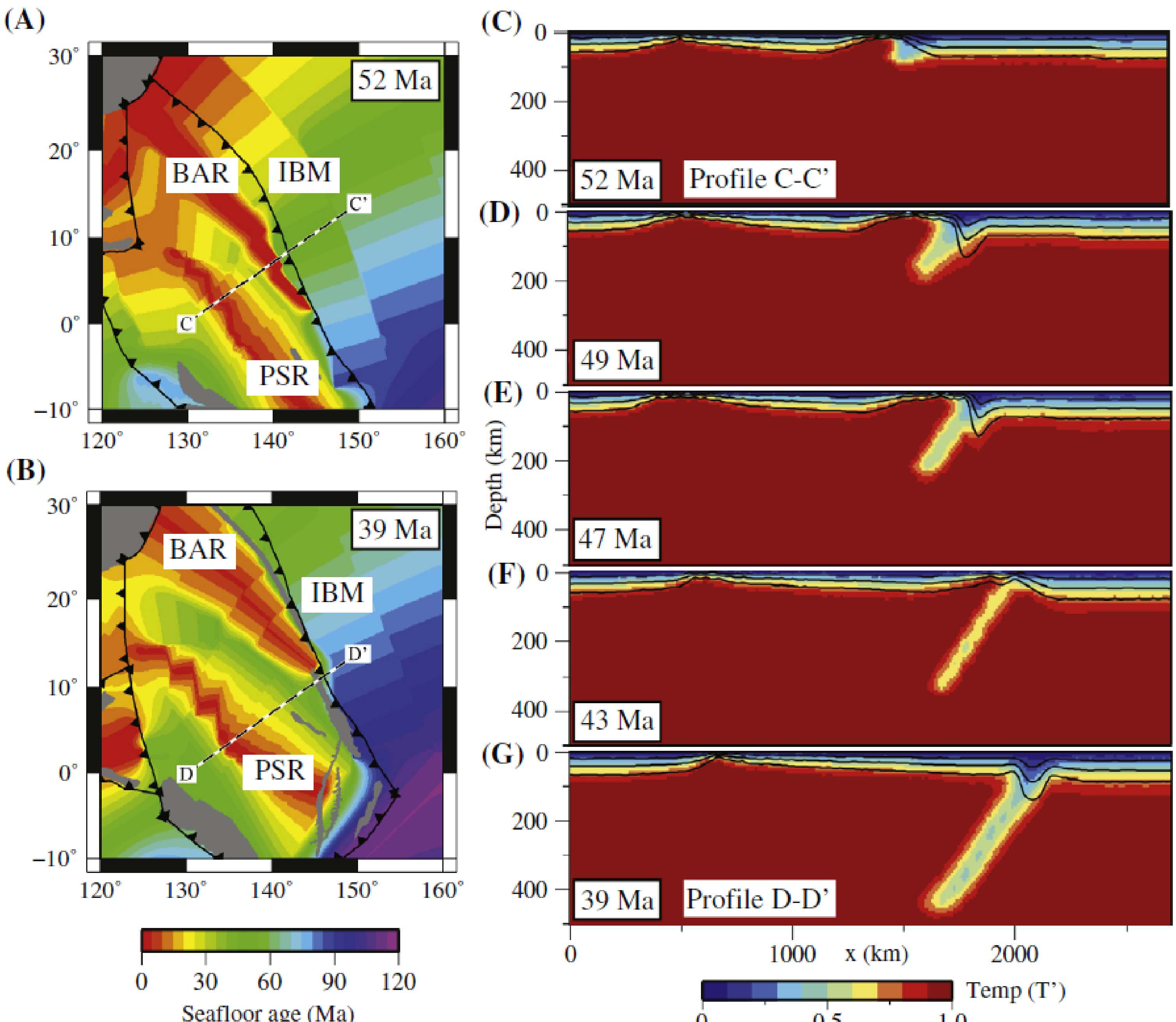

Bower et al. (2014)

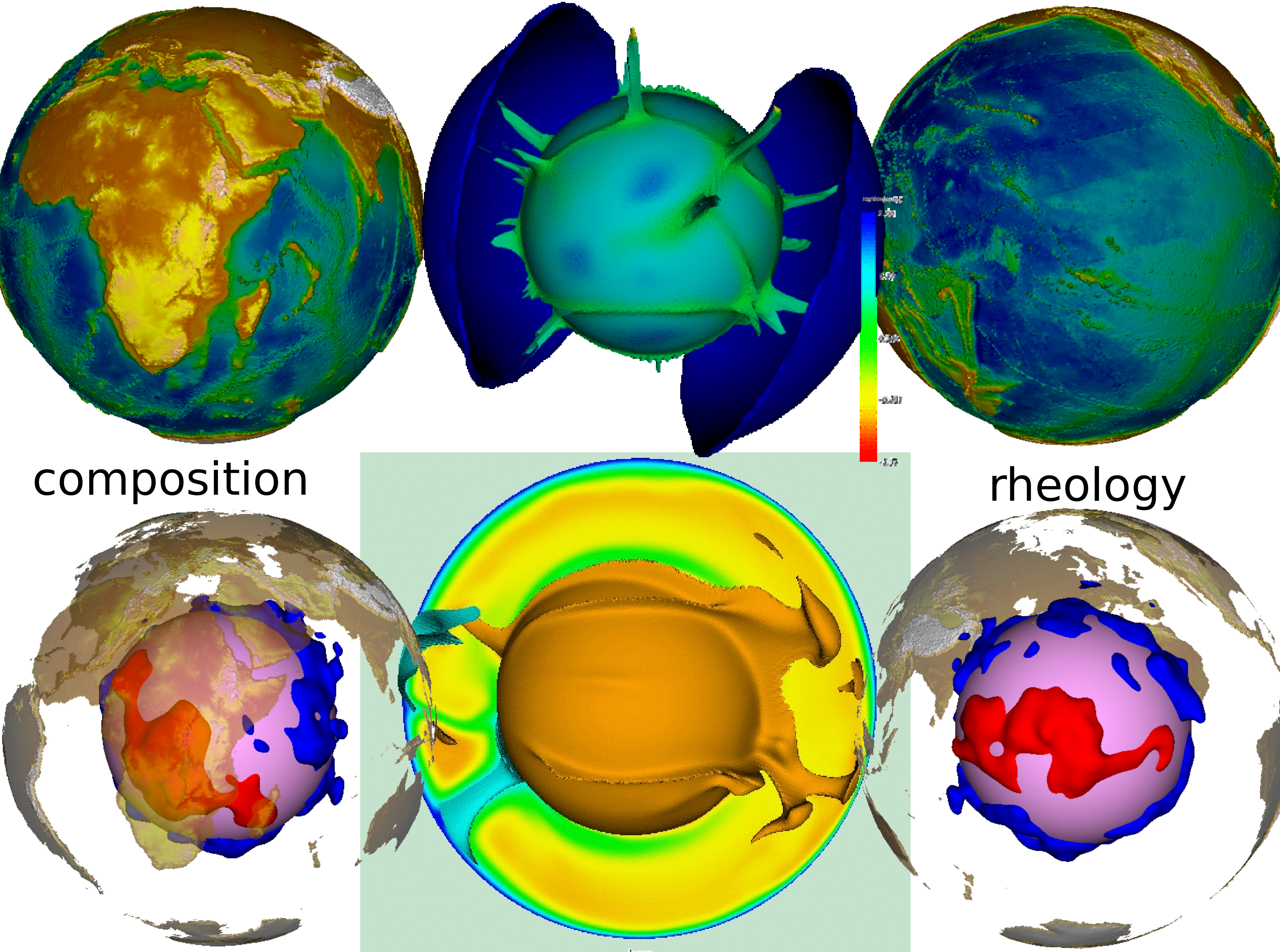
composition
rheology

Geophysical constraints on global mantle dynamics (applied geodynamics)

- Plate velocities
- Topography
- Geoid
- Seismic tomography
- Seismic anisotropy

Plate velocities

(net rotation, relative plate motions, distribution of strain-rate, toroidal vs. poloidal; now and in past)

MORVEL-56 in SA reference frame

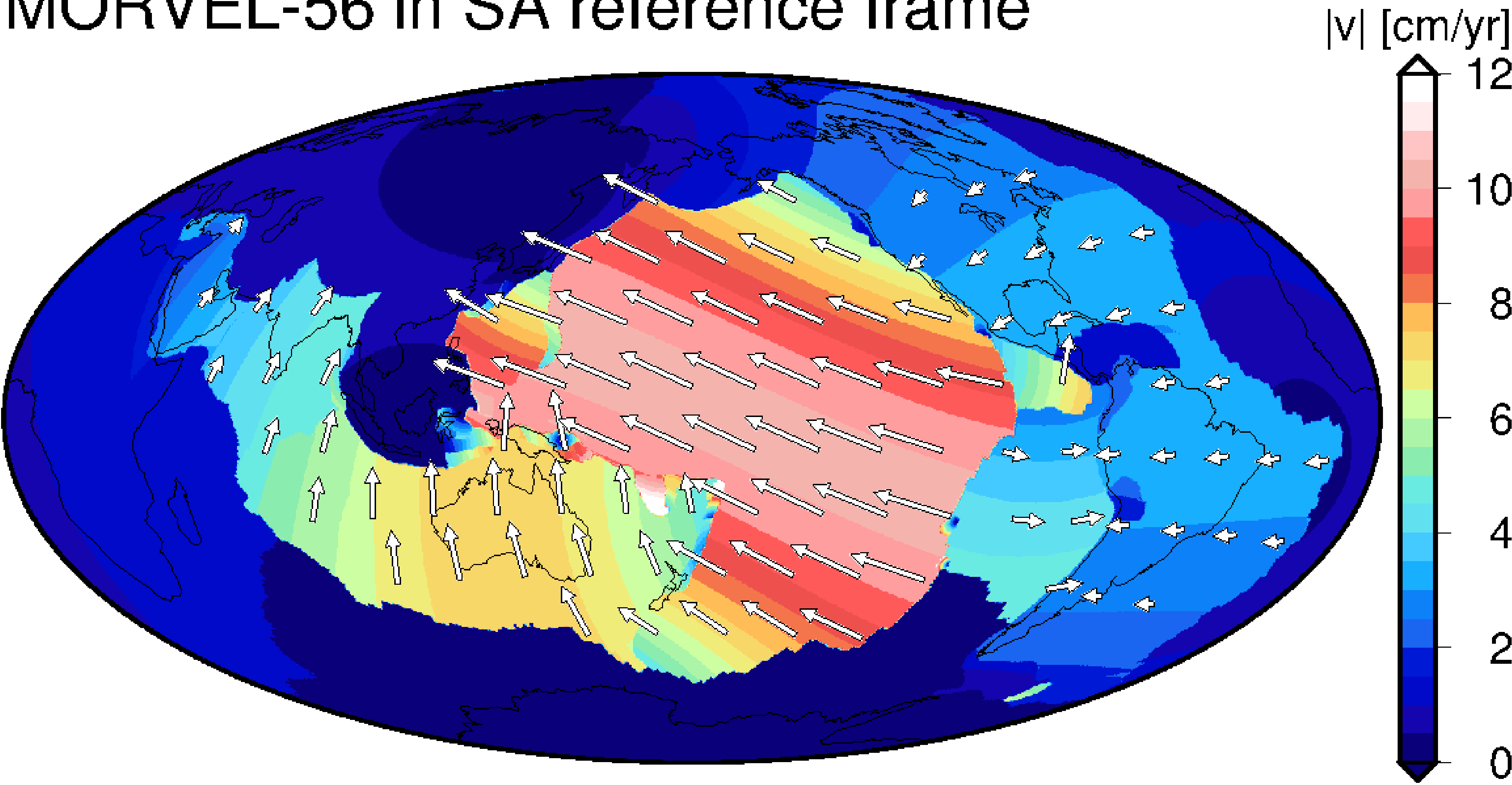

Argus et al. (2011), Becker et al. (2015)

Helmholtz decomposition

into irrotational (poloidal) and divergence free (toroidal) fields

$$\underline{v}_h \equiv \underline{v}_{h,\mathrm{pol}} + \underline{v}_{h,\mathrm{tor}} \equiv \underline{\nabla}_h \varphi + \underline{\nabla} \times (\psi \hat{z})$$

$$\nabla^2 \varphi = \underline{\nabla}_h \bullet \underline{v}_h ; \nabla^2 \psi = \mathrm{vort}_z(\underline{v}_h)$$

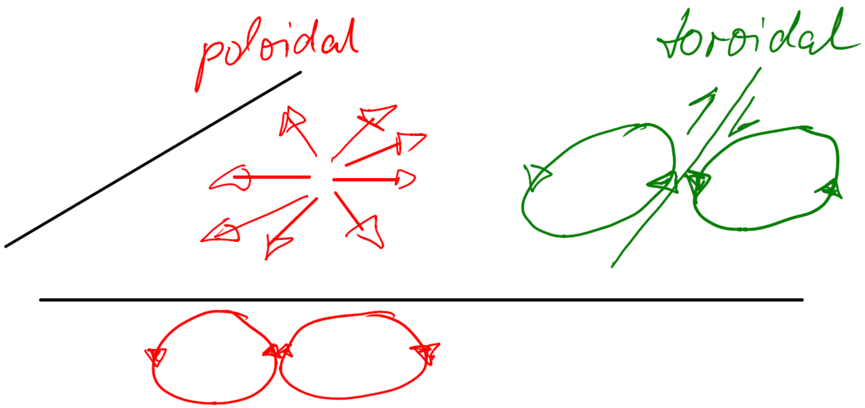

Or, in *vector* spherical harmonics (use *generalized* spherical harmonics for orientational, 2ϕ):

$$\mathbf{V}(\theta,\phi) = \sum_{l\,m} Re\{b_{lm}\mathbf{B}_{lm}(\theta,\phi) + c_{lm}\mathbf{C}_{lm}(\theta,\phi)\}$$

$$\mathbf{B}_{lm}(\theta,\phi) = \frac{1}{L}\frac{\partial P_{lm}(\theta)}{\partial\theta}e^{im\phi}\mathbf{e}_\theta + \frac{im}{L\sin\theta}P_{lm}(\theta)e^{im\phi}\mathbf{e}_\phi$$

$$\mathbf{C}_{lm}(\theta,\phi) = \frac{im}{L\sin\theta}P_{lm}(\theta)e^{im\phi}\mathbf{e}_\theta - \frac{1}{L}\frac{\partial P_{lm}(\theta)}{\partial\theta}e^{im\phi}\mathbf{e}_\phi$$

Time-evolution of plate kinematic diagnostics

Mueller et al. (2016)

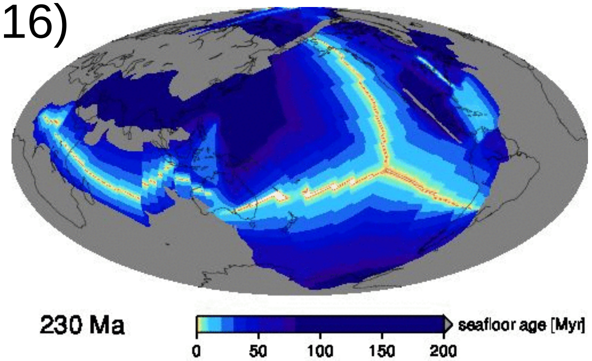

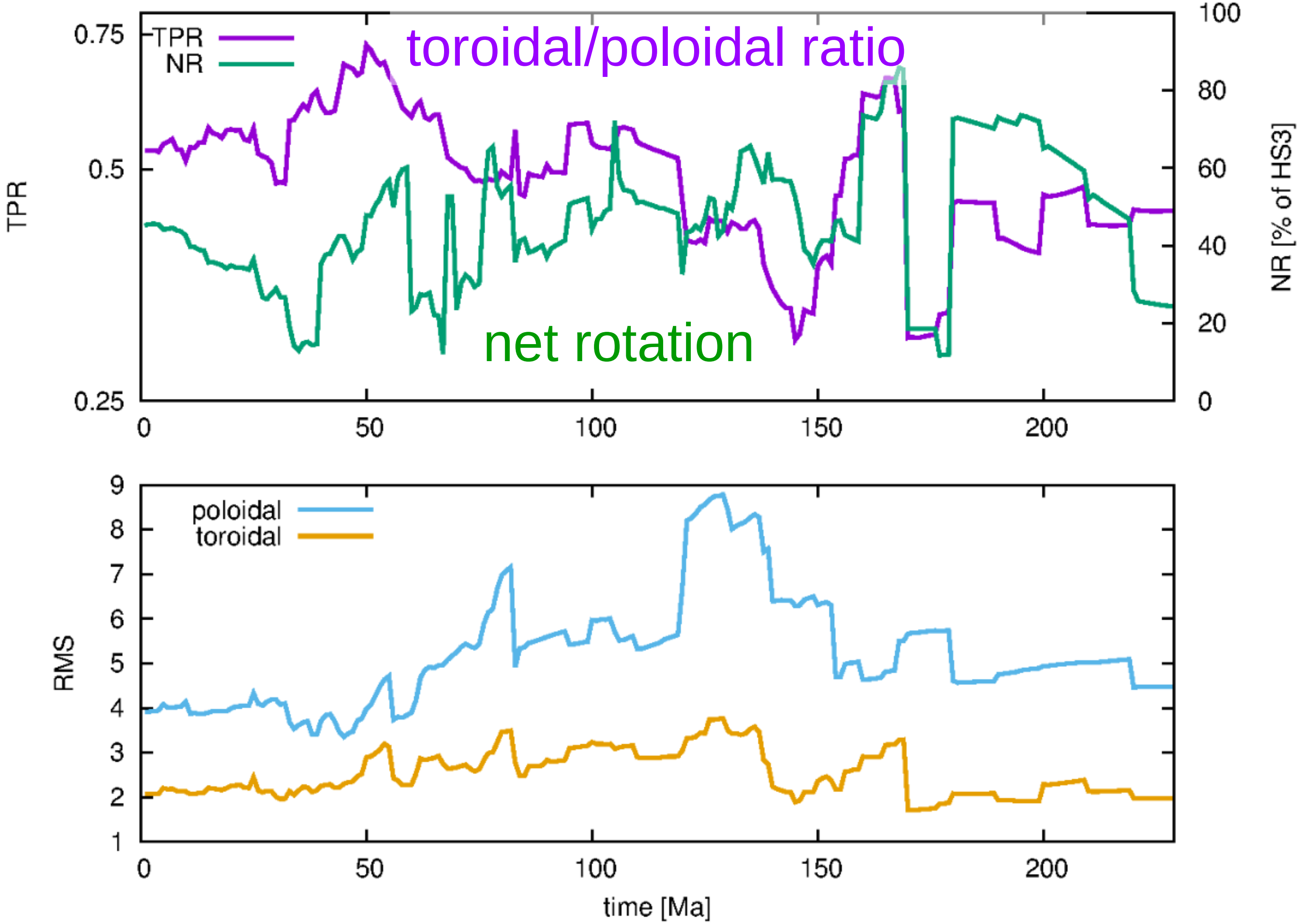

Surface topography

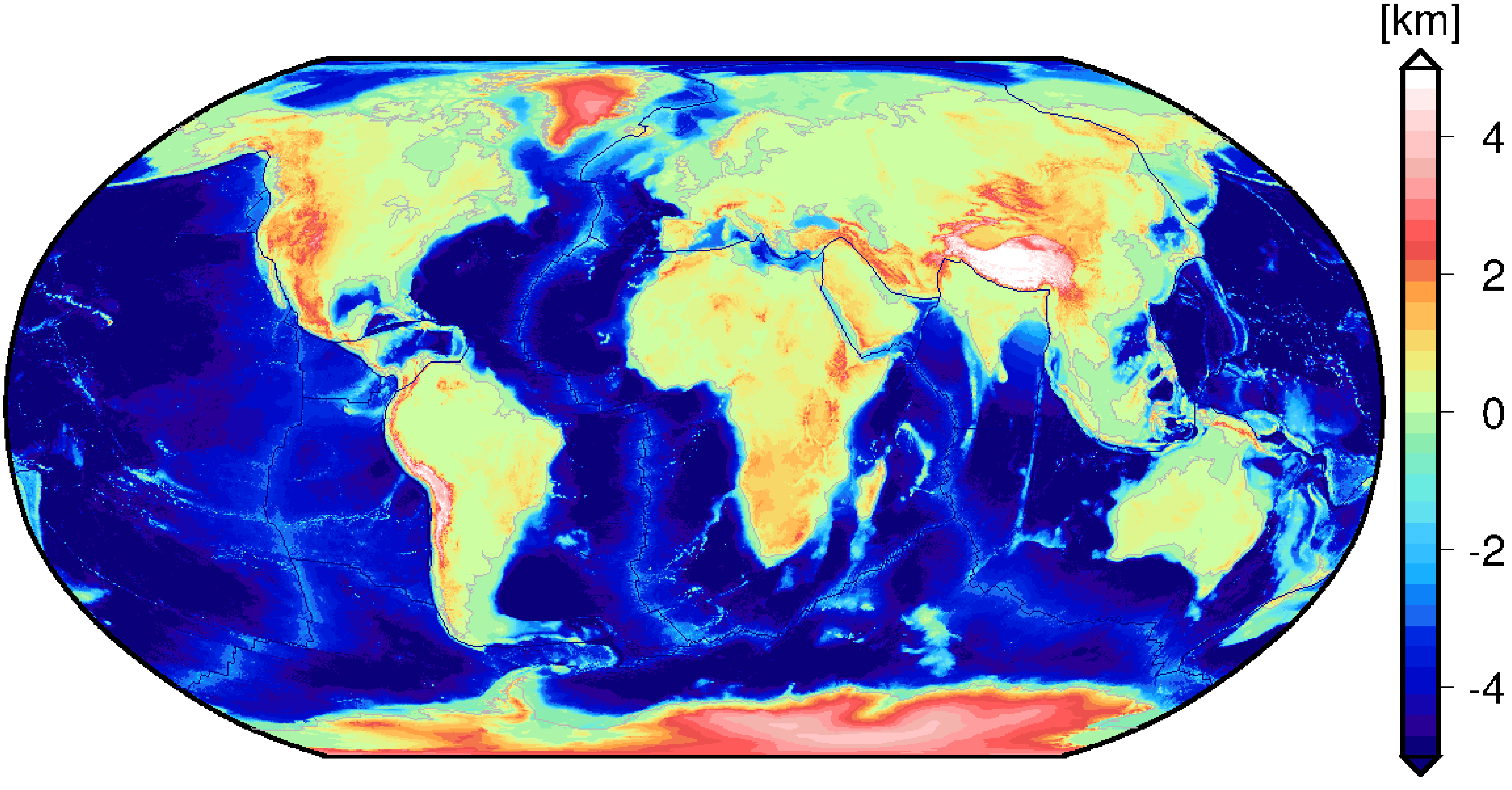

Isostasy

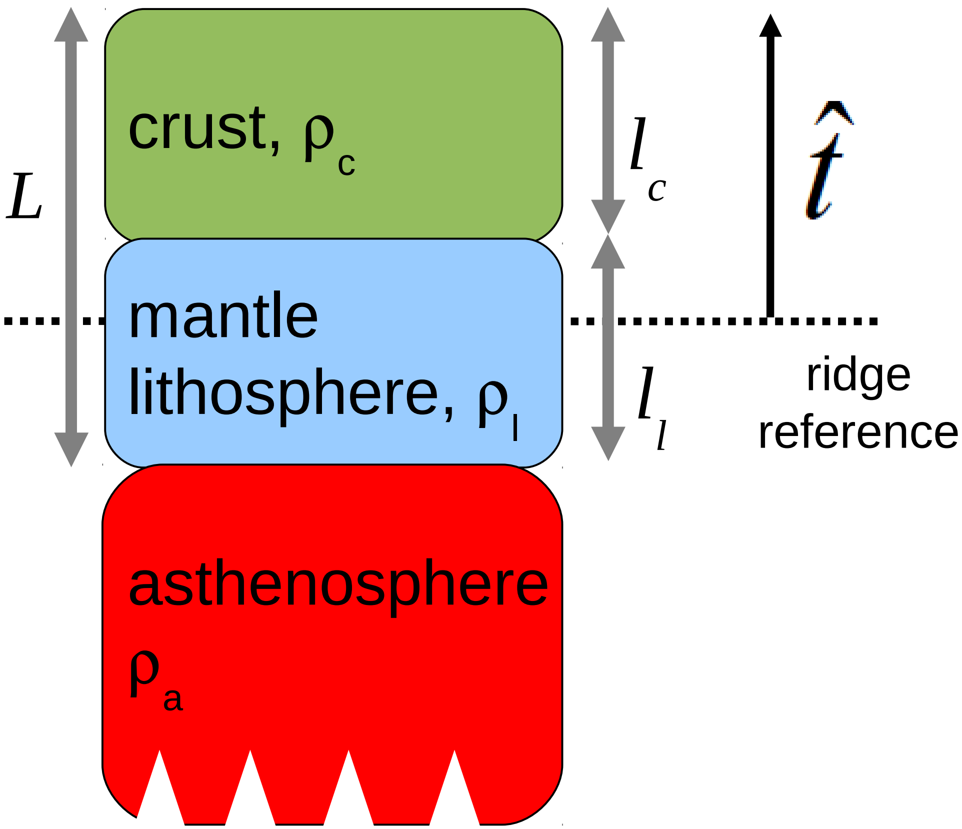

$$\hat{t} = f_1 l_c + f_2 l_l$$

$$f_1 = \frac{\rho_a - \rho_c}{\rho_a}, \quad f_2 = \frac{\rho_a - \rho_l}{\rho_a}$$

$$f_1 \approx 0.12 \qquad f_2 \approx -0.01$$

Airy : ρ const. (~continents)
Pratt: *l* const. (~oceans)

p = const. @ compensation level

actual topography

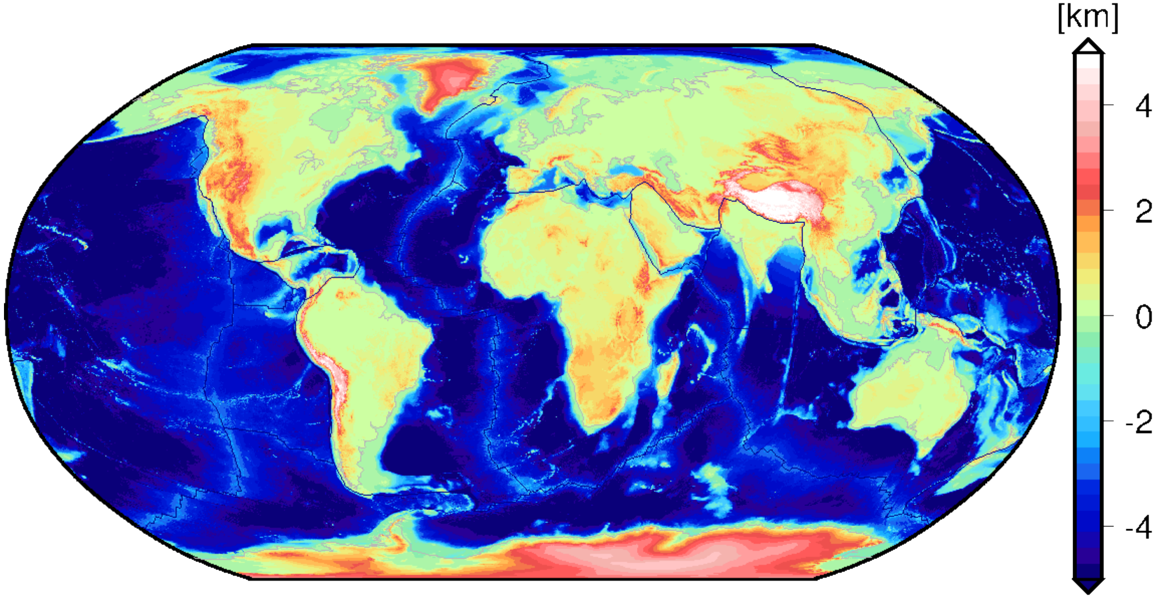

crustal thickness

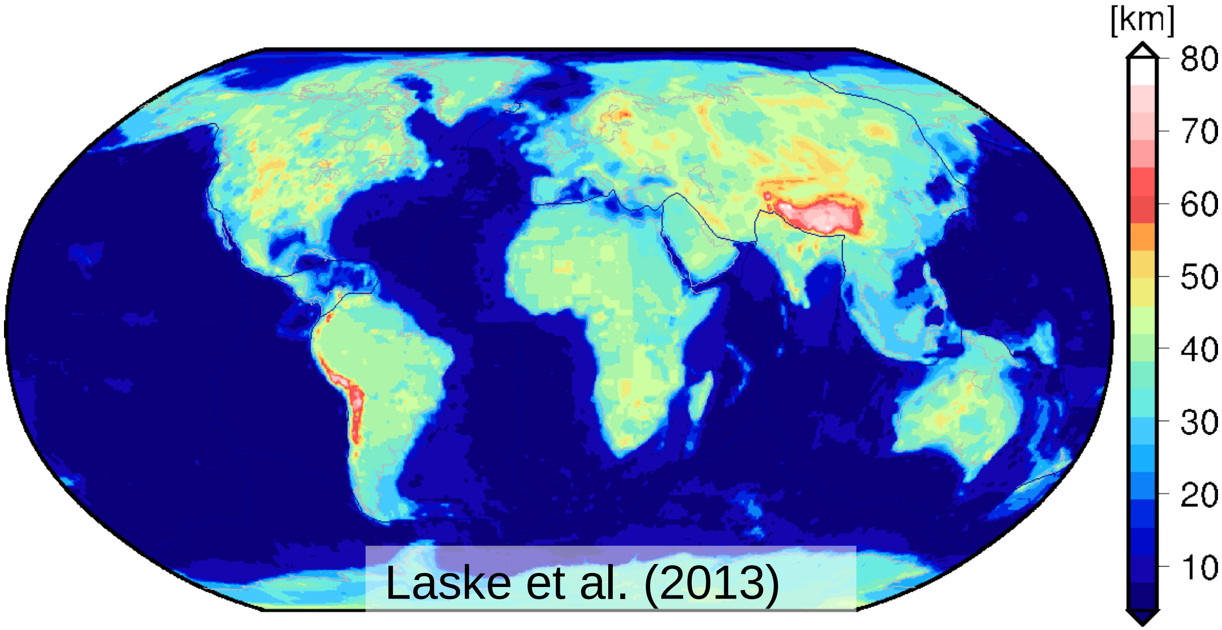

Note:
very uneven coverage.
active source best, RF next best thing

actual topography

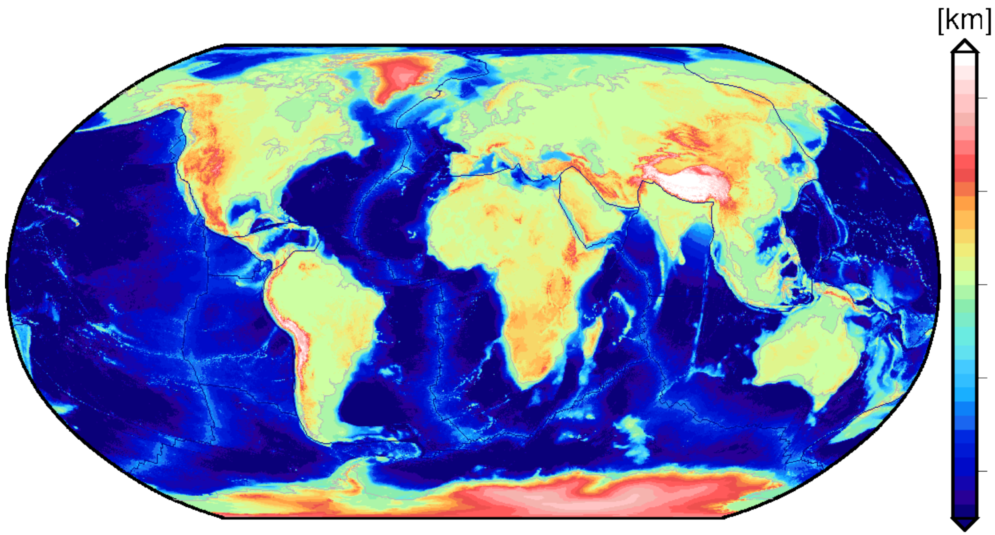

$$\hat{t} = f_1 l_c + f_2 l_l$$

$$f_1 = \frac{\rho_a - \rho_c}{\rho_a} \qquad f_2 = \frac{\rho_a - \rho_l}{\rho_a}$$

crustal thickness from CRUST1.0

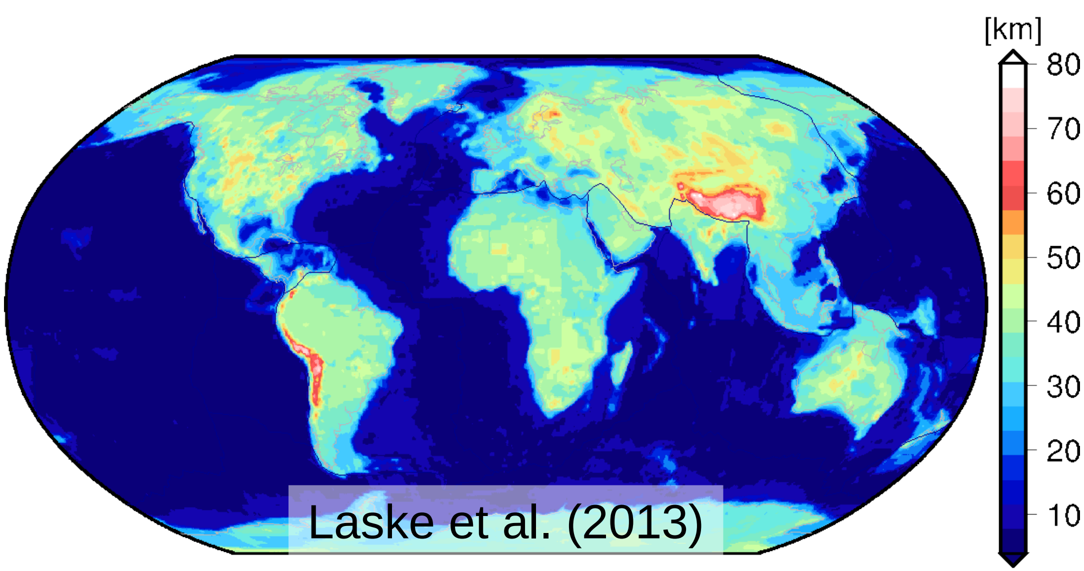

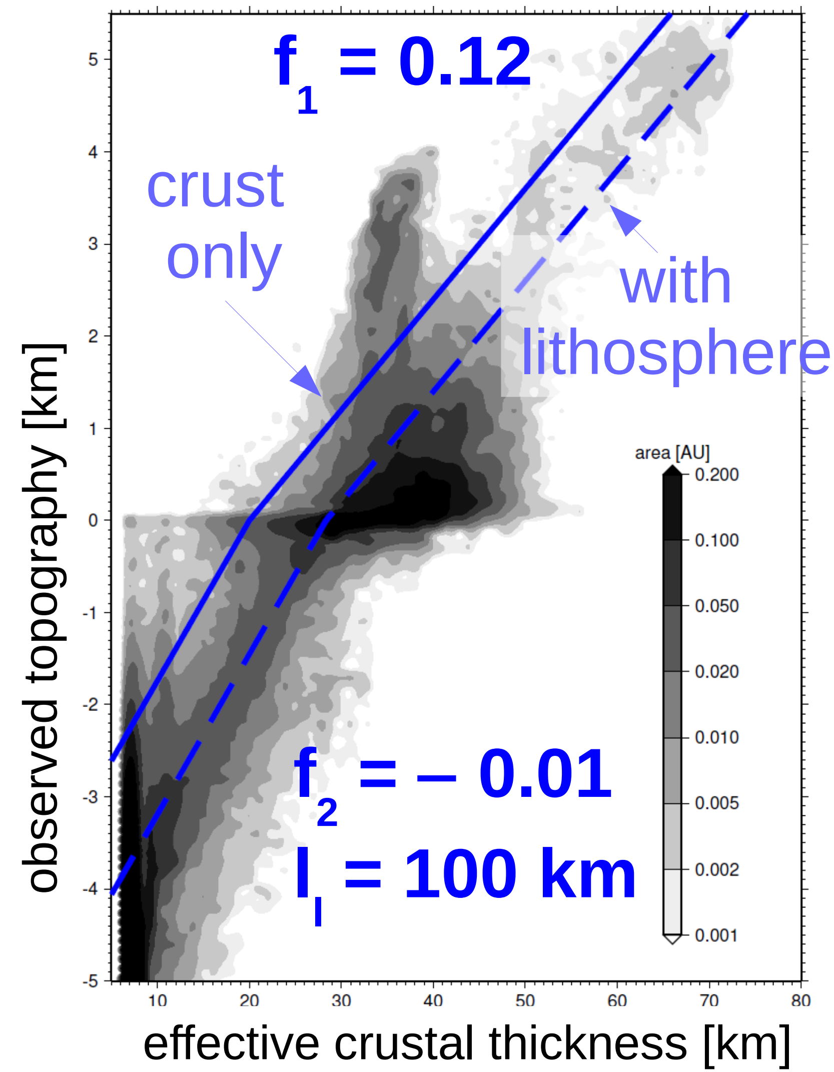

actual topography

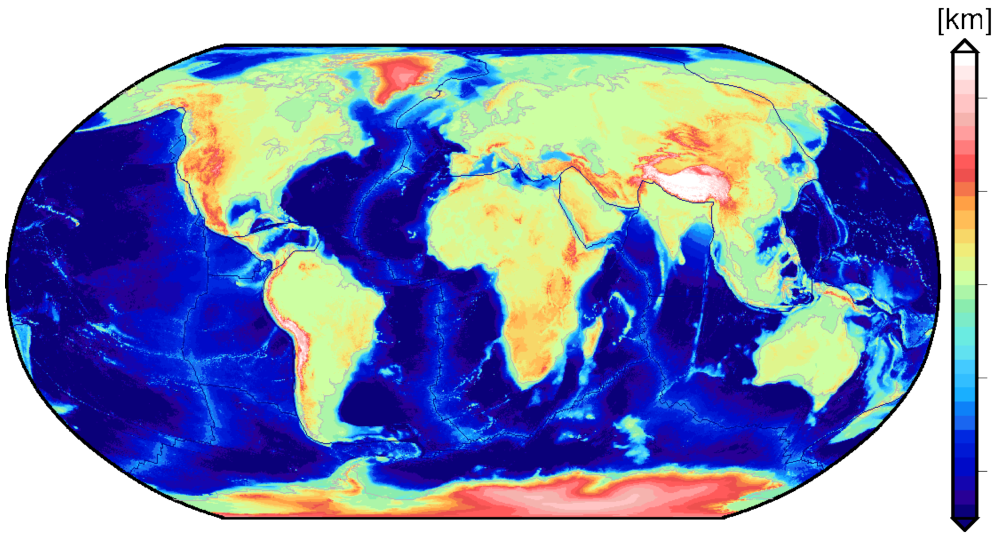

crustal thickness from CRUST1.0

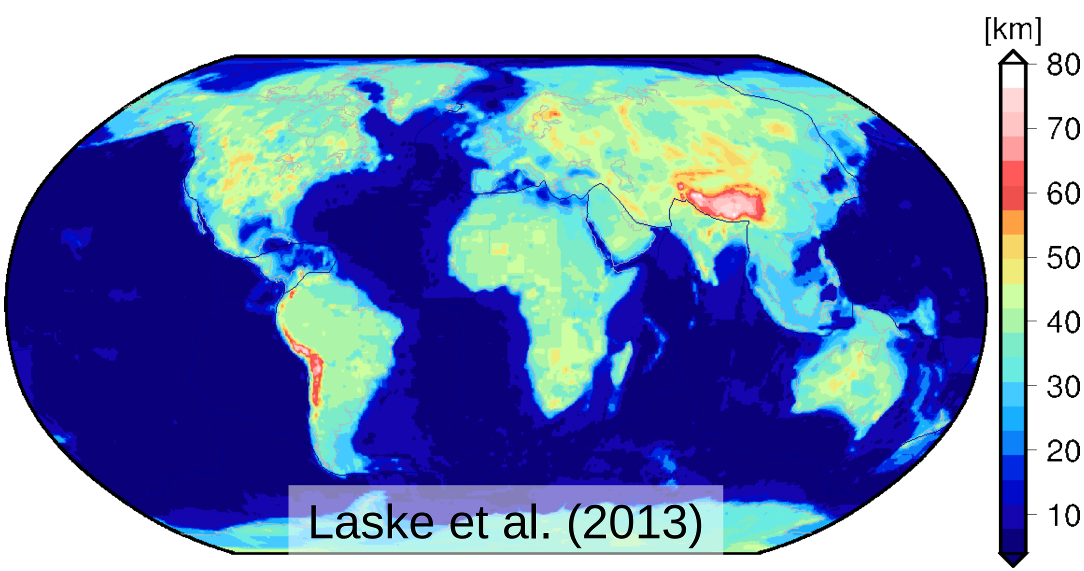

$$\hat{t} = f_1 l_c + f_2 l_l$$

$$f_1 = \frac{\rho_a - \rho_c}{\rho_a} \qquad f_2 = \frac{\rho_a - \rho_l}{\rho_a}$$

thickness vs. topography

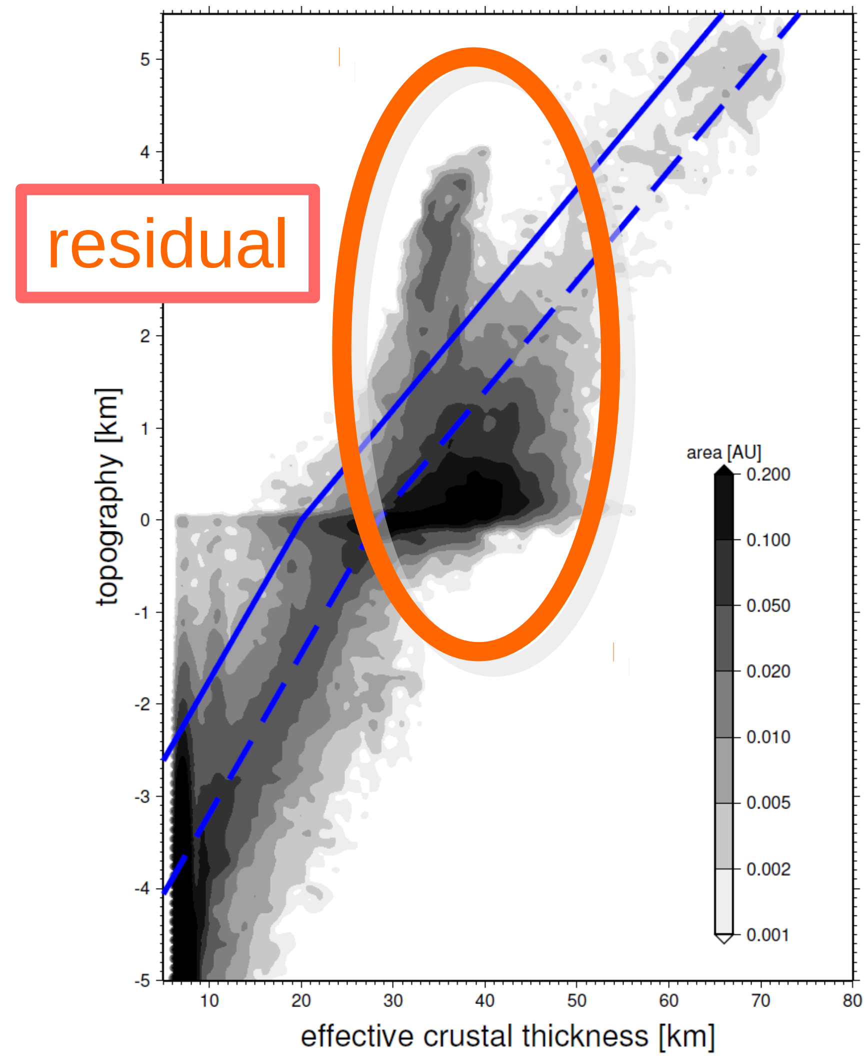

Global crustal residual topography

topography

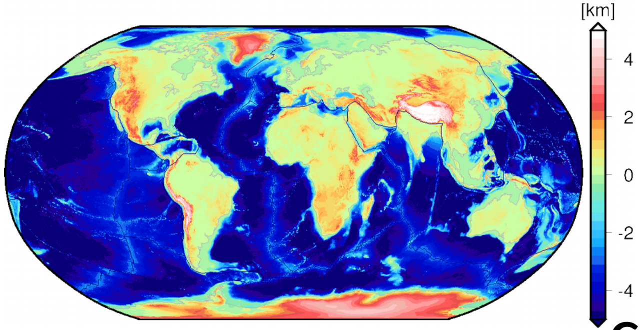

crustal model

−

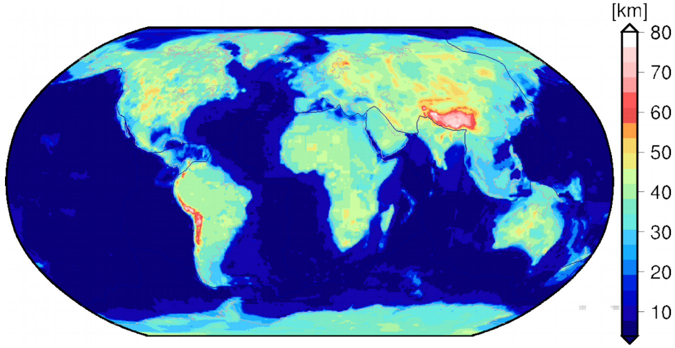

Note: Like oh so many things, “model”, not “data”

=

Non-isostatic, ~Airy residual topography

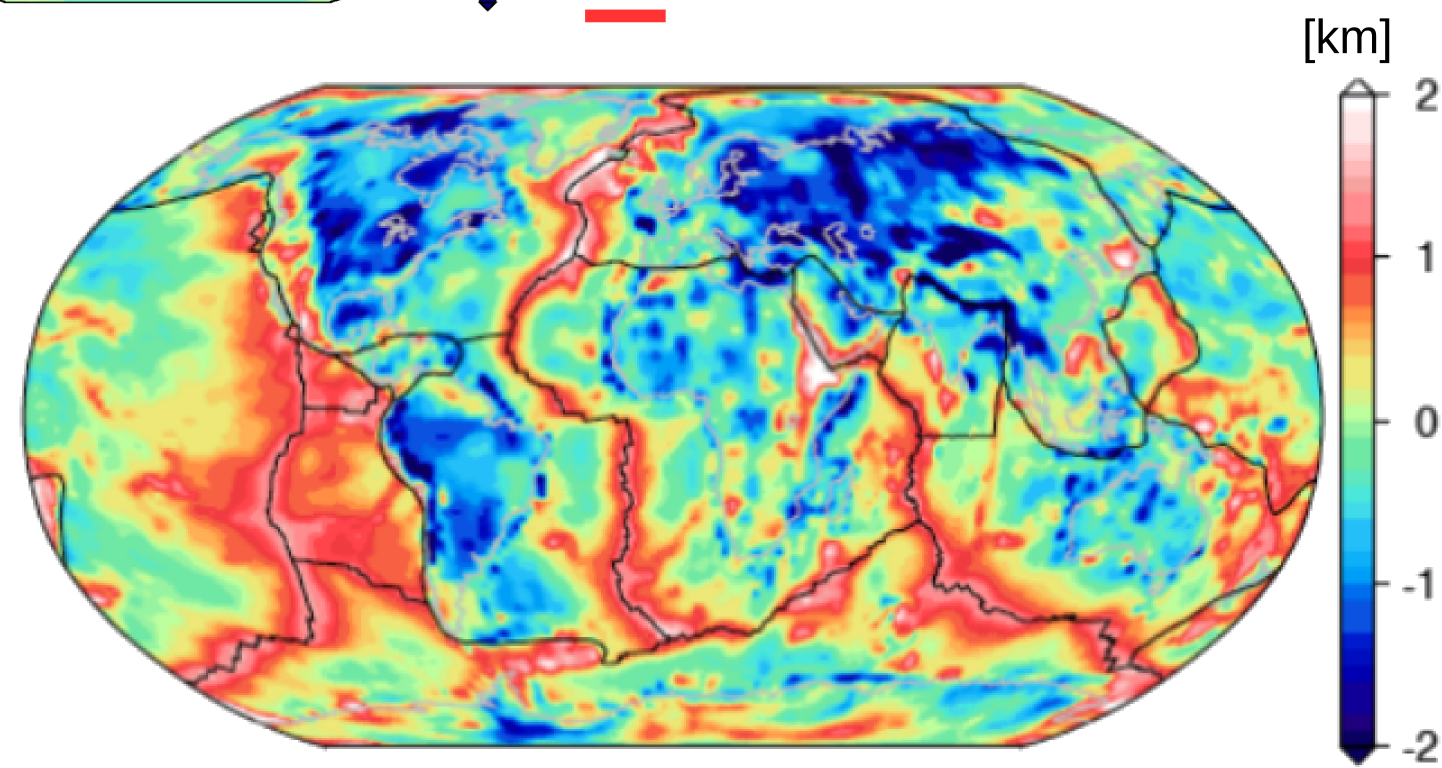

Geoid anomalies

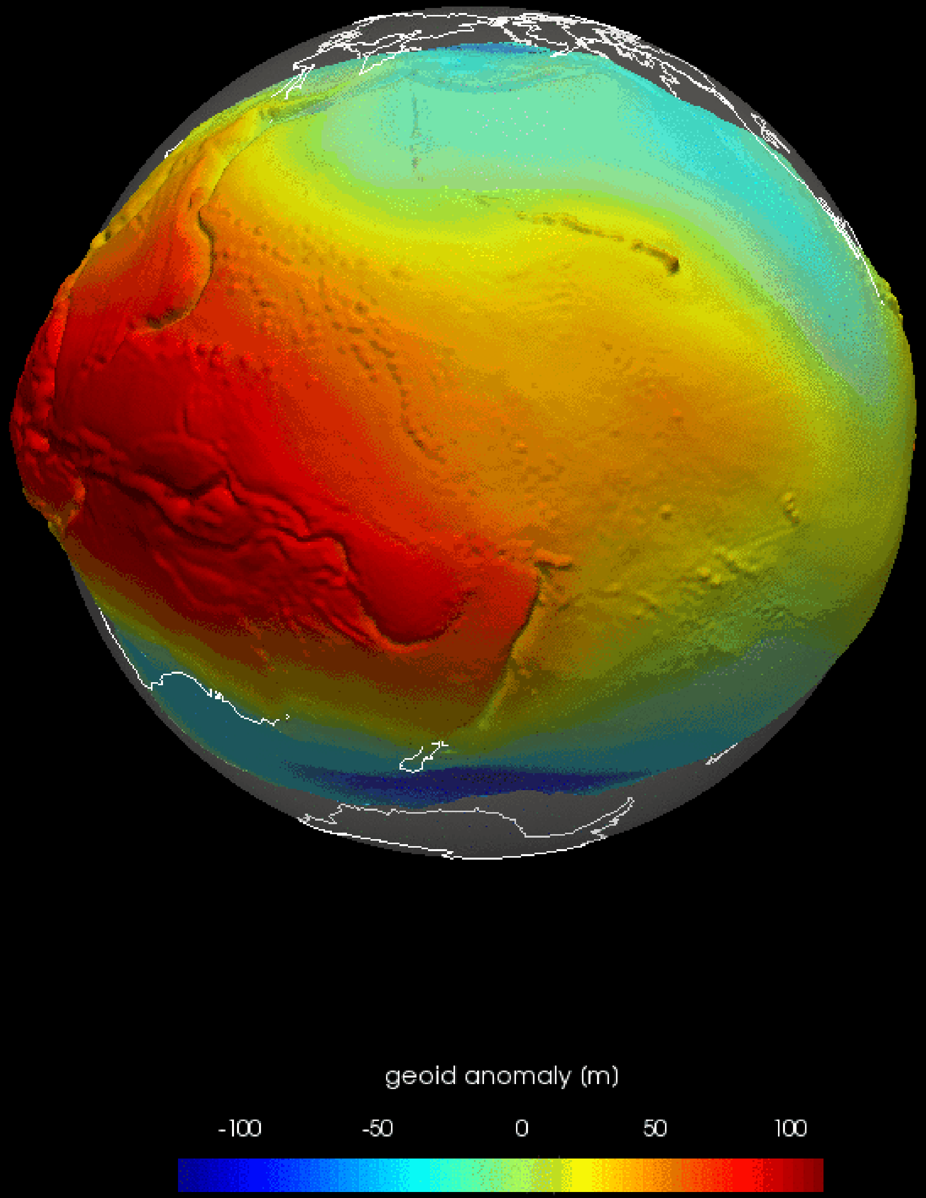

(corrected for *hydrostatic* shape)

Potential field constraints

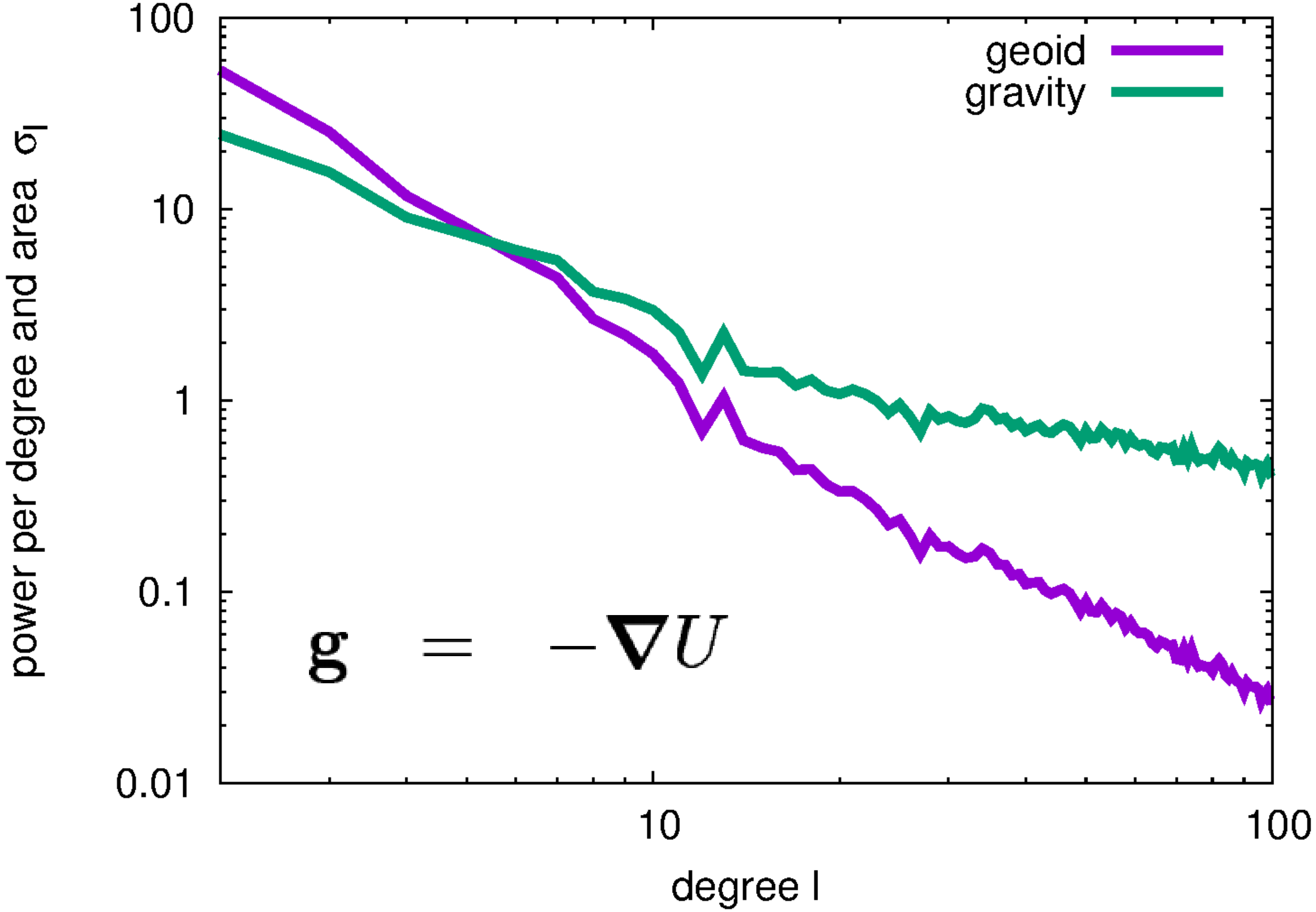

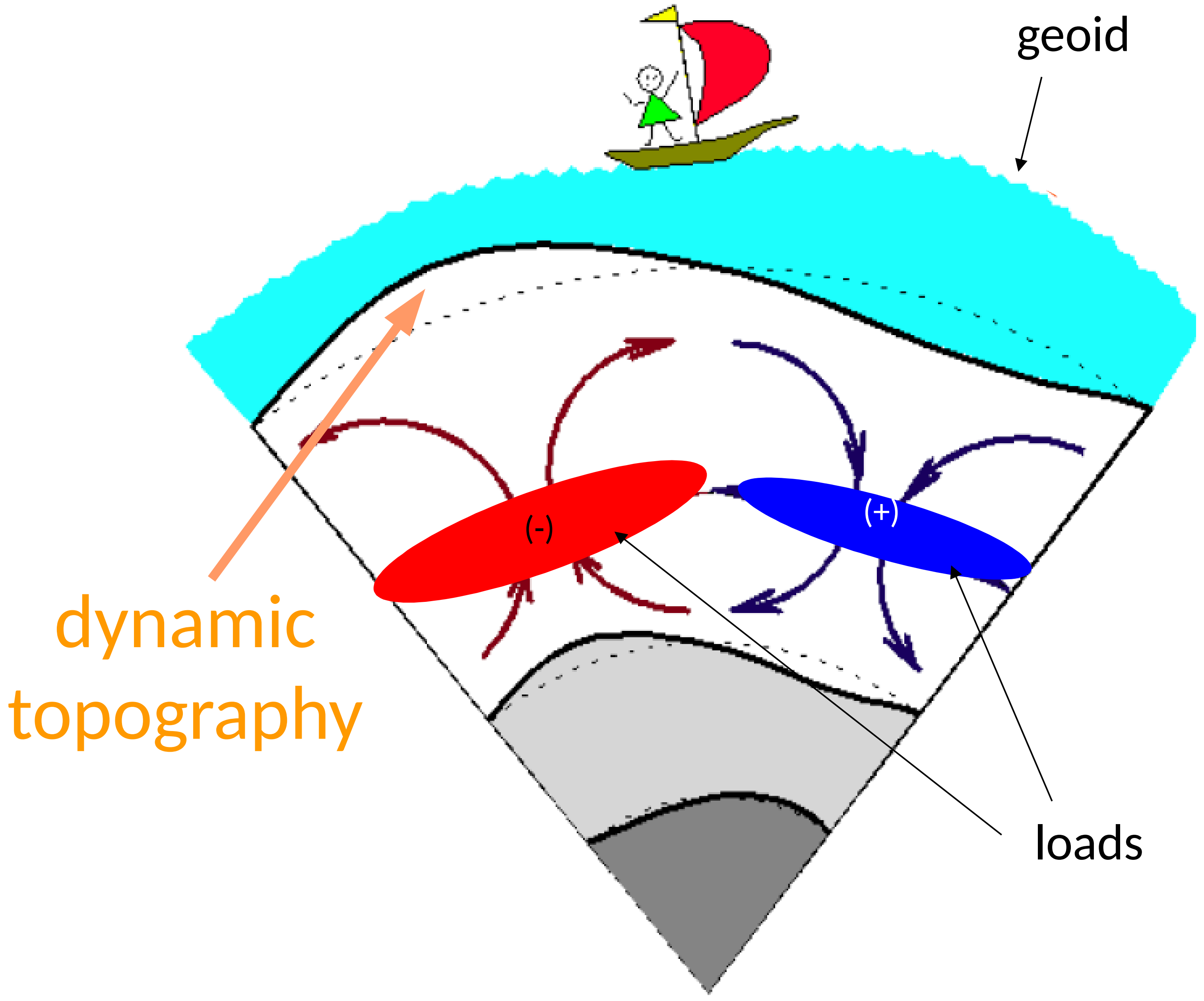

Figure from Y. Ricard

How do we build a deep Earth density model?

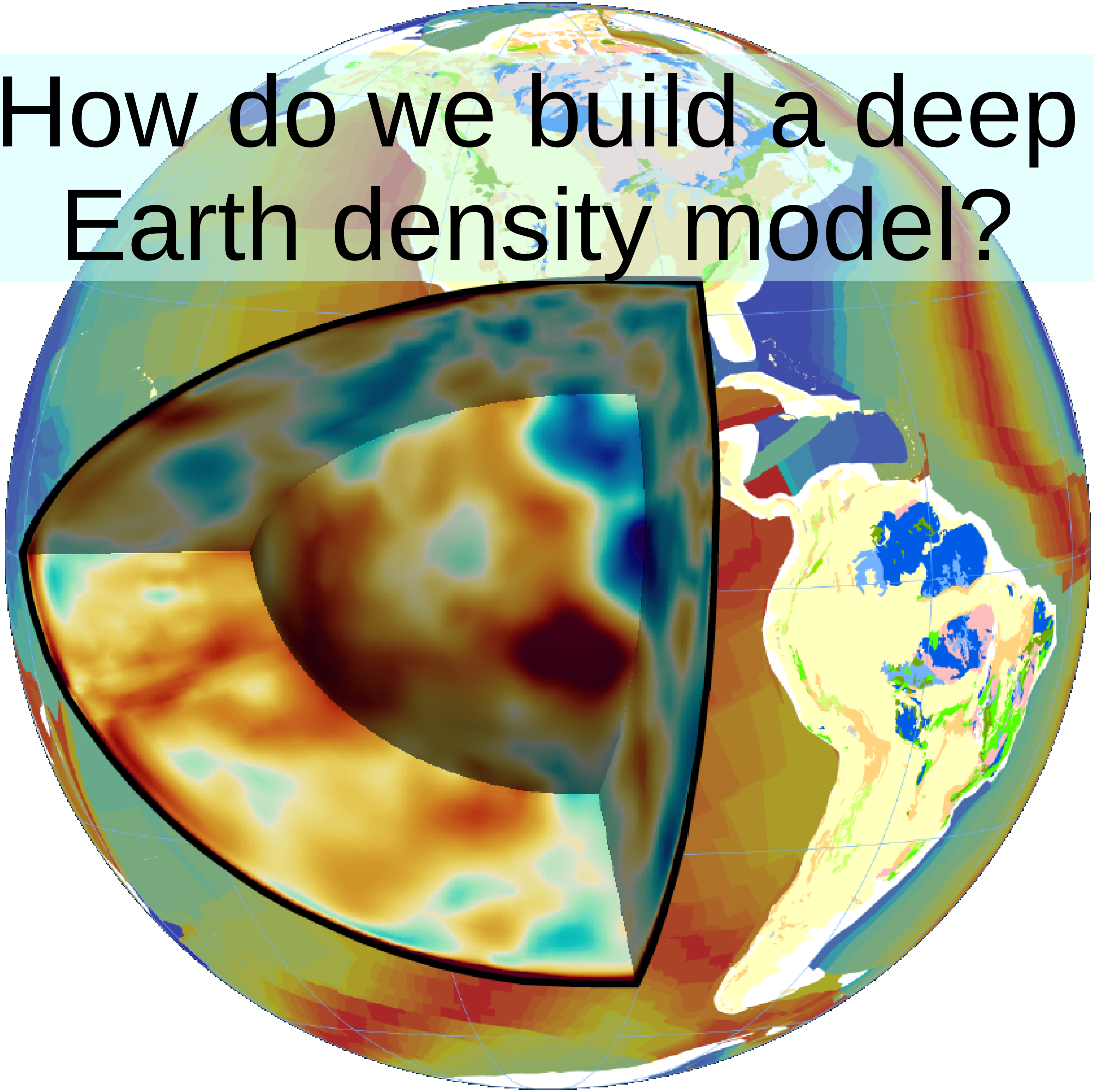

Upper mantle slabs from Wadati-Benioff zones

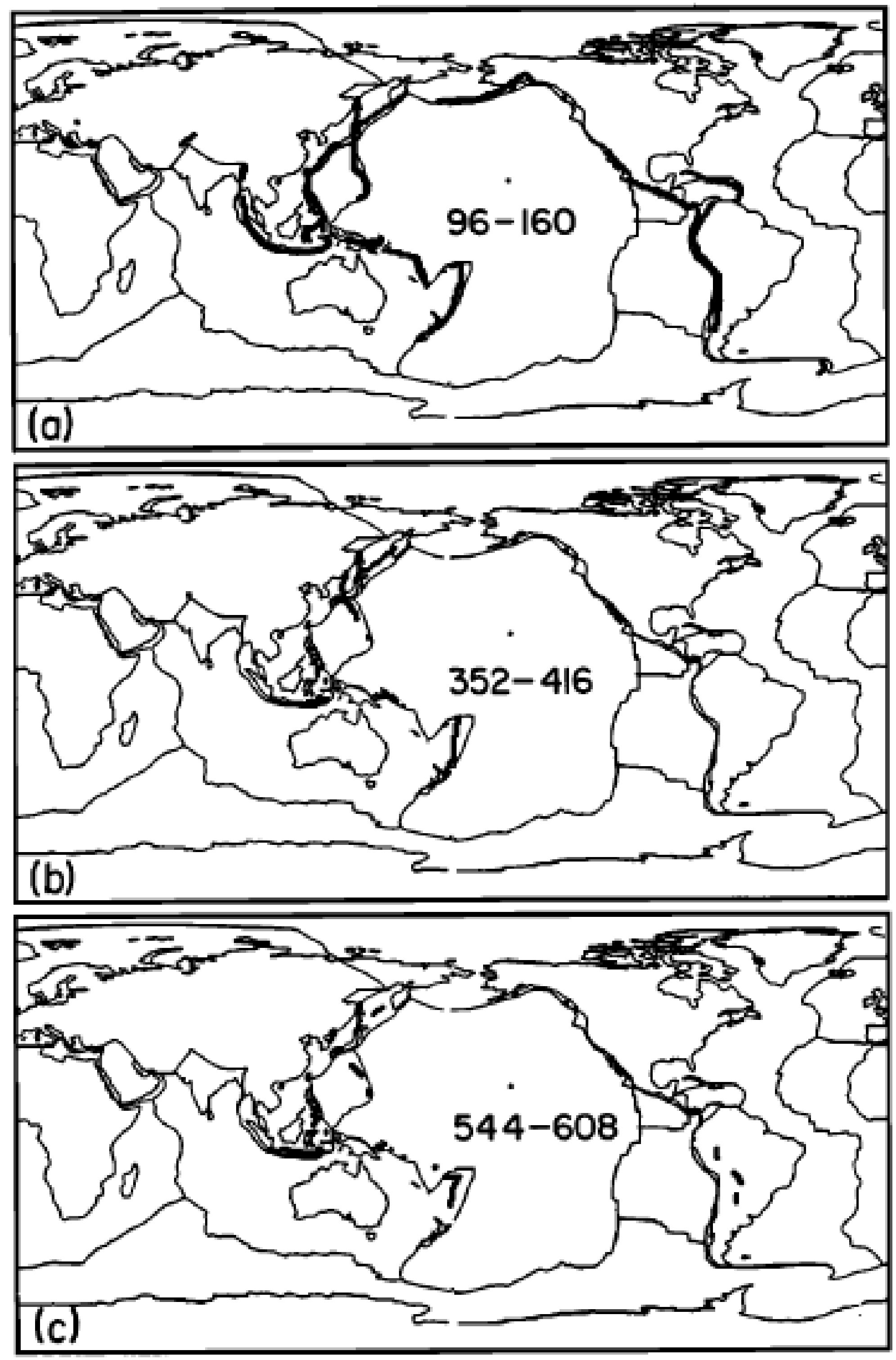

Hager (1984)

Mueller et al. (2016)

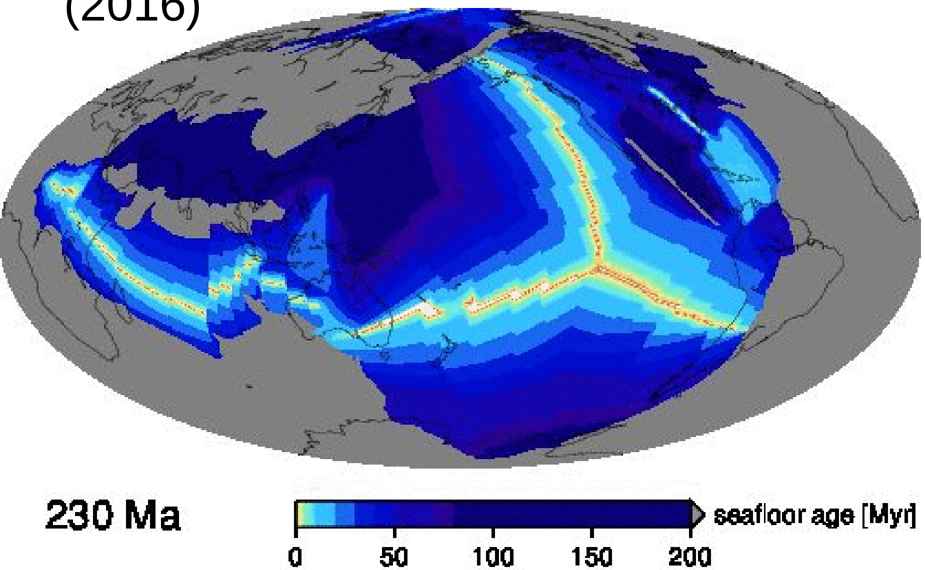

Stokeslets link subduction history to mantle structure

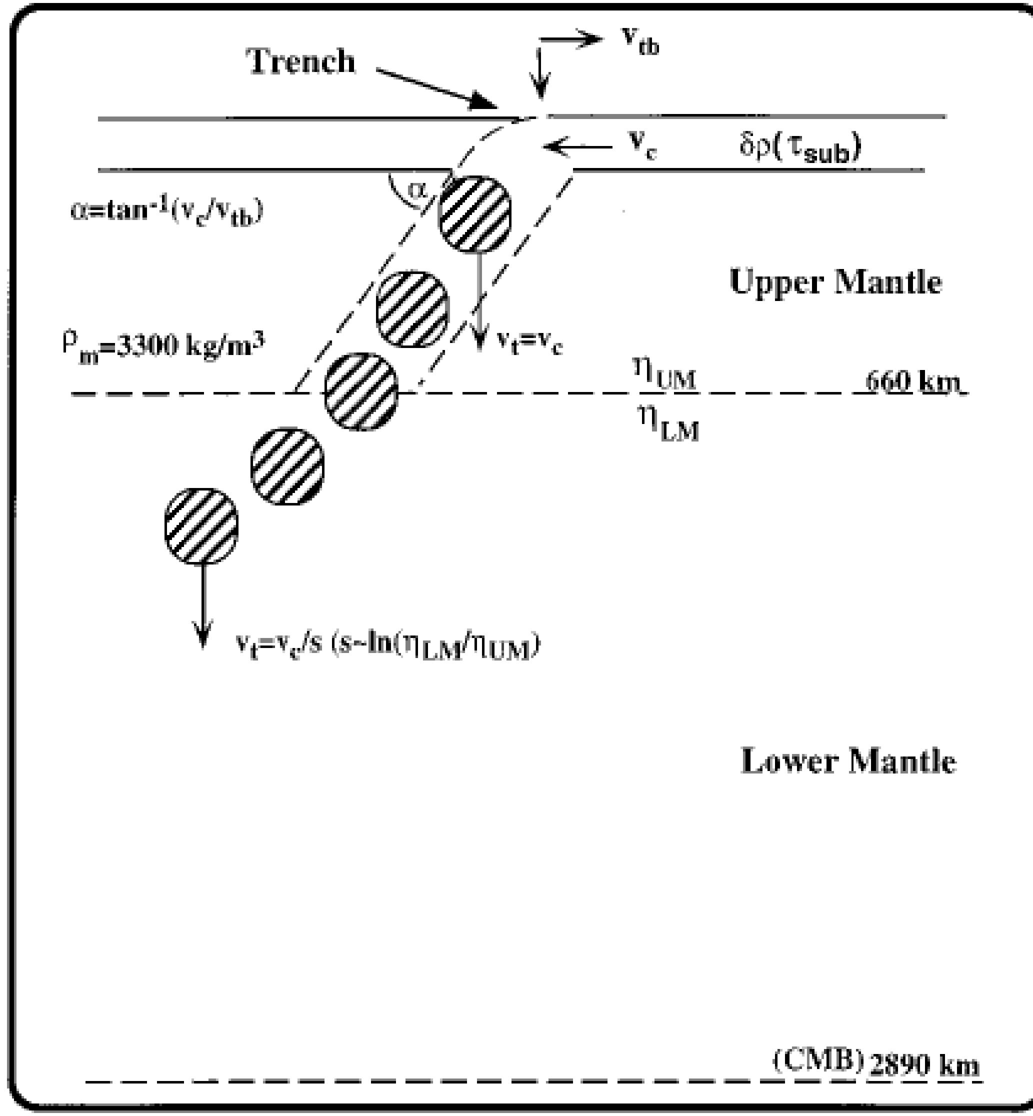

Ricard et al. (1993); Lithgow-Bertelloni et al. (1993, 1998)

Seismic tomography shows slabs in lower mantle

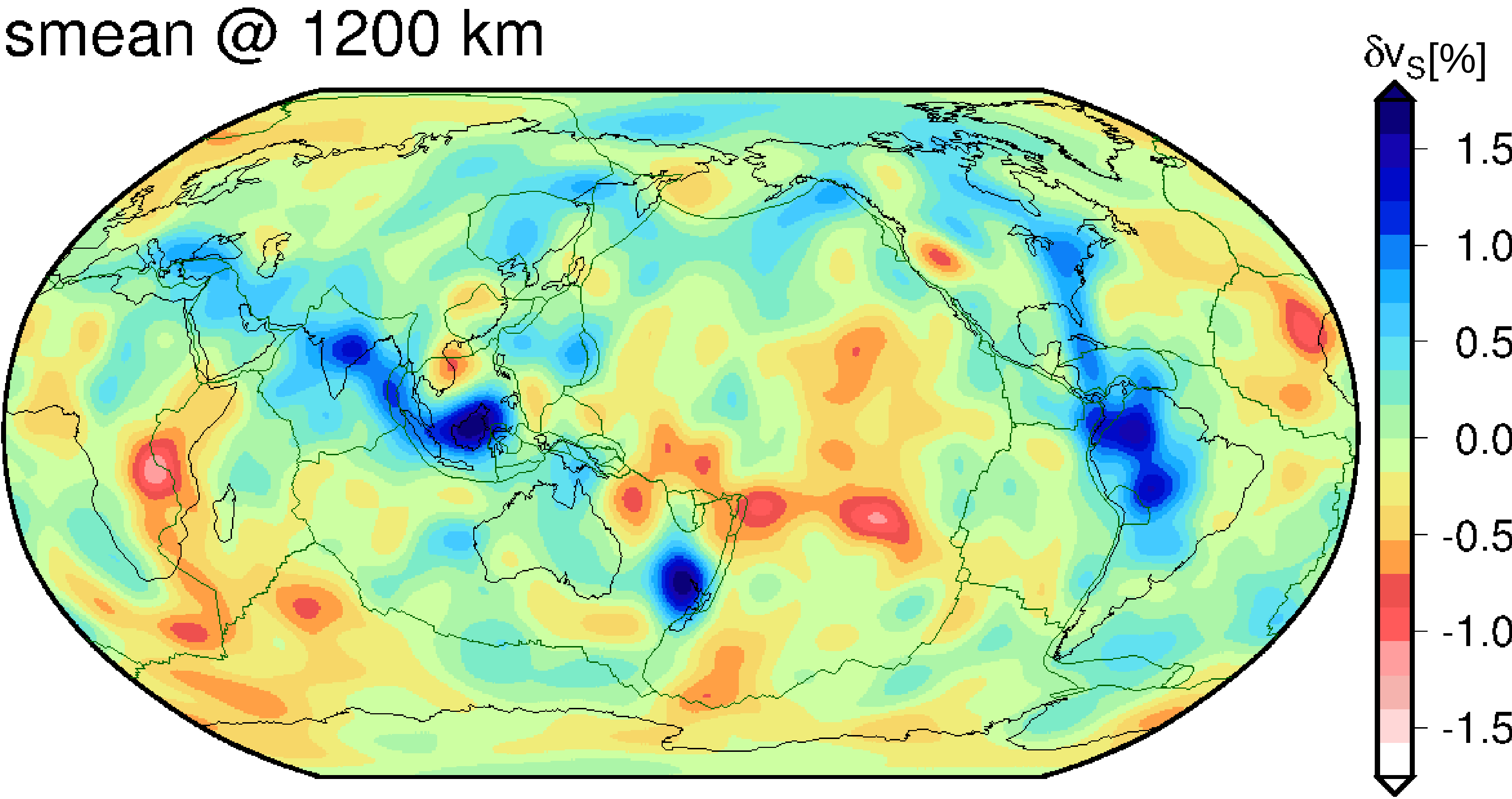

Becker and Boschi (2002)

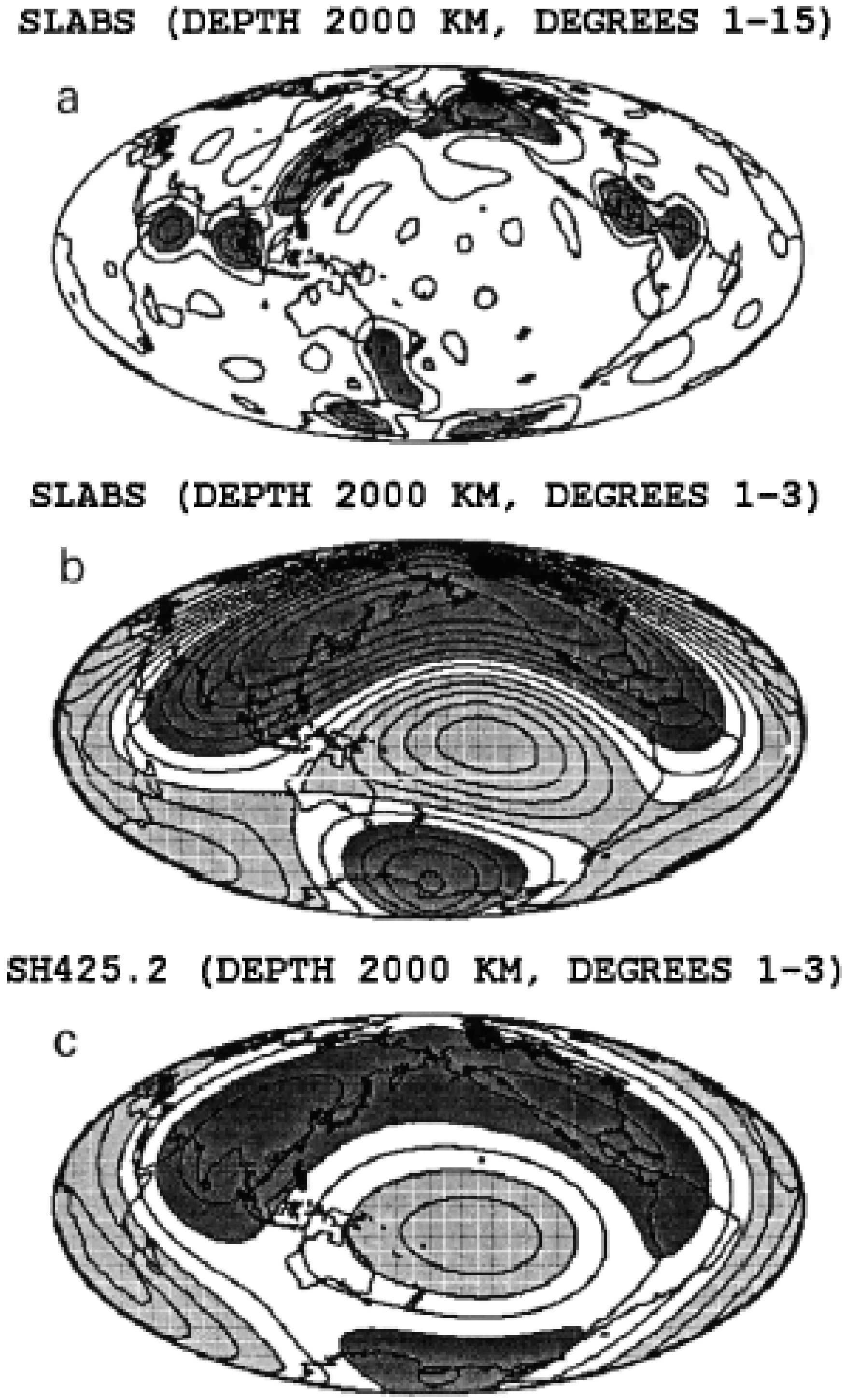

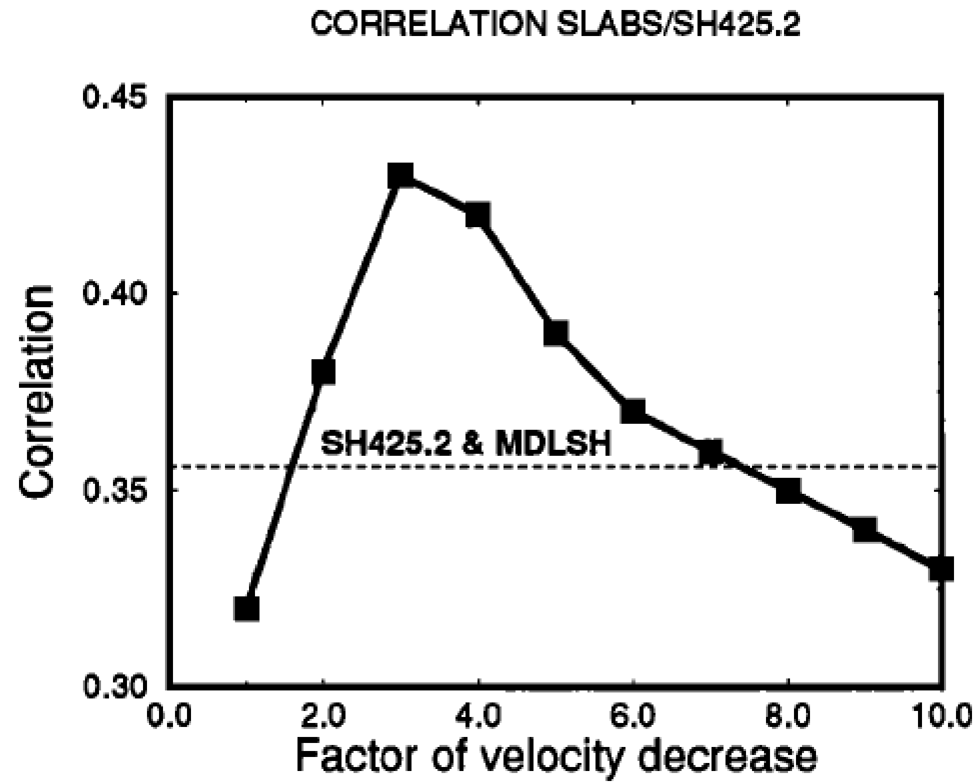

Ricard et al. (1993)

Mantle structure as *f*(*t*) from subduction

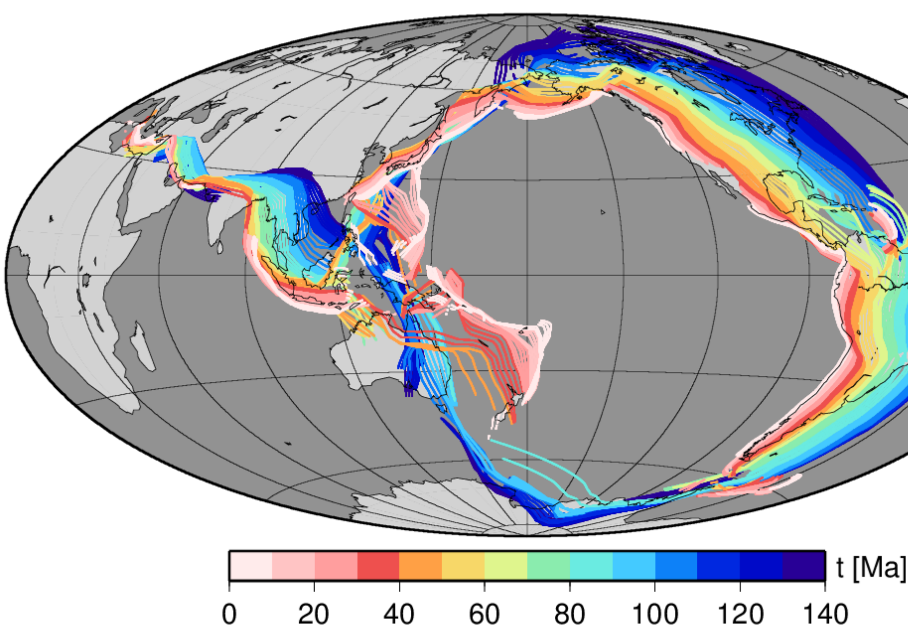

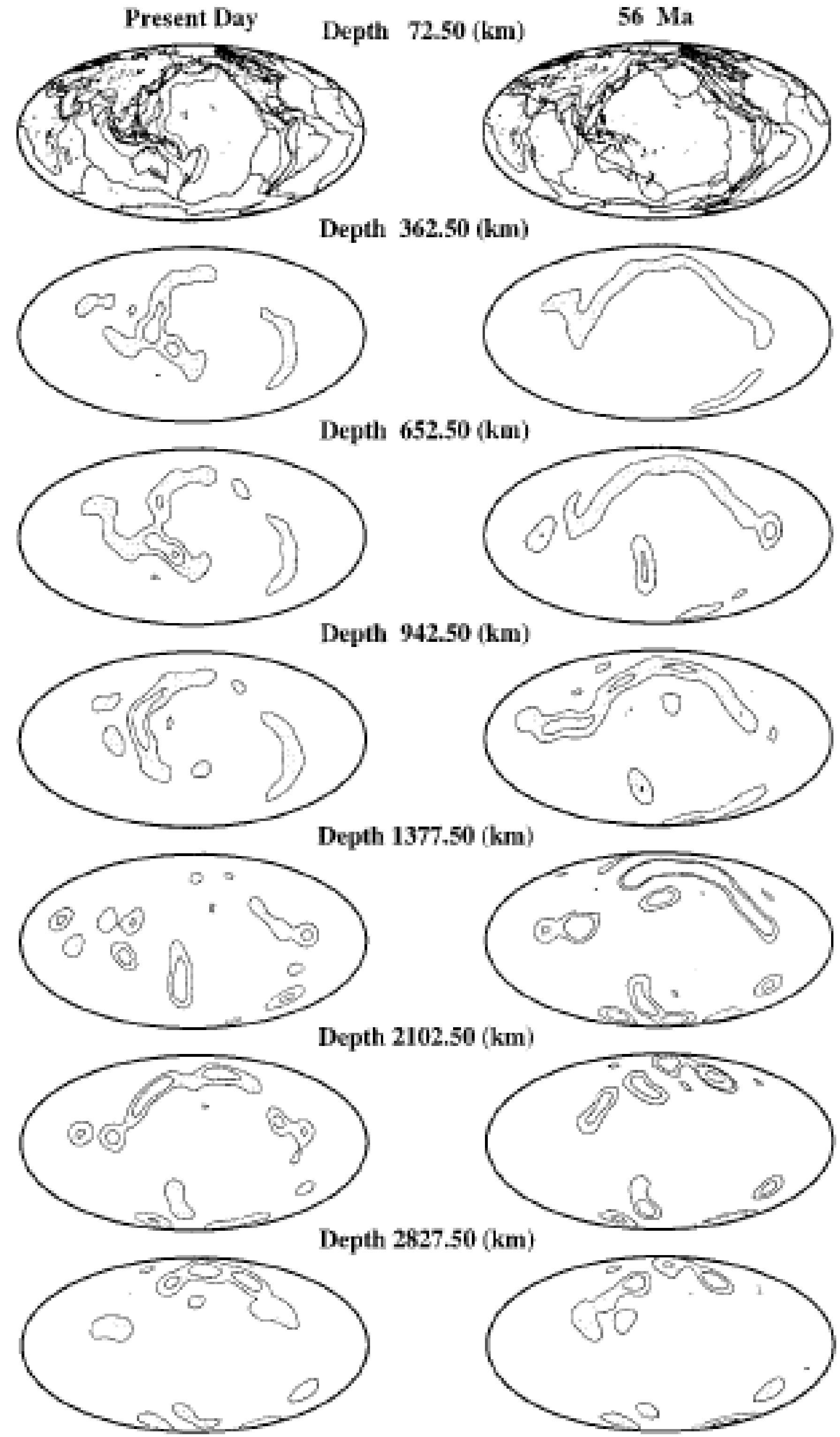

Ricard et al. (1993); Lithgow-Bertelloni & Richards (1998);
Steinberger (2000); Spasojevich et al. (2009); Steinberger and Torsvik (2010)
Steinberger et al. (2014); Bower et al. (2015)

Possible reference frame
(but sinking rates uncertain)

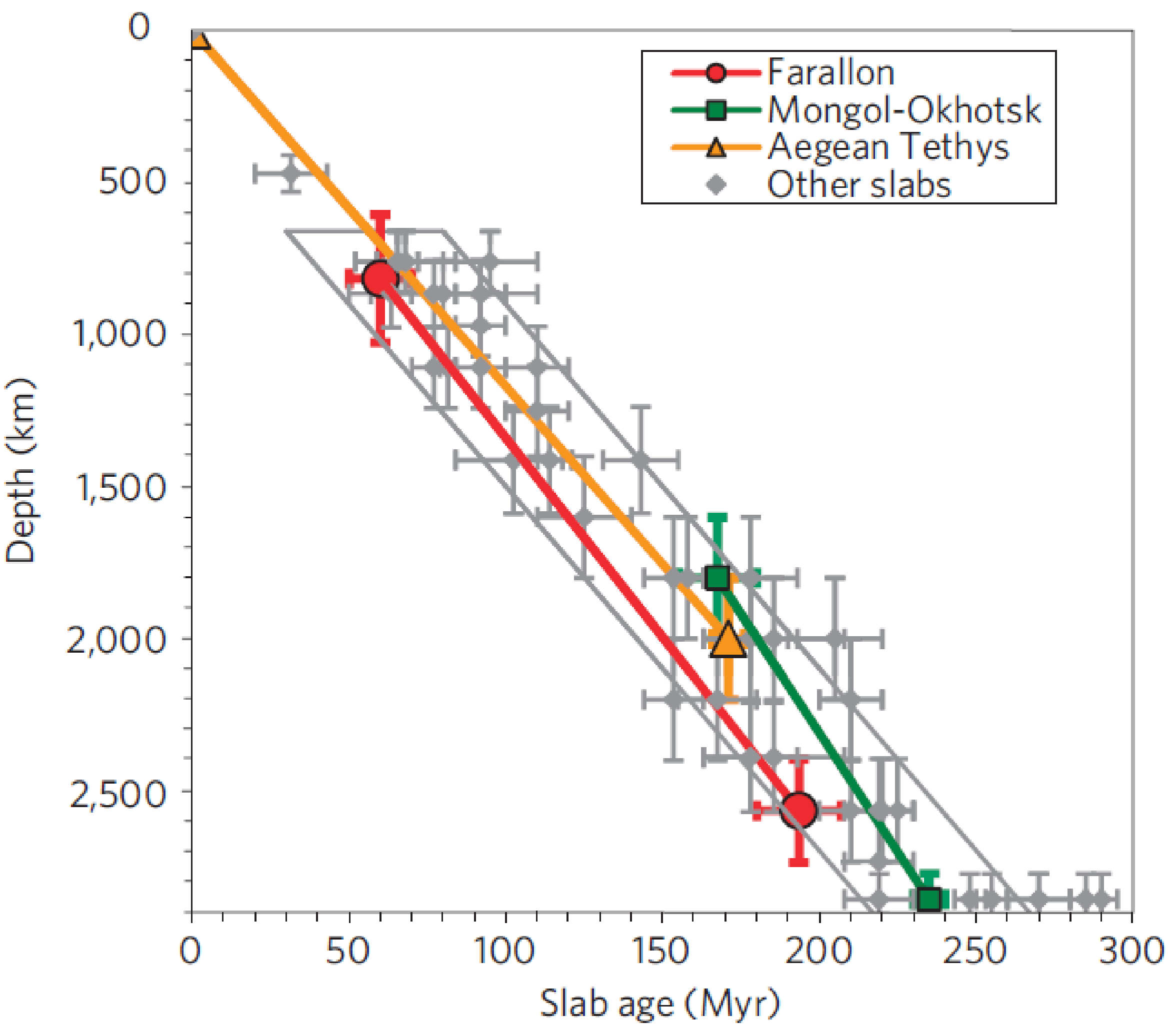

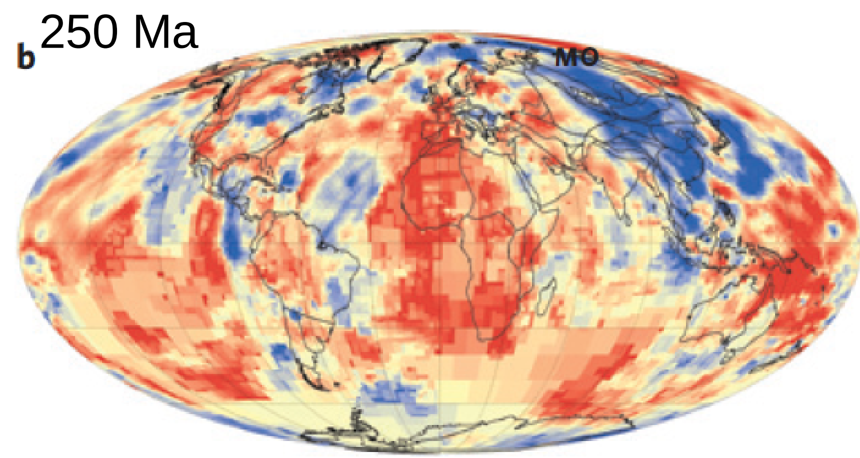

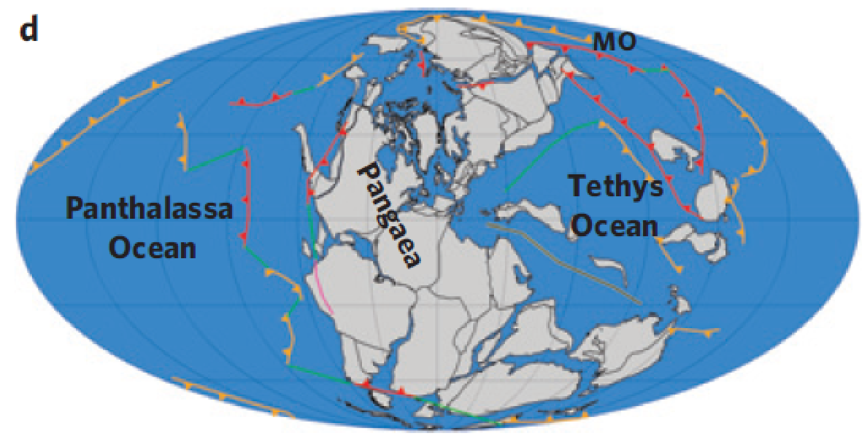

van der Meer et al. (2009)

Correlation: Advected slabs vs. tomography

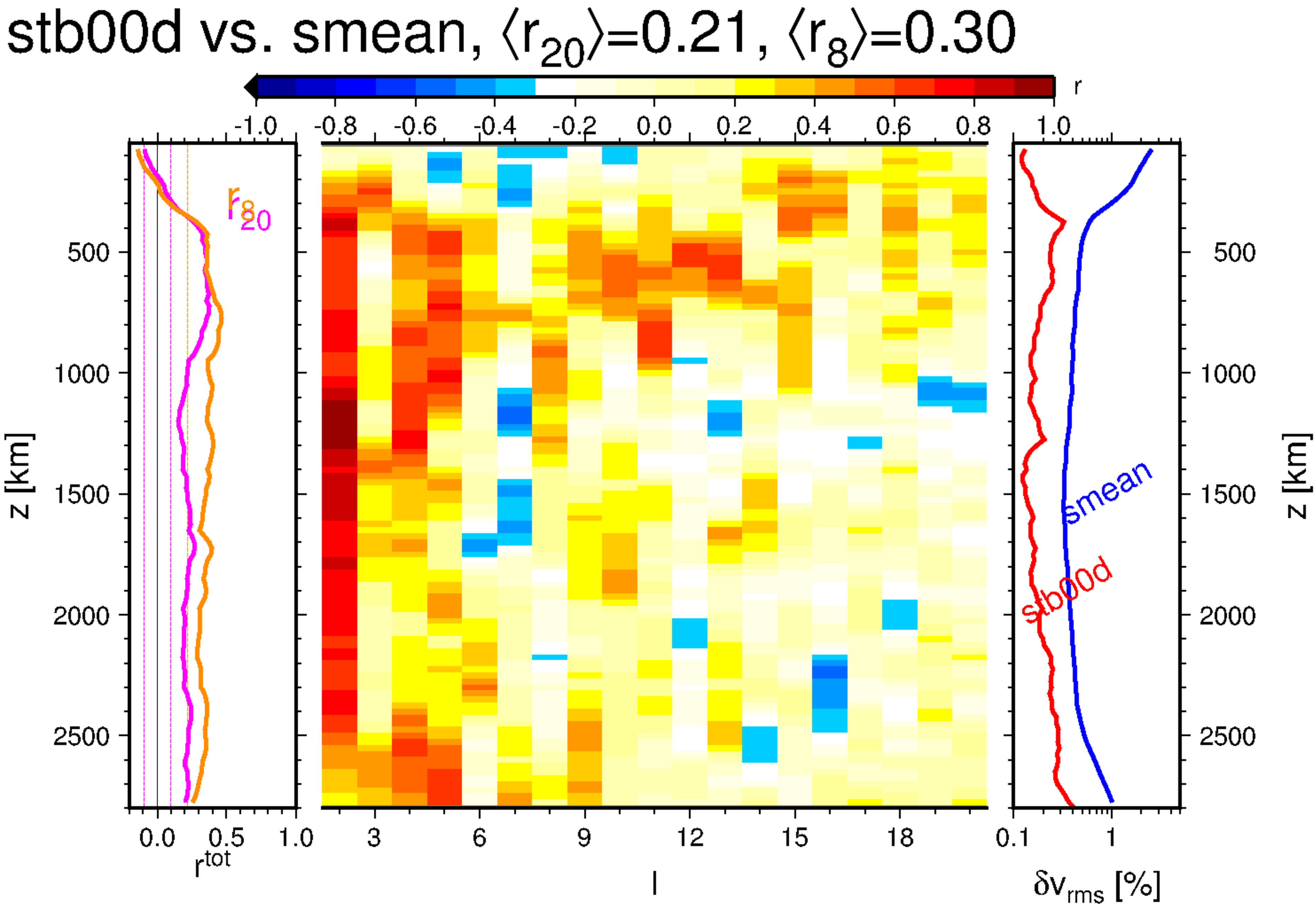

Lithgow-Bertelloni & Richards (1998); Steinberger (2000); Bunge & Grand (2000); Spasojevic & Gurnis (2009)

Becker & Boschi (2002)

Advected plumes vs. tomography

(Steinberger flow model conduits)

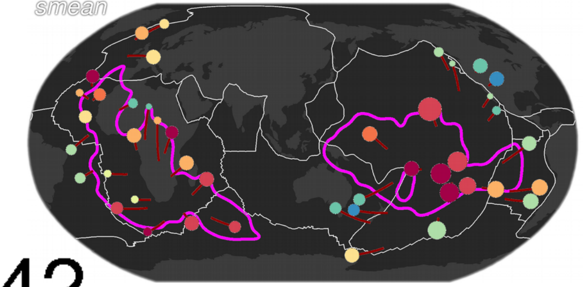

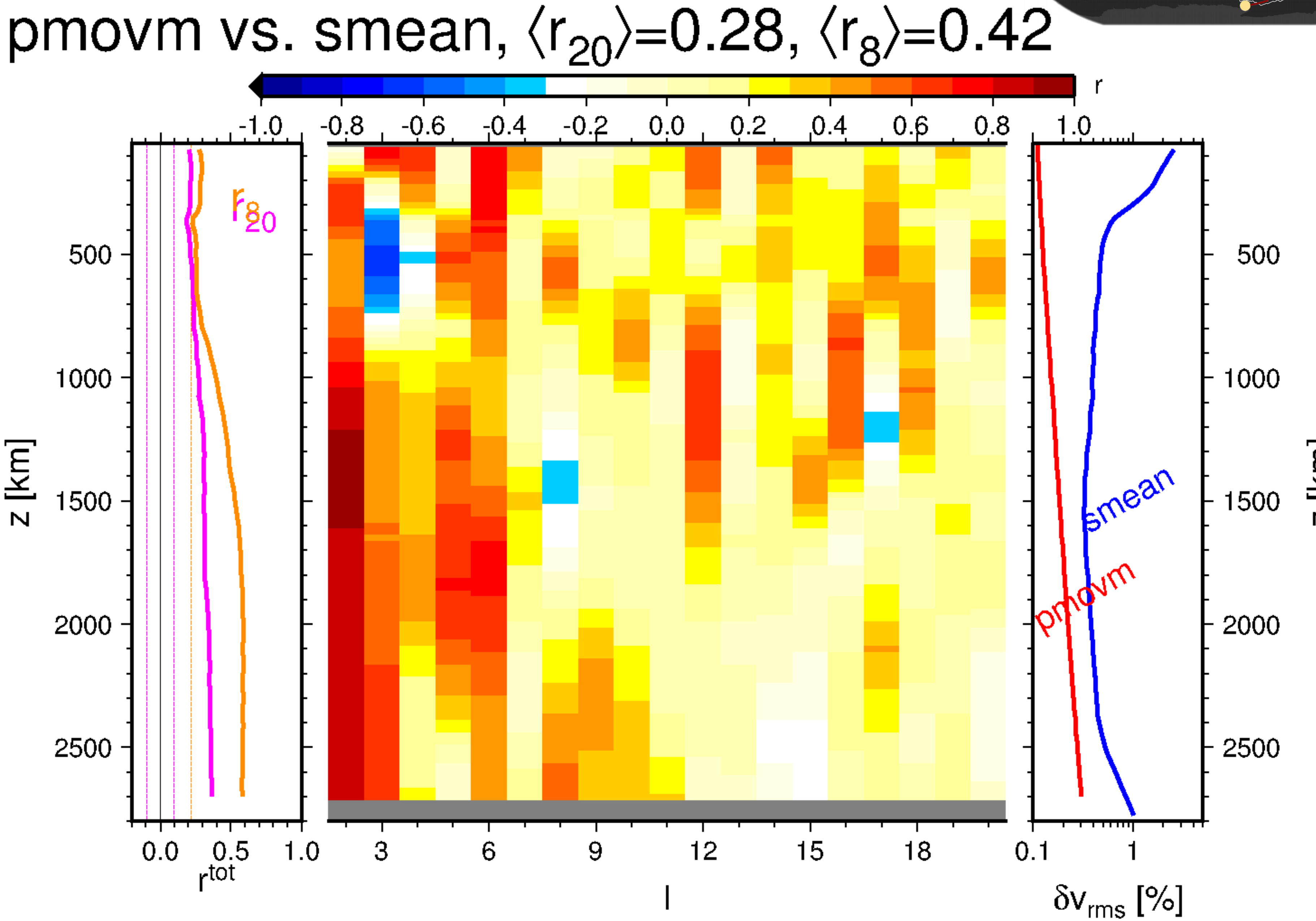

Note: Correlation with *moving* plumes **better** than with slabs

Boschi et al. (2007, 2008)

Advected plumes vs. tomography

(Steinberger flow model conduits)

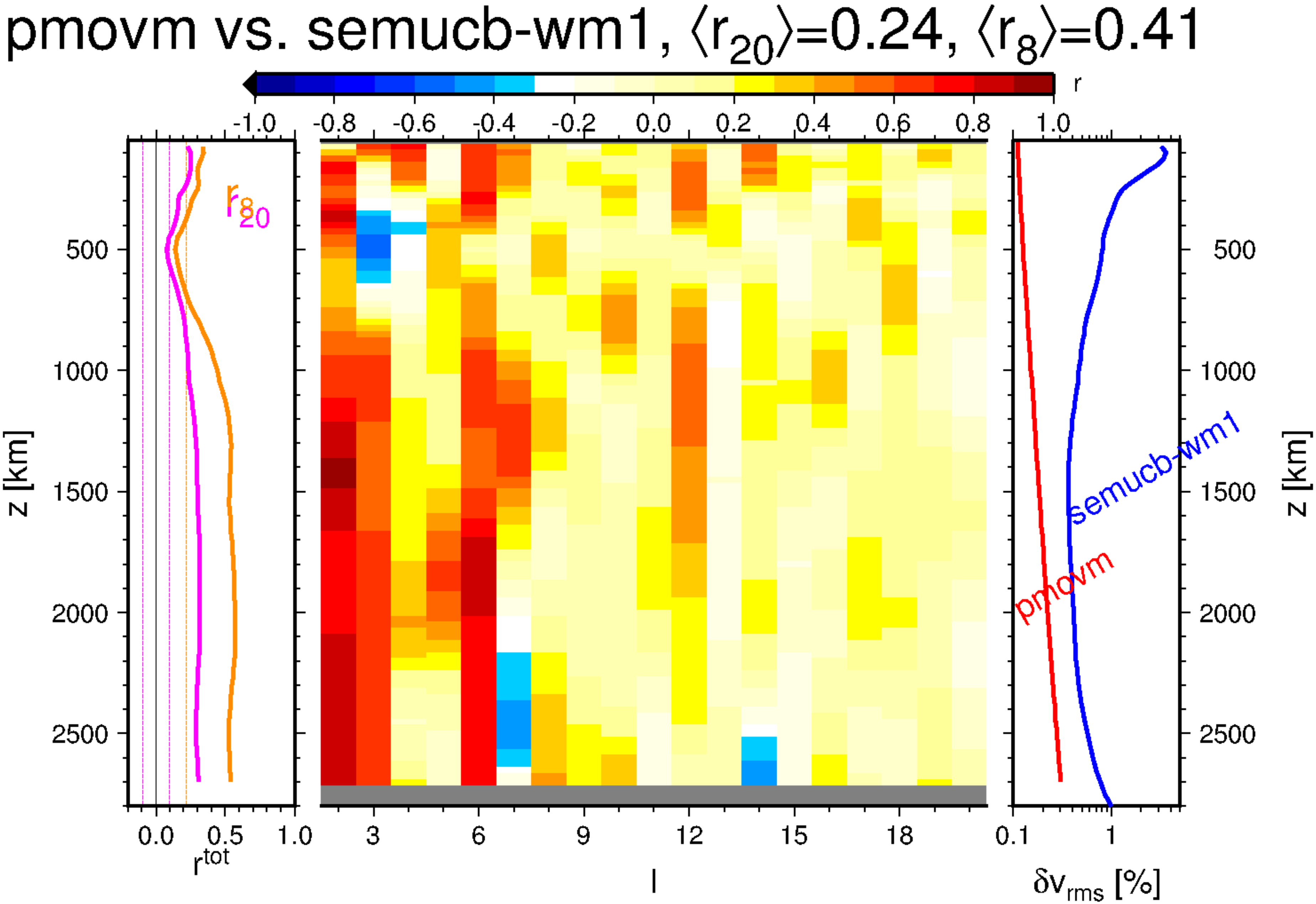

Boschi et al. (2007, 2008)

Building a model of Earth from slabs and plumes

Input: Slabs and plumes

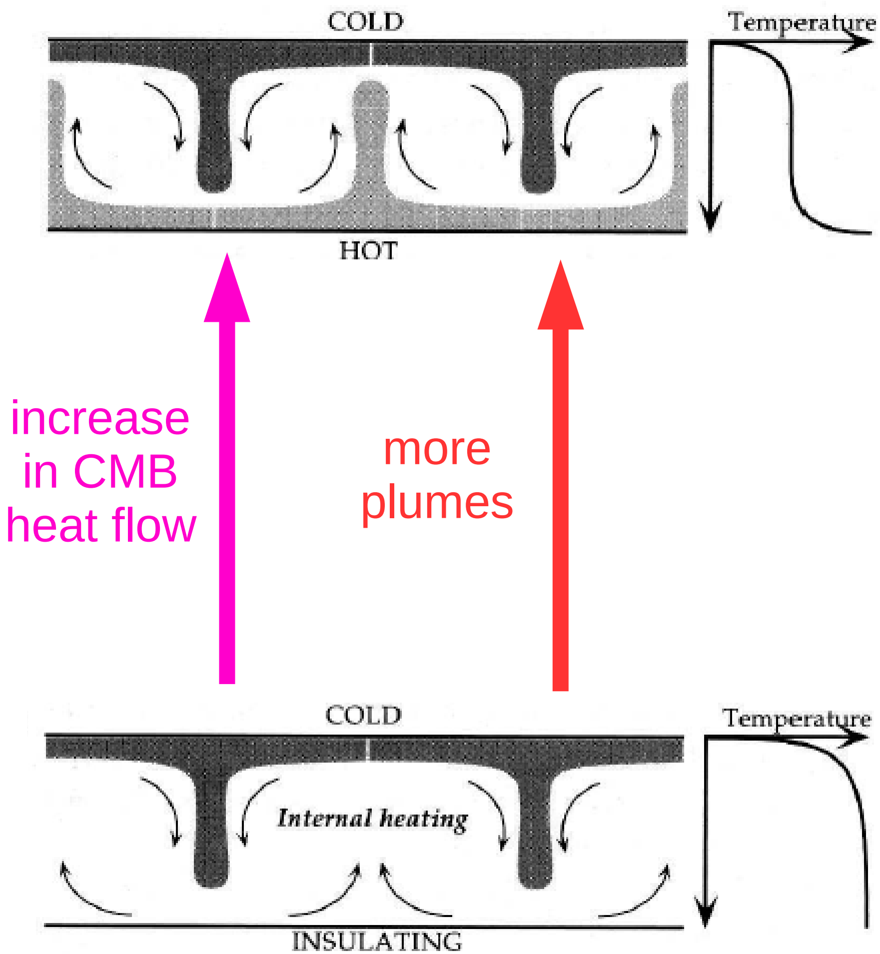

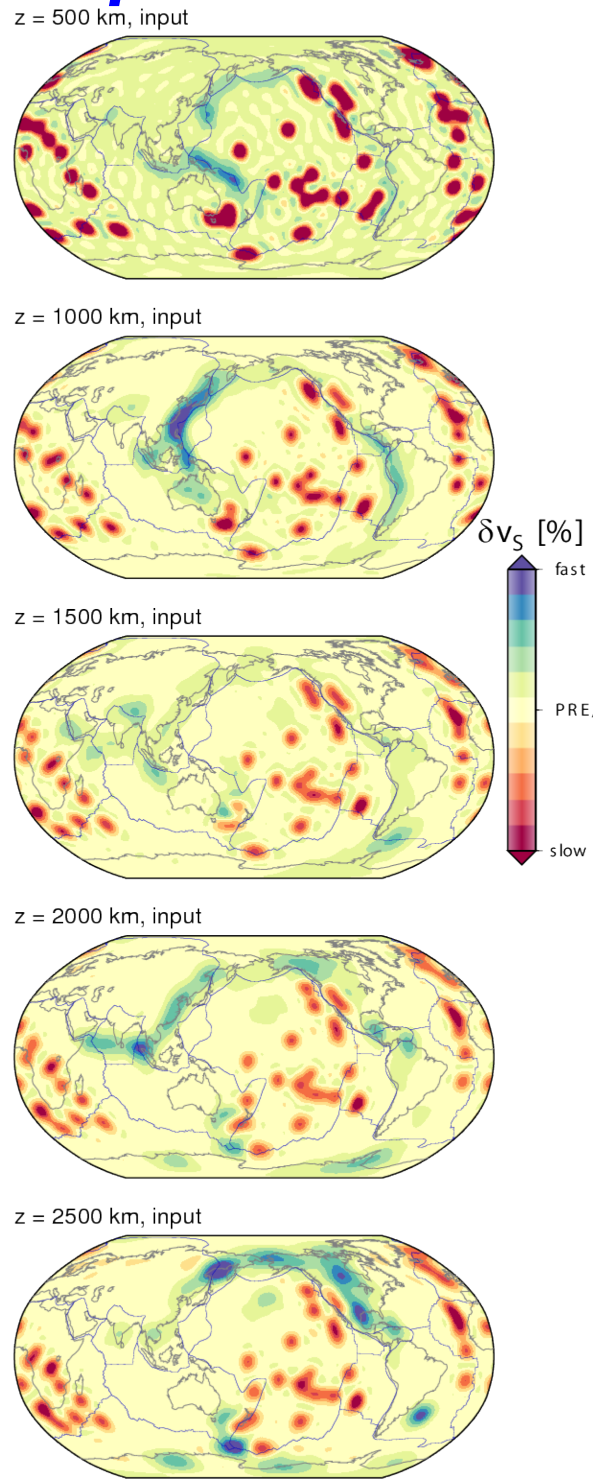

Resolving power of tomography

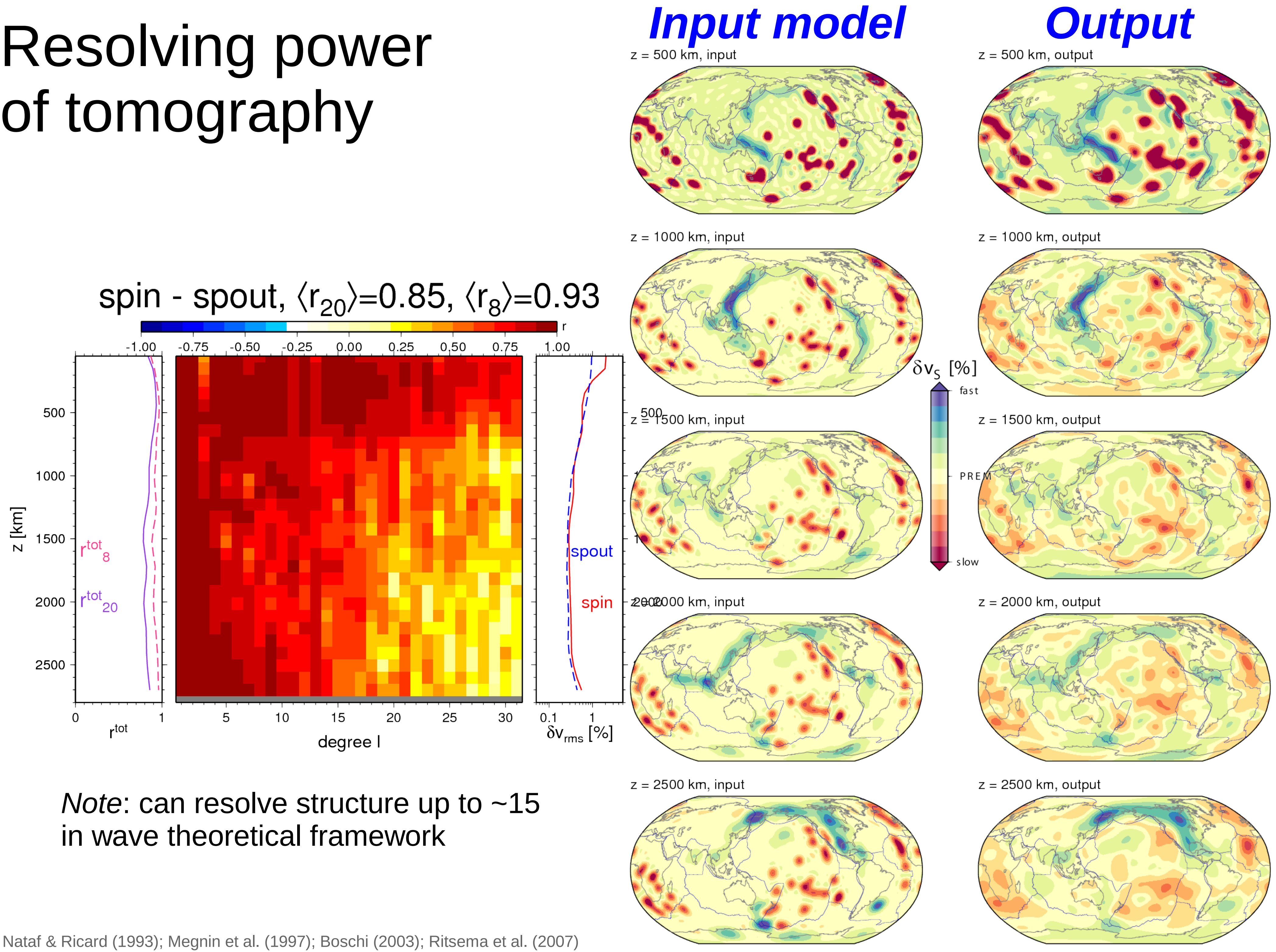

Note: can resolve structure up to ~15 in wave theoretical framework

Nataf & Ricard (1993); Megnin et al. (1997); Boschi (2003); Ritsema et al. (2007)

Inter tomography-model correlation

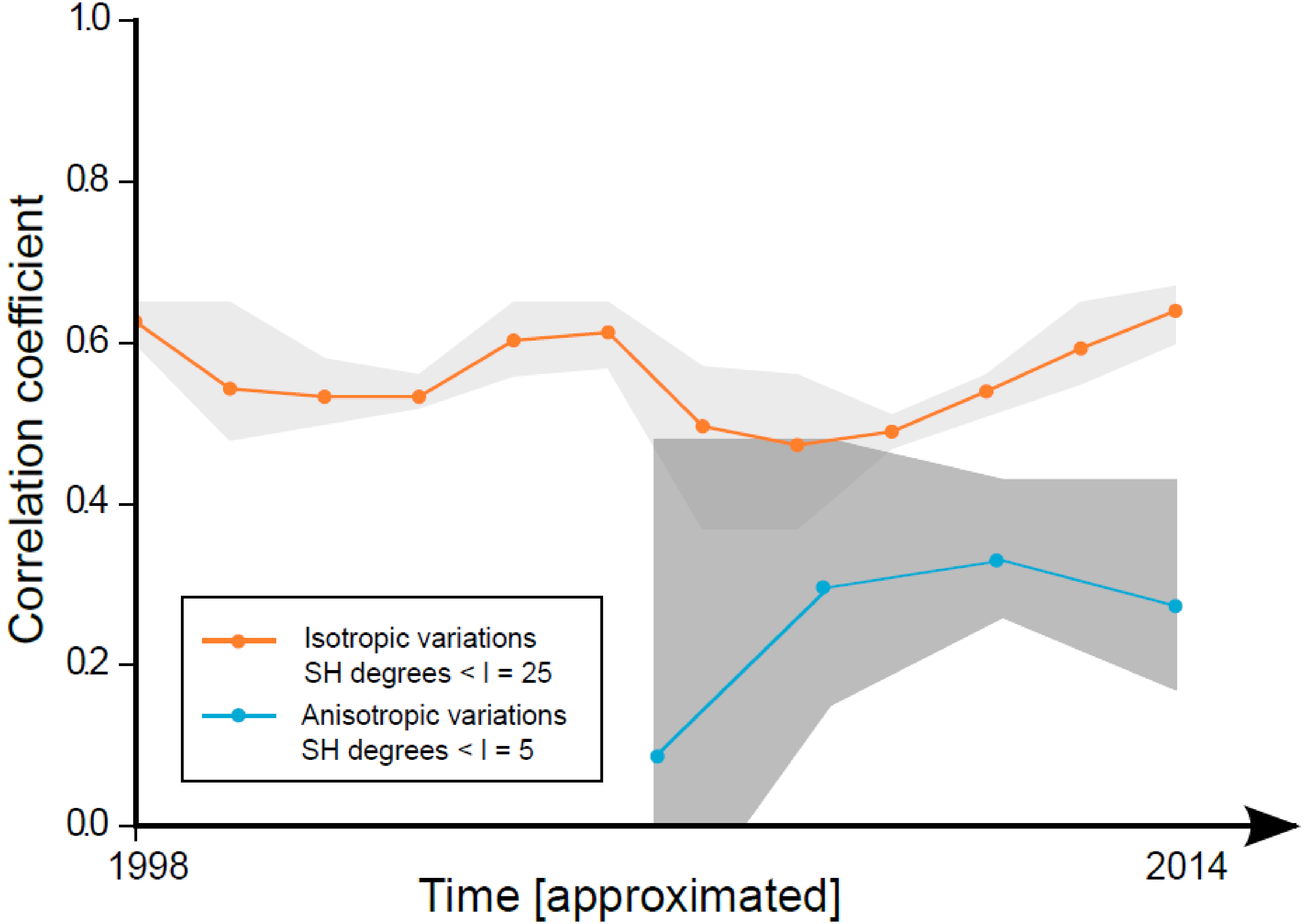

Note: data *and* theory matter

Auer (2016)

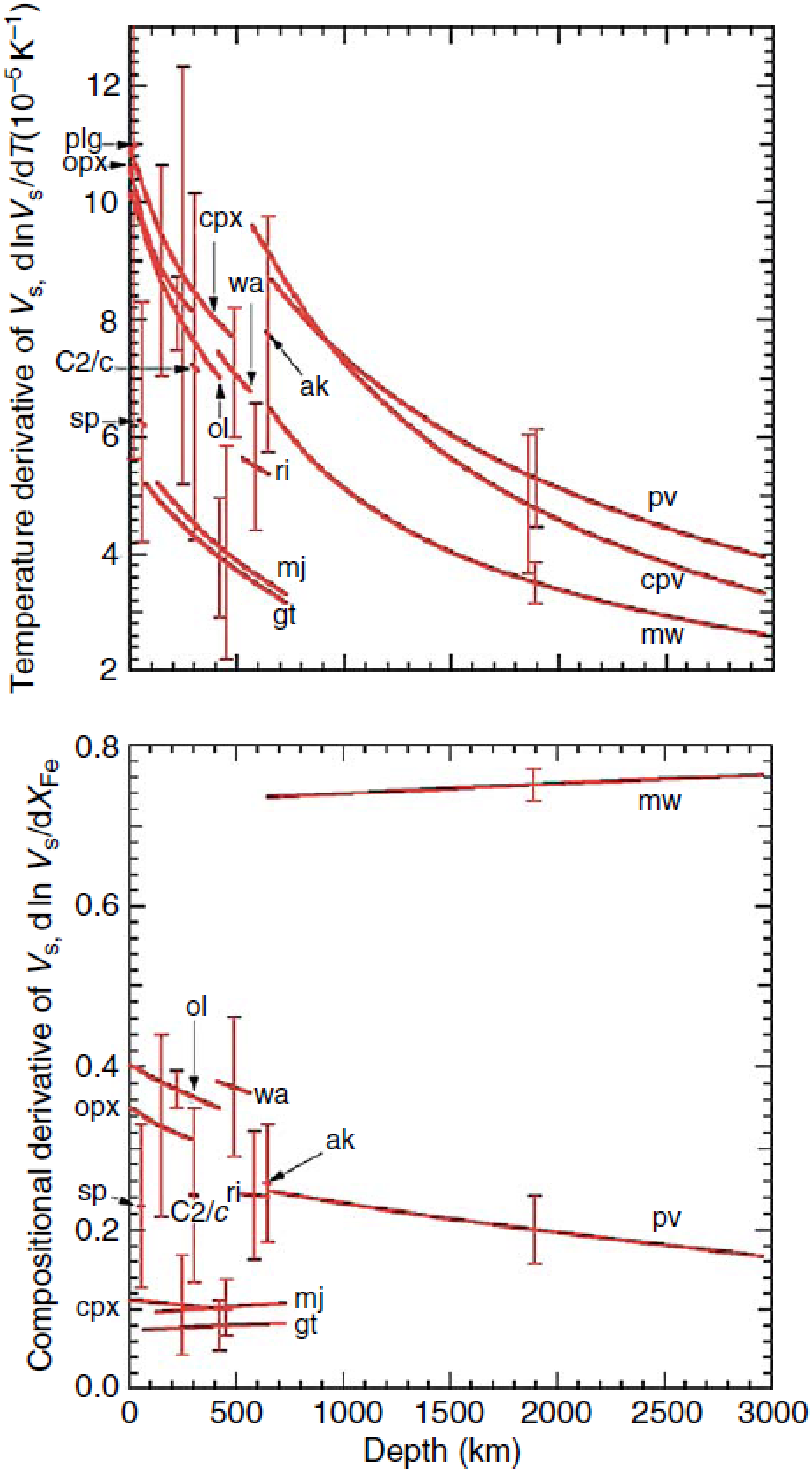

How to convert tomography to density anomalies?

I. Take it from mineral physics and

composition from…


Stixrude and Jeanloz (2009)

II. Best-fit scaling and composition as inverse problems

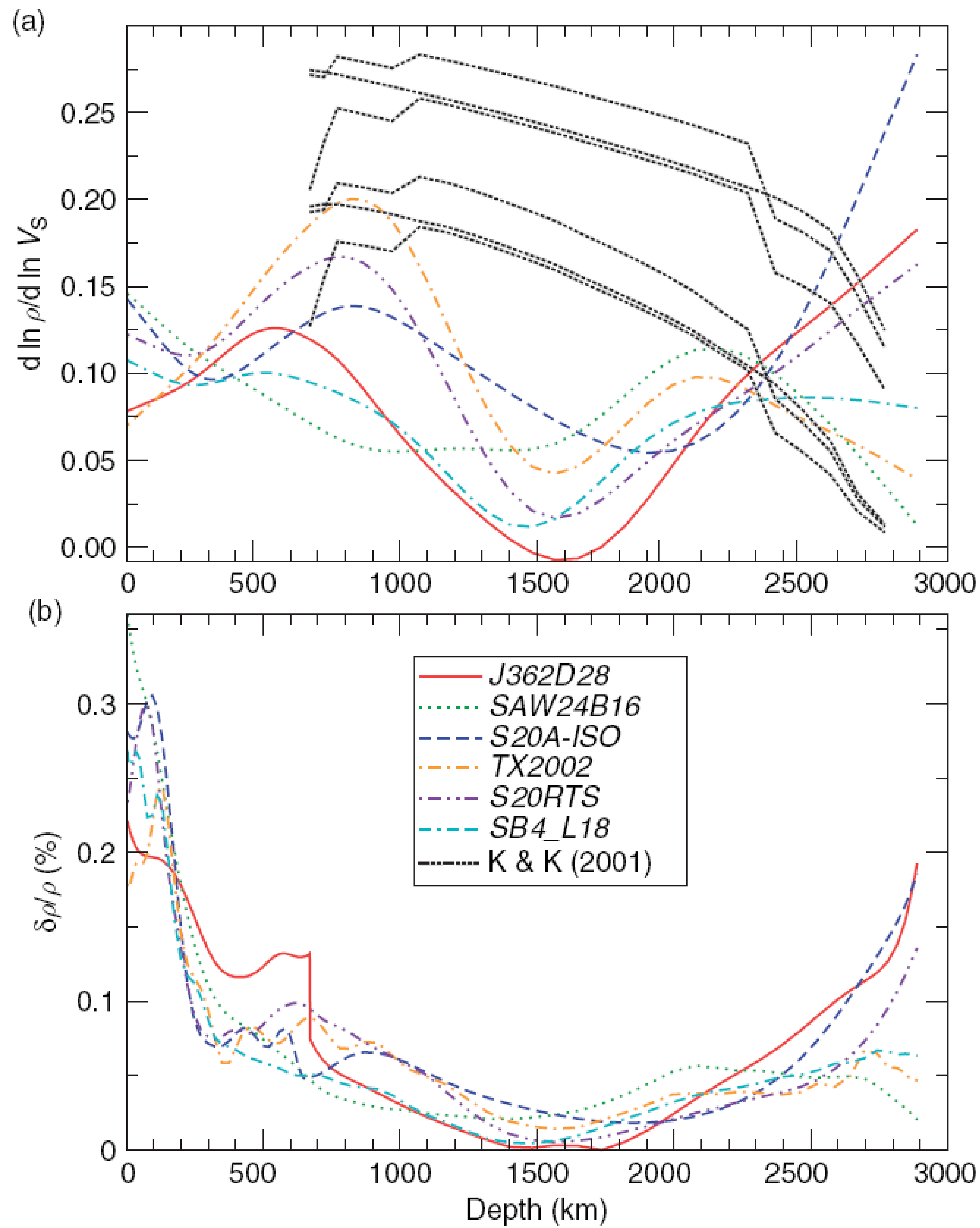

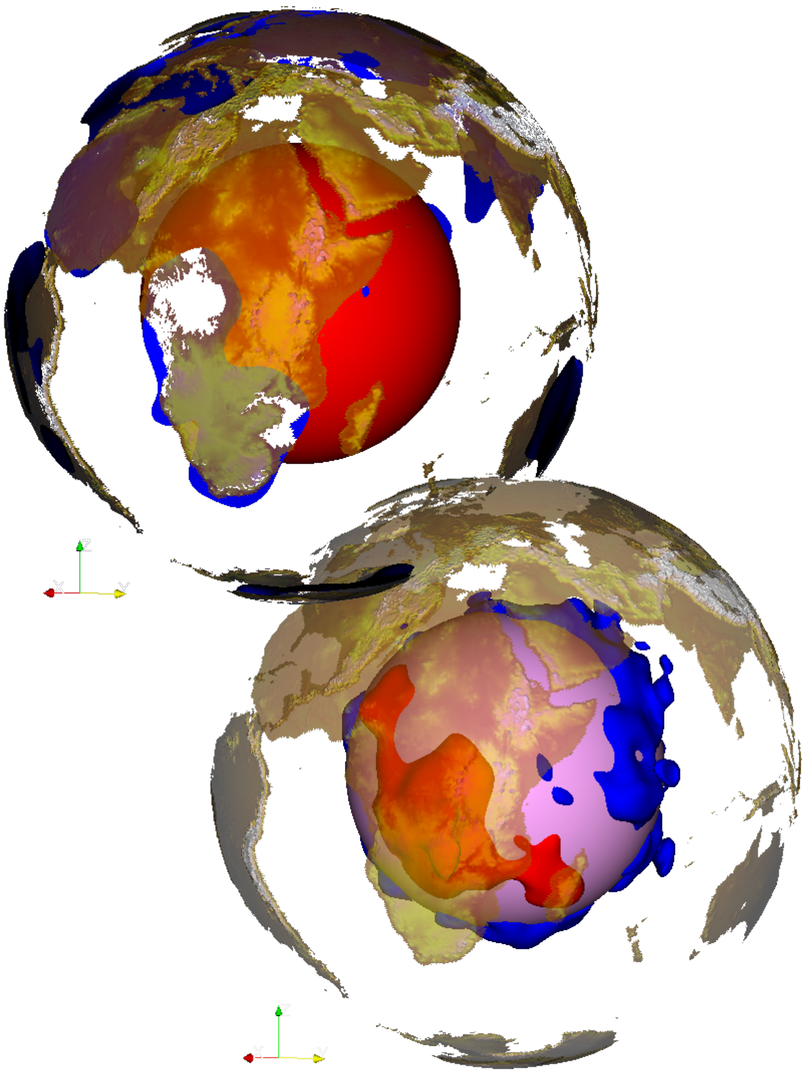

cf. Simmons et al. (2008, 2010),
Soldati et al. (2014), Forte et al. (2015)

Besides cratons and piles: dln ρ/d ln v_s = 0.2

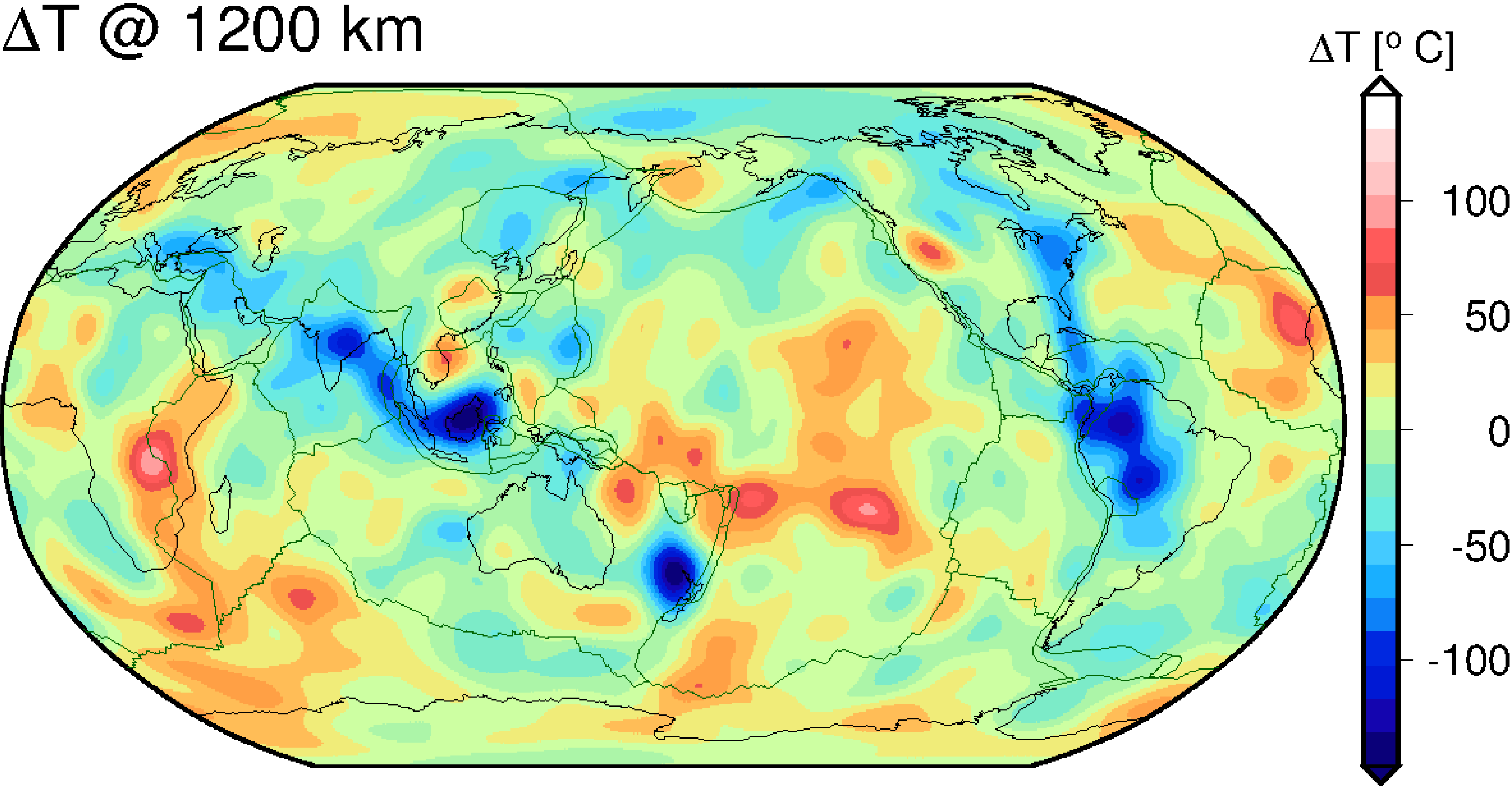

- Use mineral physics to convert velocity into temperature (density) anomalies

How to compute flow?

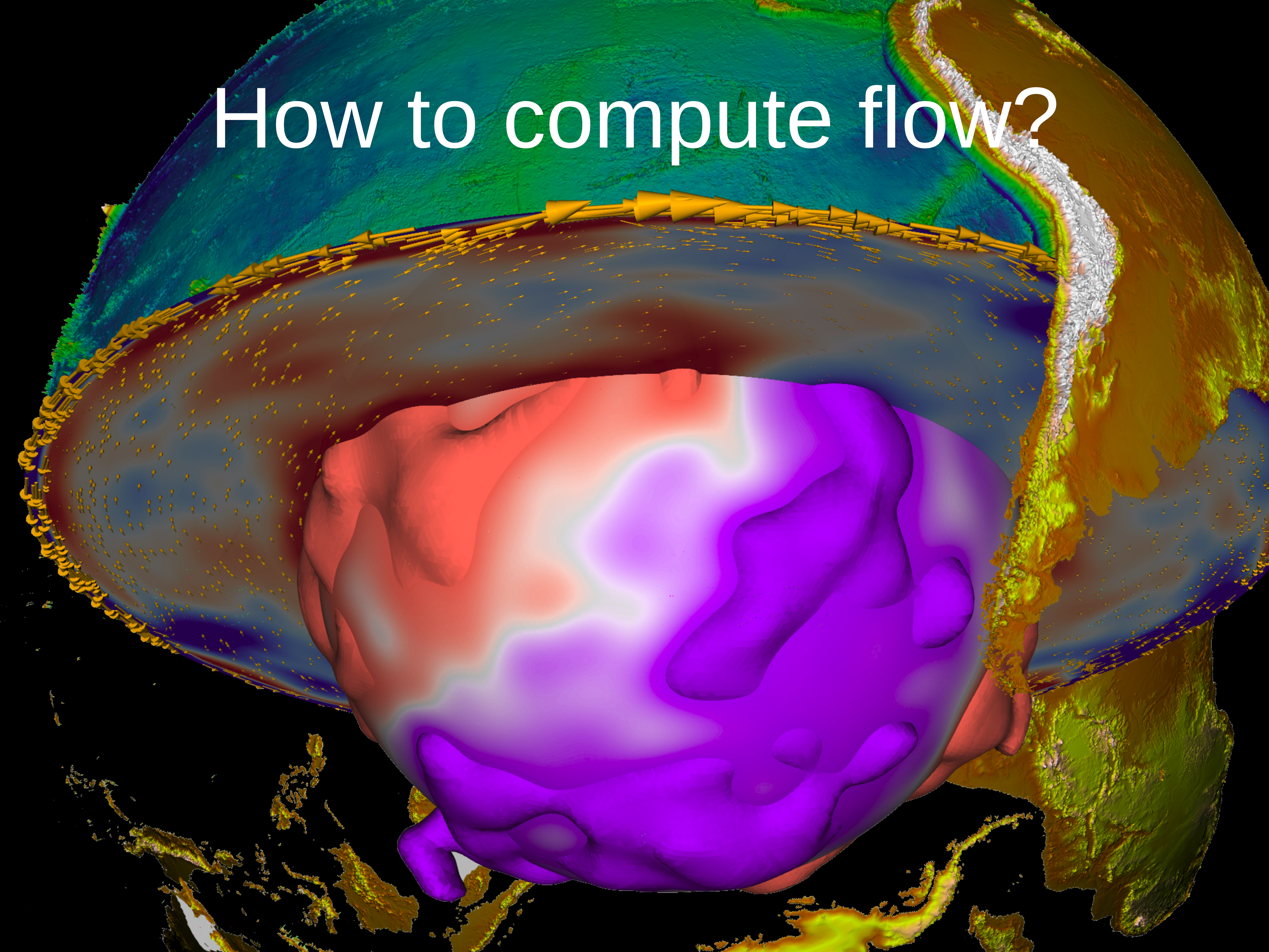

Mantle circulation

- Treat mantle and lithosphere as a fluid
- Infinite Prandtl number (no inertia) approximation
    - Navier-Stokes turns into Stokes equation
- Instantaneous solution for given density and boundary conditions
    - Can solve in <~1 s for spherical Earth without lateral viscosity variations (LVVs)

force balance
(conservation of momentum)

$$\frac{\partial \sigma_{ij}}{\partial x_j} = - Ra \, \Delta T \, \delta_{ir}$$

viscous drag

thermal buoyancy

constitutive equation
(rheology)

$$\sigma_{ij} = -P\delta_{ij} + 2\eta\left(\frac{\partial u_i}{\partial x_j} + \frac{\partial u_j}{\partial x_i}\right)$$

stress tensor

dynamic pressure

Newtonian viscosity

strain-rate

e.g. Hager & O'Connell (1981), Ricard & Vigny (1989)

$$\Delta T$$

$$v \propto \frac{Ra\,\Delta T}{\eta} = \frac{\Delta\rho}{\eta}$$

Stokes sphere

$$V_{\mathrm{Stokes}} = C\,\frac{\Delta\rho g a^2}{\eta_m}$$

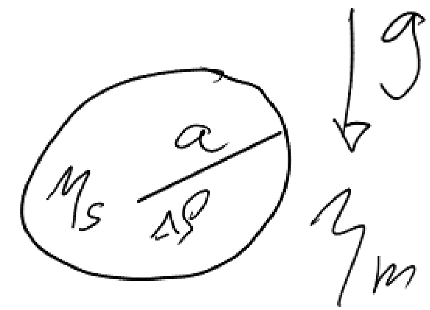

$$C = \frac{2+2\eta'}{6+9\eta'} \quad \text{where} \quad \eta' = \frac{\eta_s}{\eta_m}$$

Asides:

- A needle, as opposed to sphere, will sink with 0.5...2 v_{Stokes}
- Pe # = ratio of diffusive to convective time scale = t_d / t_c

  $t_c = a^2 / \kappa$, $t_c = a / v_{\mathrm{Stokes}}$, $\Delta\rho = \Delta T \alpha \rho_0$, then Pe → Ra (with a instead of L)

Mantle circulation

- Thermo-chemical heterogeneity and complex rheologies make things interesting
- Finite element methods best suited for lateral viscosity variations (we can now solve all of this, at < km resolution without approximations)

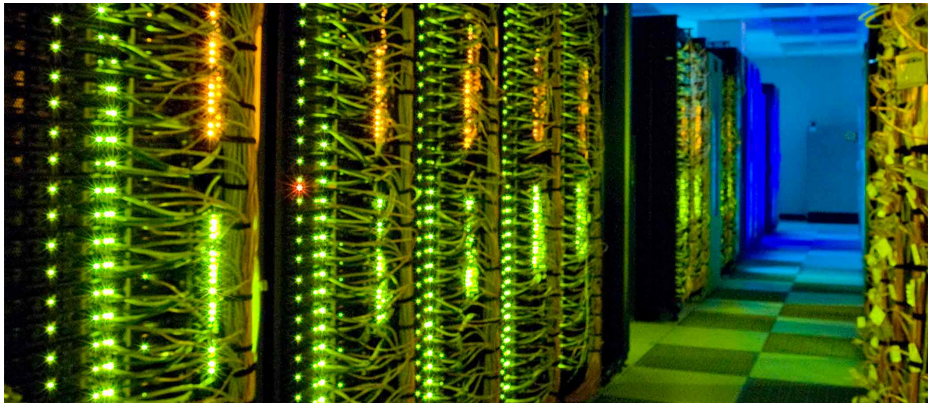

force balance
(conservation of momentum)

$$\frac{\partial \sigma_{ij}}{\partial x_j} = - Ra\,\Delta T\,\delta_{ir} - Ra_C\,\Delta C\,\delta_{ir}$$

chemical buoyancy

constitutive law
(rheology)

$$\sigma_{ij} = -P\delta_{ij} + 2\eta(\sigma, T, d, H_2O, \varepsilon)\varepsilon_{ij}$$

non-Newtonian viscosity with memory

Mantle convection

- Energy equation introduces time-dependence
- Coupling between velocity and temperature introduces non-linearity
    - Can time reverse advection, but not diffusion

force balance
(conservation of momentum)

$$\frac{\partial \sigma_{ij}}{\partial x_j} = - Ra\,\Delta T \delta_{ir} - Ra_C\,\Delta C \delta_{ir}$$

constitutive law
(rheology)

$$\sigma_{ij} = -P\delta_{ij} + 2\eta(\sigma, T, d, H_2O, \varepsilon)\dot{\varepsilon}_{ij}$$

conservation of energy

$$\frac{\partial T}{\partial t} = \underbrace{-u_i \frac{\partial T}{\partial x_i}}_{\text{advection}} + \underbrace{\kappa \frac{\partial^2 T}{\partial x^2}}_{\text{diffusion}} + \underbrace{H}_{\text{heat production}}$$

Global circulation models

show that plate-motion induced shear cannot always be guessed from surface motions

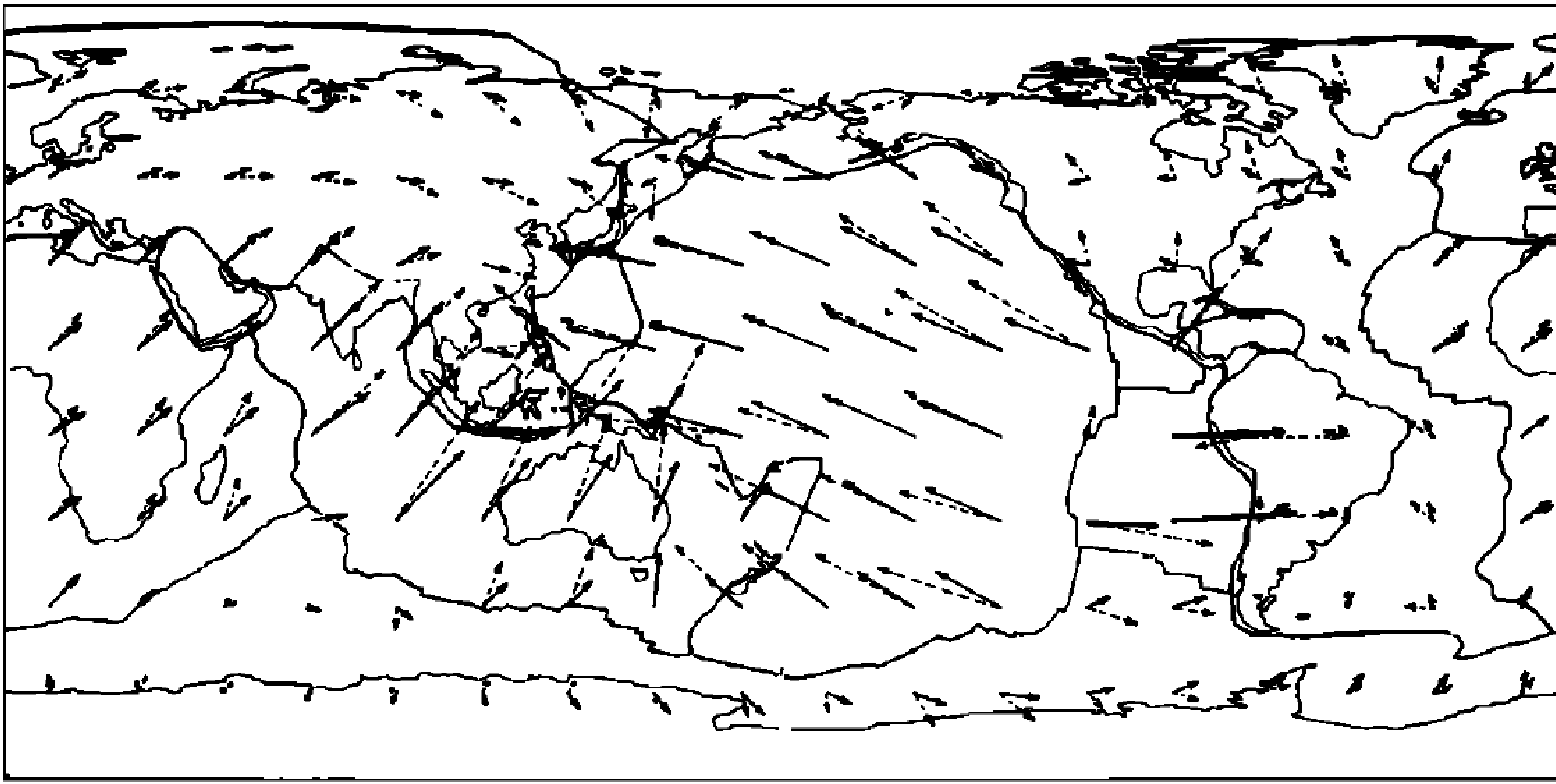

SHEAR STRESS AT BASE OF LITHOSPHERE

Simple Drag

Flow Model

Hager & O'Connell (1979)

Let's fit the geoid: Static effect of slablet

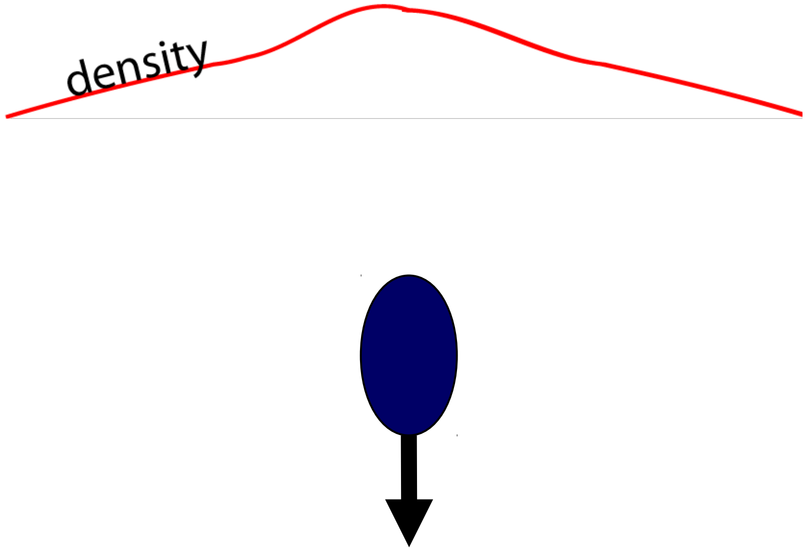

sketch from M. Billen's MYRES talk
cf. Hager & Richards (1984); Ricard (1984)

Combined static and dynamic geoid effect of slablet

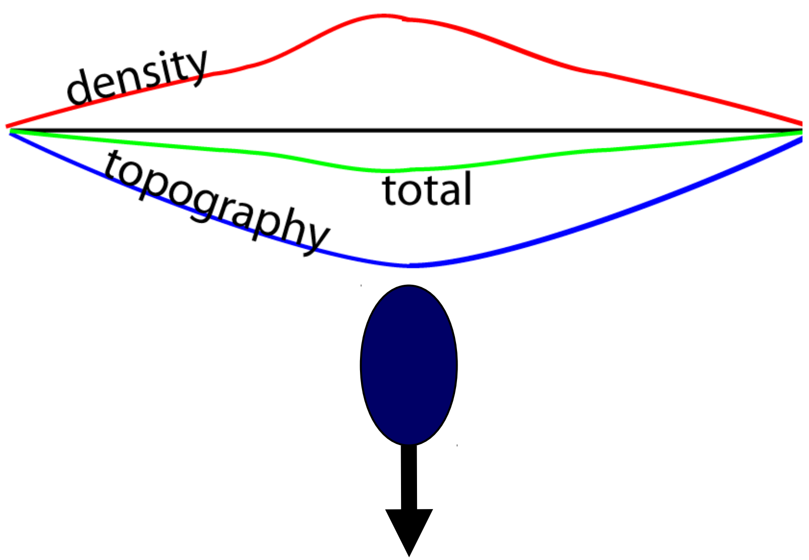

sketch from M. Billen's MYRES talk
cf. Hager & Richards (1984); Ricard (1984)

Kernels for homogeneous mantle

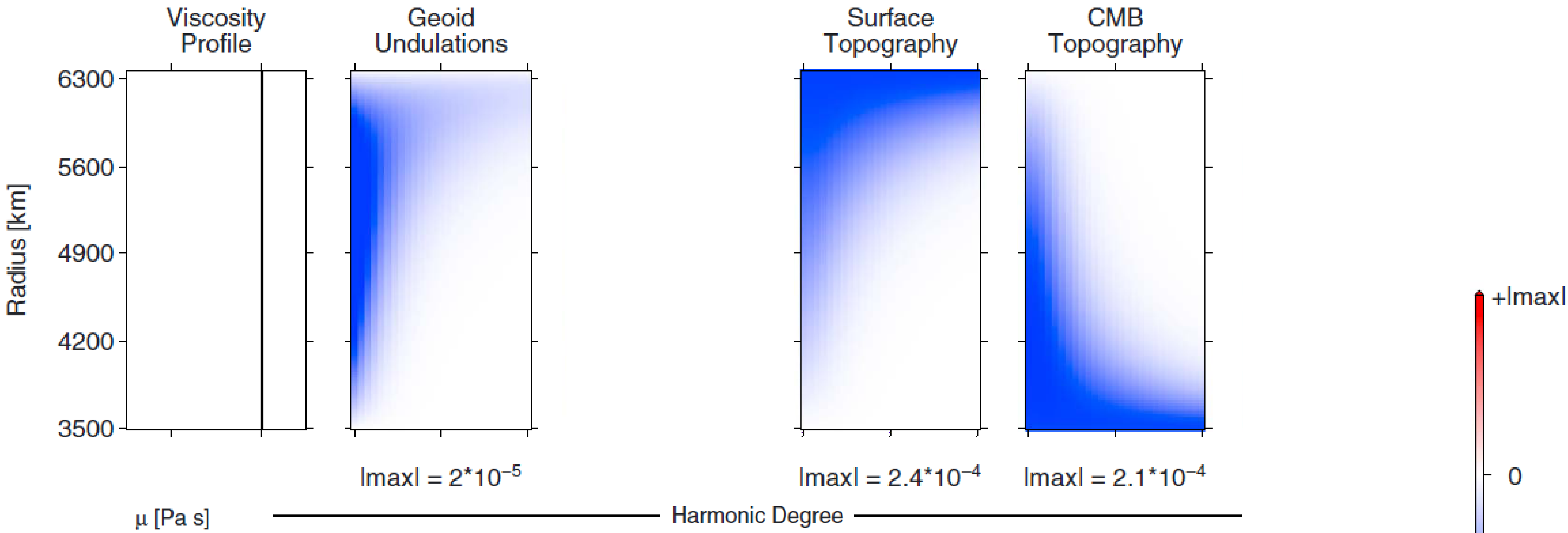

response to density anomalies as *f*(*z*, *l*)

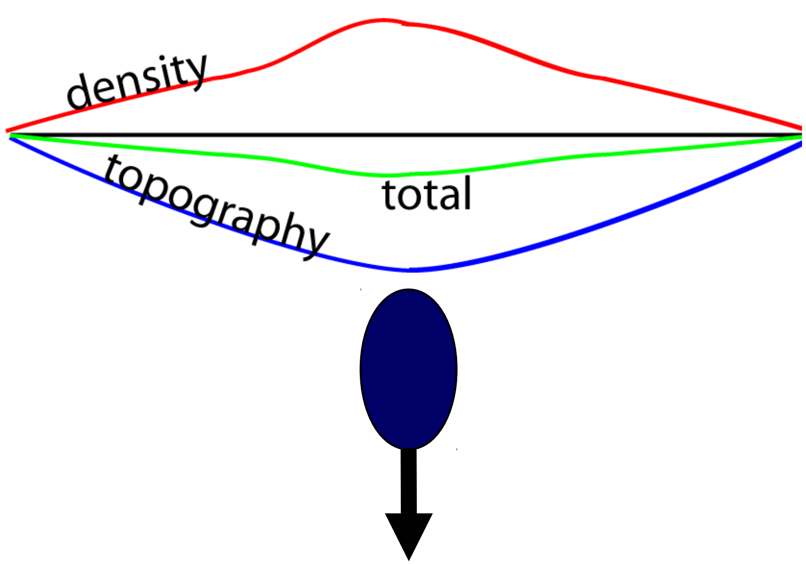

Colli et al. (2016), sketch from M. Billen
cf. Hager & Richards (1984); Ricard (1984)

Kernels for layered viscosity mantle

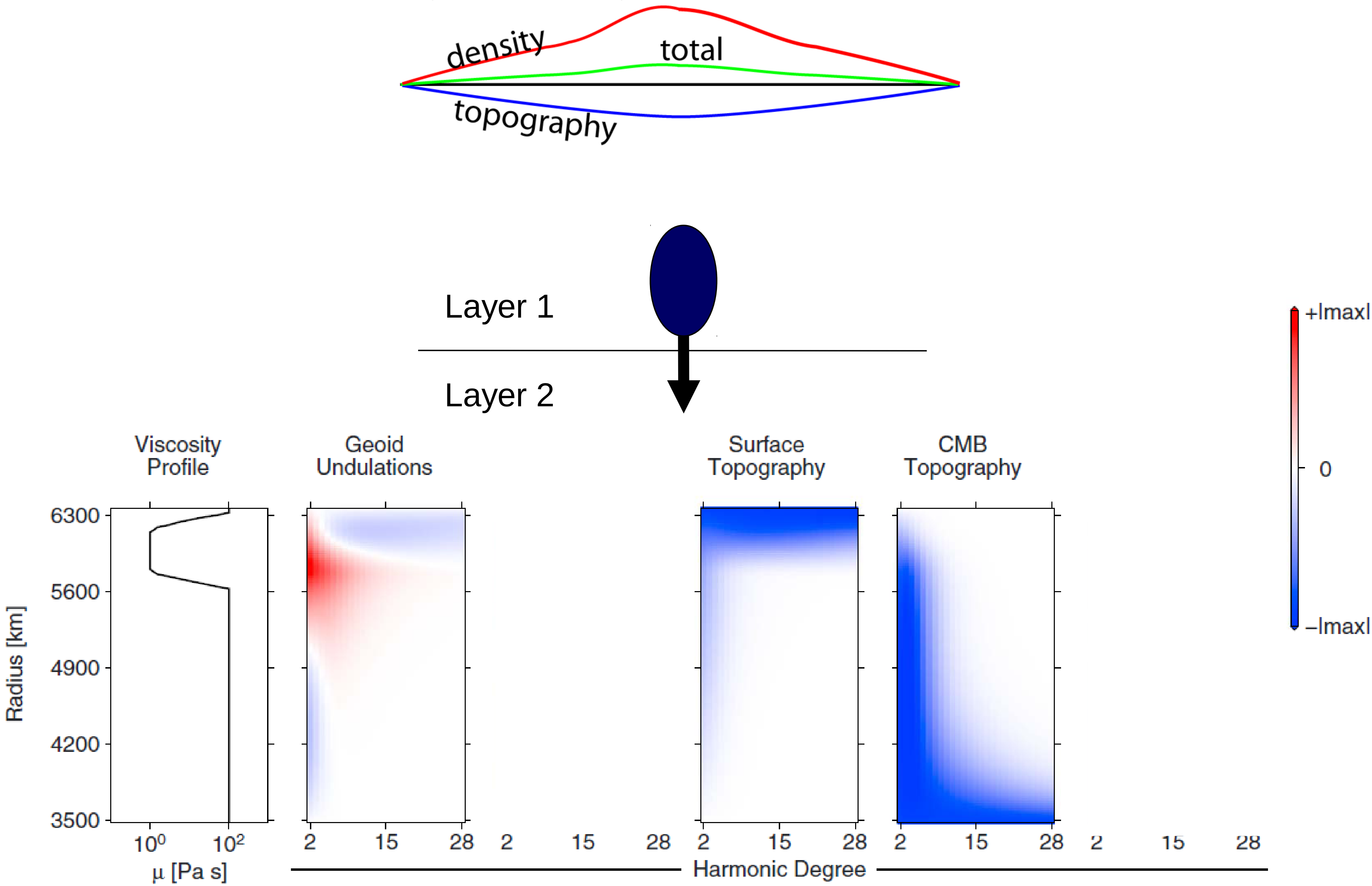

Colli et al. (2016), sketch from M. Billen cf. Hager & Richards (1984); Ricard (1984)

Geoid for tomography driven flow

- Isoviscous – free slip surface boundary condition

Constant
d ln ρ/d ln v_s

geoid prediction

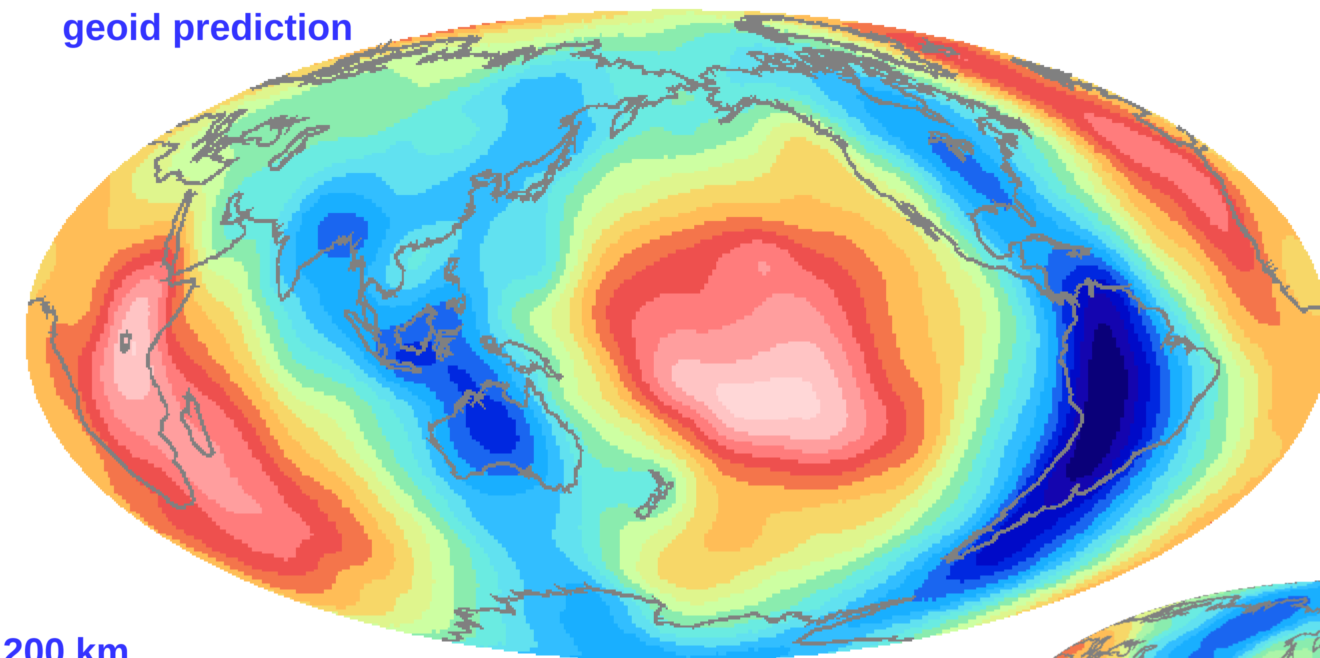

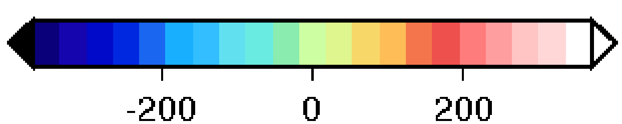

tomography @ 1200 km

$r_{1\text{-}20} = 0.28$

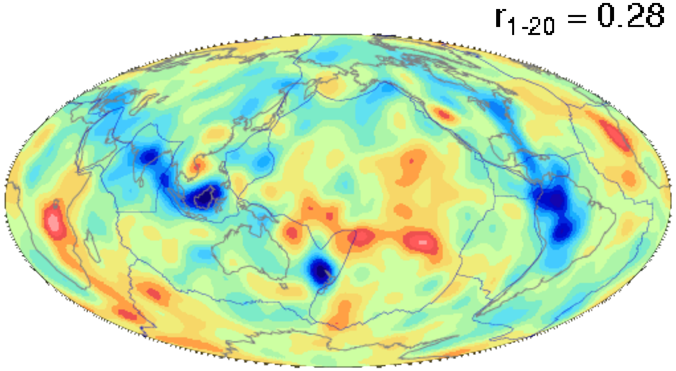

observed geoid

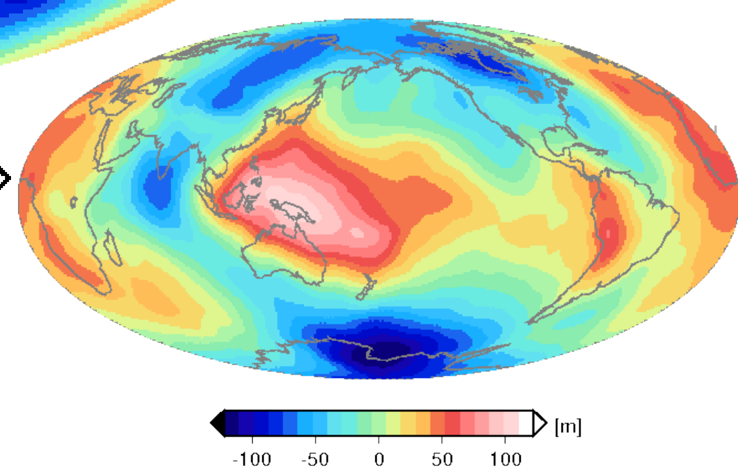

Geoid for tomography driven flow

- Four layer model with viscosity increase in lower mantle

geoid prediction

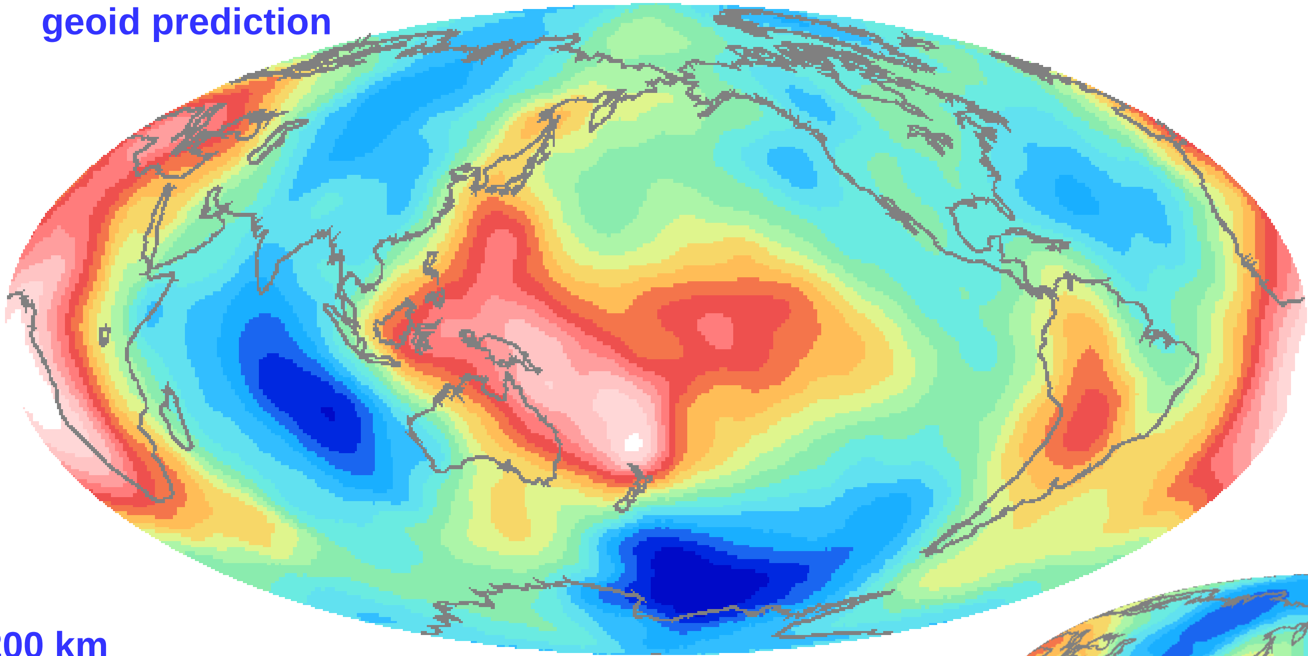

tomography @ 1200 km

$r_{1\text{-}20} = 0.79$

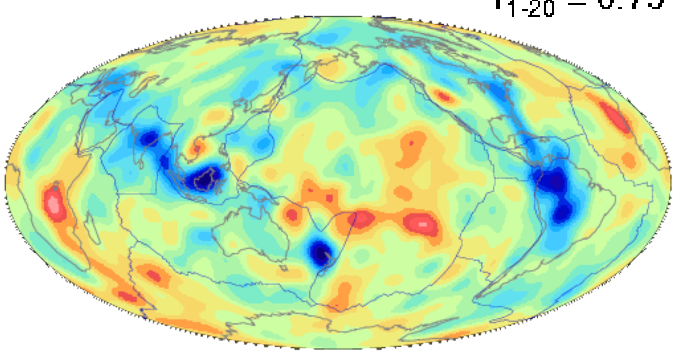

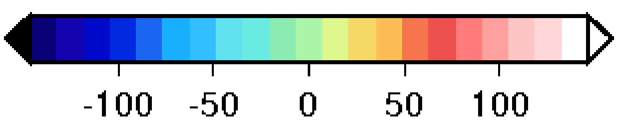

observed geoid

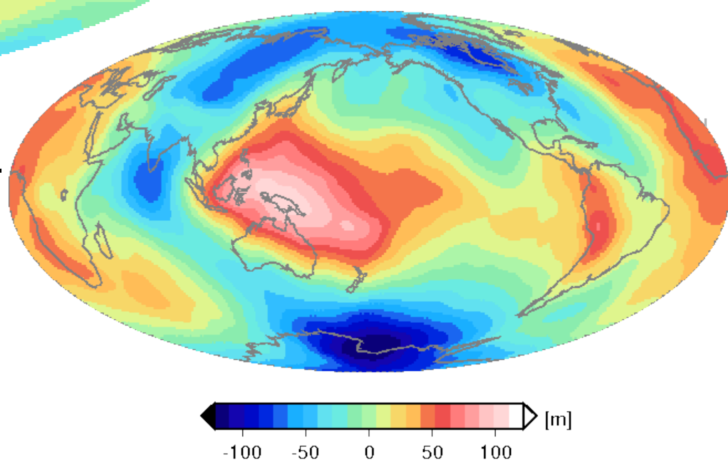

“Airy” residual surface topography: mainly due to half-space cooling

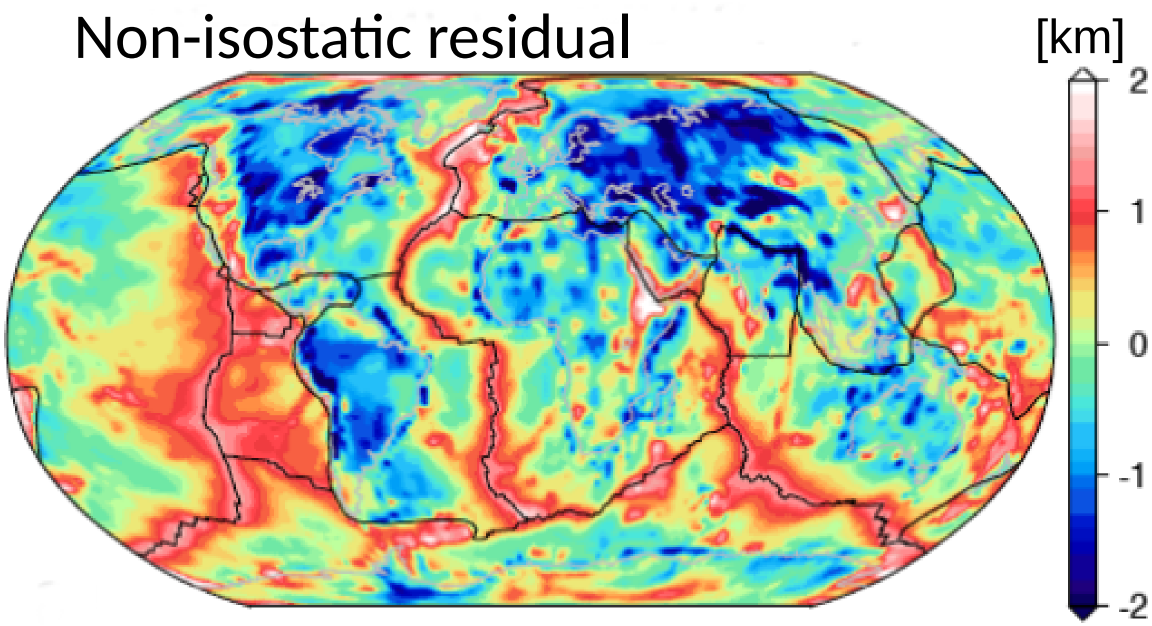

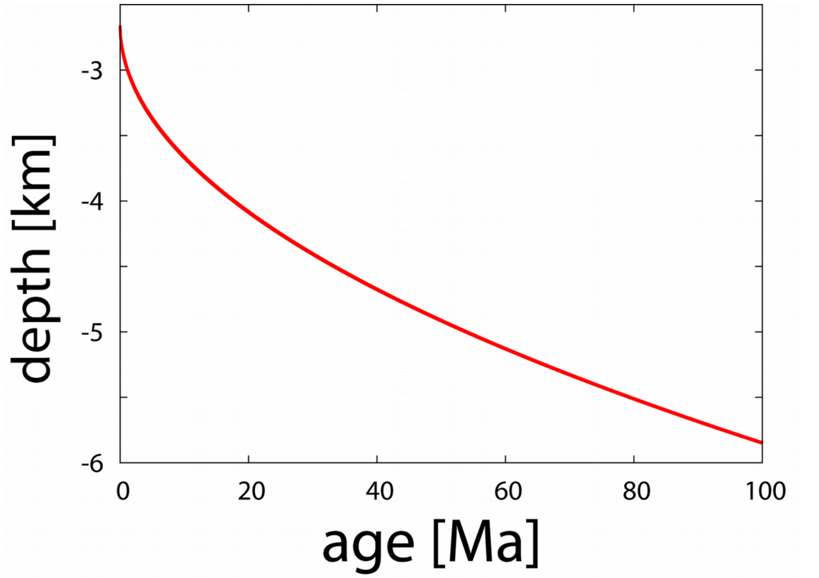

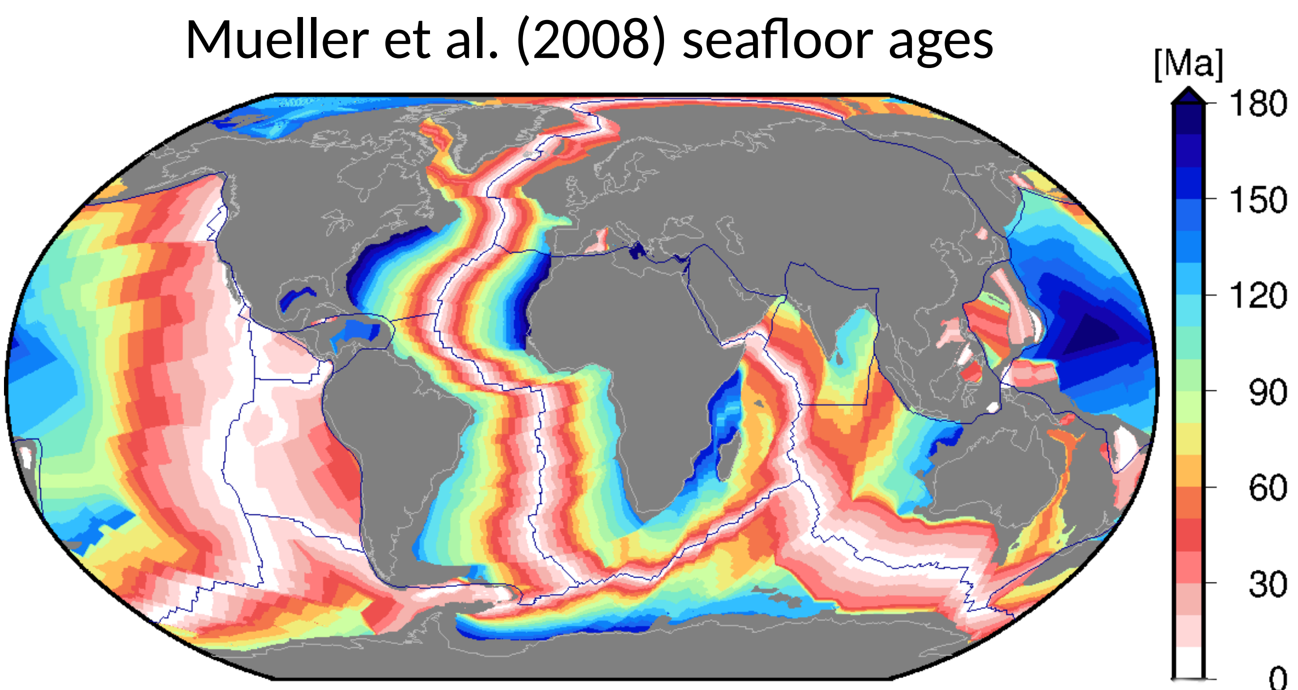

- the outstanding performance of this geodynamic “model” complicates attribution of anomalous topography

Non half-space cooling residual topography

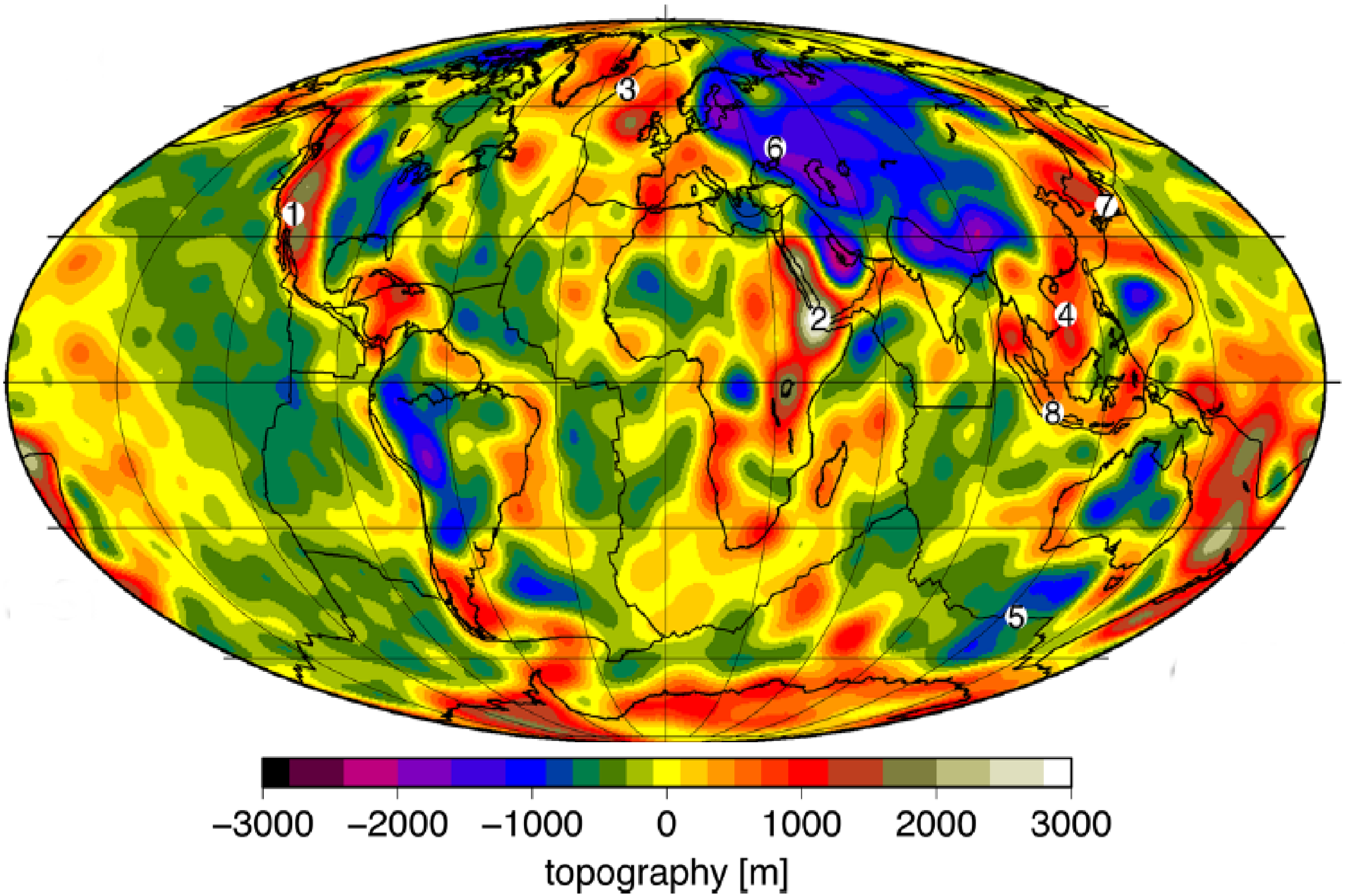

Topography corrected for Airy isostasy, half-space cooling, and lithospheric model (Steinberger, 2016)

Dynamic topography physics: “plume” case

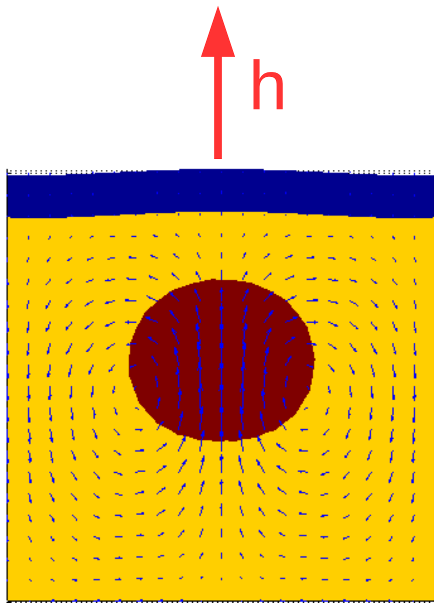

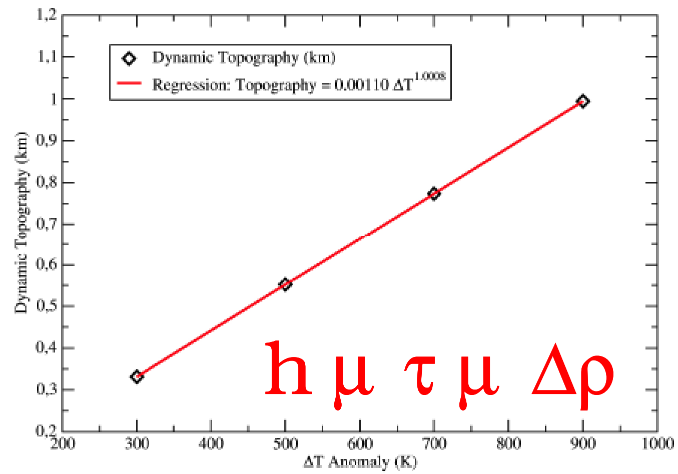

- dynamic topography h μ with density (temperature anomaly), $\Delta\rho$ (here = ΔT)

Stokes' sphere velocity/stress:

$$v_{\mathrm{Stokes}} \; \mu \; \Delta\rho/\eta$$

$$\tau \qquad \mu \; \Delta\rho$$

Notes:

- Often, we infer equivalent topography from σ_{zz} pushing on a free slip surface
- this works remarkably well in most cases ($\lambda \ll L$)

Dynamic topography physics: "plume" case

h, dh/dt

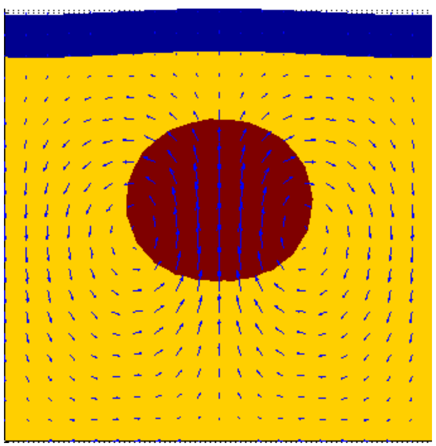

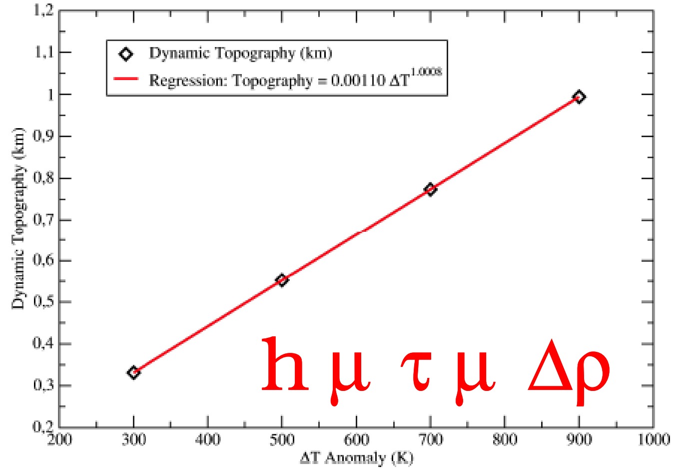

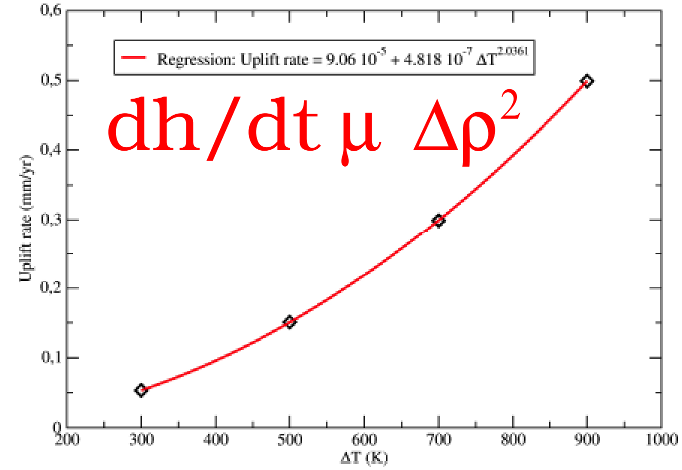

➔ dynamic topography *h* µ with density (temperature anomaly), Δρ (here = Δ*T*)

v µ Δρ/η

h µ τ µ Δρ

dh/dt µ v h

µ Δρ^2/η

Note:

- ➔ Match topography and velocity, constrain both Δρ and η,
- ➔ match uplift, even better!

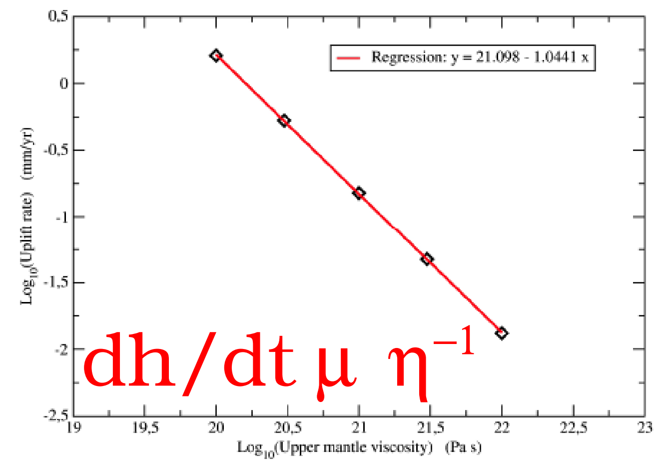

➔ uplift rate, d*h*/dt µ inverse of viscosity, 1/η (and density anomaly squared)

Match of dynamic topography from mantle flow models to surface residual topography

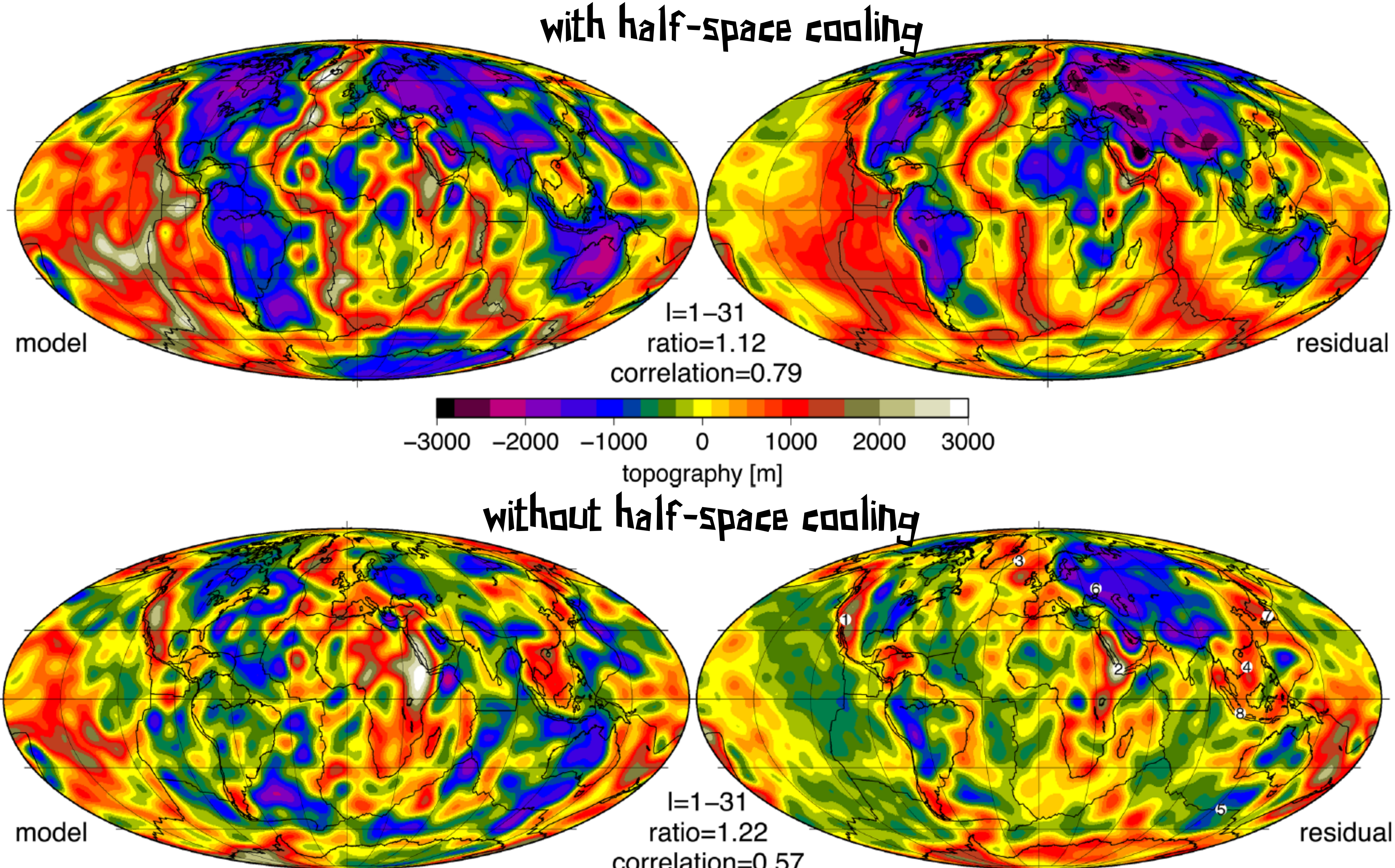

Steinberger (2016)

Isochemical, $\Delta\rho = 1$

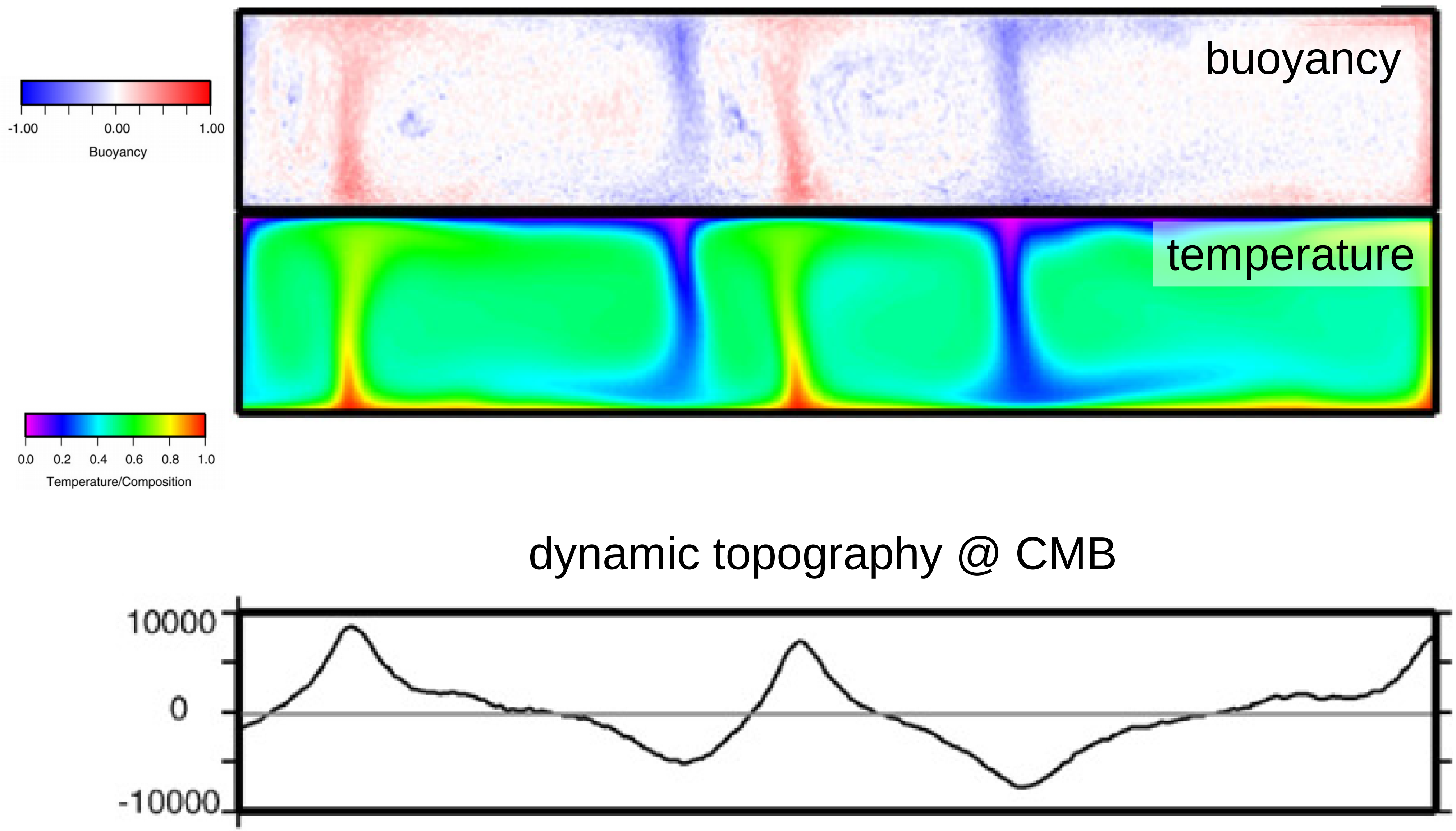

Lassak et al. (2008)

Pilotania, $\Delta\rho = 1$

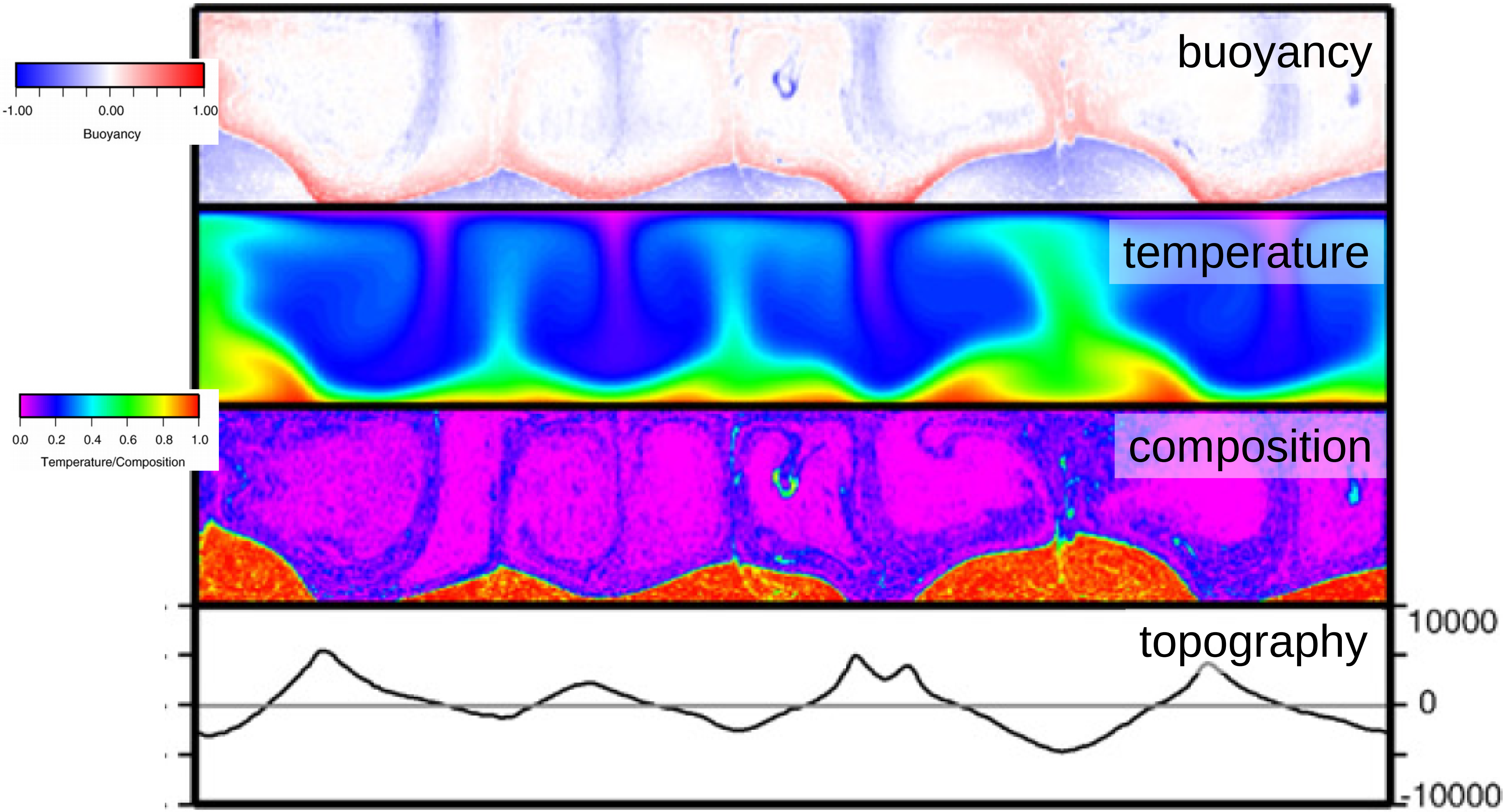

Lassak et al. (2008)

Pilotania, $\Delta\rho = 1{,}000$

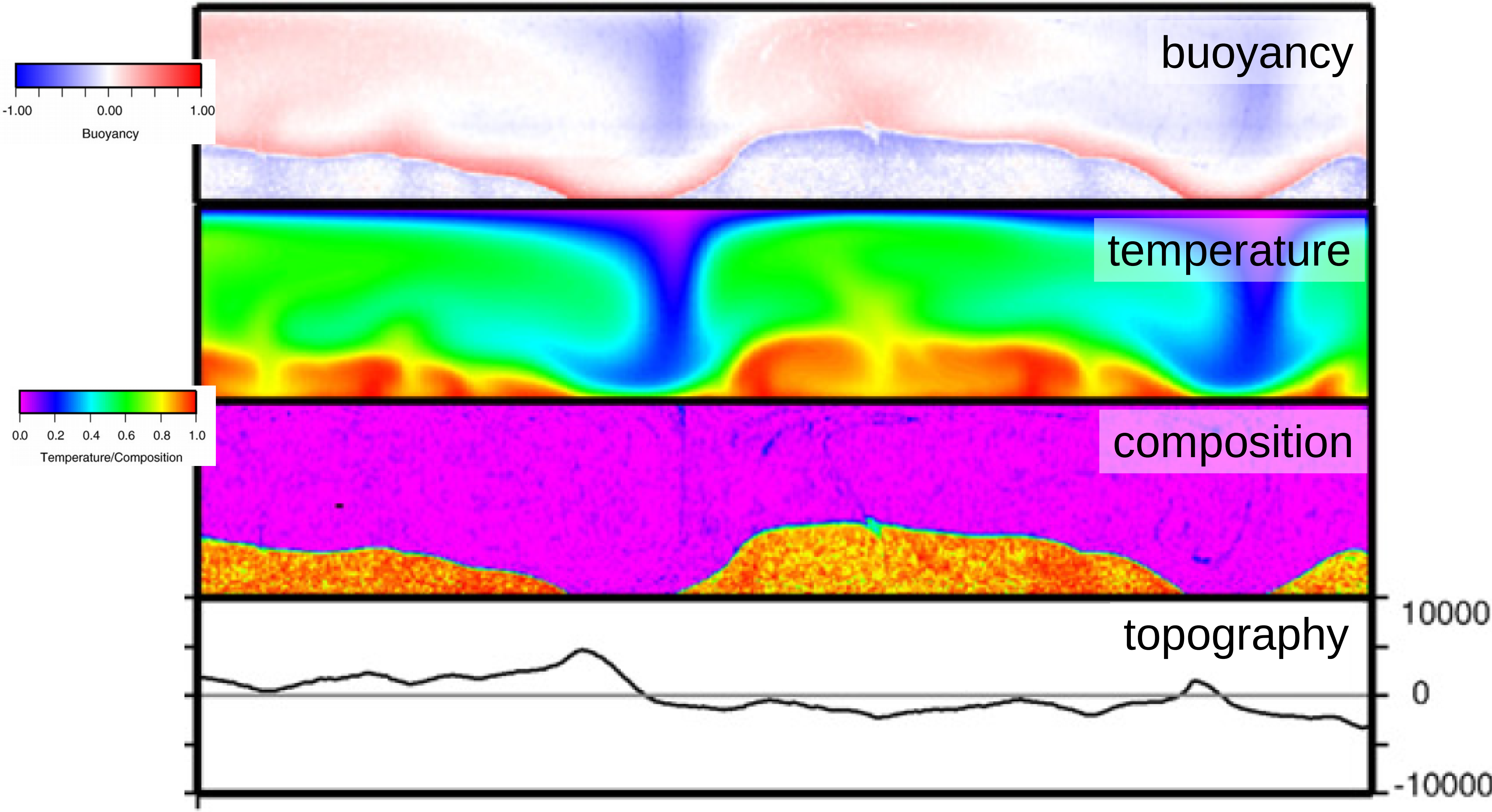

Lassak et al. (2008)

Viscosity inversions are non-unique
(Monte Carlo approach,
based on geoid and surface dyn. topo)

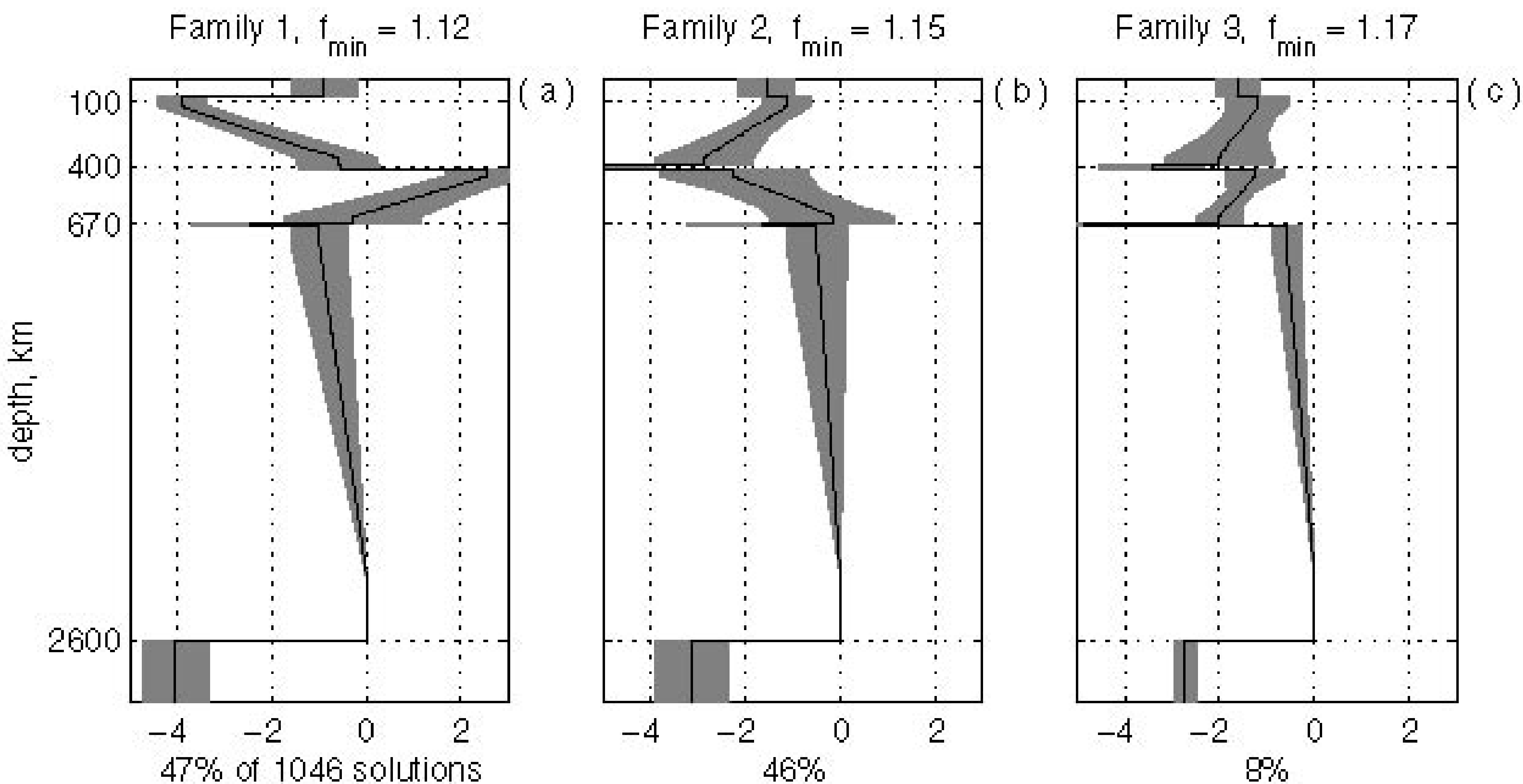

Panasyuk & Hager (2000)

Combining post-glacial rebound (GIA) and geoid
(still need to close loop with ice models)

Notes:

- geoid gives relative η with depth
- GIA gives absolute value
- "Haskell constraint" is ~10^{21} Pas for *average* down to ~1200 km (under cratons...)

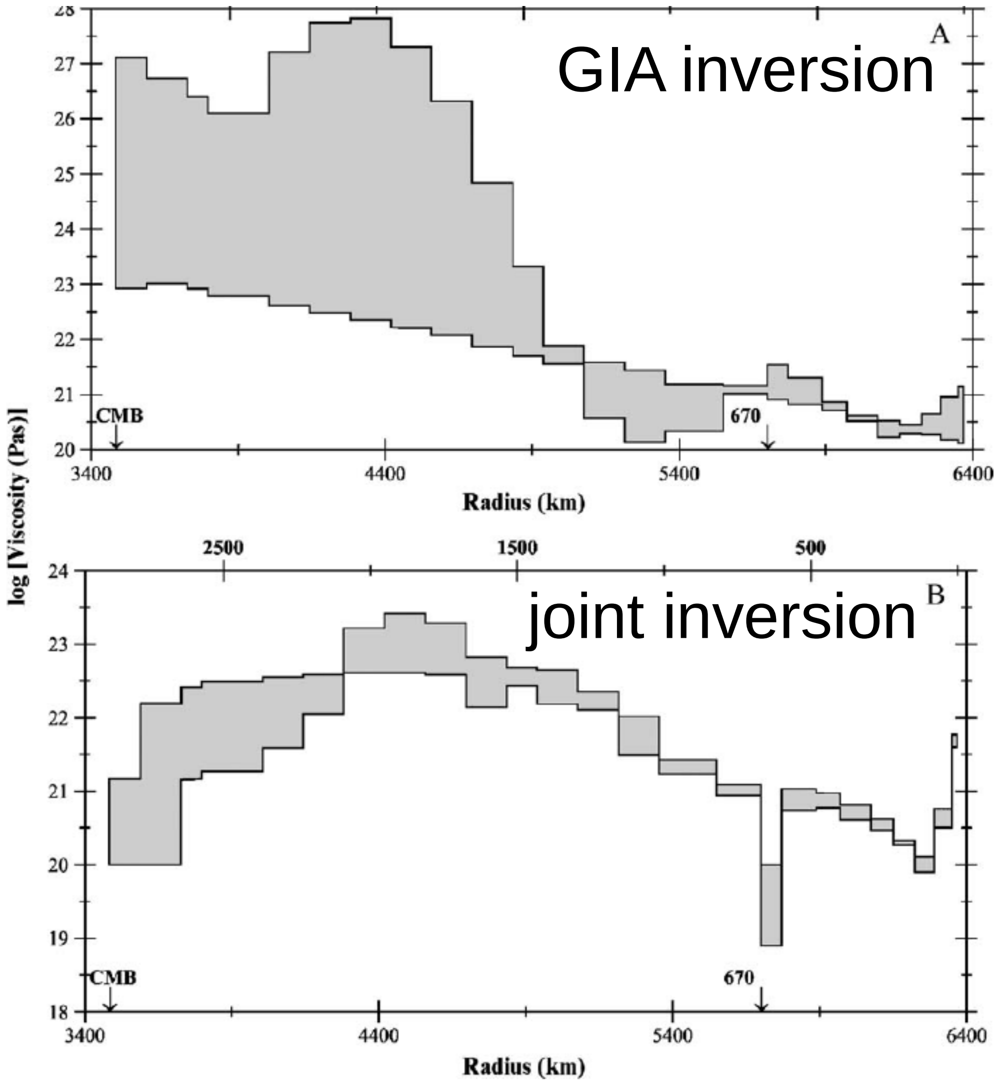

Mitrovica & Forte (2004)

Slab ponding diversity and viscosity stratification in transition zone

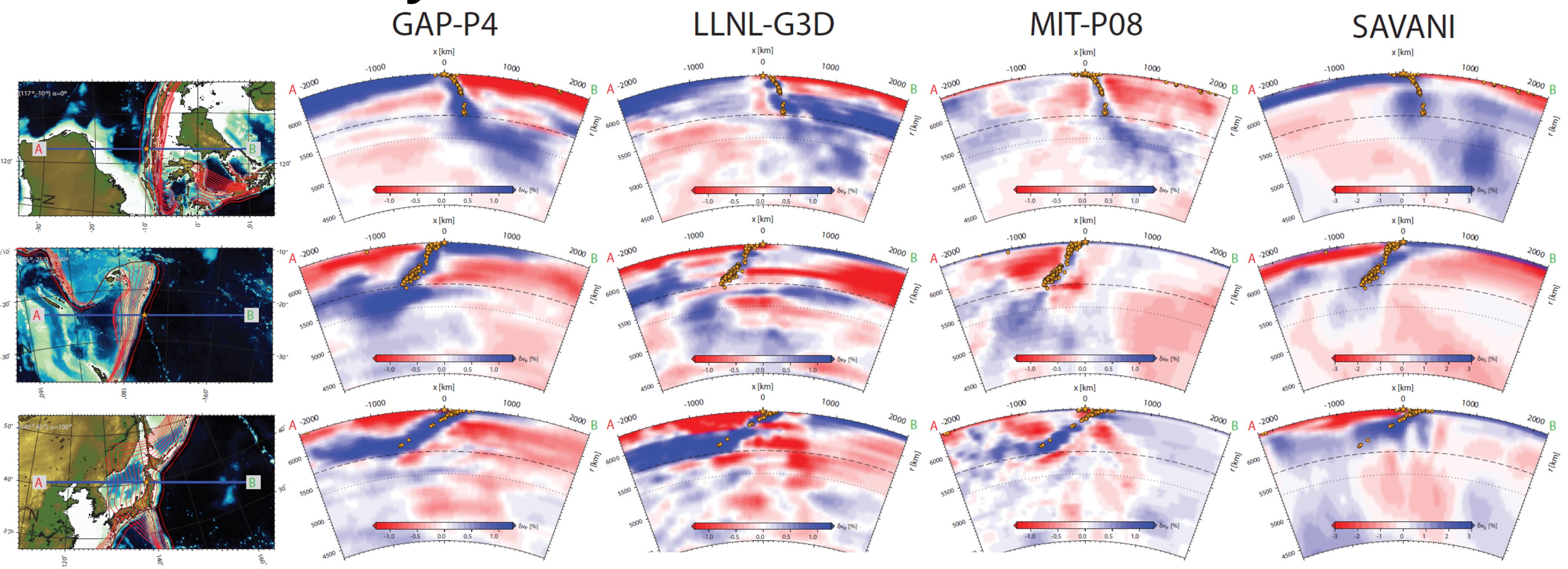

cf. Fukao and Obayashi (2013)

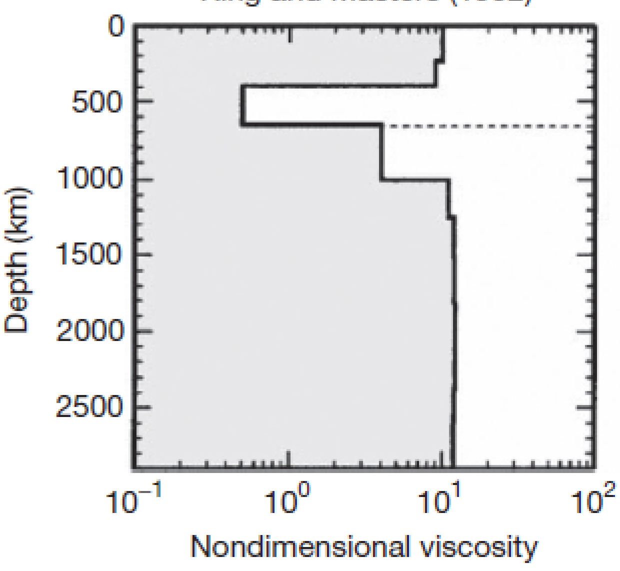

Genetic algorithm inversion based on geoid

Global, stochastic view:
Radial correlation functions

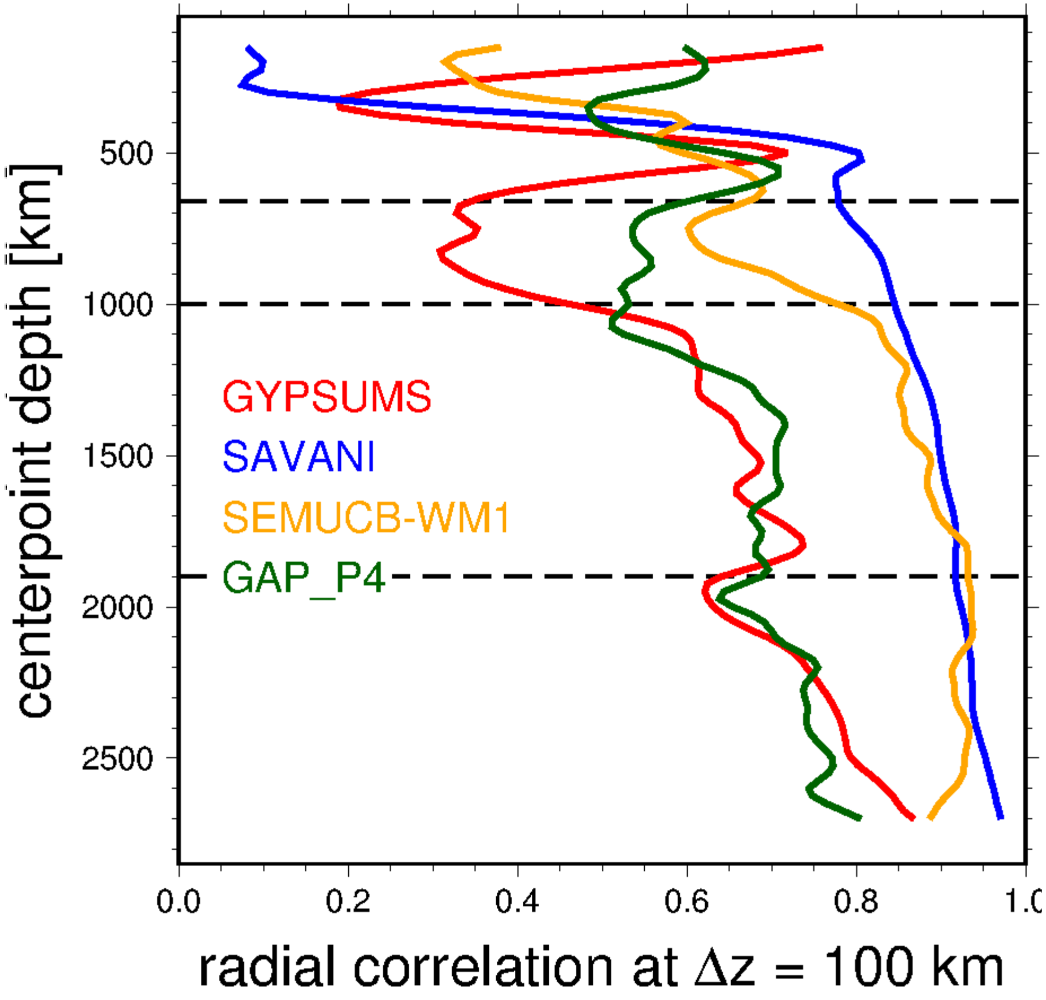

cf. Puster and Jordan (1997),
Tackley (1998, 2002)

Query data for discontinuity depth

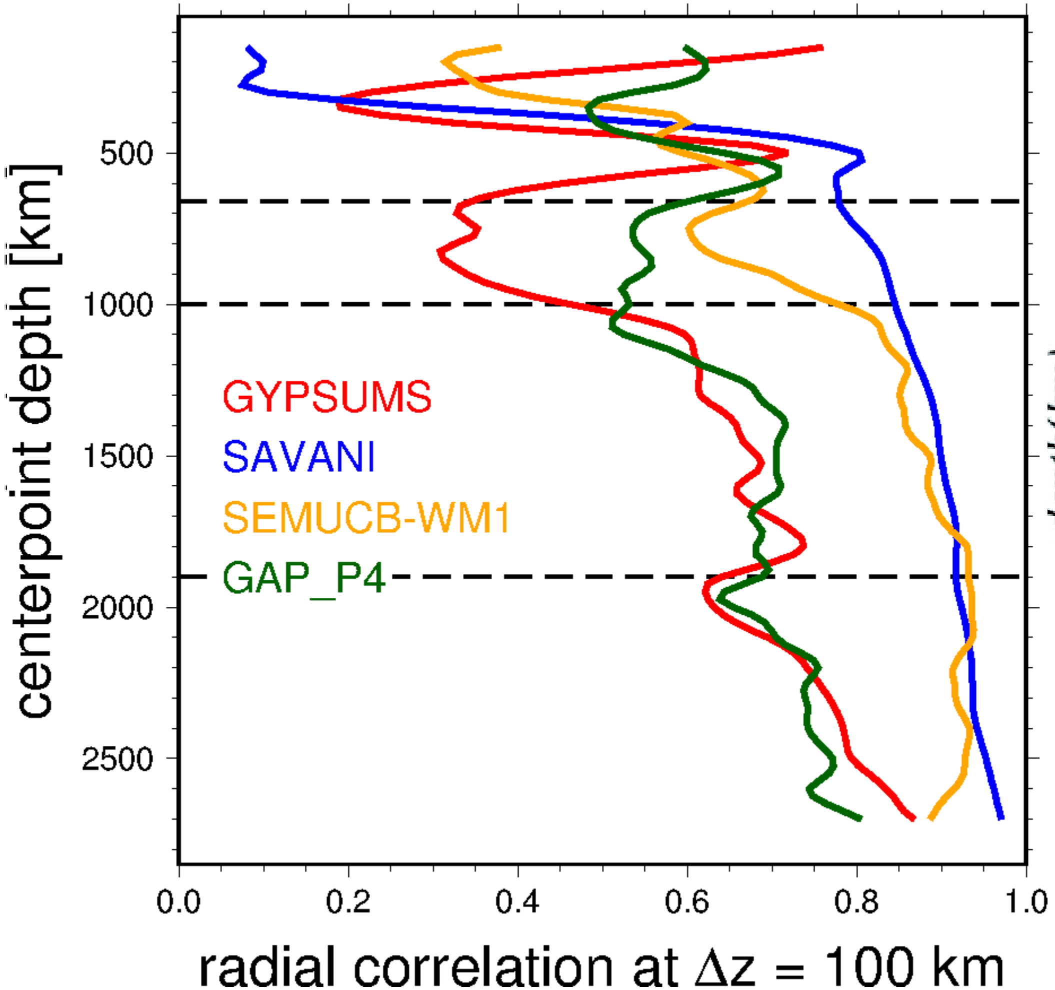

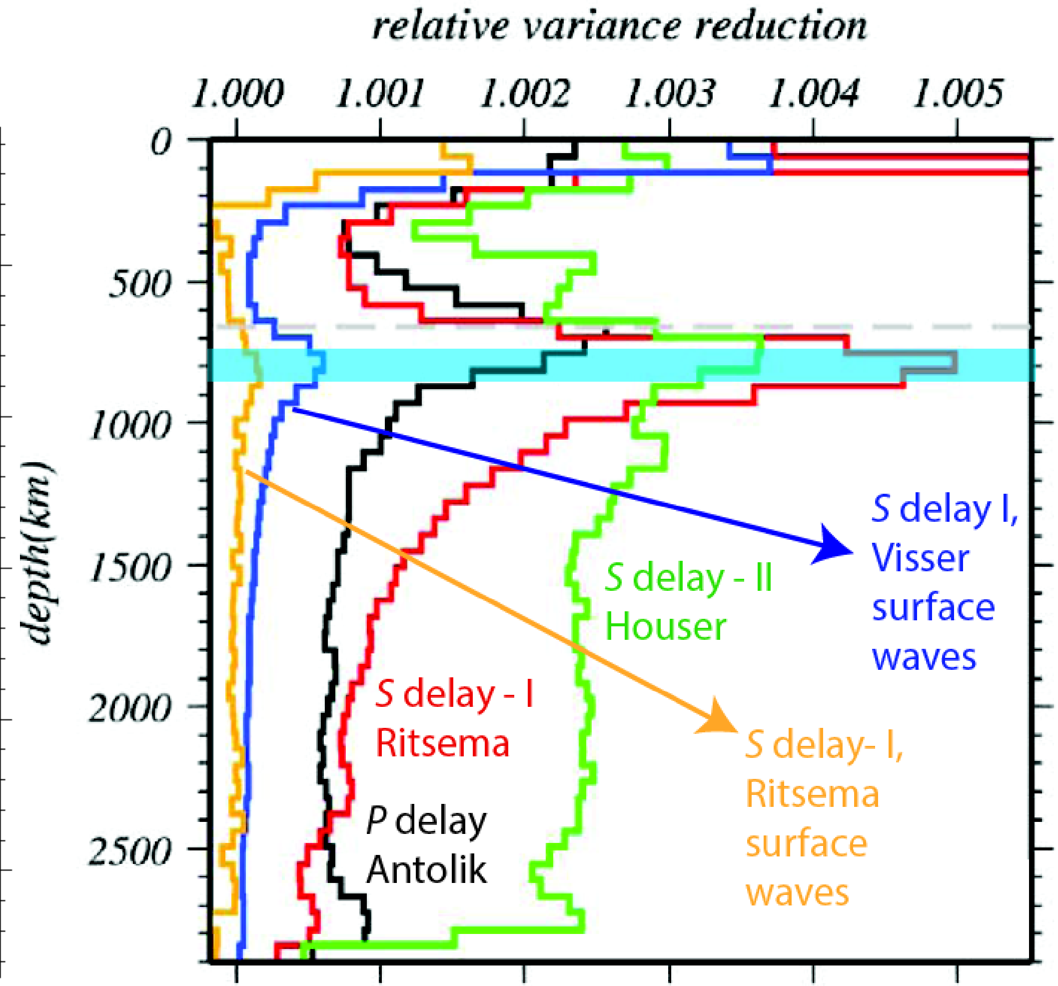

Becker and Boschi (2011)

cf. Puster and Jordan (1997), Tackley (1998, 2002)

see Max Rudolph talk on Rudolph et al. (2015)

Adding a constraint: Predicting plate motions

Flow model with only radial viscosity variations

Poloidal component

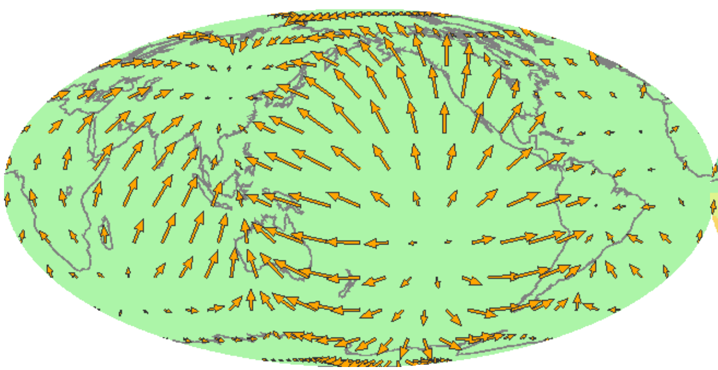

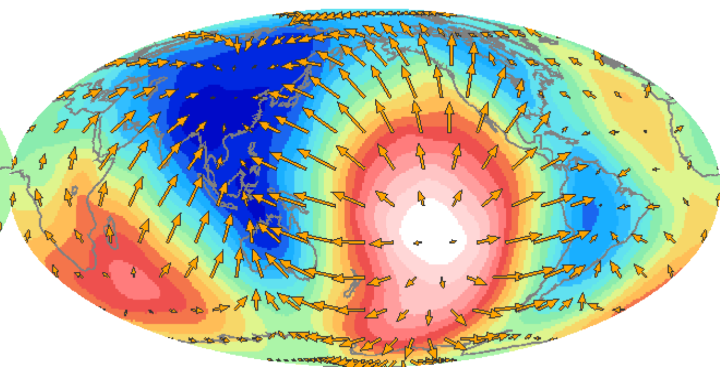

- No toroidal flow without lateral viscosity variations (no PT coupling)
- Strain-rates not very plate-like

Observed plate velocities in hot spot reference frame

Poloidal component

Toroidal component

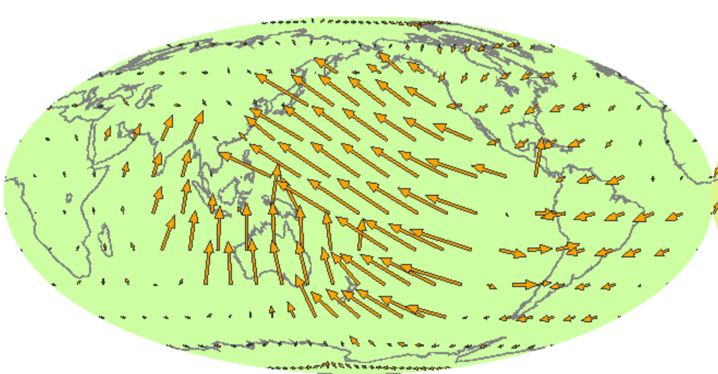

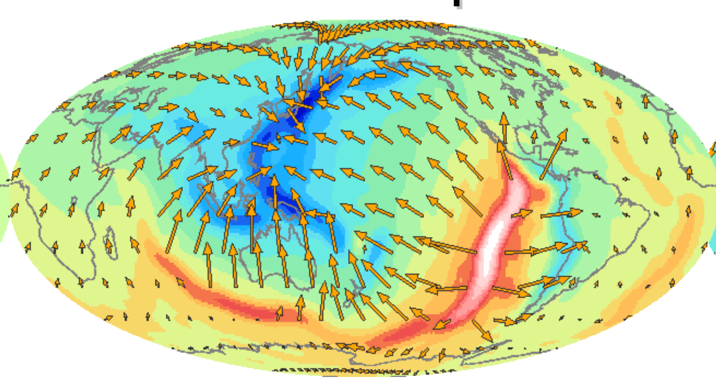

Sources and sinks

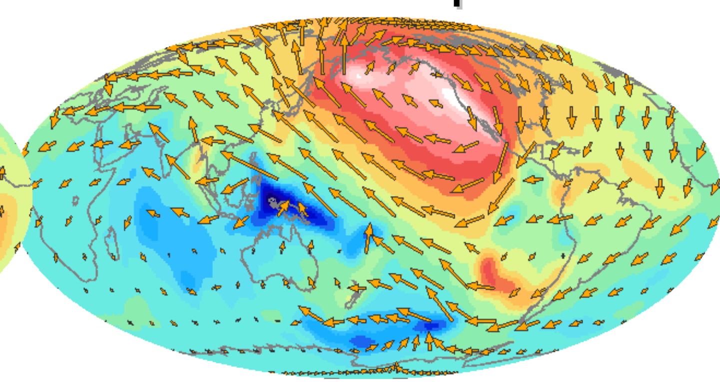

Strike slip motion, spin

O'Connell et al. (1991); Ricard et al. (1991); Ribe (1993); Forte & Peltier (1993); Thoraval & Richards (1997); Moucha et al. (2008); Ghosh et al. (2009)

Rigid plate motions for weak boundaries

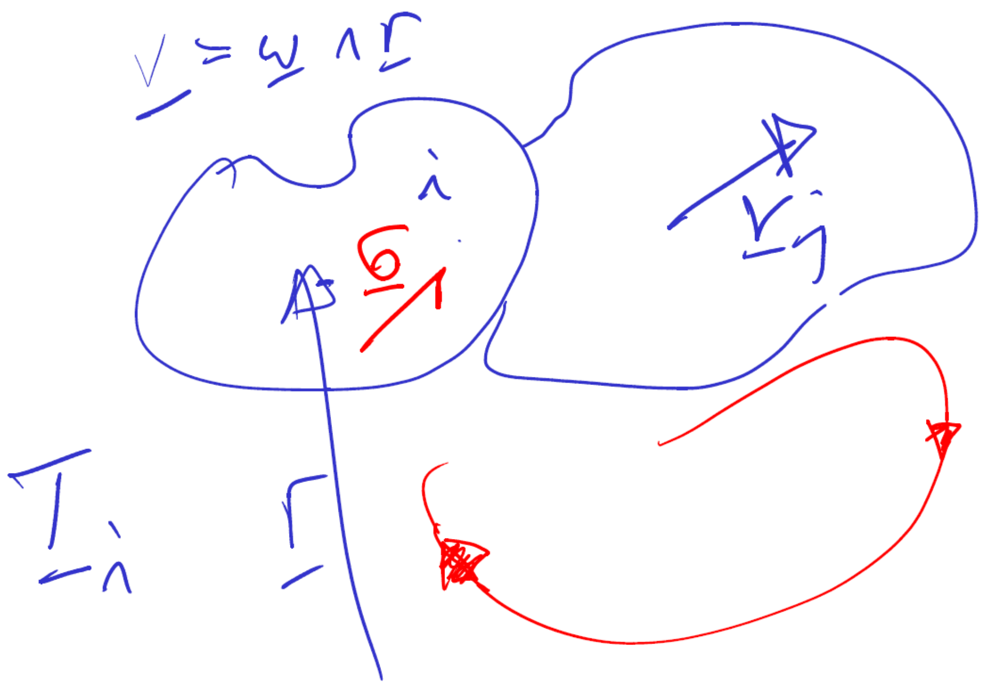

$$\mathbf{T}_i = \int_{\text{plate}} dA \; \mathbf{r} \times \boldsymbol{\sigma}$$

$$\mathbf{T}_{vd} = \mathbf{P} \cdot \boldsymbol{\omega} = \sum_{i}^{M} \mathbf{T}_i$$

Note: Can construct plate motion interaction matrix **P**, for any LVVs

cf. Ricard and Vigny (1989), Forte (1993), van Summeren et al. (2010)

Match to observed plate motions

- Velocity model
  - Prescribe weak plate boundaries
  - Compute plate drag coupling and driving torques
  - Solve for Euler vectors for rigid plates
- Correlations good, but oceanic plates move as fast as continental ones

Observed plate motions

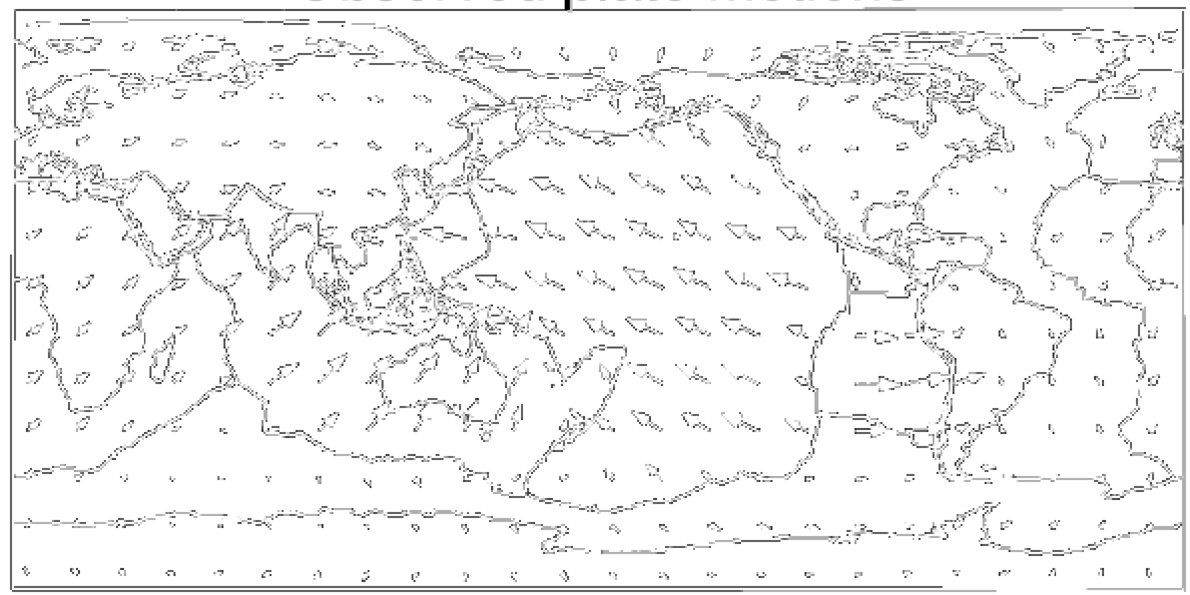

Modeled plate motions

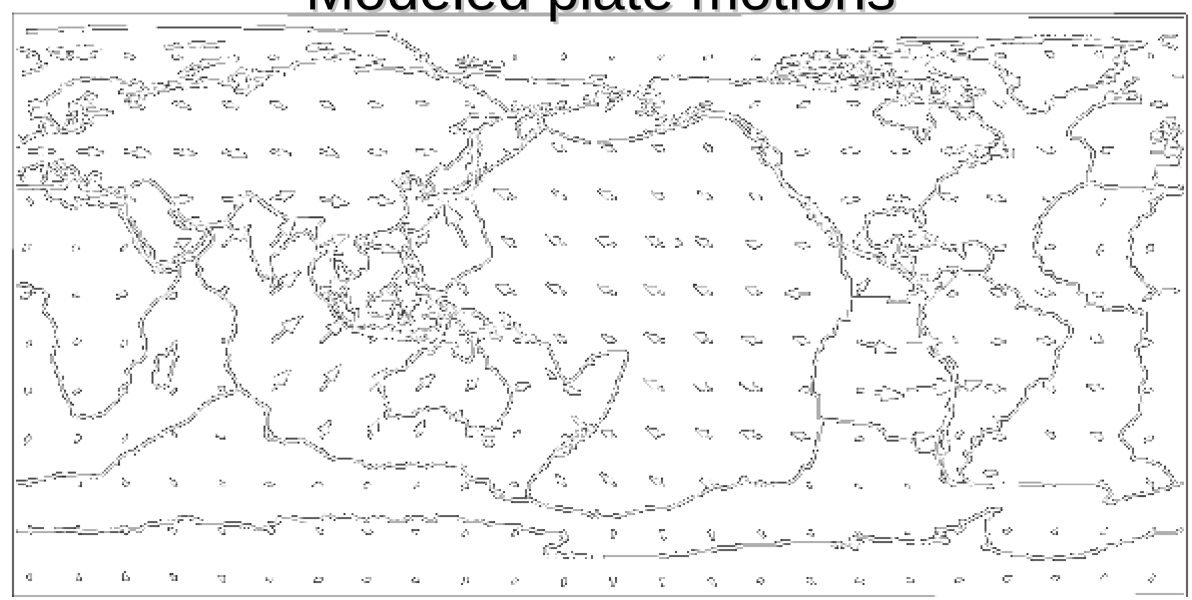

Ricard & Vigny (1989)

Ricard & Vigny (1989); Lithgow-Bertelloni & Richards (1998); Becker & O'Connell (2001); Conrad & Lithgow-Bertelloni (2002); Becker (2006); van Summeren et al. (2010; Alisic et al. (2014)

Adding edge forces to basal shear from flow

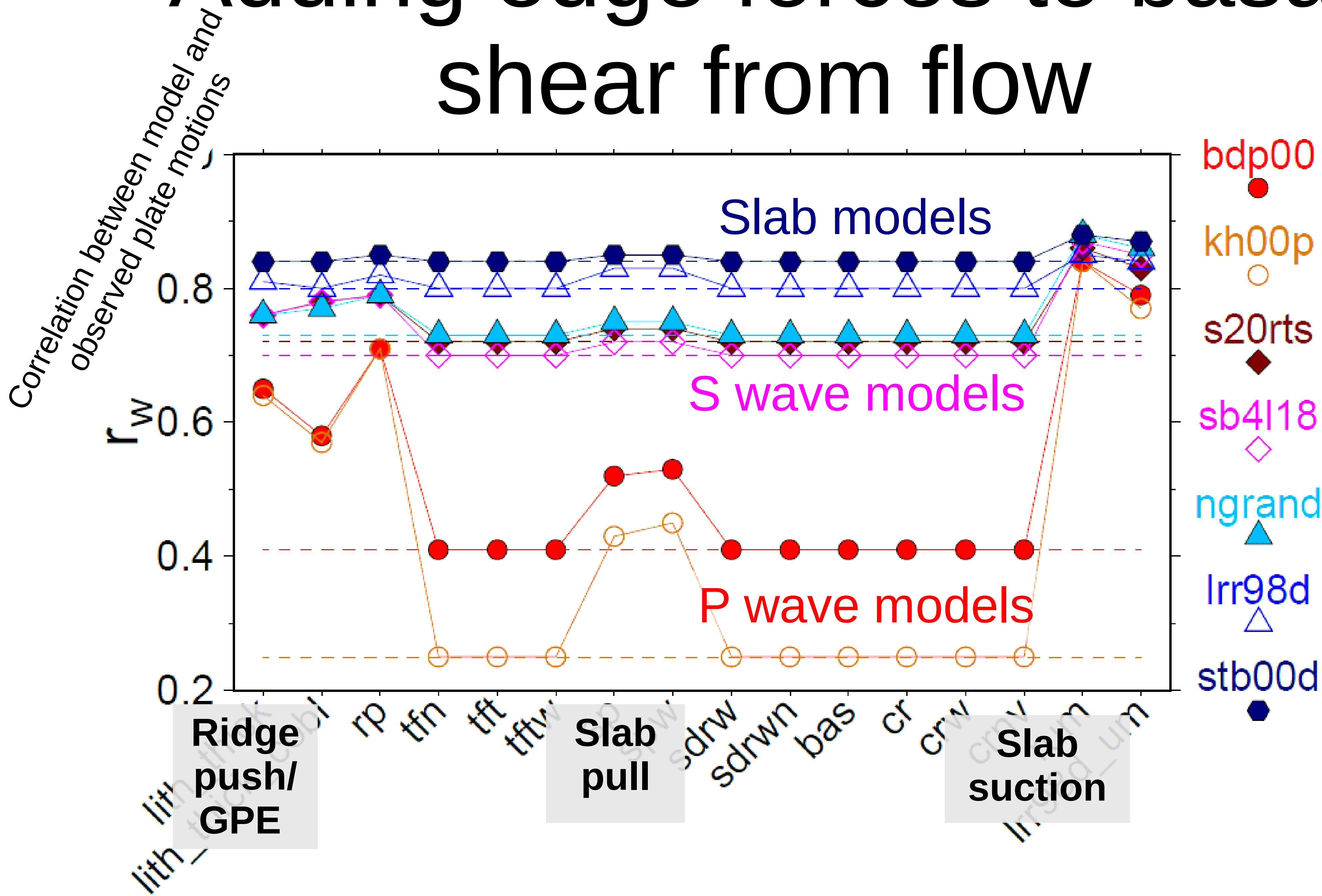

Becker & O'Connell (2001)

Ricard & Vigny (1989); Lithgow-Bertelloni & Richards (1998); Zhong et al. (2000); Becker & O'Connell (2001); Conrad & Lithgow-Bertelloni (2002); Becker (2006)

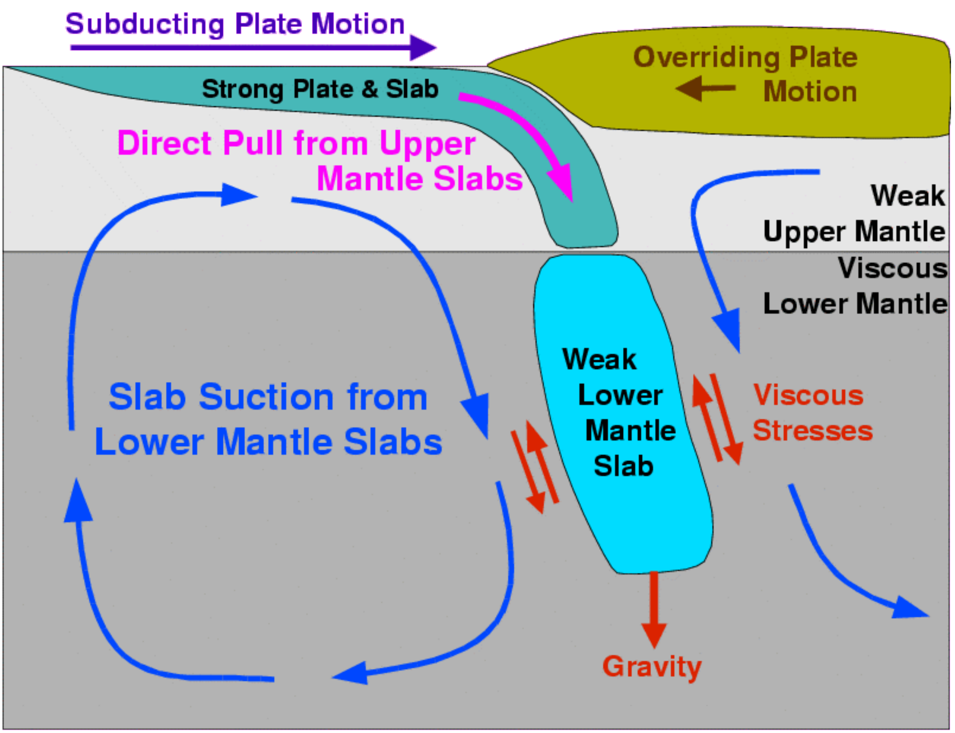

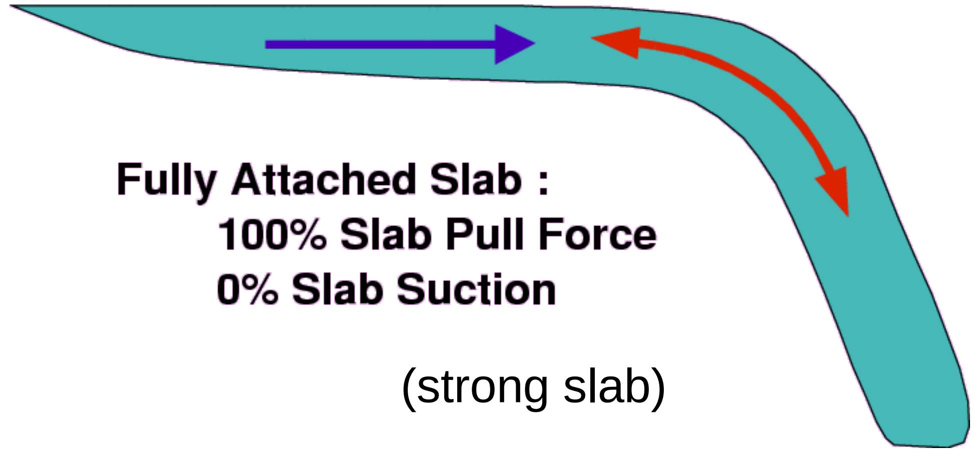

Which slabs must be detached to produce the best fit to plate motions?

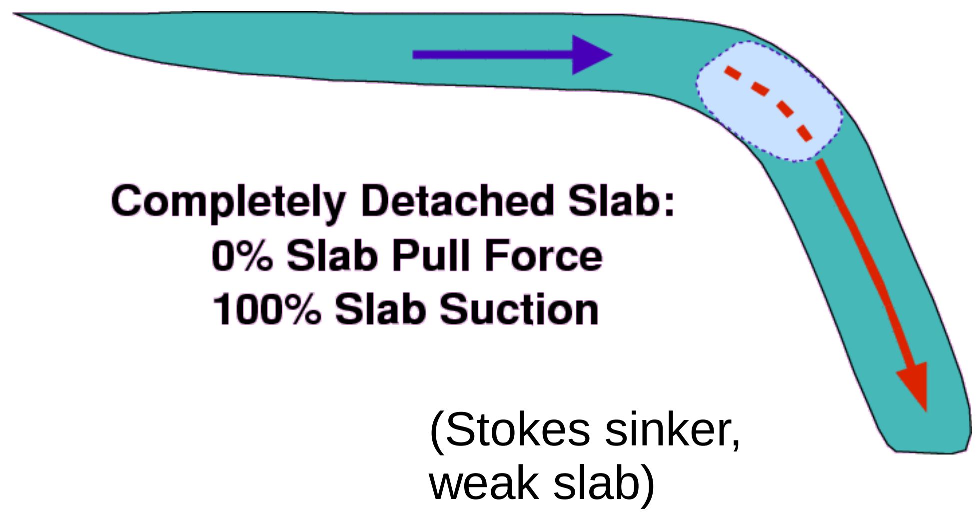

Slide courtesy of C. Lithgow-Bertelloni

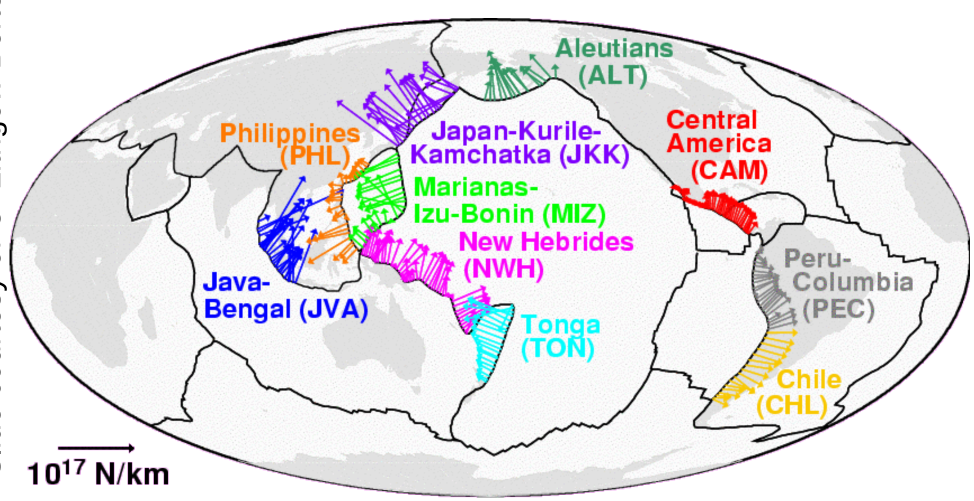

Conrad and Lithgow-Bertelloni (2004)

Mantle rheology

η: viscosity
$\dot{\varepsilon}$: strain-rate

- use generic temperature and/or stress dependence of viscosity on top of radial variations
- use effective, olivine creep law with diffusion & dislocation creep

$$\dot{\varepsilon}_0 = \dot{\varepsilon}_{\mathrm{disl}} + \dot{\varepsilon}_{\mathrm{diff}}$$

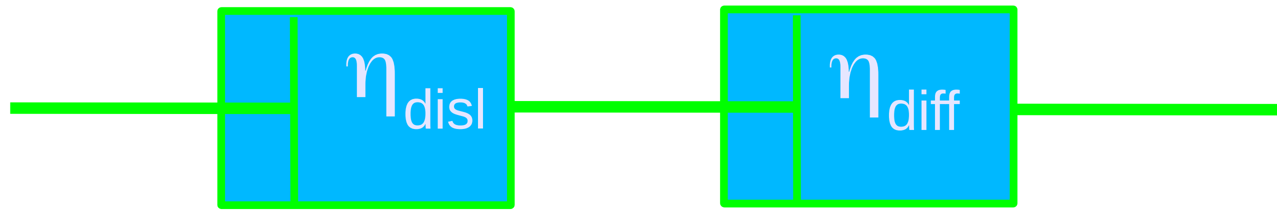

$$\eta_{\mathrm{eff}} = \frac{\eta_{\mathrm{disl}}\eta_{\mathrm{diff}}}{\eta_{\mathrm{disl}} + \eta_{\mathrm{diff}}}$$

$$\eta = \left(\frac{d^m}{A'}\right)^{\frac{1}{n}} \dot{\varepsilon}_{II}^{\frac{1-n}{n}} \exp\left(\frac{E^* + pV^*}{nRT_r(T_c + T)}\right)$$

Sub-oceanic vs. continental speeds
(LVV GCM @ 250 km)

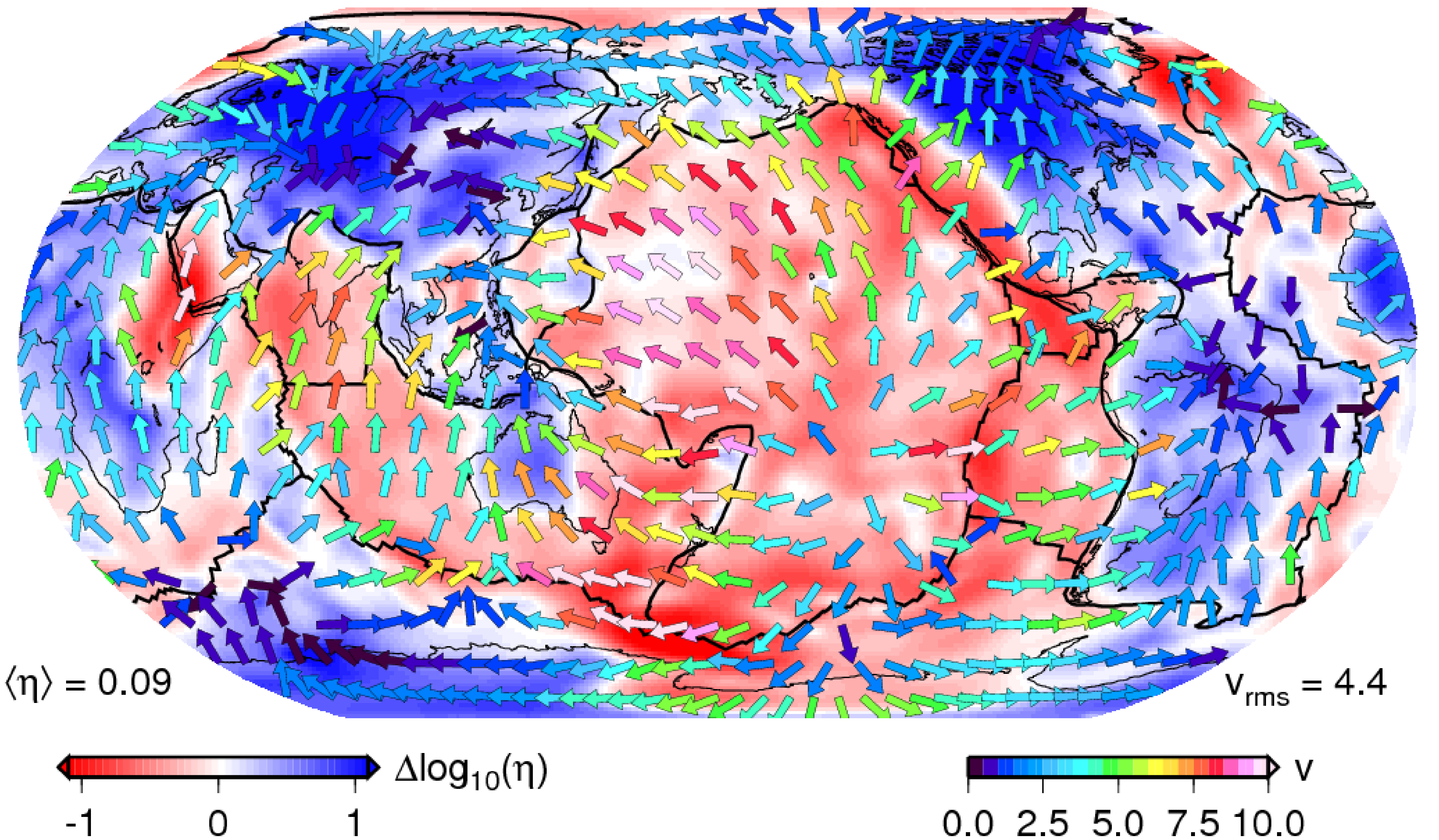

Hager & O'Connell (1981); Ricard & Vigny (1989); Zhang & Christensen (1993); Cadek & Fleitout (2003); Becker (2006);

Stadler et al. (2010); Alisic et al. (2014)

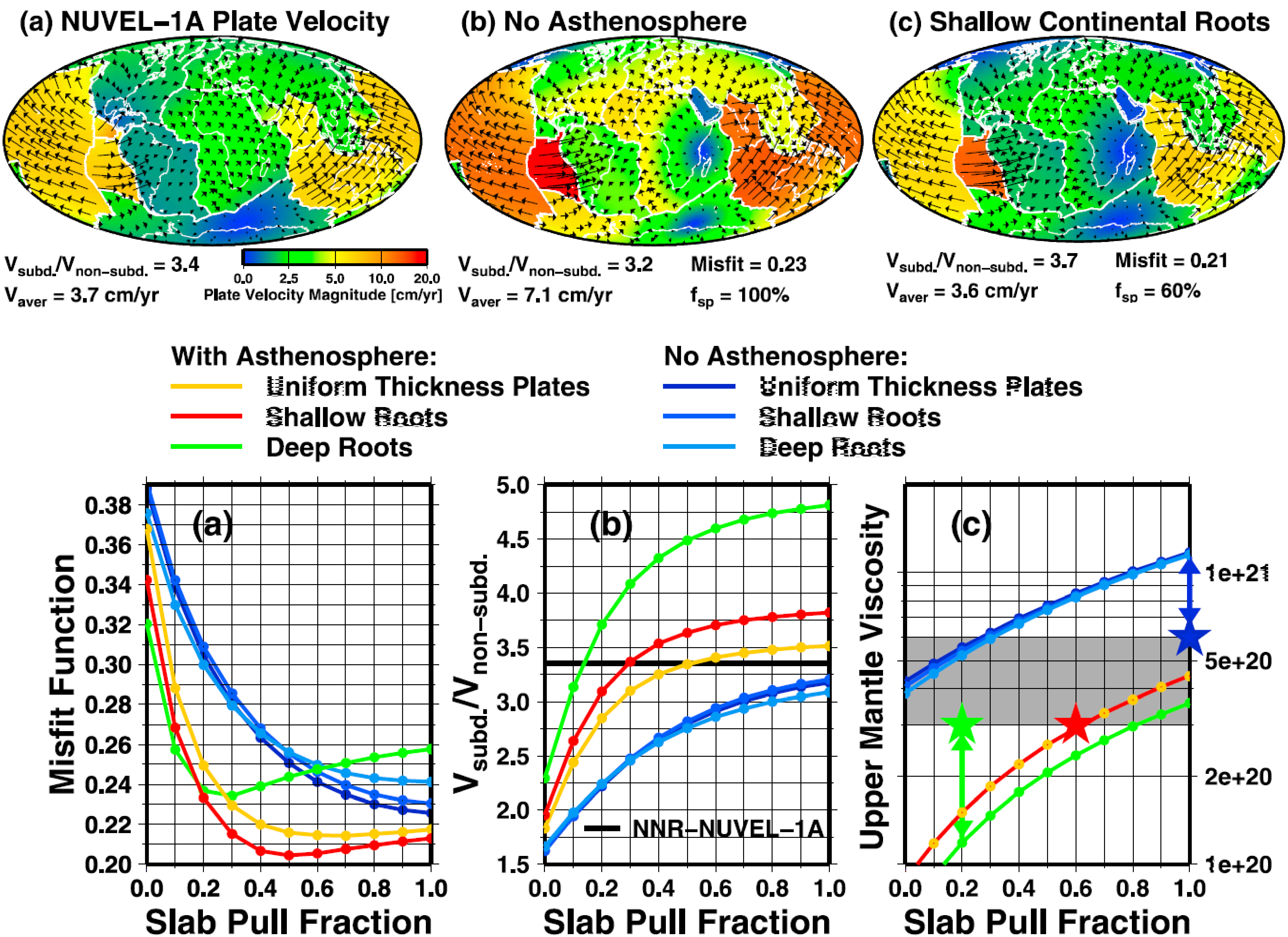

van Summeren et al. (2012)

Average mantle viscosities for olivine

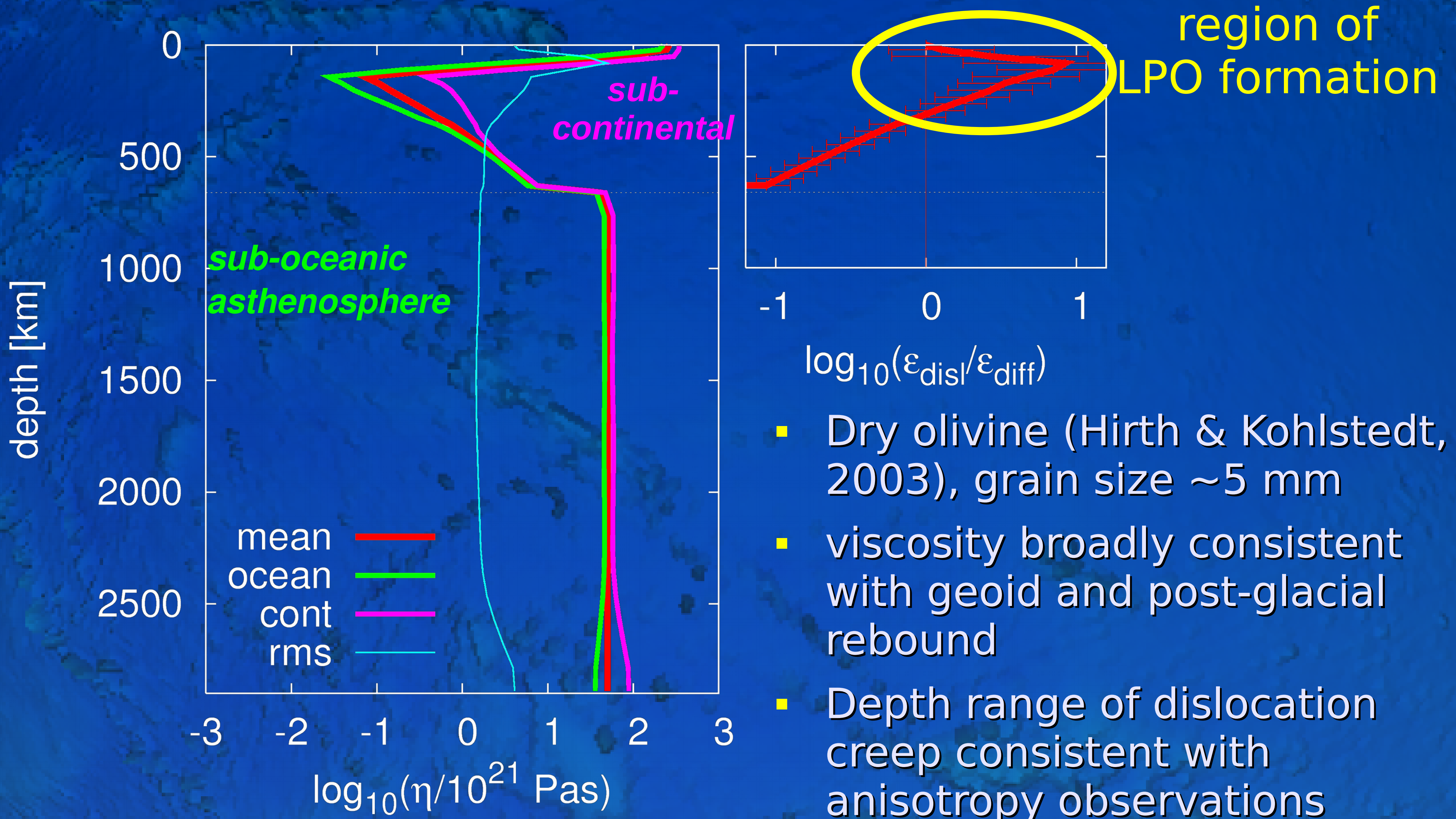

- Dry olivine (Hirth & Kohlstedt, 2003), grain size ~5 mm
- viscosity broadly consistent with geoid and post-glacial rebound
- Depth range of dislocation creep consistent with anisotropy observations

Cadek & Fleitout (2003); McNamara et al. (2003);

Podolevsky et al. (2005); Becker (2006)

Seismic anisotropy from flow

2) LPO prediction

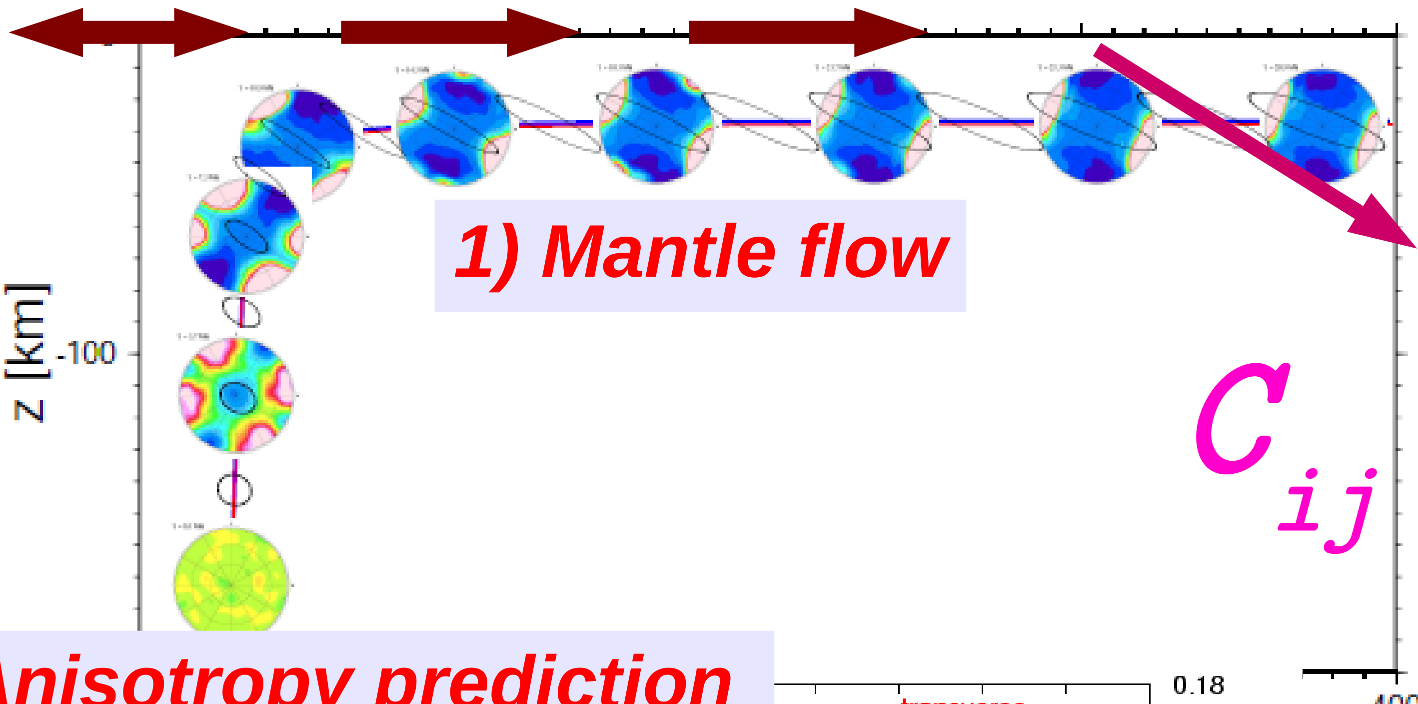

1) Mantle flow

C_{ij}

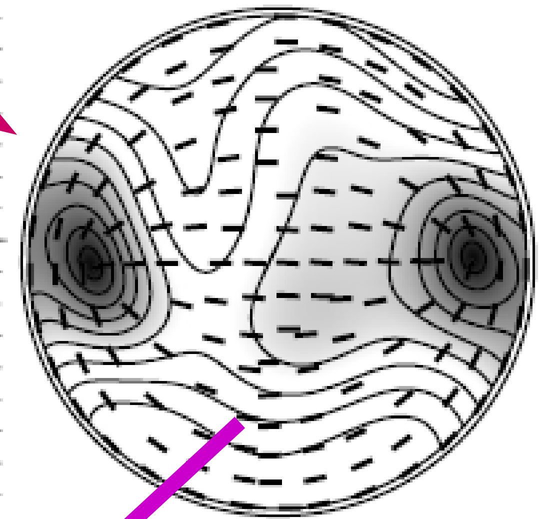

(80% hex, 12% orth.
@ 75% SC saturation)

3) Anisotropy prediction

model synthetics

S wave splitting

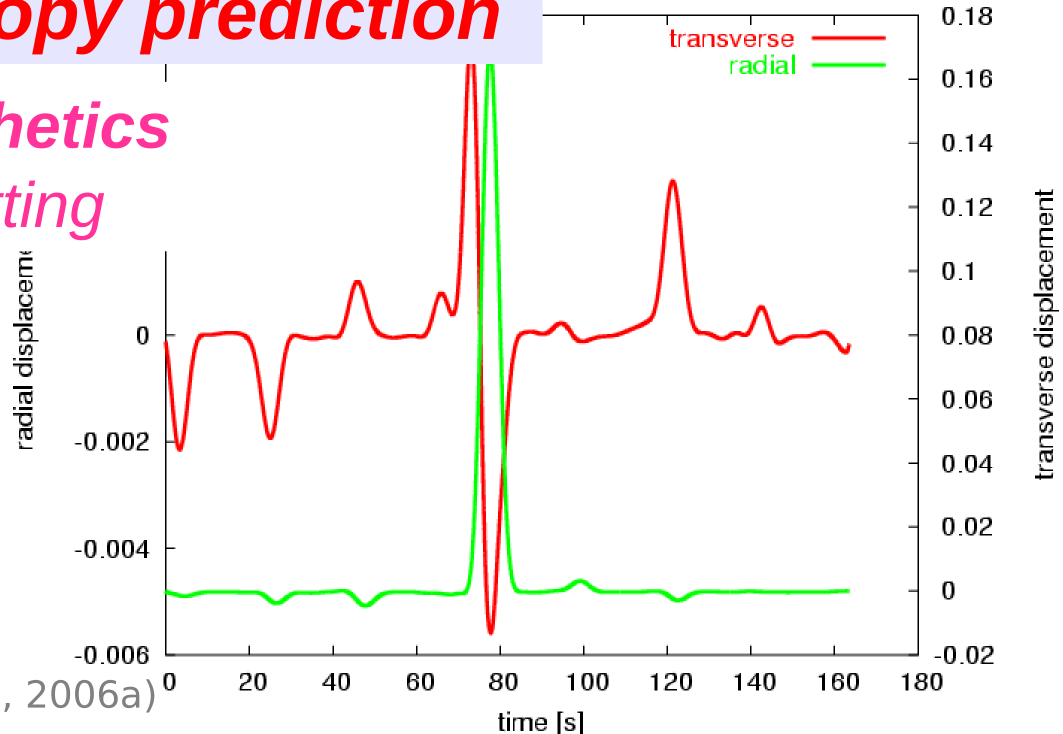

generate synthetic waveforms from 3D anisotropic model

Becker et al. (2006, 2006a)

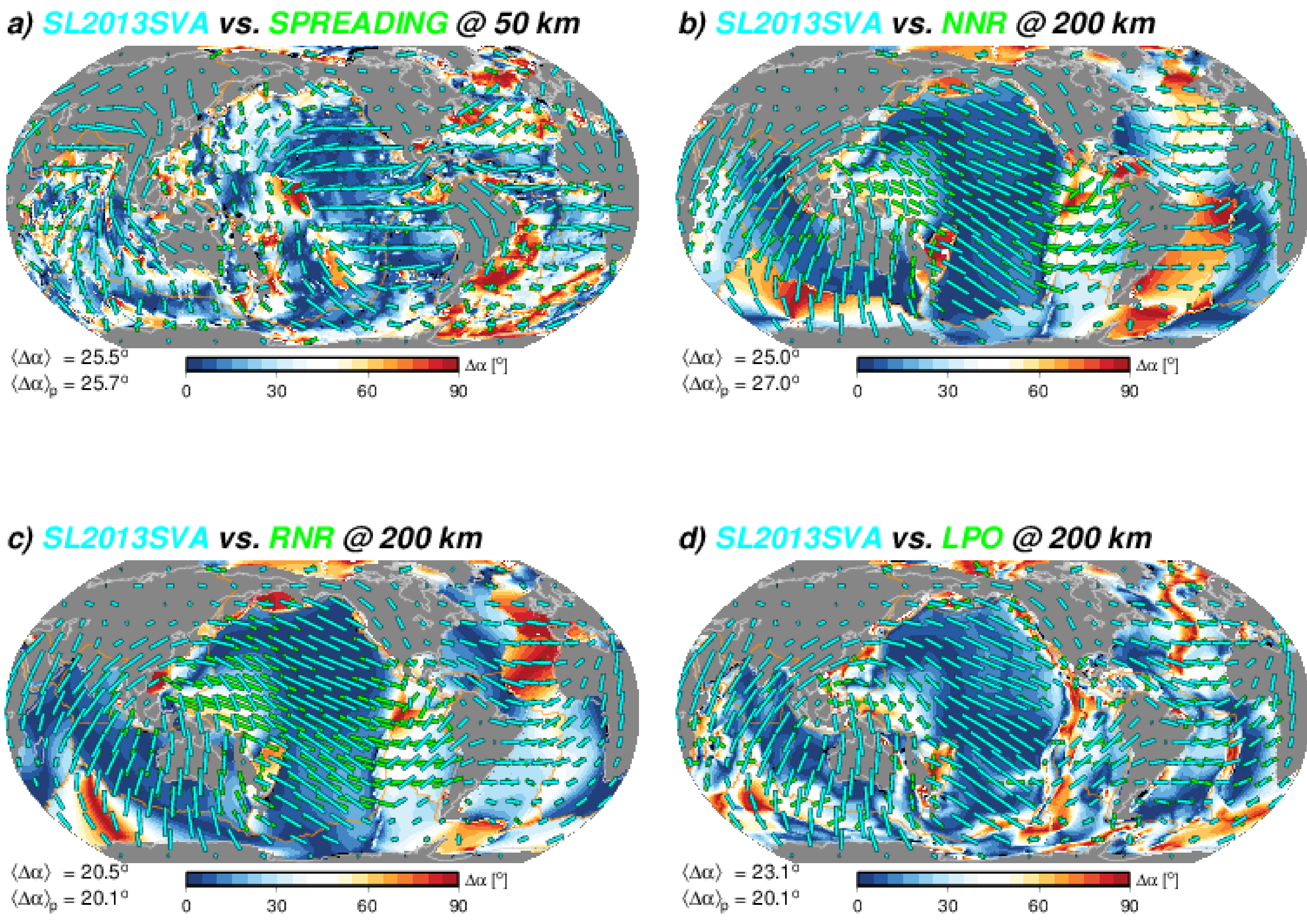

Becker et al. (2014), using SL2013SV

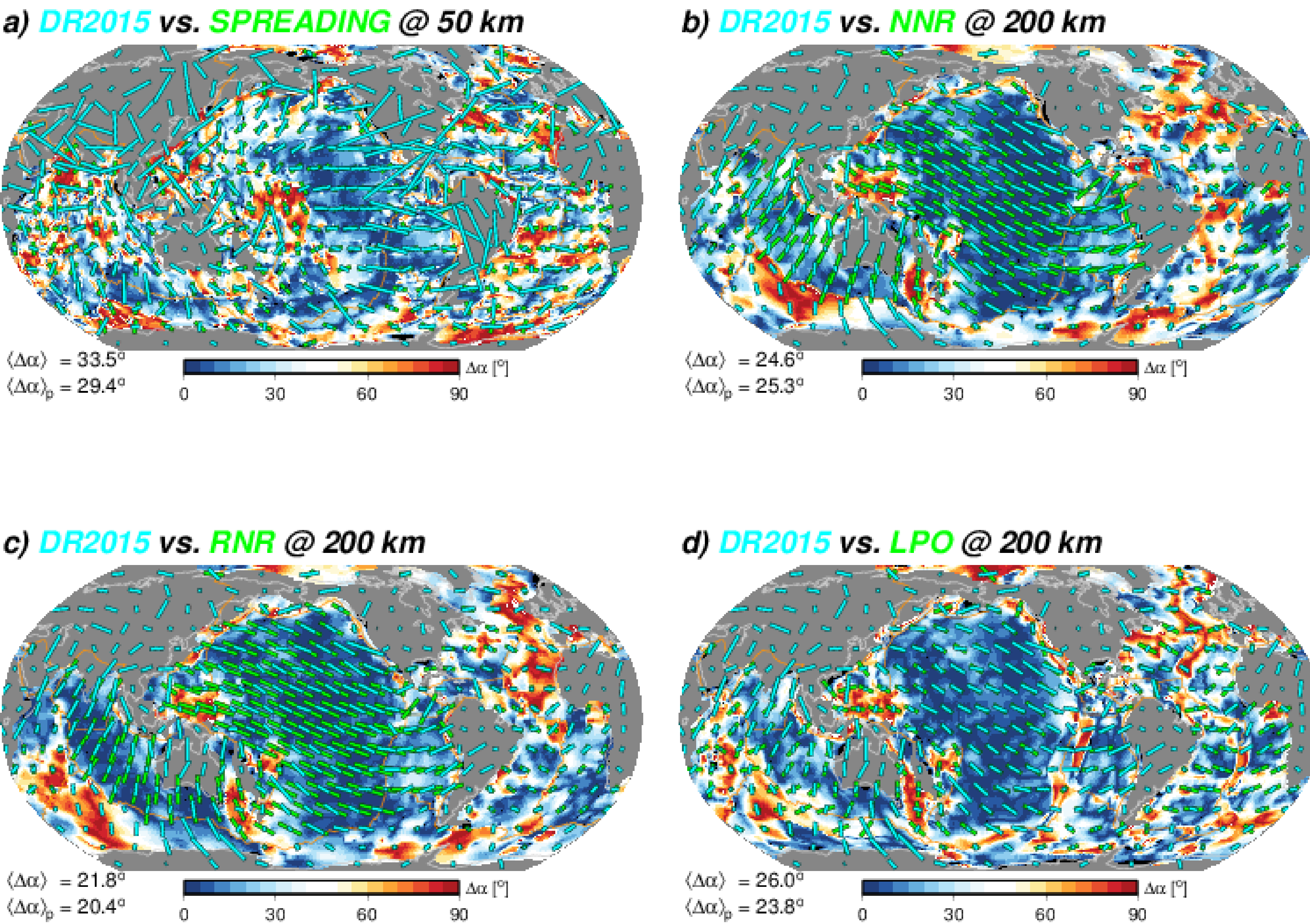

using Debayle et al.'s (2015) model

Test for decoupling layer

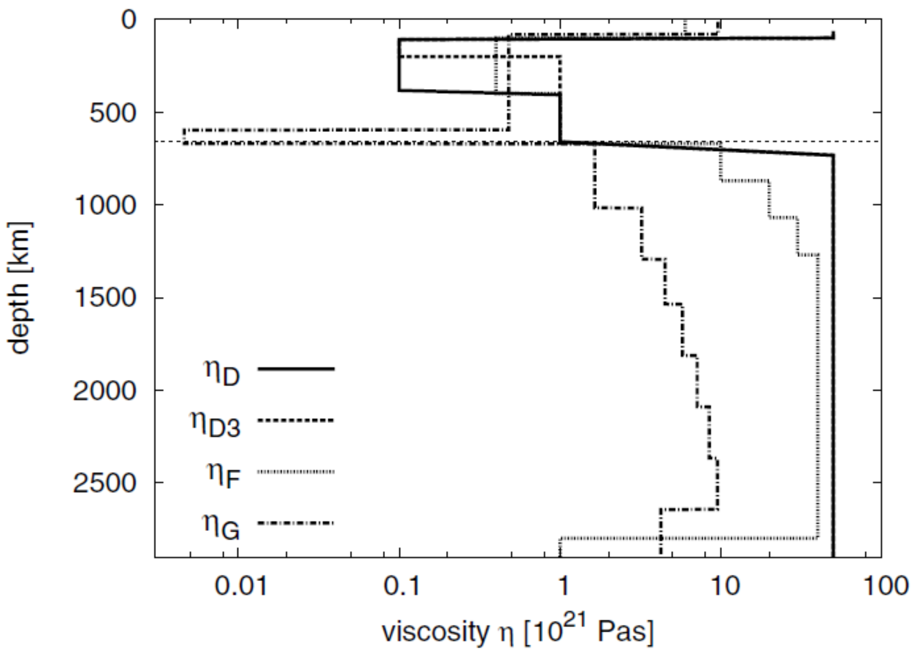

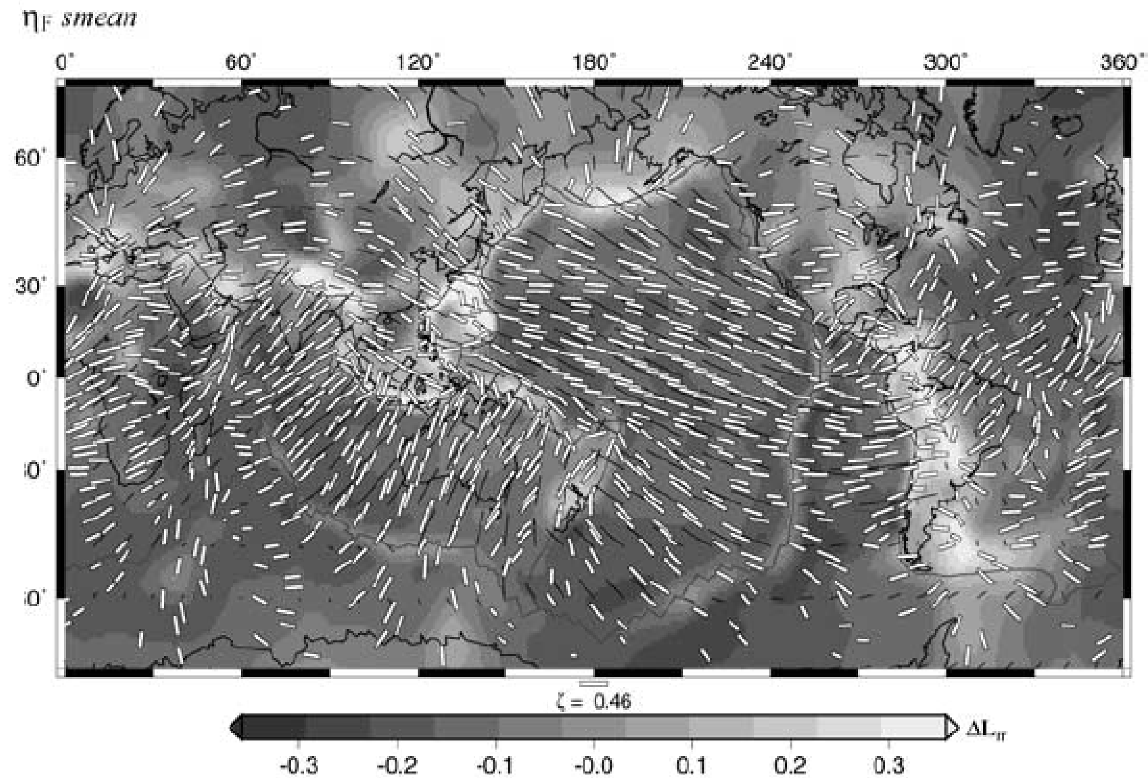

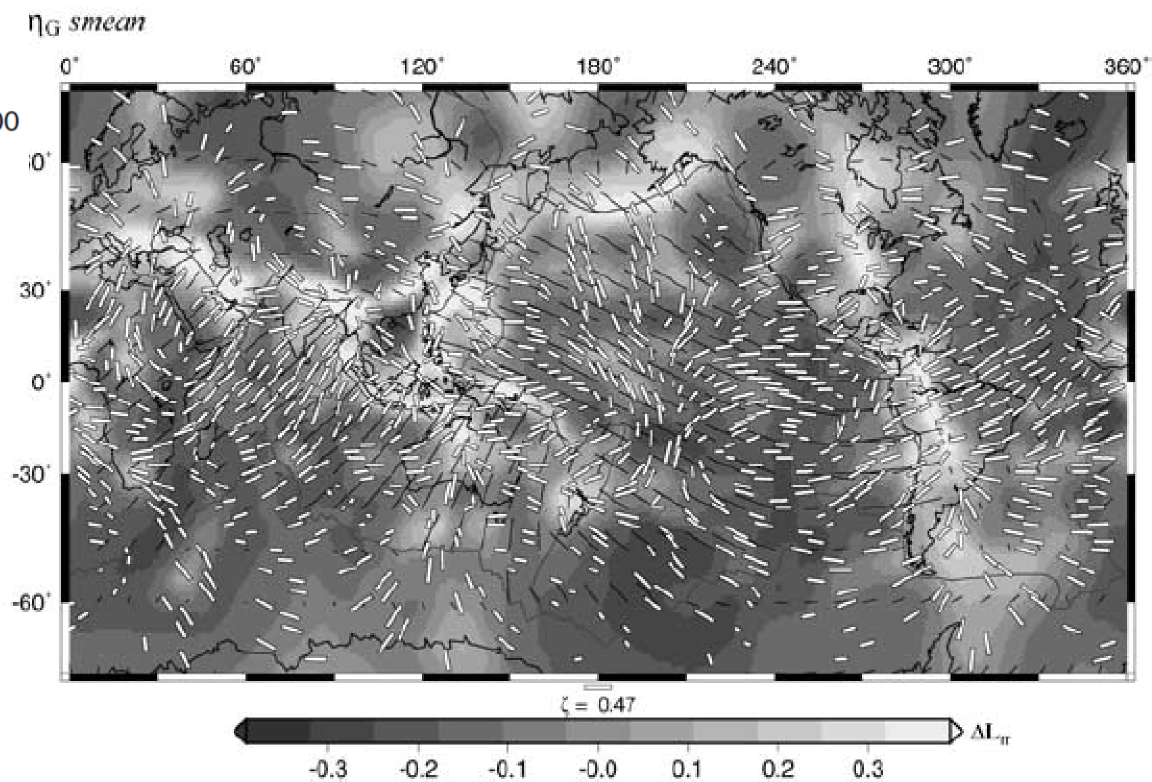

Becker et al. (2003)

Regional *SKS* splitting

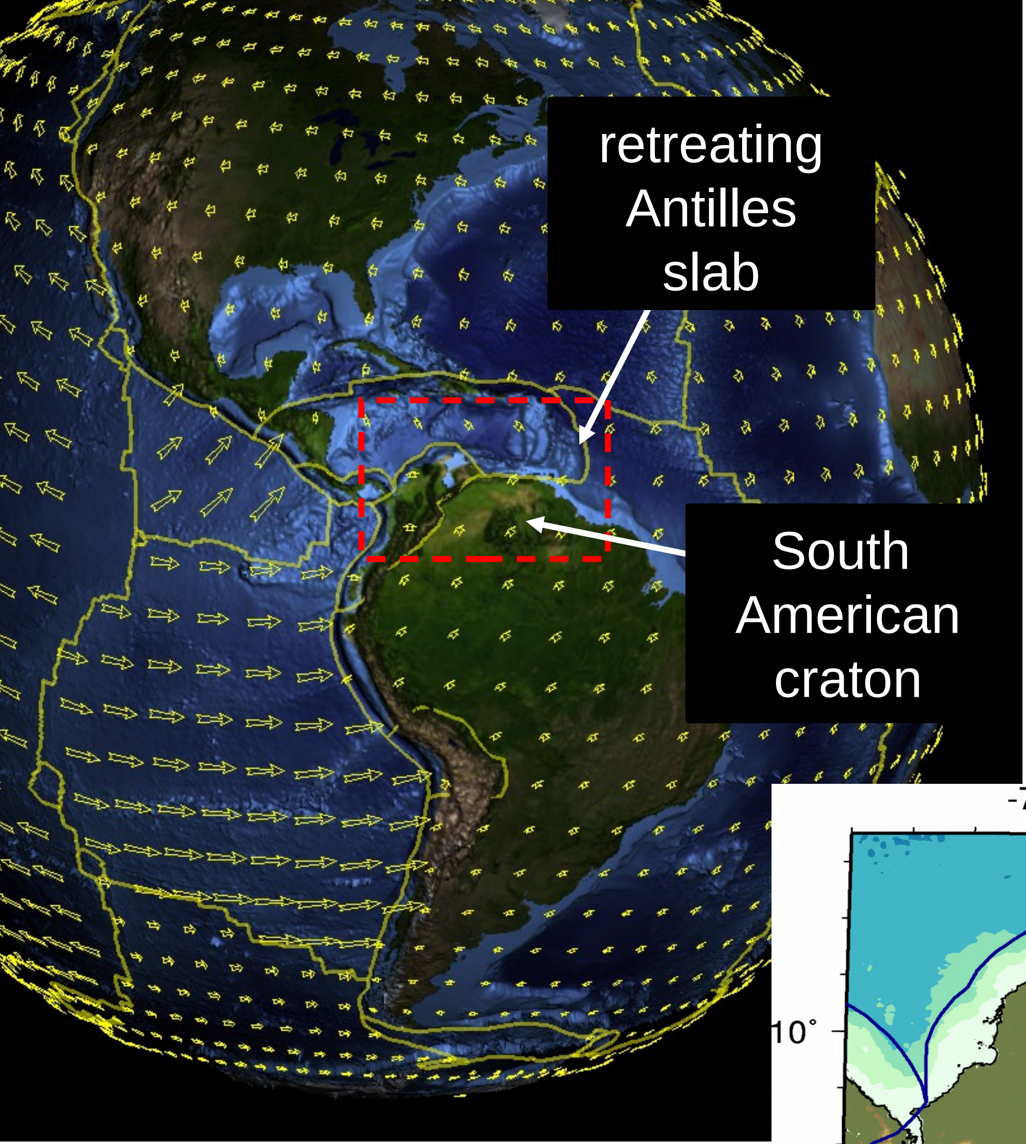

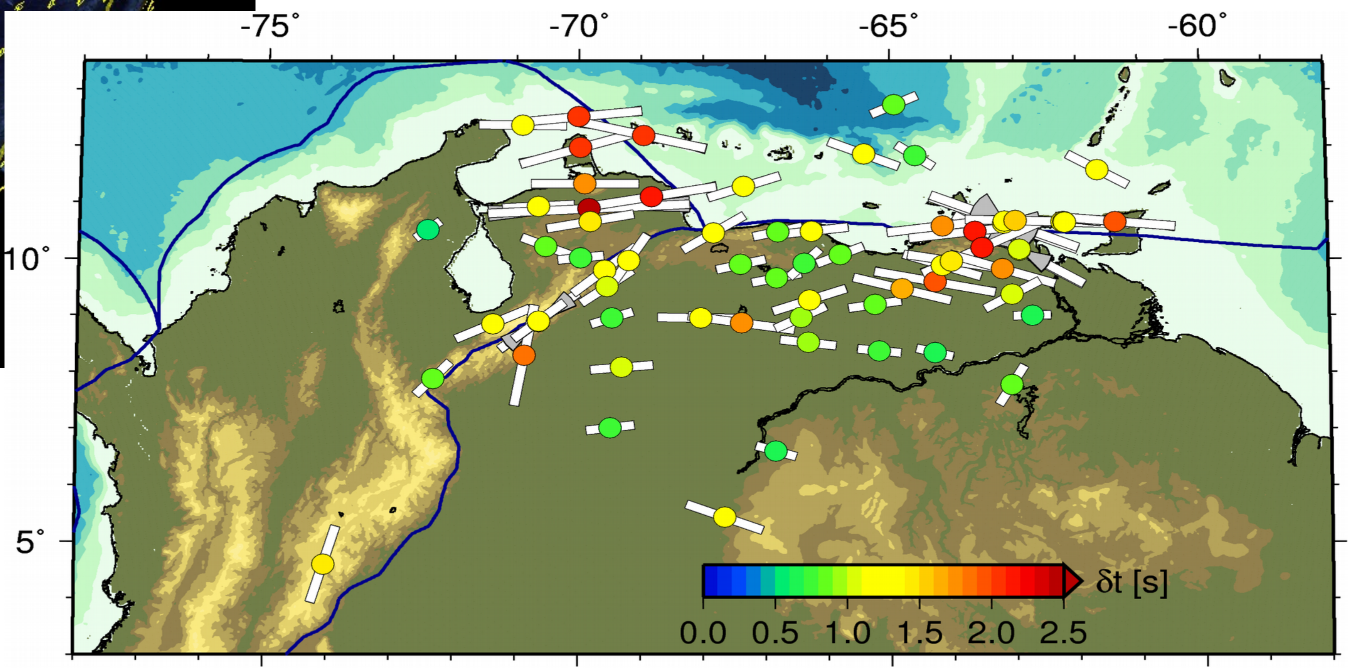

Growdon et al. (2009); Masy et al. (2011)

SKS splitting from reference model (tomography driven)

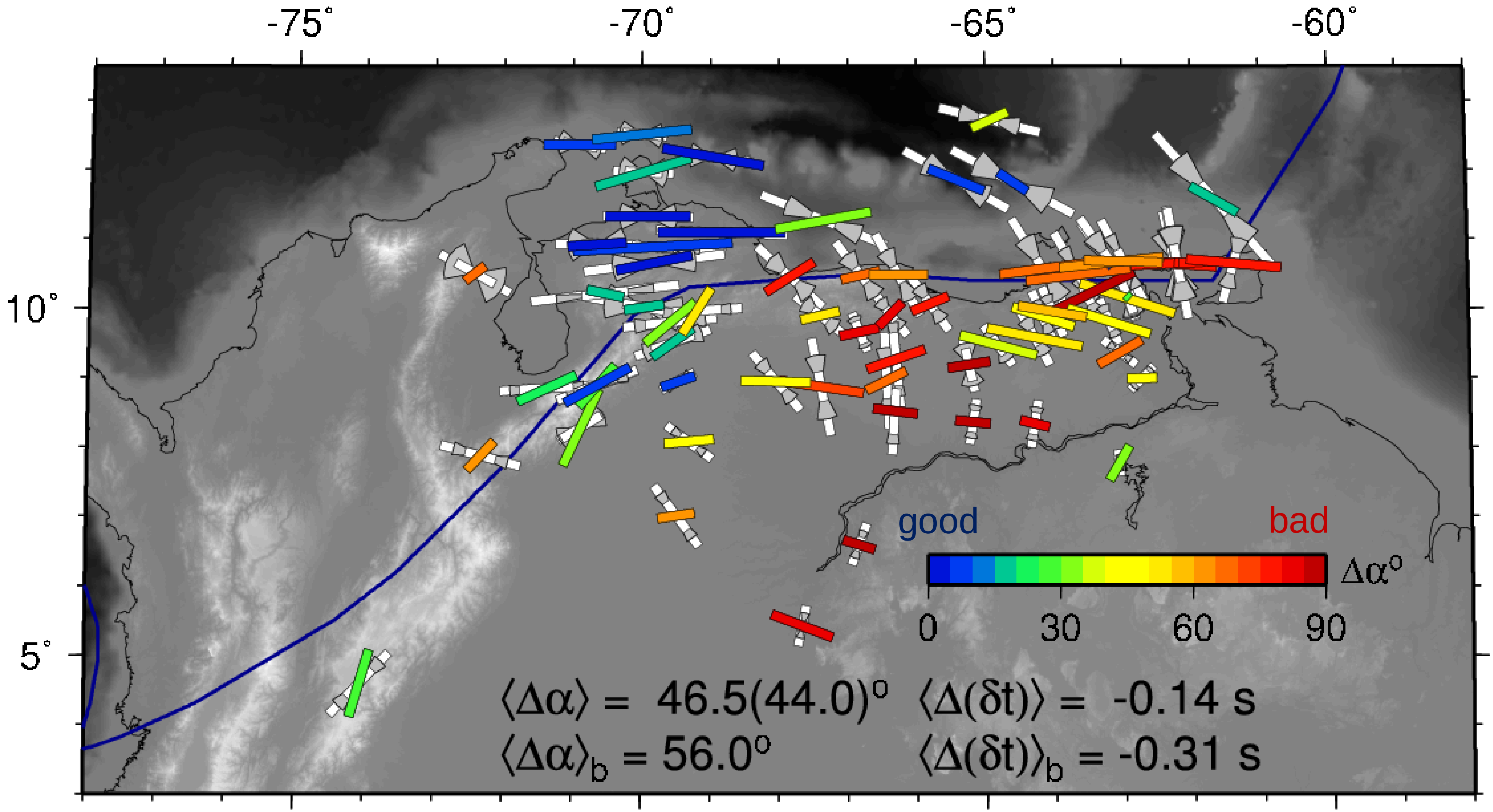

Colored bars: measurements colored by misfit

White bars: predictions from full waveform modeling, wedges indicating back-azimuthal variation of δt, α

Miller and Becker (2012)

Splitting from slab model with a weak asthenosphere and keel

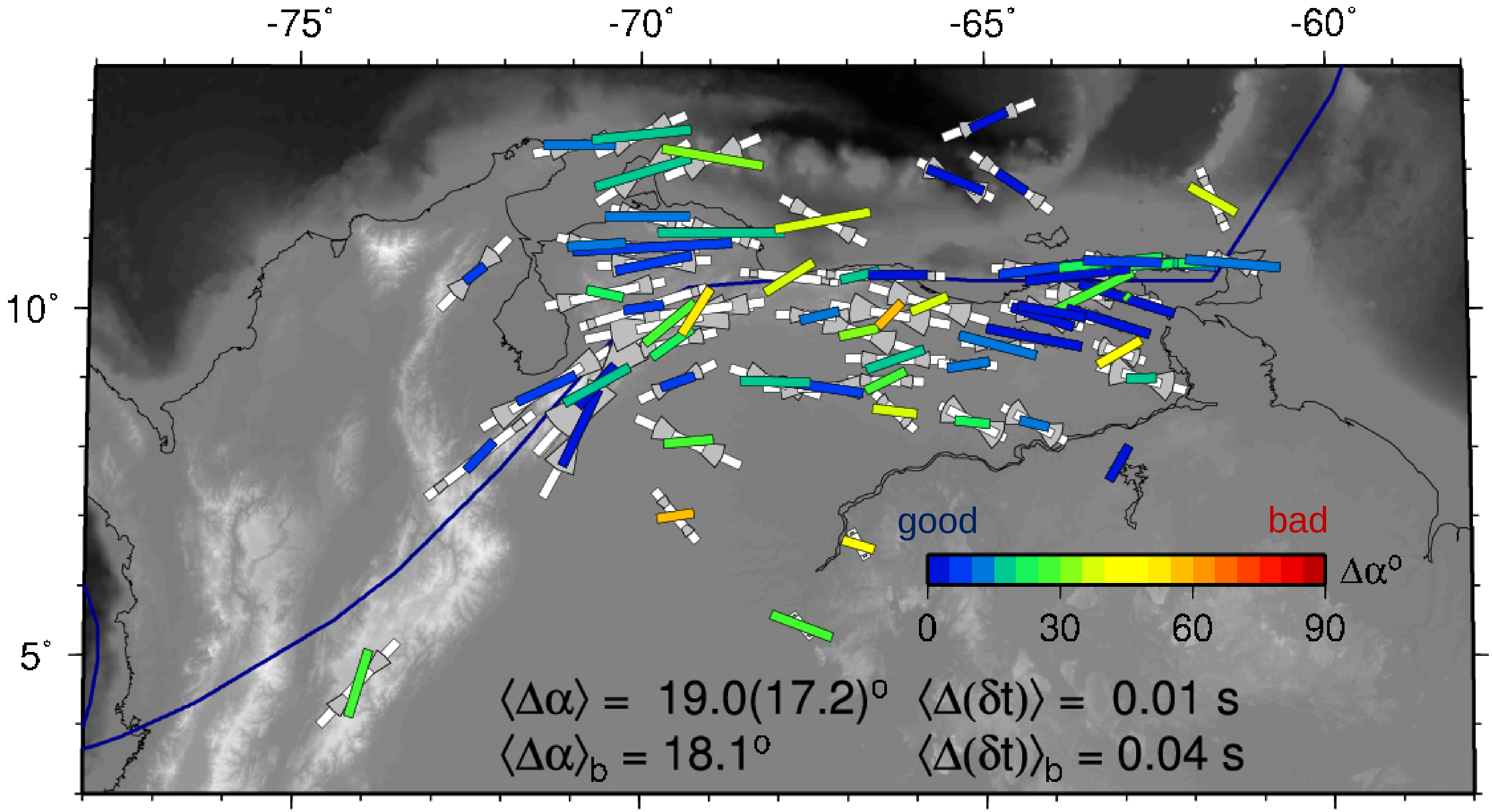

mean angular misfit

mean delay time misfit

Miller and Becker (2012)

Inverse geodynamics:
Regional splitting azimuth misfit

$$u \propto \frac{\Delta \rho}{\eta}$$

viscosity models, η

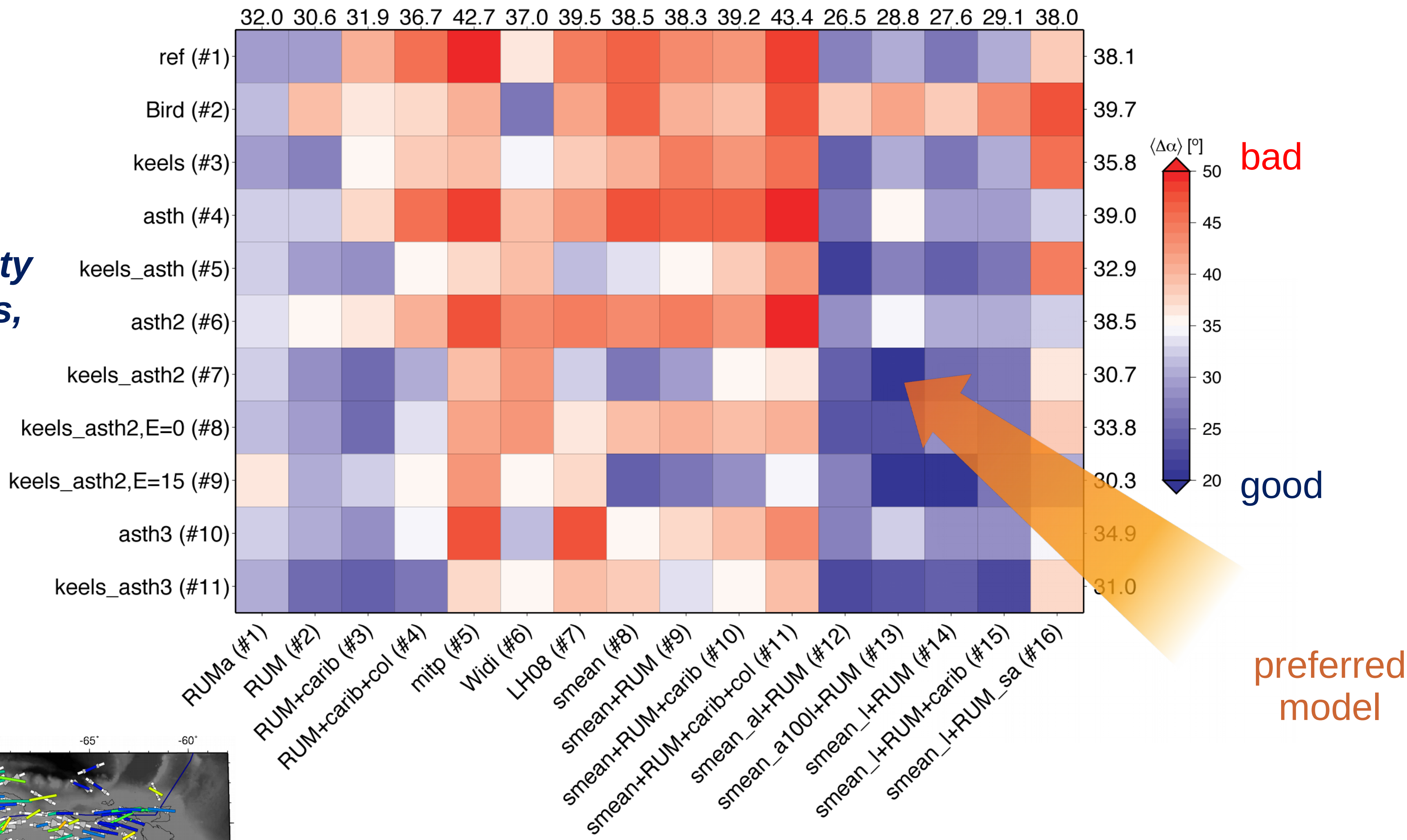

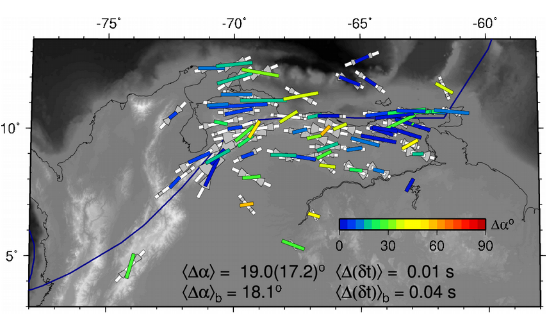

density models, $\Delta\rho$

Miller and Becker (2012)

How to resolve some of the non-uniqueness and uncertainties?

Verticals

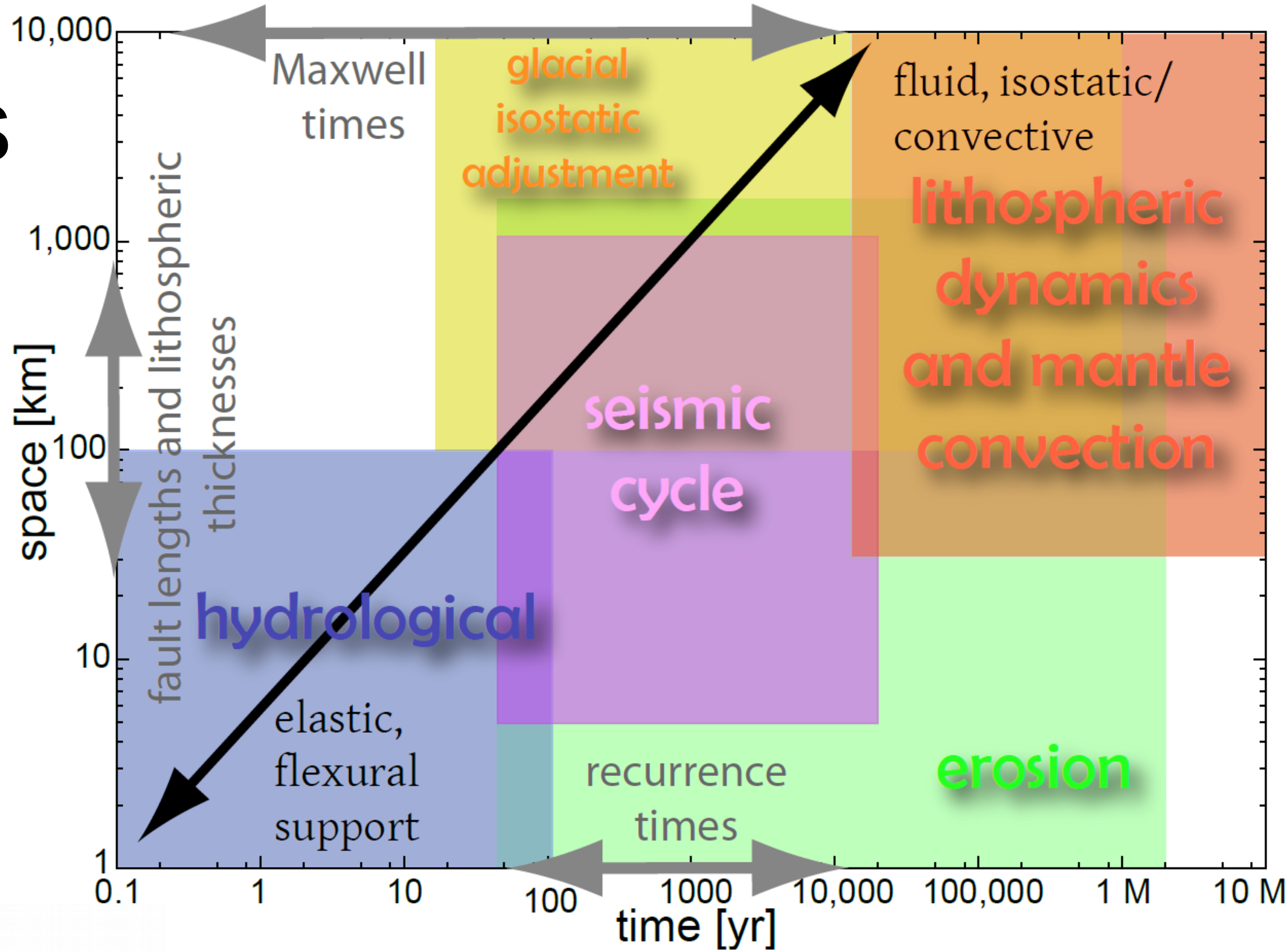

10,000
1,000
100
10
1
0.1
1
10
100
1000
10,000
100,000
1 M
10 M
space [km]
time [yr]
Maxwell times
glacial isostatic adjustment
fluid, isostatic/ convective
lithospheric dynamics and mantle convection
fault lengths and lithospheric thicknesses
seismic cycle
hydrological
elastic, flexural support
recurrence times
erosion

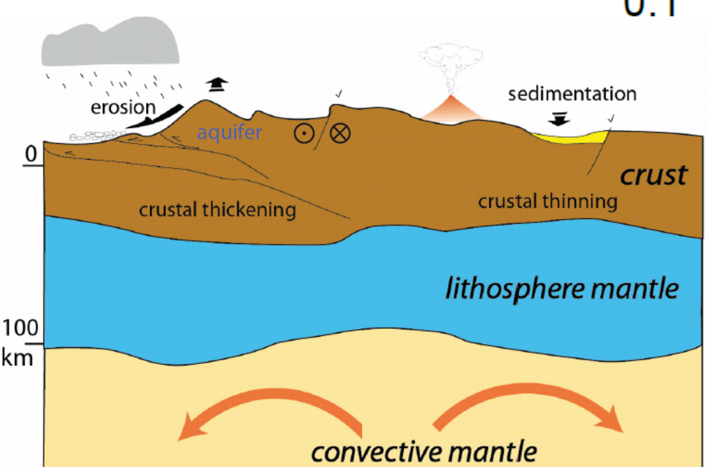

erosion
aquifer
sedimentation
0
crust
crustal thickening
crustal thinning
lithosphere mantle
100 km
convective mantle

co-seismic

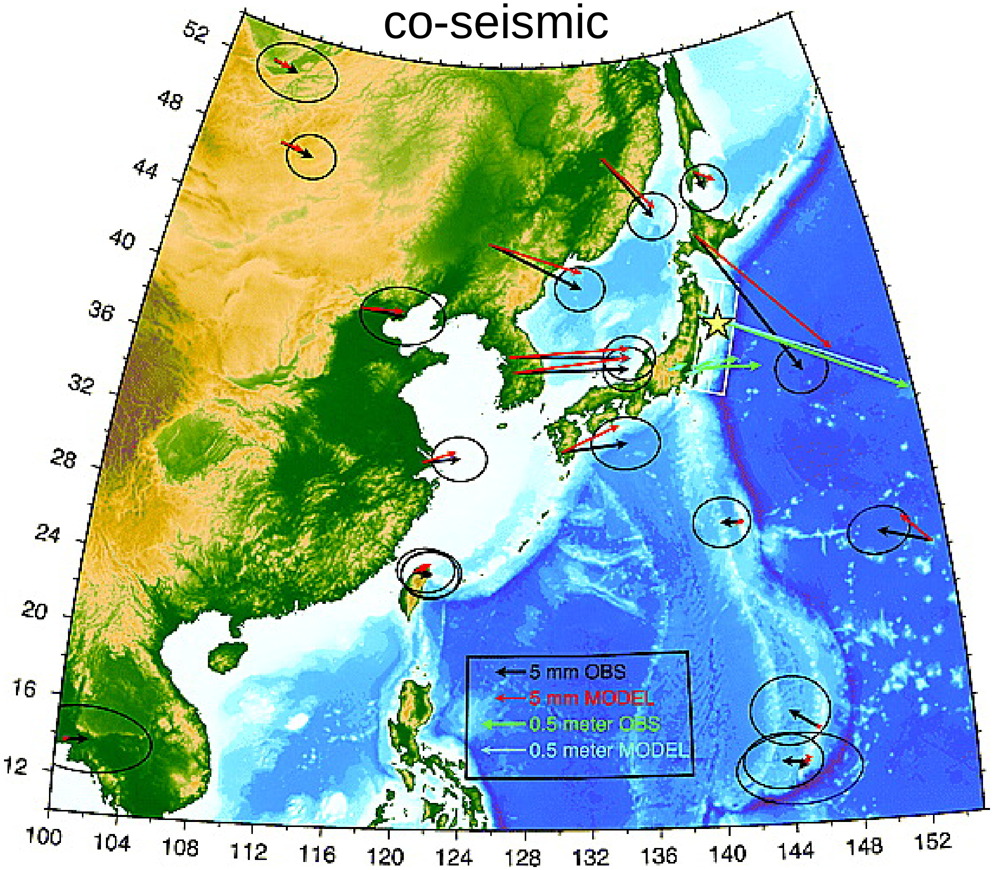

post-seismic
cumulative
(3 years)

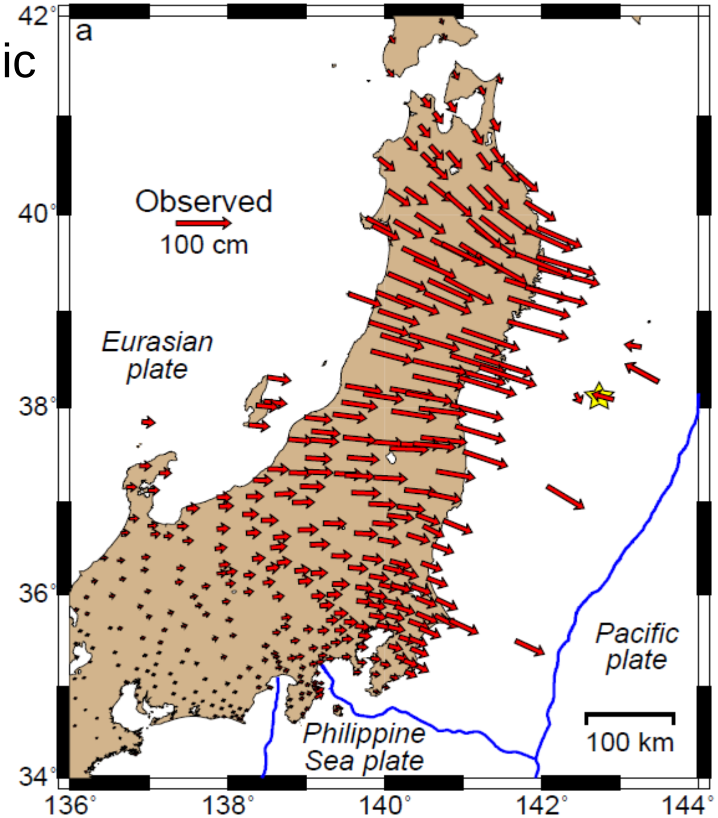

2011
Tohoku M9

Pollitz et al. (2011)

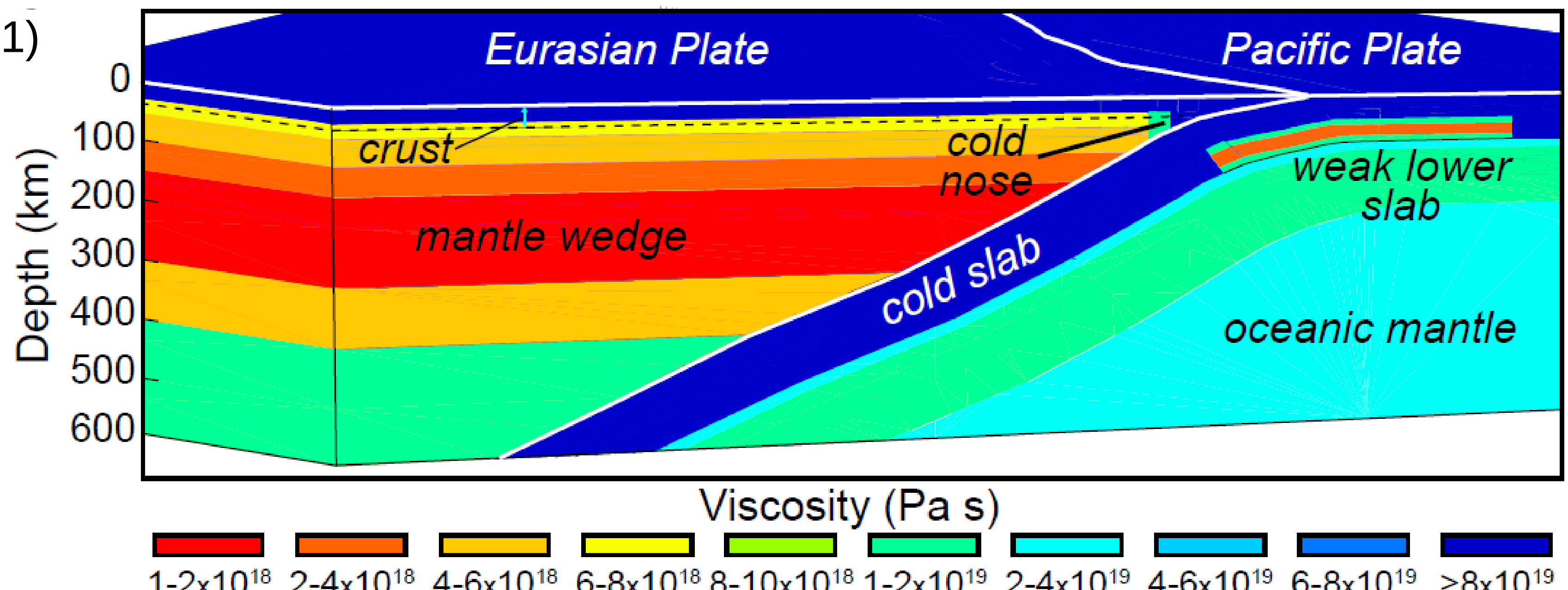

Freed et al. (submitted)

Geodynamic inversions

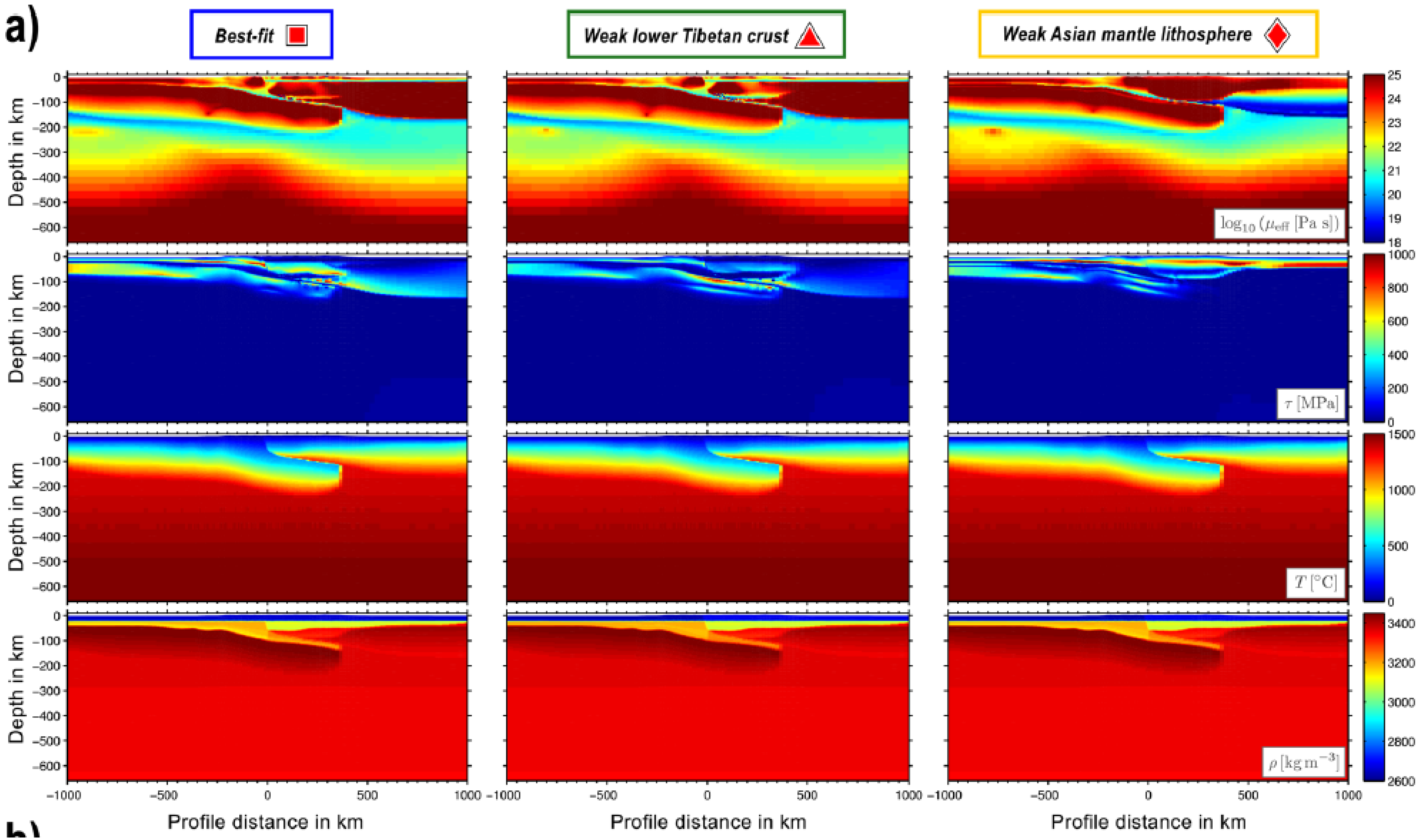

Baumann and Kaus (2015)

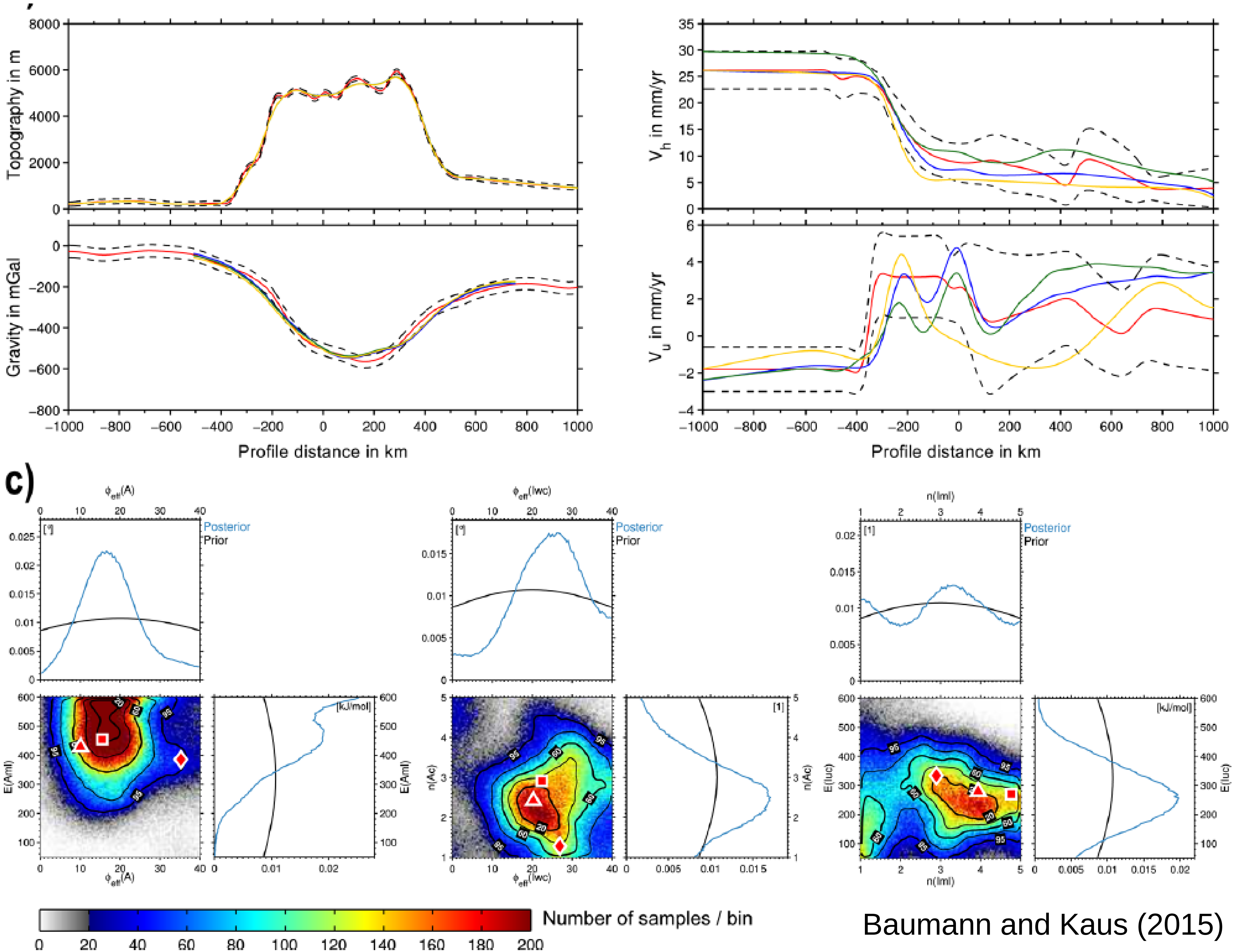

Baumann and Kaus (2015)

State of affairs

- Can explain plate velocities, geoid, dynamic topography and ~seismic anisotropy with global mantle circulation models
- Provides constraints on rheology and effective density distribution, needed to understand terrestrial planet evolution
- Frontiers: Time evolution and continental dynamics, e.g.
    - predict intraplate deformation
    - experimental design/hypothesis testing

Additional slides

Seismic anisotropy

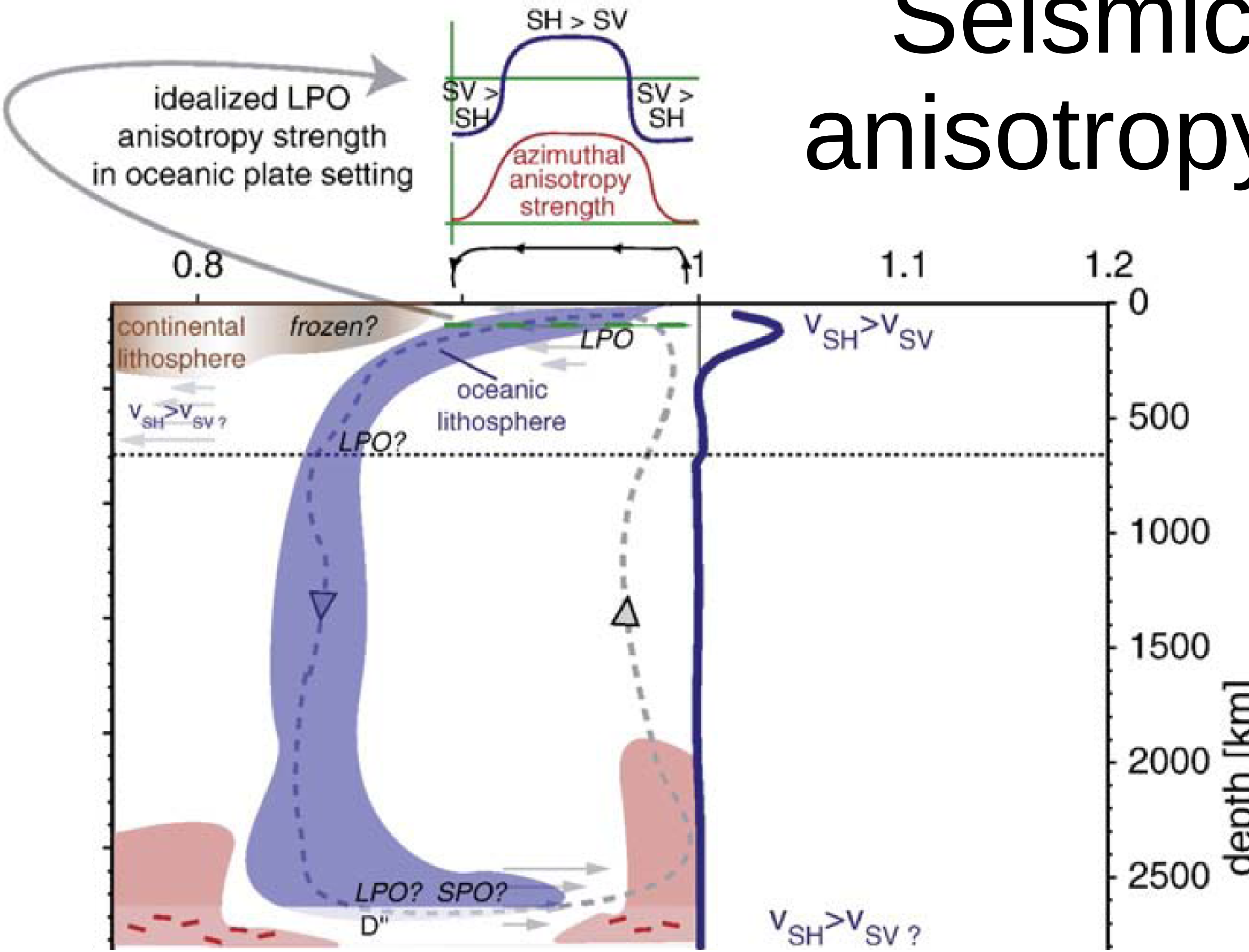

Long and Becker (2010)

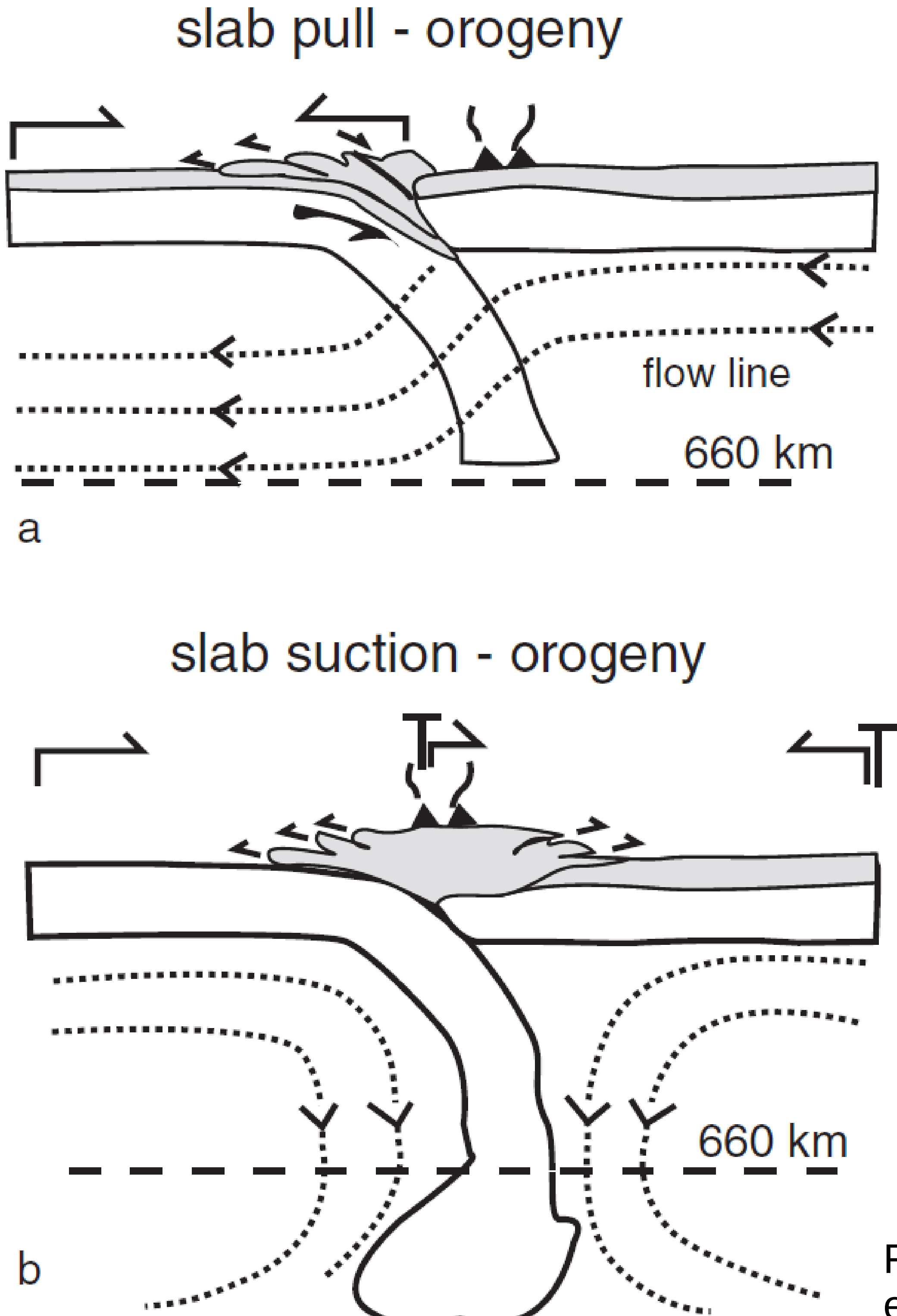

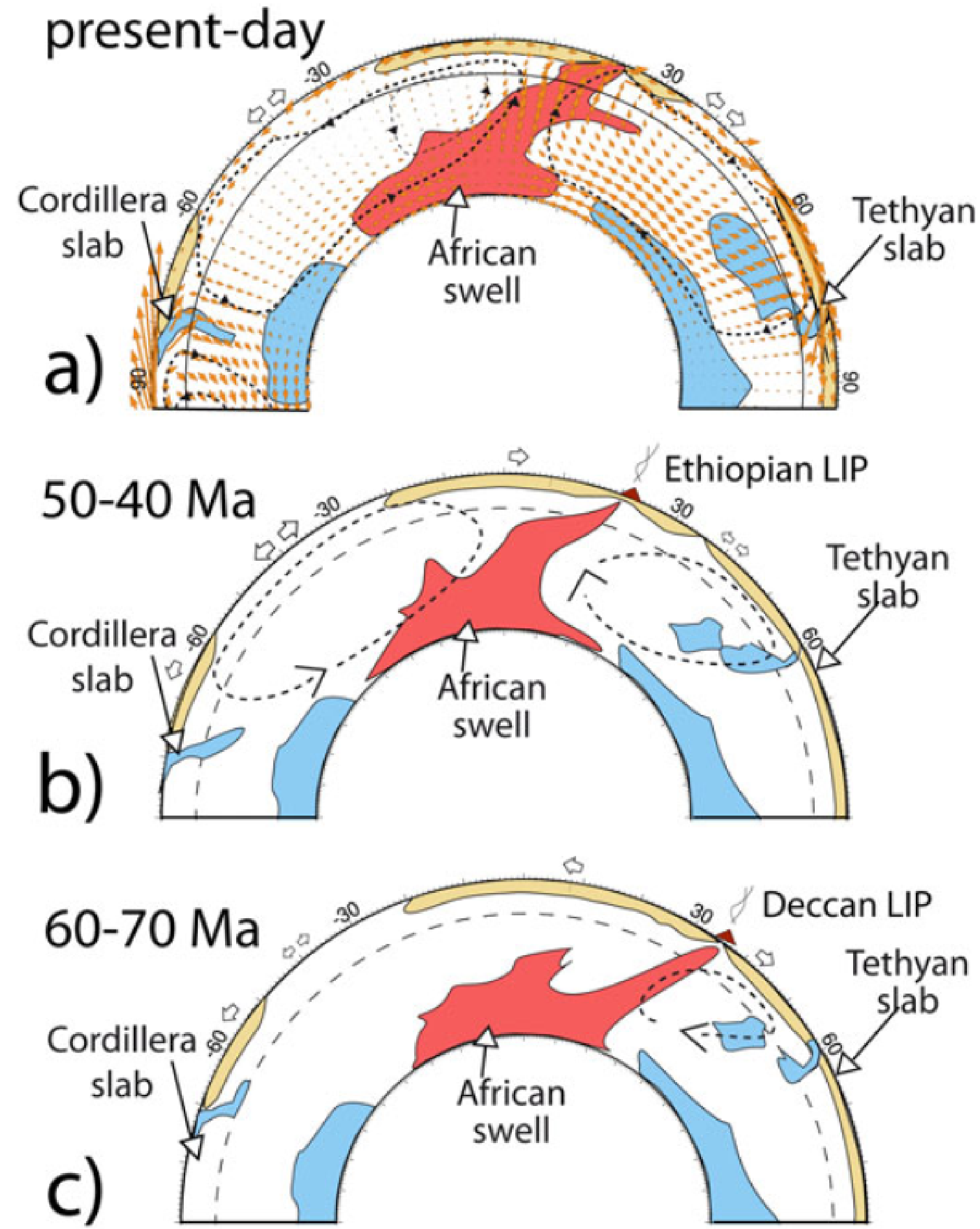

Faccenna et al. (2013)

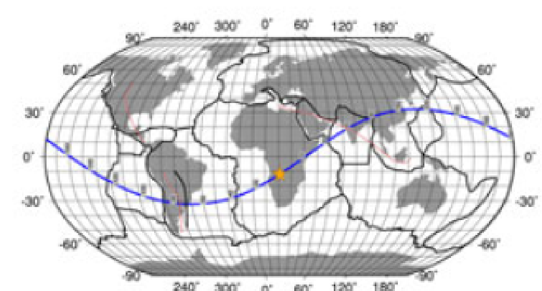

Residual topography models

Hoggard et al. (2016)

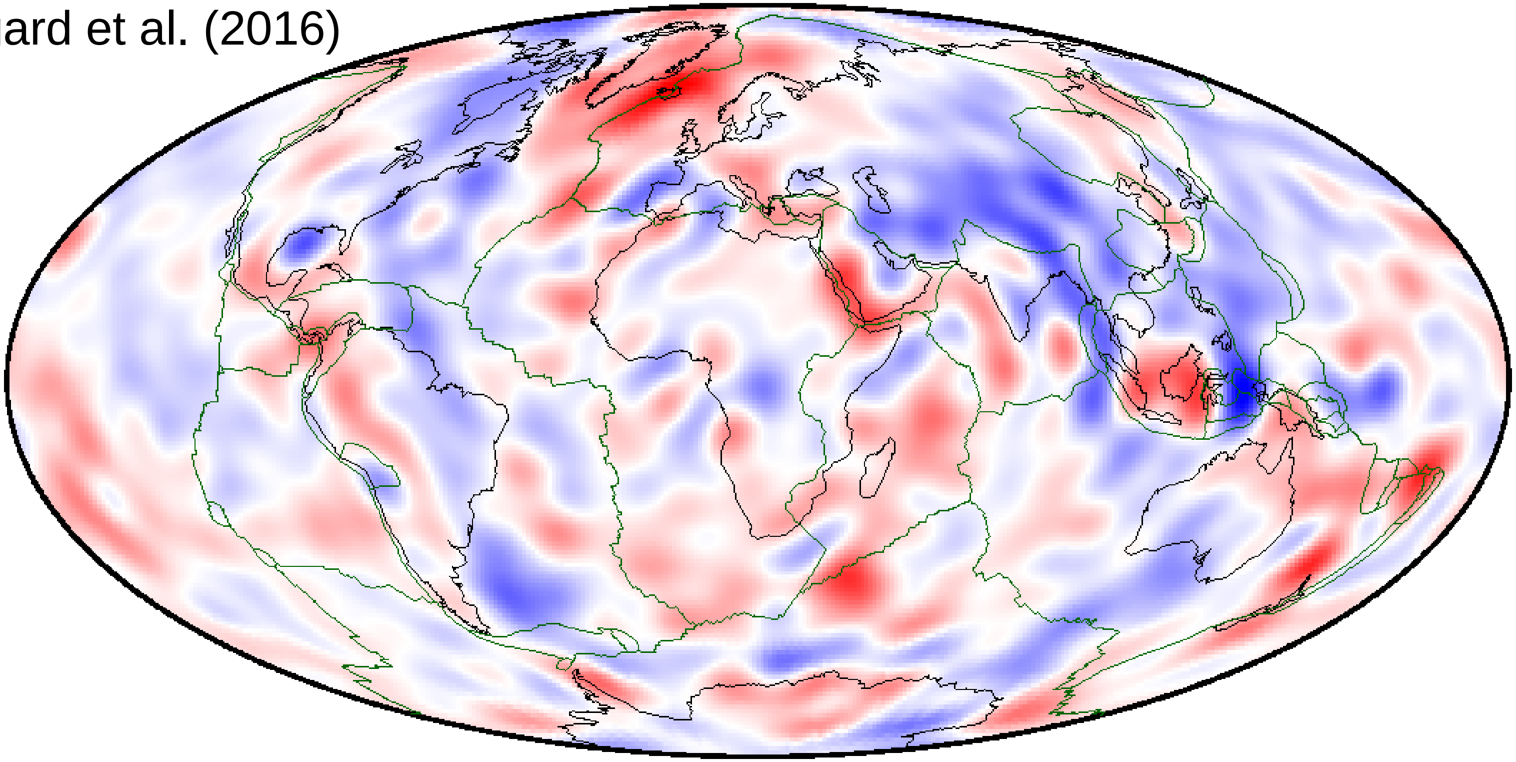

crust for sparse, oceanic sites from active source, corrected to plate model, *continental areas from free-air*

Steinberger (2016)

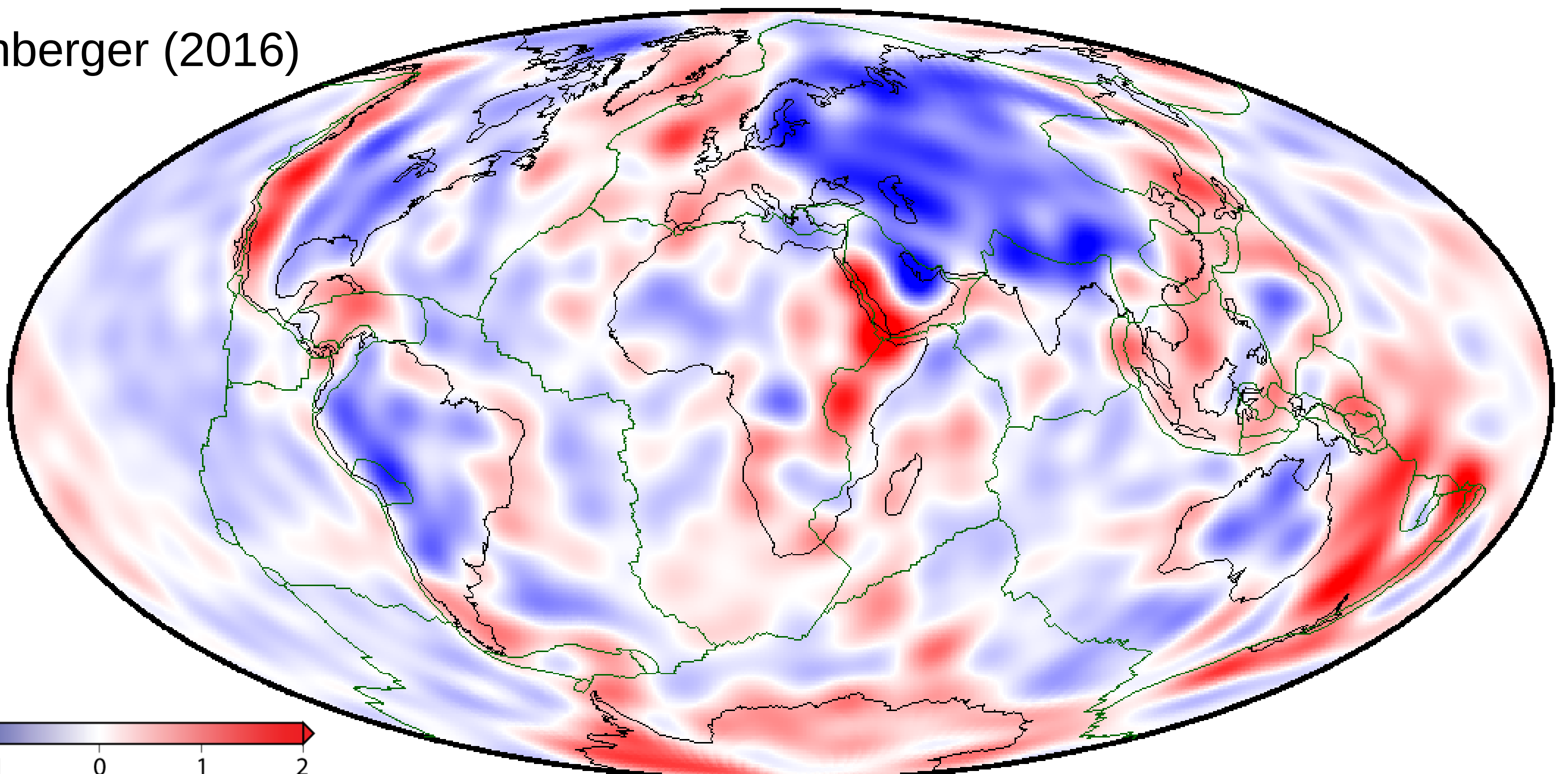

crust from CRUST1, lithospheric Model, corrected for half-space cooling

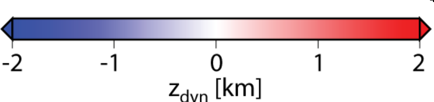

Admittance != constant

$$\frac{\text{gravity}}{\text{dynamic surface topography}} = \text{Dynamic Admittance}$$

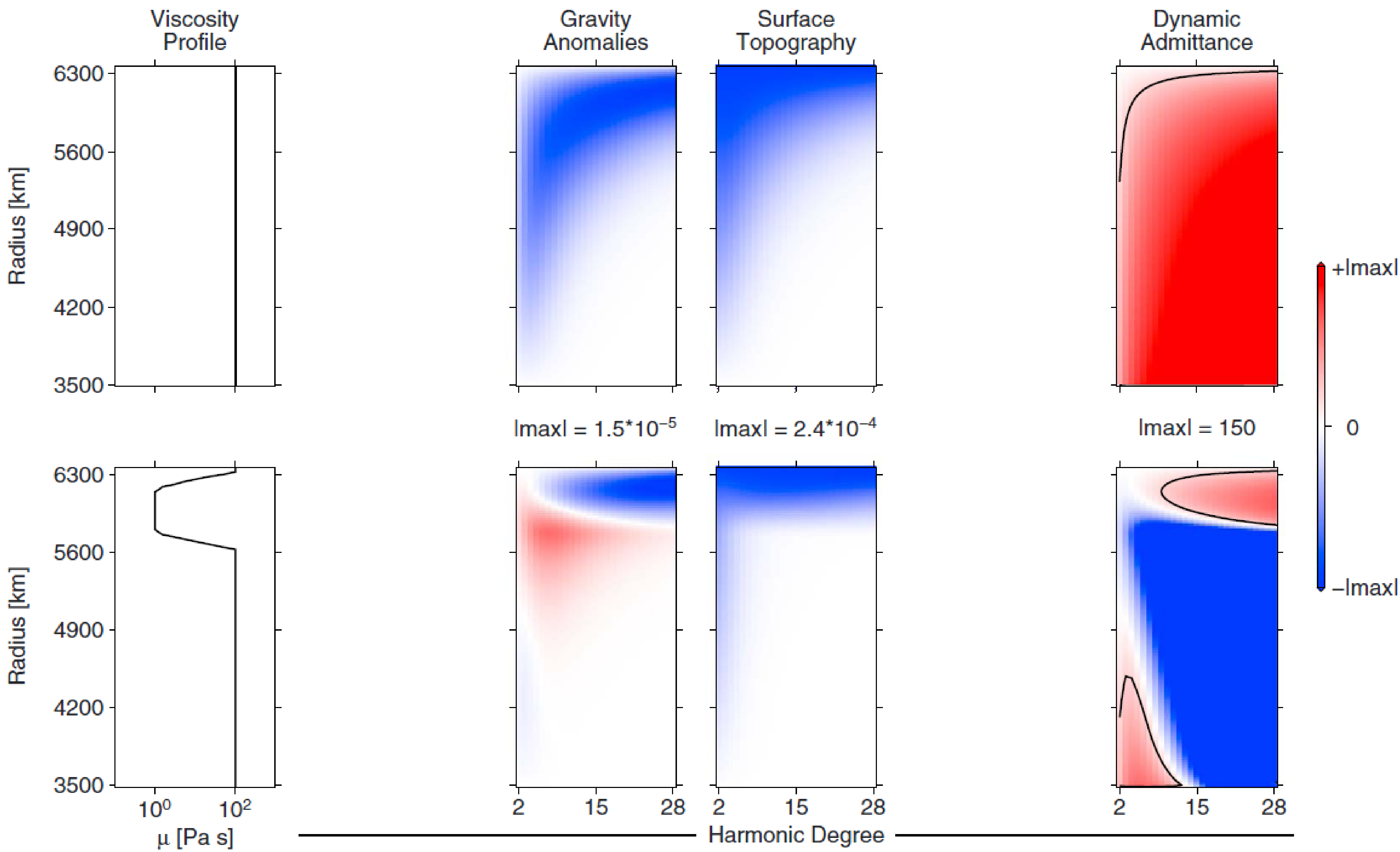

(CIDER supported...)

Colli et al. (2016) cf. Hager & Richardson (1984); Ricard (1984)

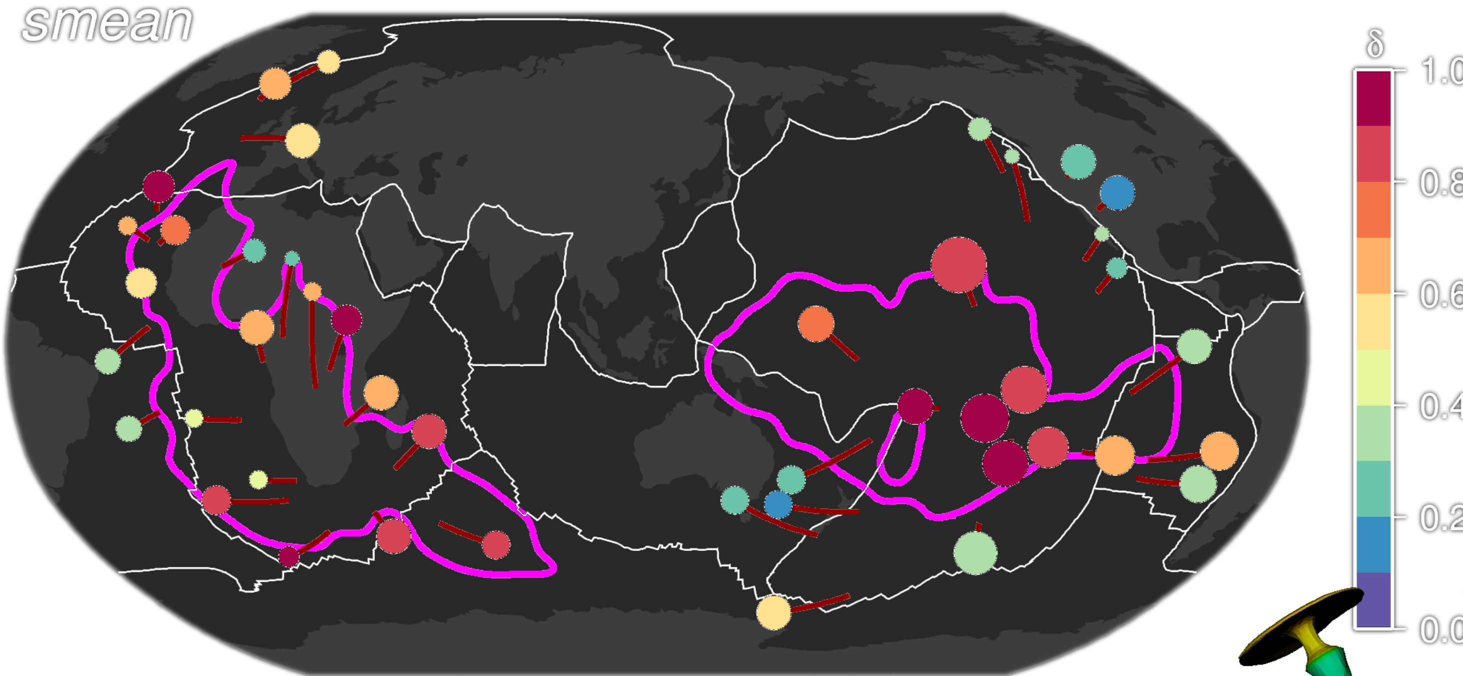

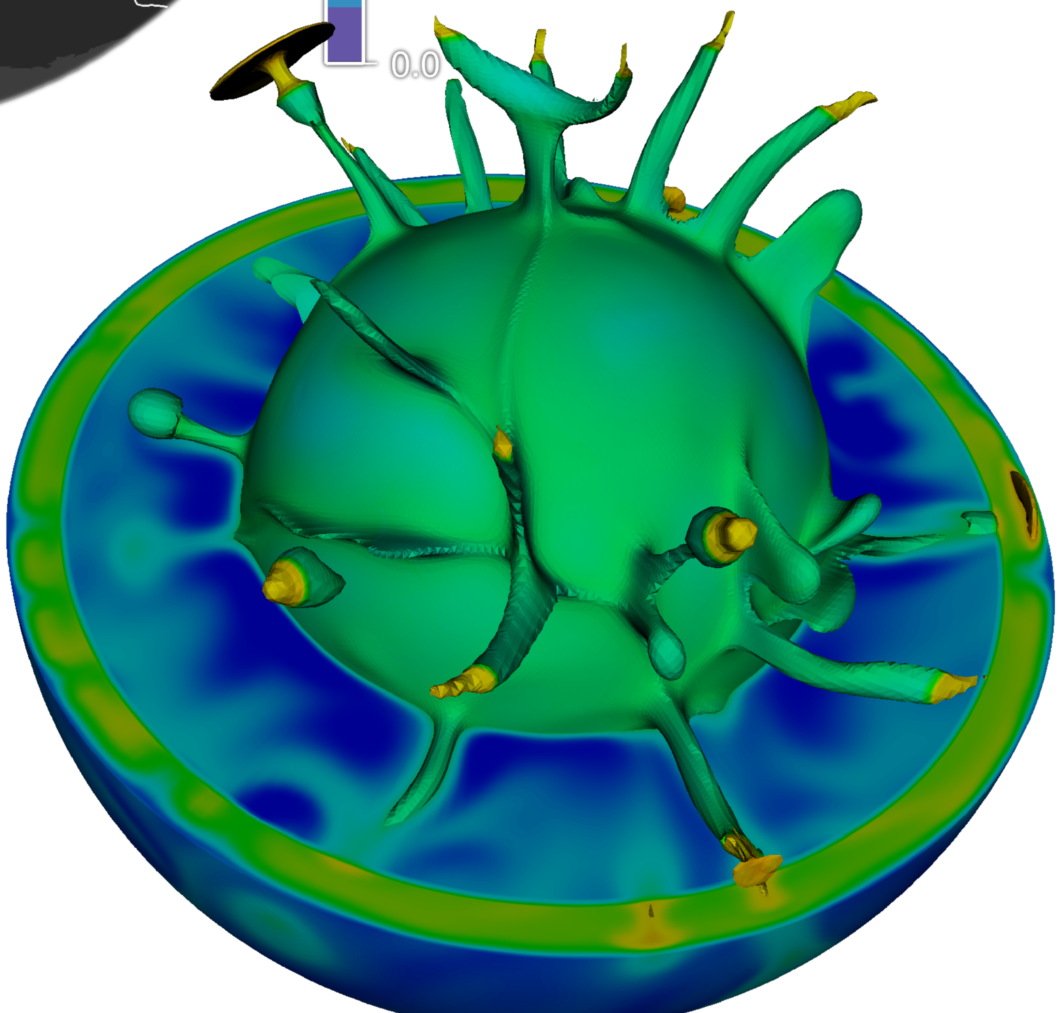

Steinberger and O'Connell (1998)
Steinberger and Arntretter (2006)
Boschi et al. (2007, 2008)

Prediction of plate scores with LVVs

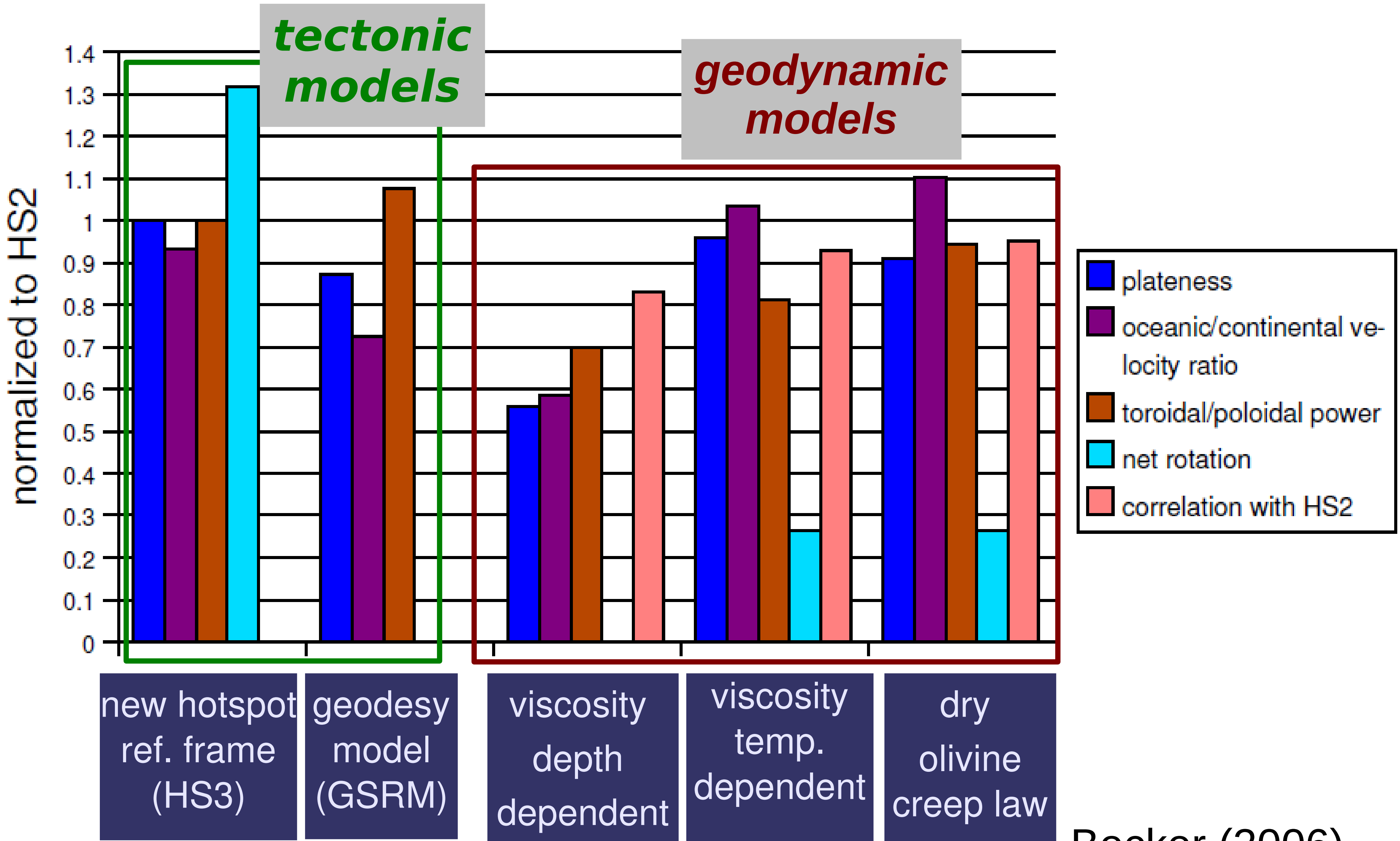

Becker (2006)

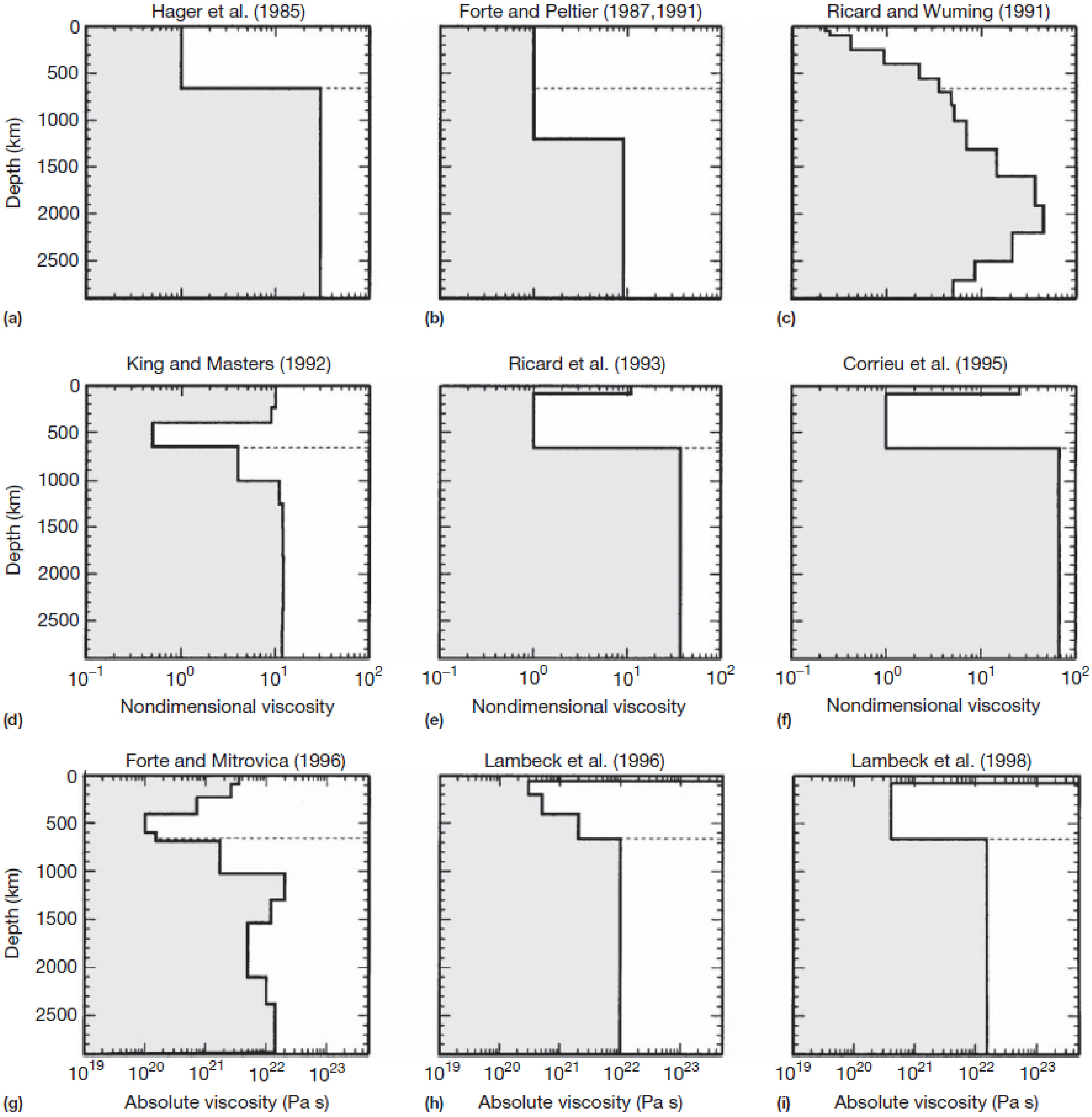

Hager et al. (1985)
Forte and Peltier (1987,1991)
Ricard and Wuming (1991)
King and Masters (1992)
Ricard et al. (1993)
Corrieu et al. (1995)
Forte and Mitrovica (1996)
Lambeck et al. (1996)
Lambeck et al. (1998)
Depth (km)
Nondimensional viscosity
Absolute viscosity (Pa s)
(a)
(b)
(c)
(d)
(e)
(f)
(g)
(h)
(i)

Forte (2015)

Geoid for tomography driven flow

- Lower mantle stiffer

geoid prediction

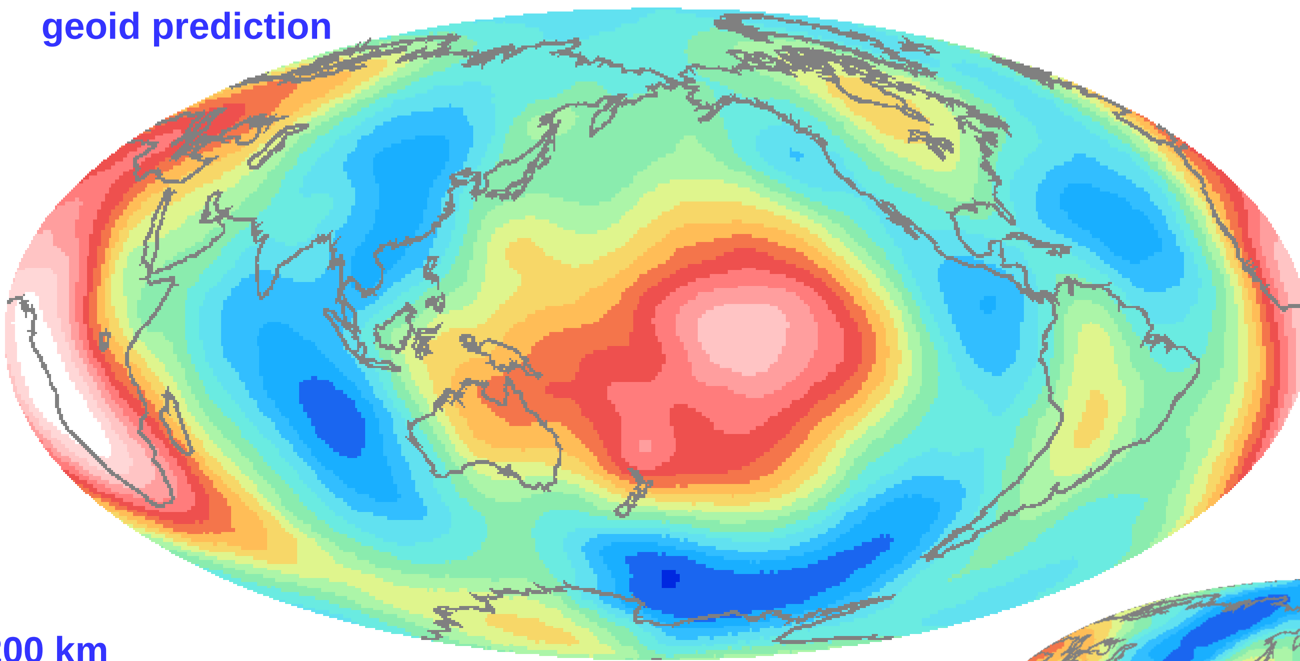

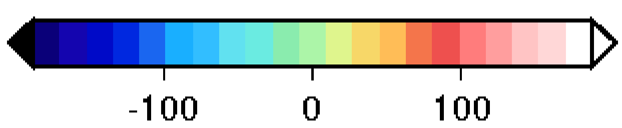

tomography @ 1200 km

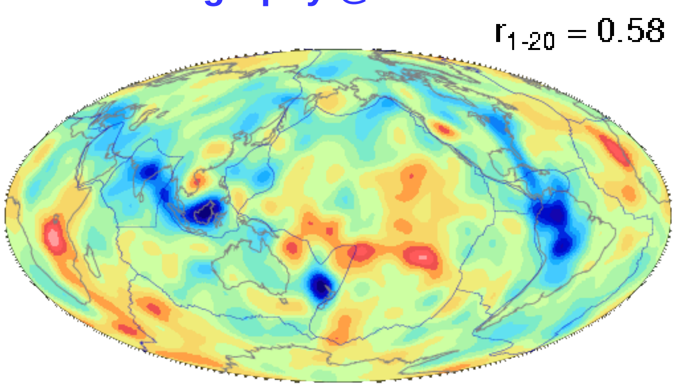

observed geoid

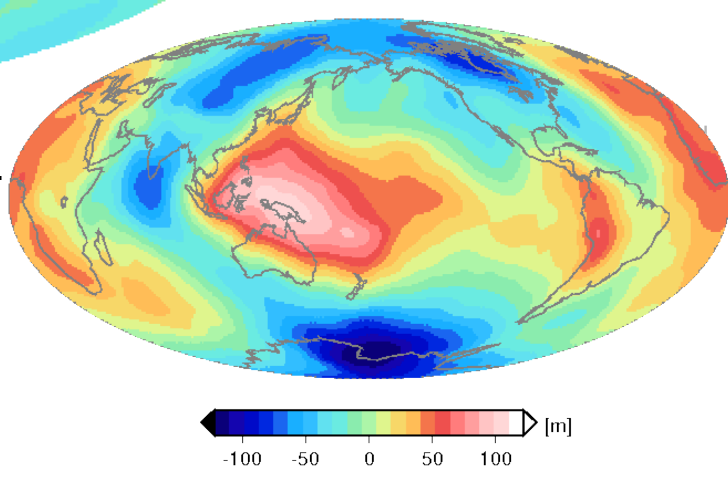

$$R = \eta_1/\eta_2$$

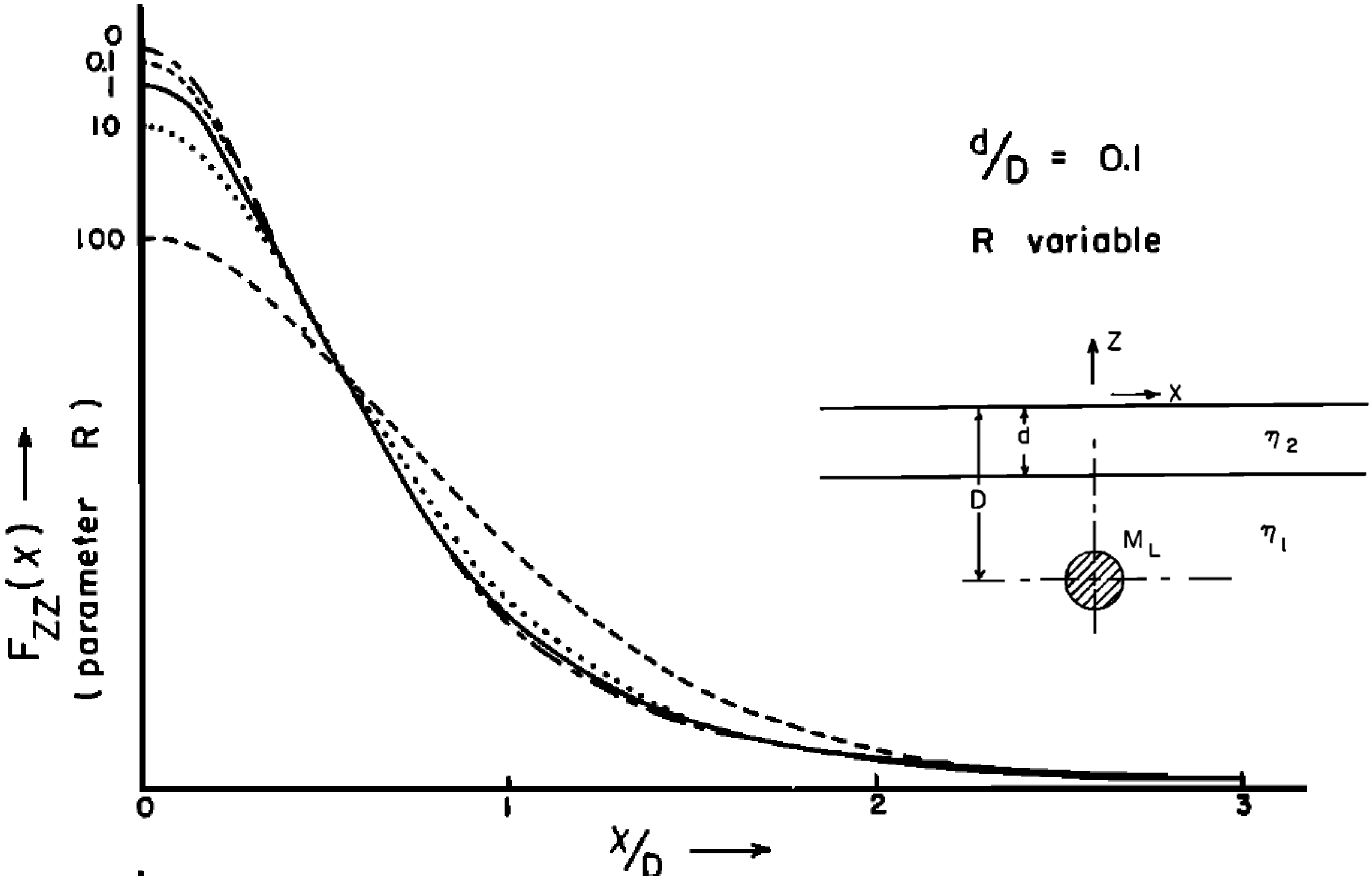

Morgan (1968)

Topography is about knowing the structure and the history, and not so much LVVs

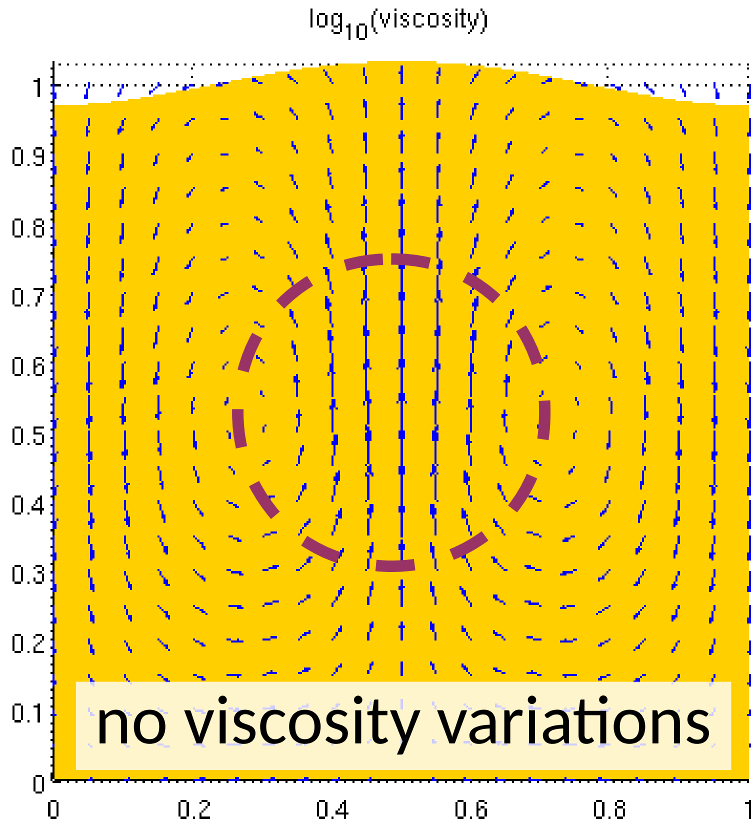

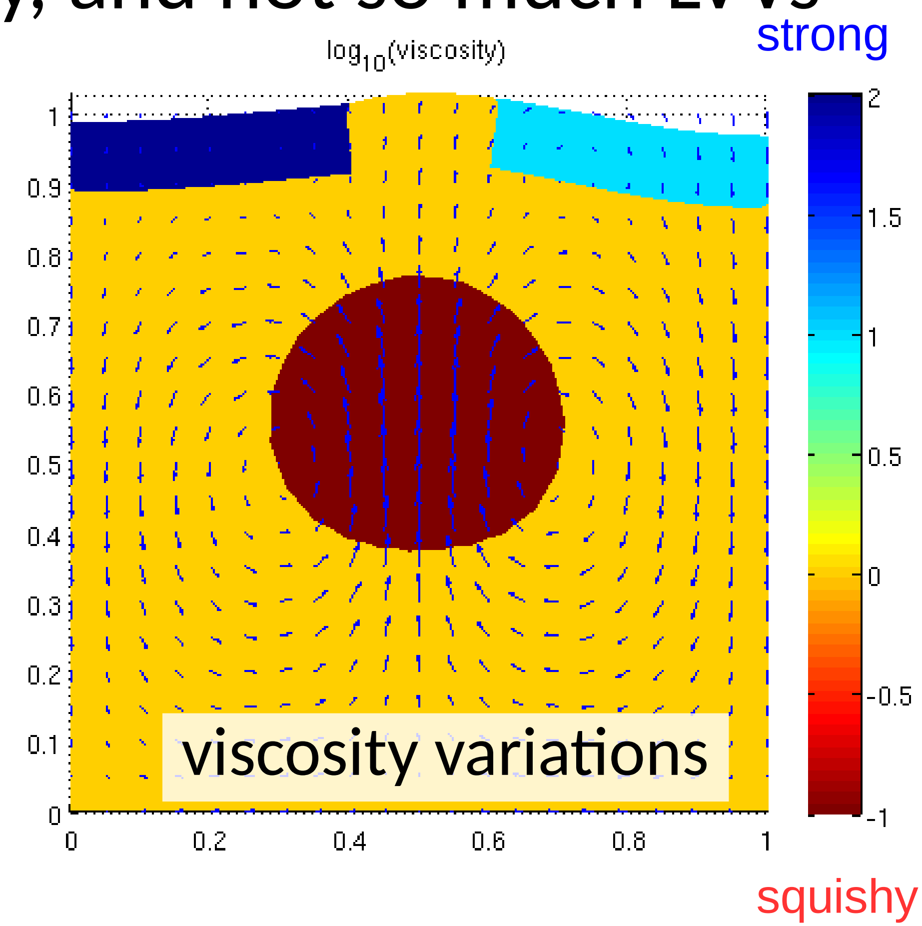

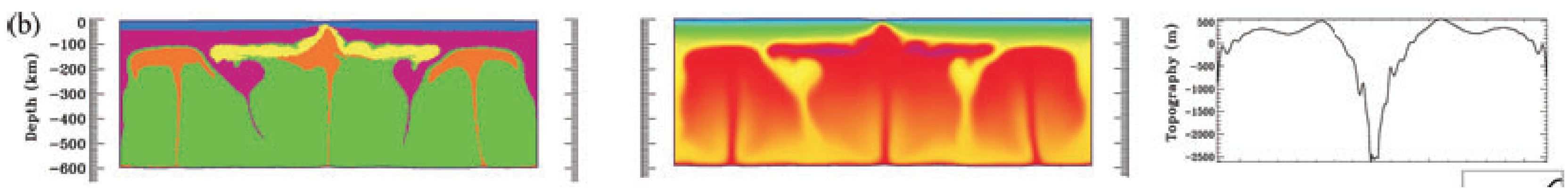

Burov et al.

Alternative age distributions for constant production rates

Subduction probability

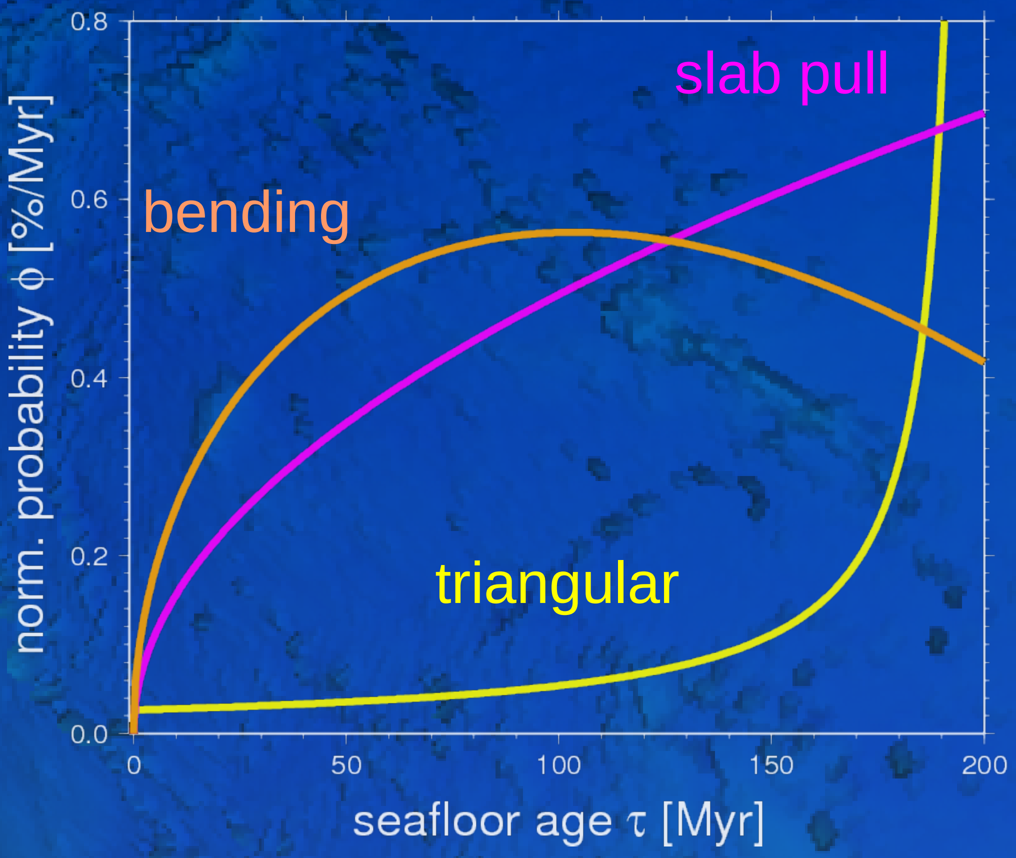

Age distribution

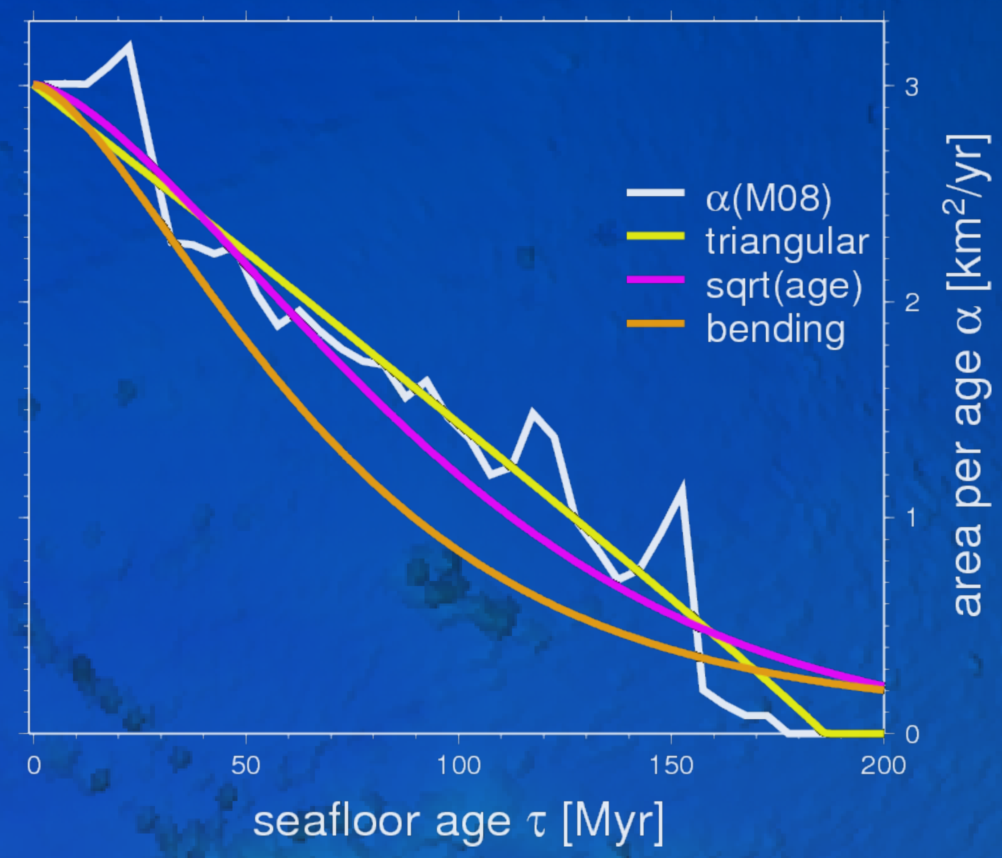

Becker et al. (2009)

Yield stress control

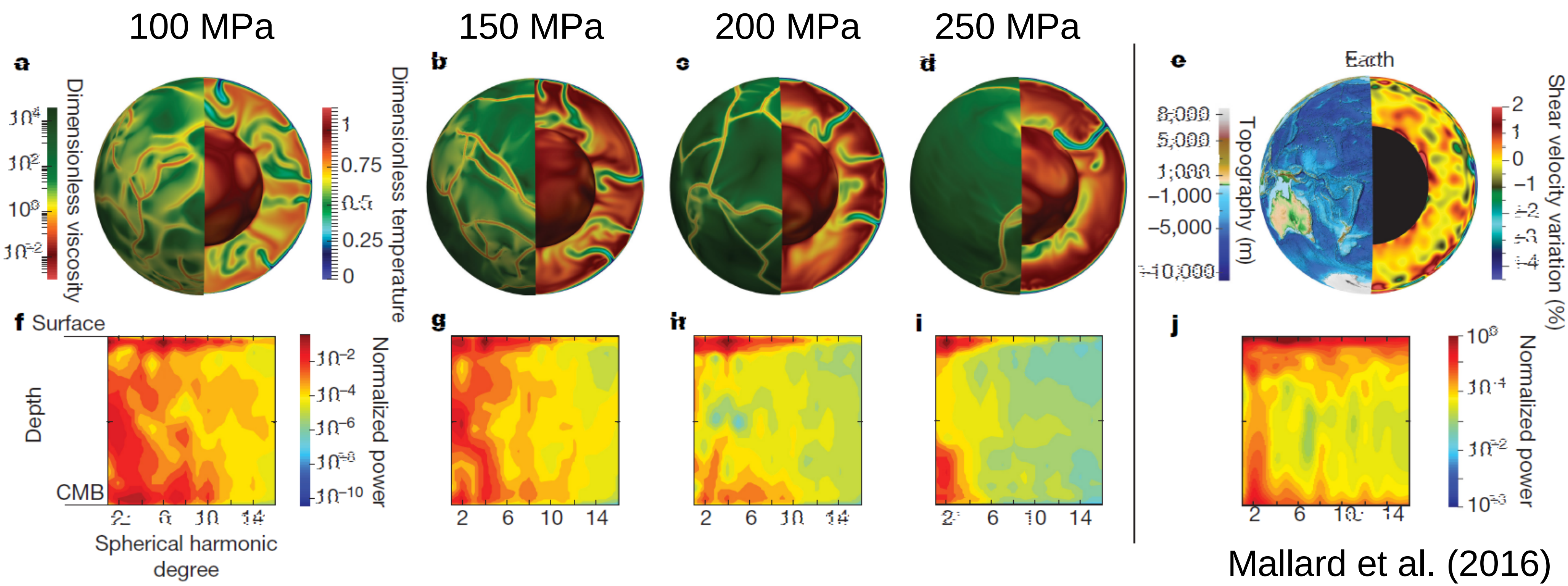

Mallard et al. (2016)

cf. Tackley (2000a,2000), Richards et al. (2001),
van Heck and Tackley (2008), Foley and Becker (2009)

But: effect of asthenosphere, internal vs. bottom heating, Ra #, continents, and damage/memory

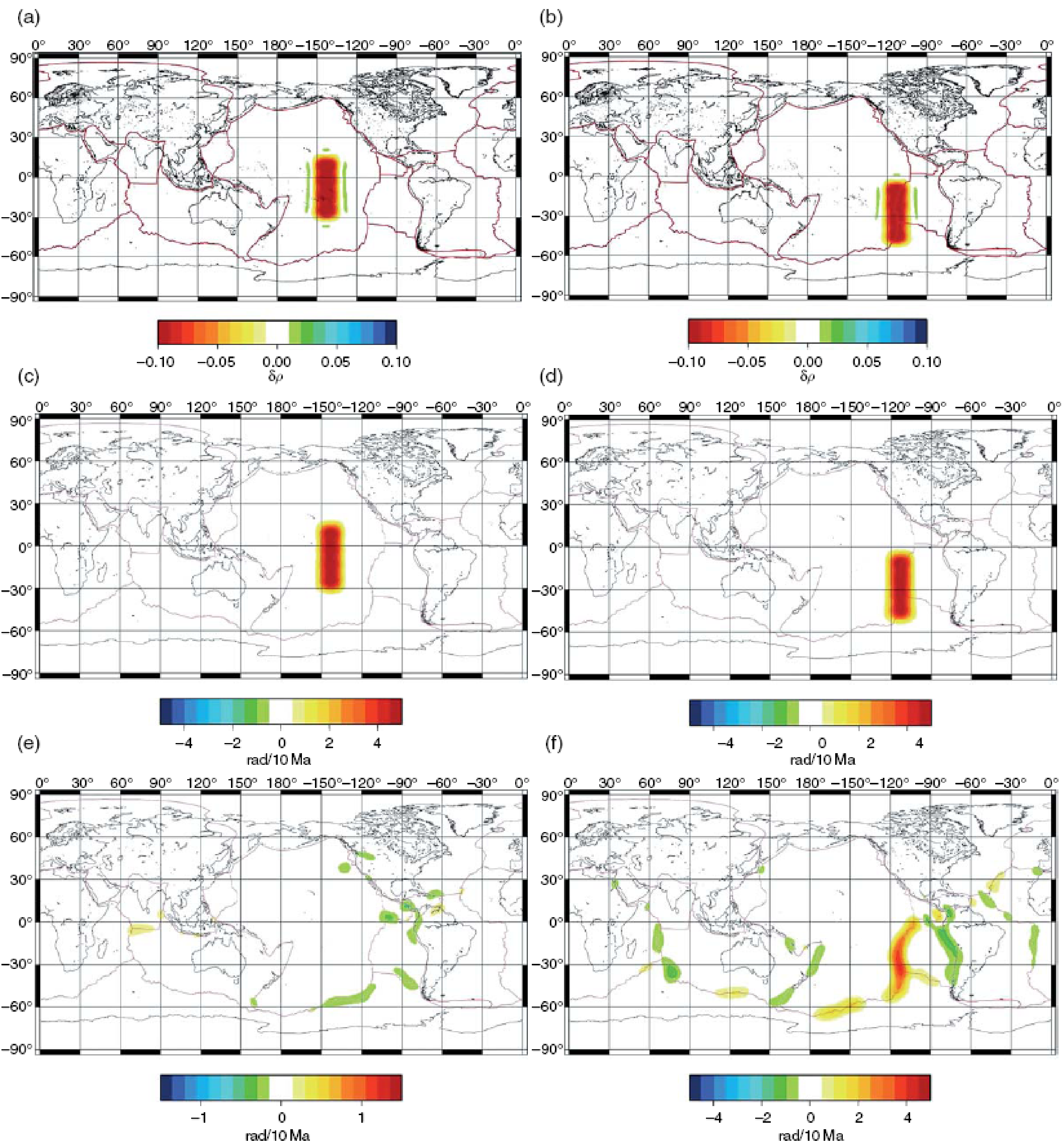

Two density sources

Free-slip solution for poloidal flow

“Plate” solution for poloidal flow

Forte (2008, 2015)

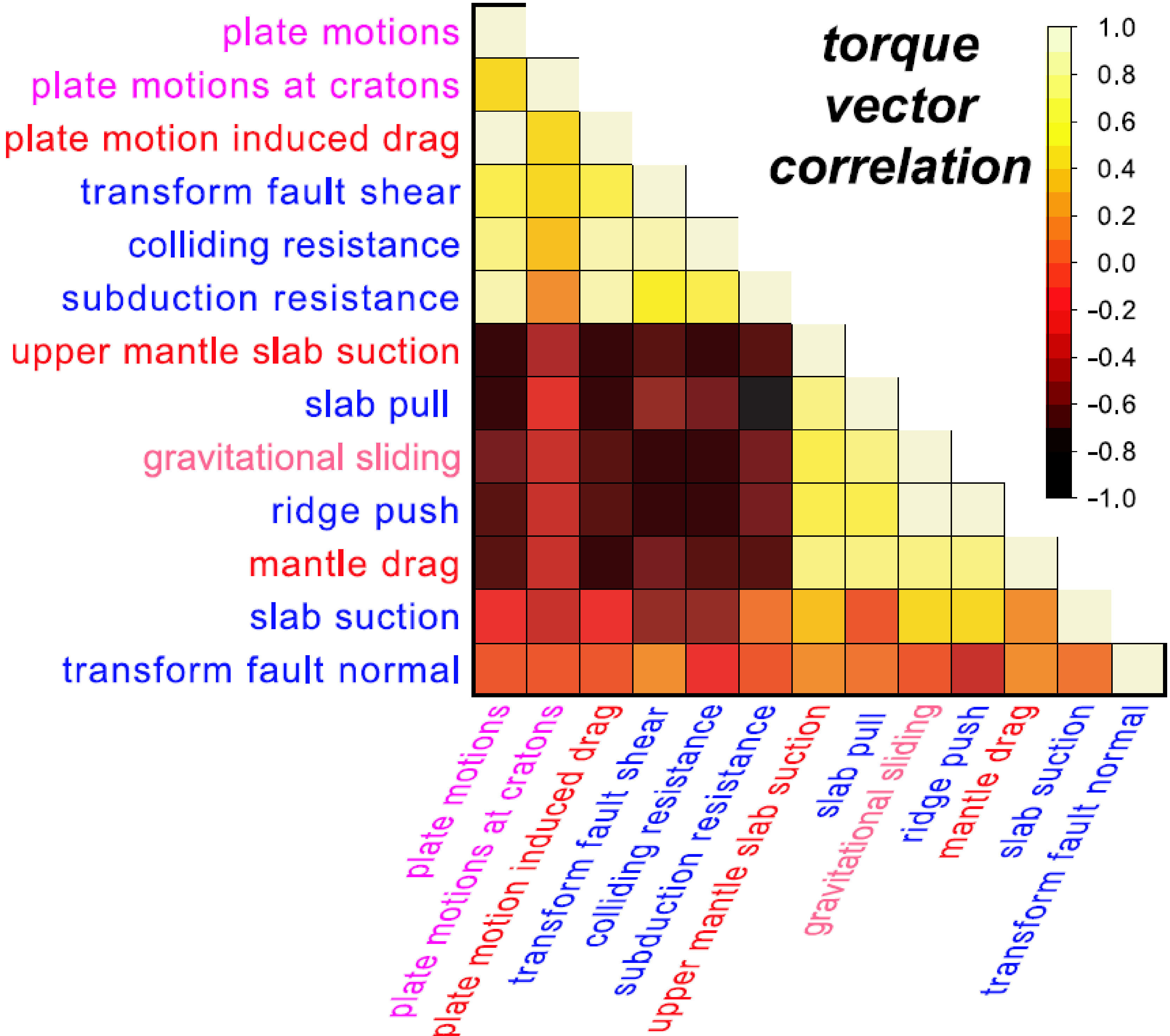

Becker & O'Connell (2001)

Geoid and LVVs

- Free slip surface
- Four layer viscosity (not optimized)
- SMEAN tomography

Correlation with observed geoid
0 < L < 20

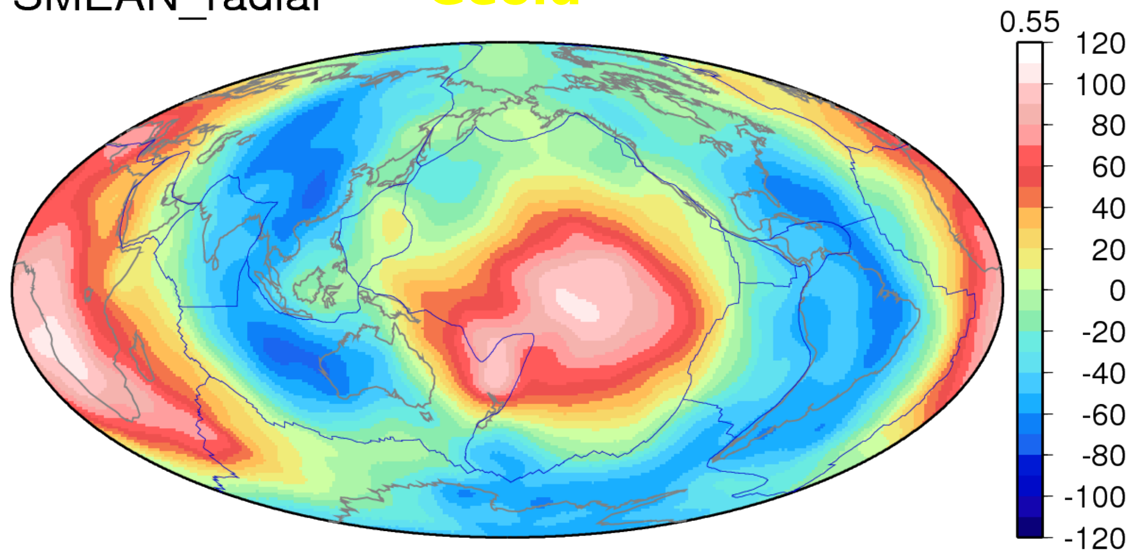

Surface velocities with viscosity in background

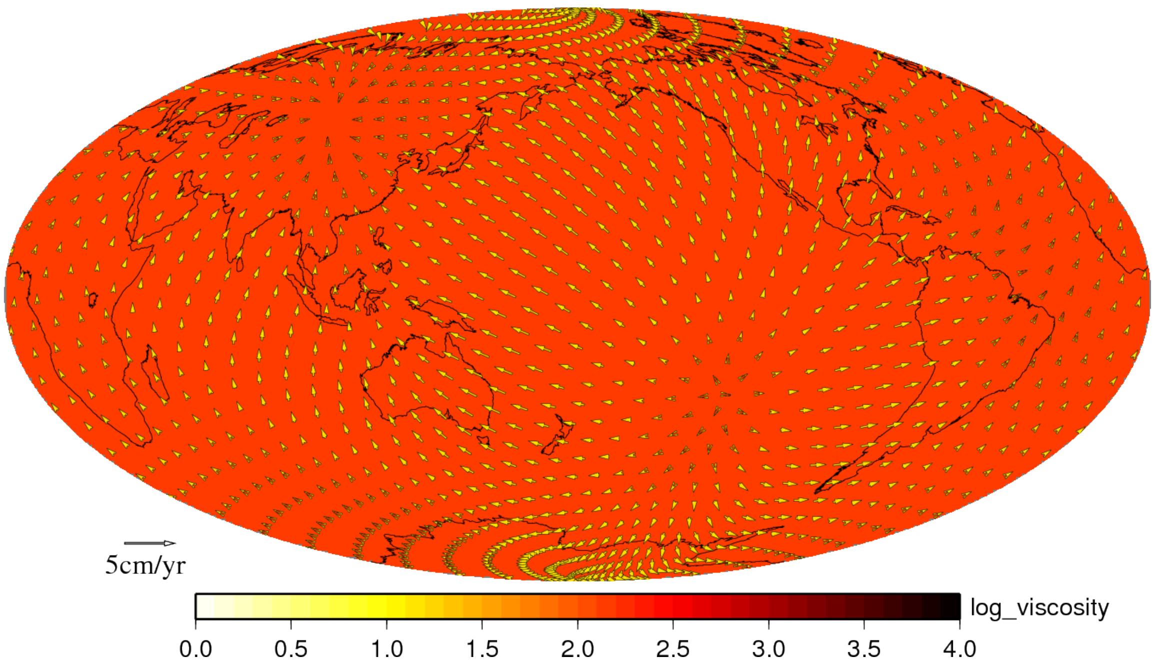

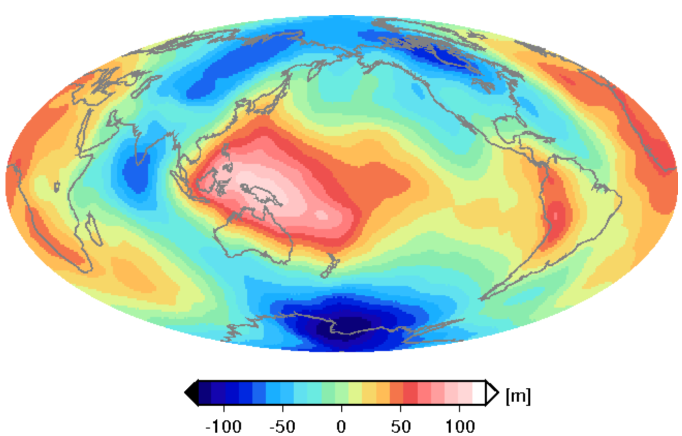

Geoid and LVVs

- Free slip surface
- Weak zones, stiff keels

Geoid

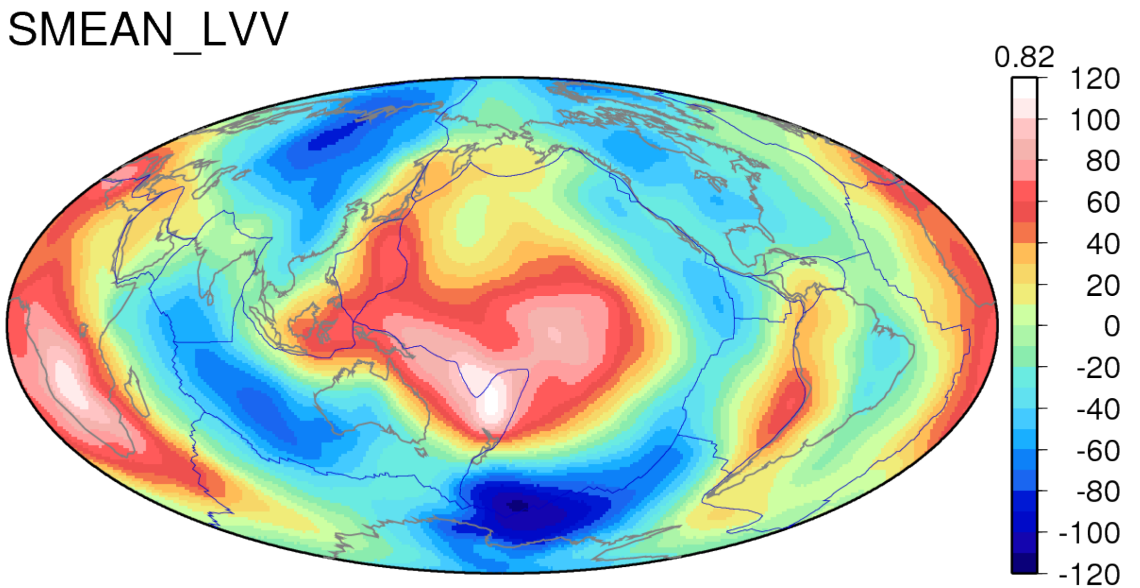

Surface velocities with viscosity in background

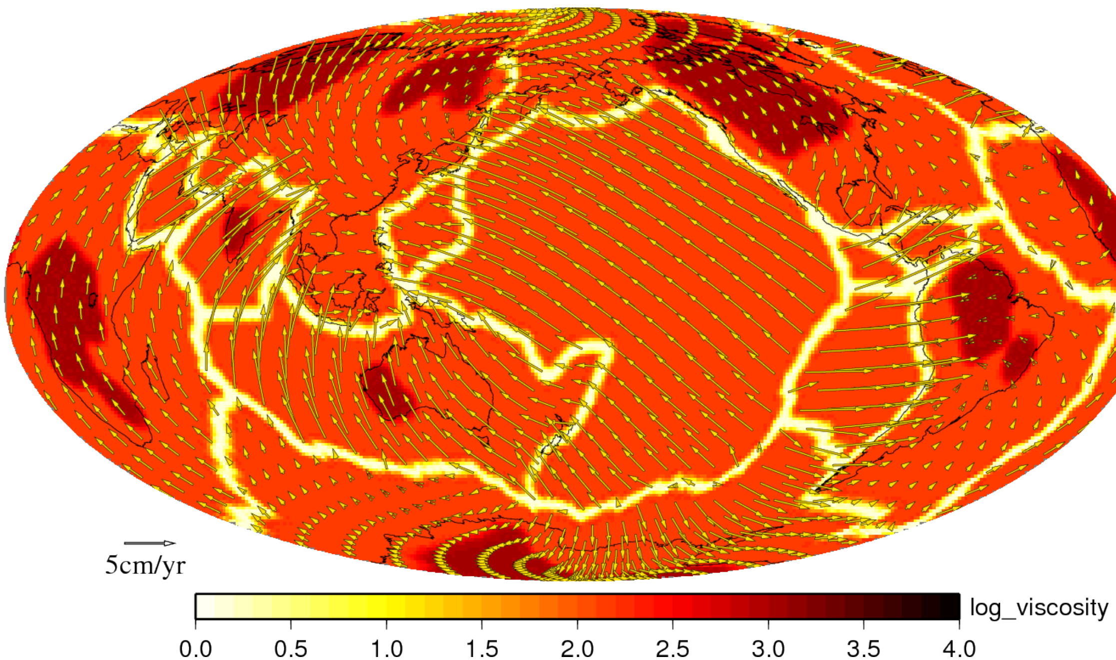

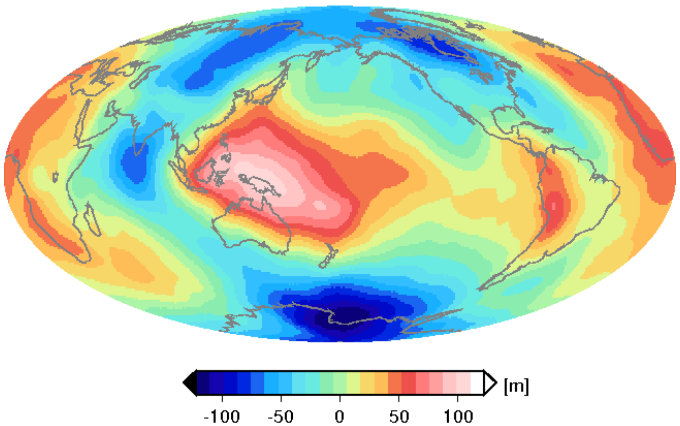

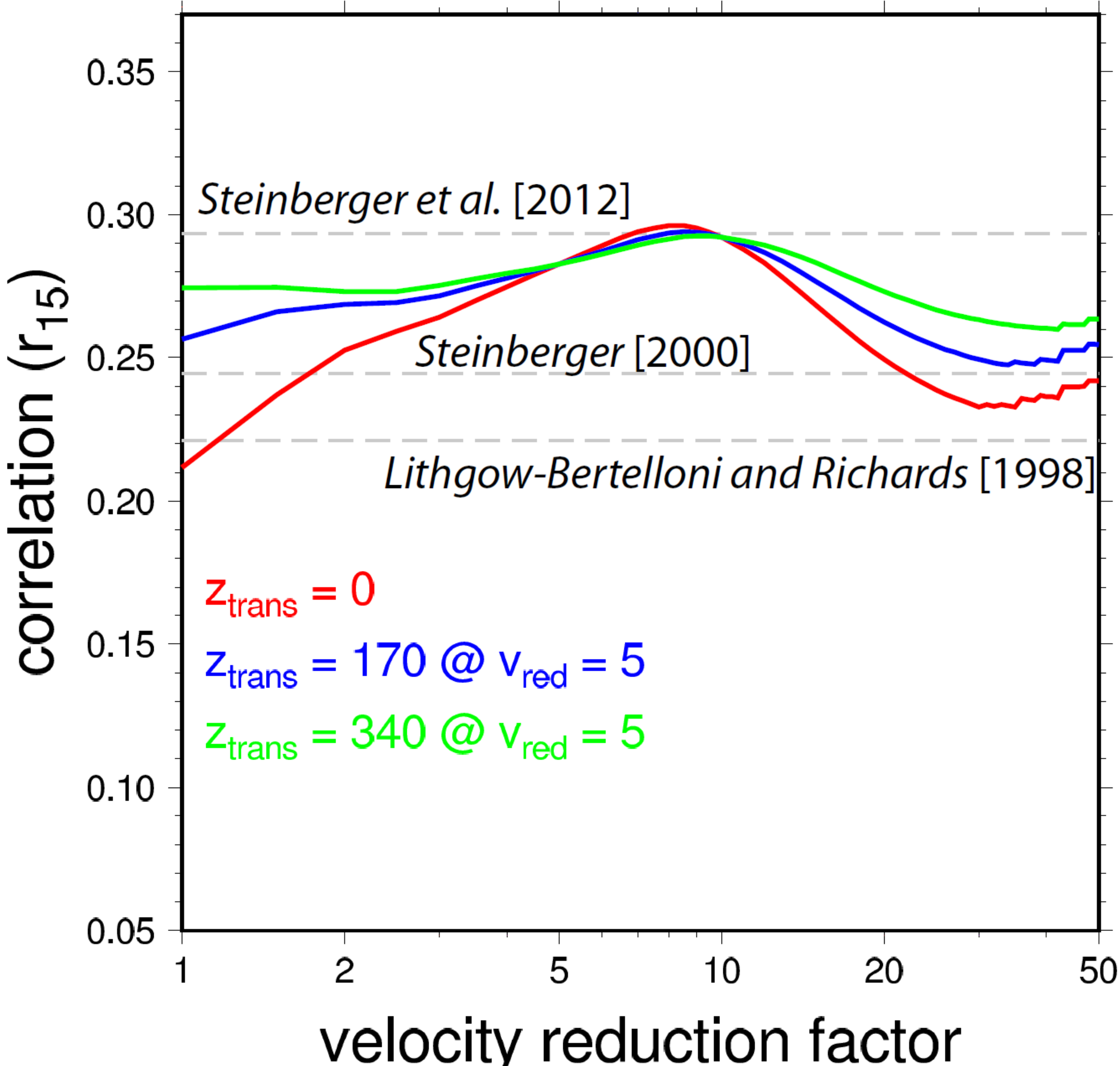

0.35
0.30
0.25
0.20
0.15
0.10
0.05
correlation (r_{15})
1
2
5
10
20
50
velocity reduction factor
Steinberger et al. [2012]
Steinberger [2000]
Lithgow-Bertelloni and Richards [1998]
z_{trans} = 0
z_{trans} = 170 @ v_{red} = 5
z_{trans} = 340 @ v_{red} = 5

Subduction velocity scaling

slab bending

mantle drag

slab pull

$$V' \approx \Delta\rho g h L / [2\eta_l (h/r)^3 + 3\eta_{\mathrm{m}} A]$$

$$V^\circ = (\Delta\rho^\circ g H^\circ h^\circ) / \eta_{\mathrm{m}}^\circ$$

$$V = V' / V^\circ$$

- Subduction velocity = modified Stokes velocity accounting for bending

Conrad and Hager (1999)

Regional models

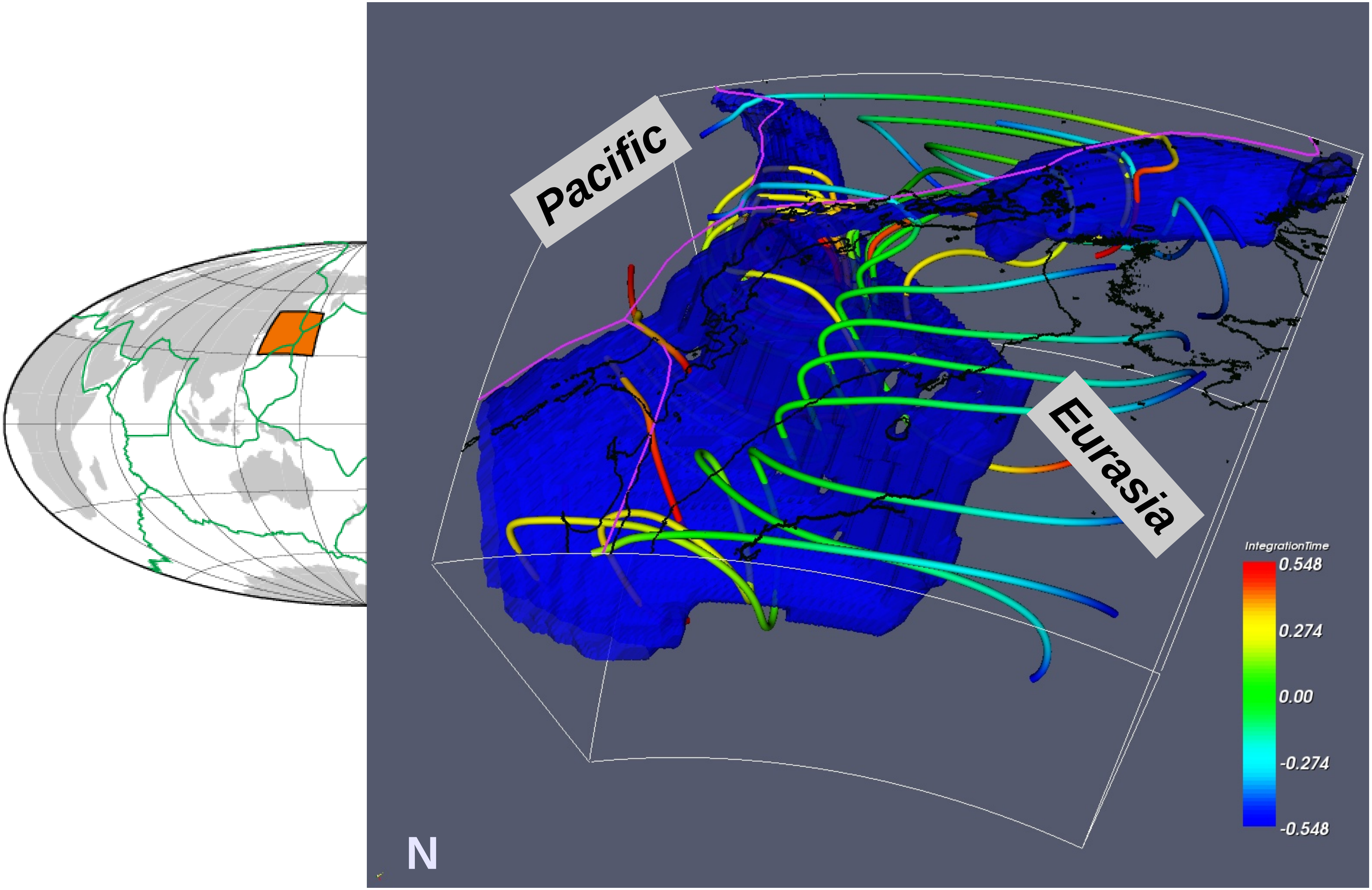

Becker & Faccenna (2009)

Global models

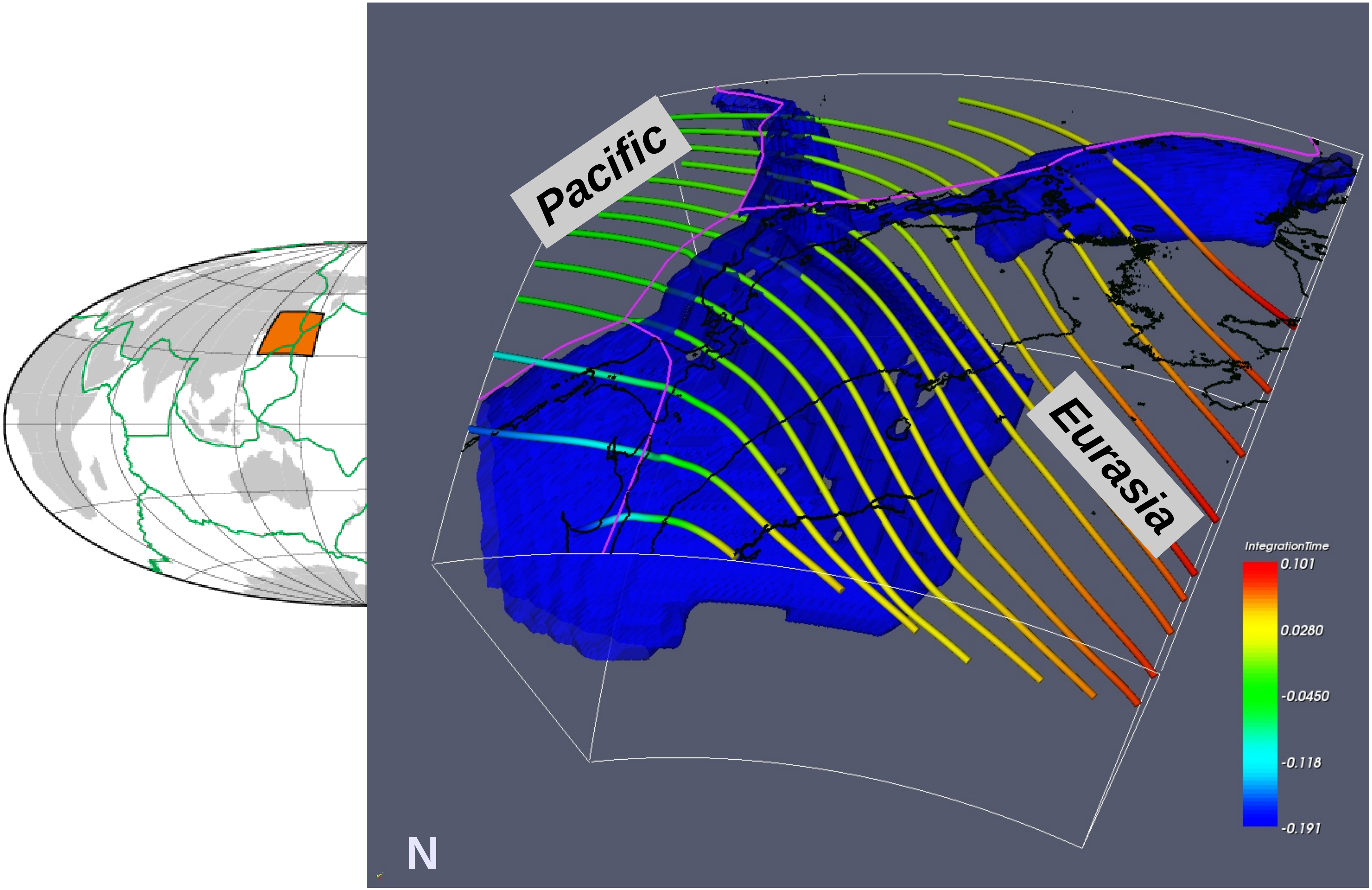

Becker & Faccenna (2009)

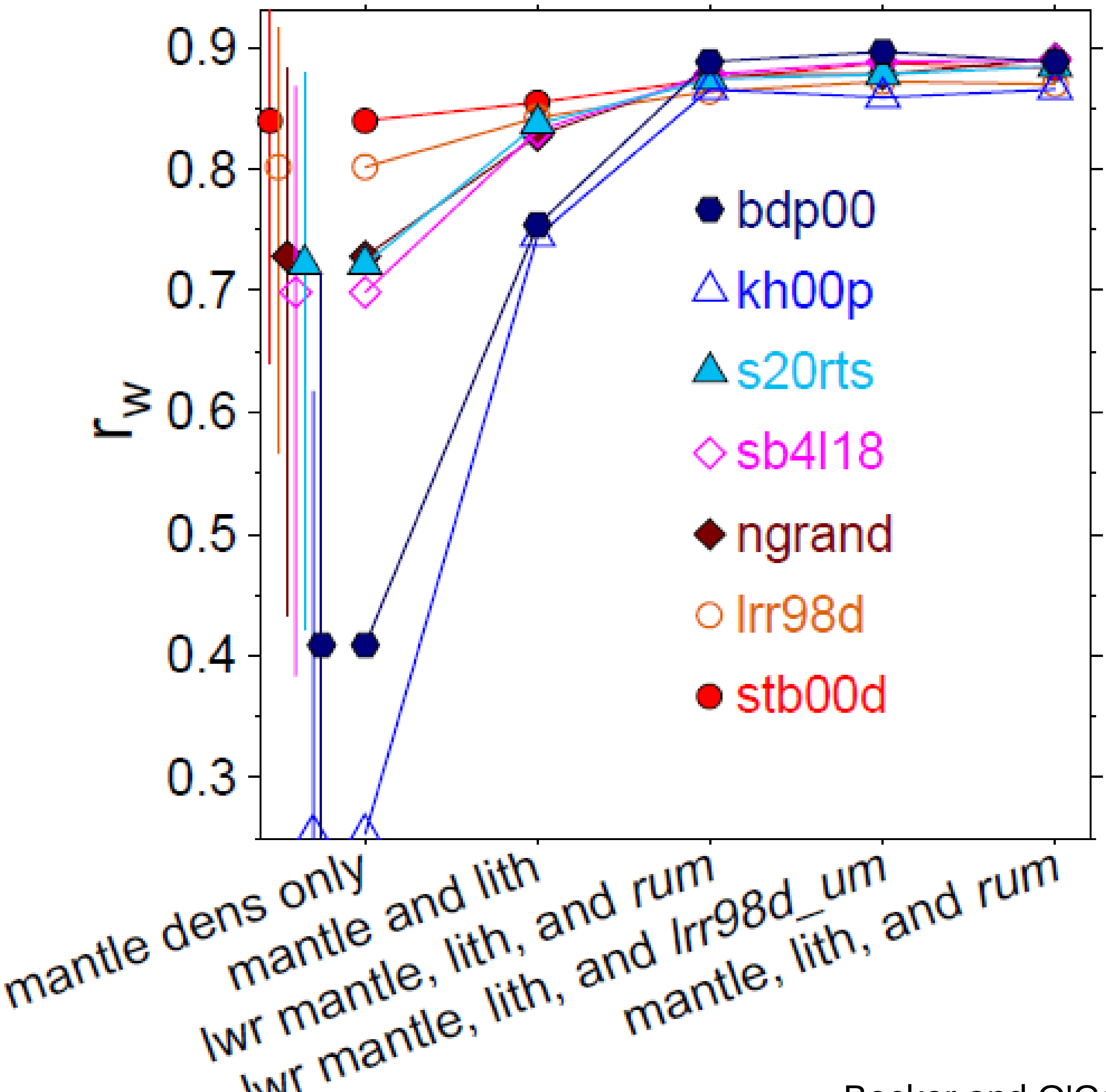

Becker and O'Connell (2001)

Gravitational potential energy

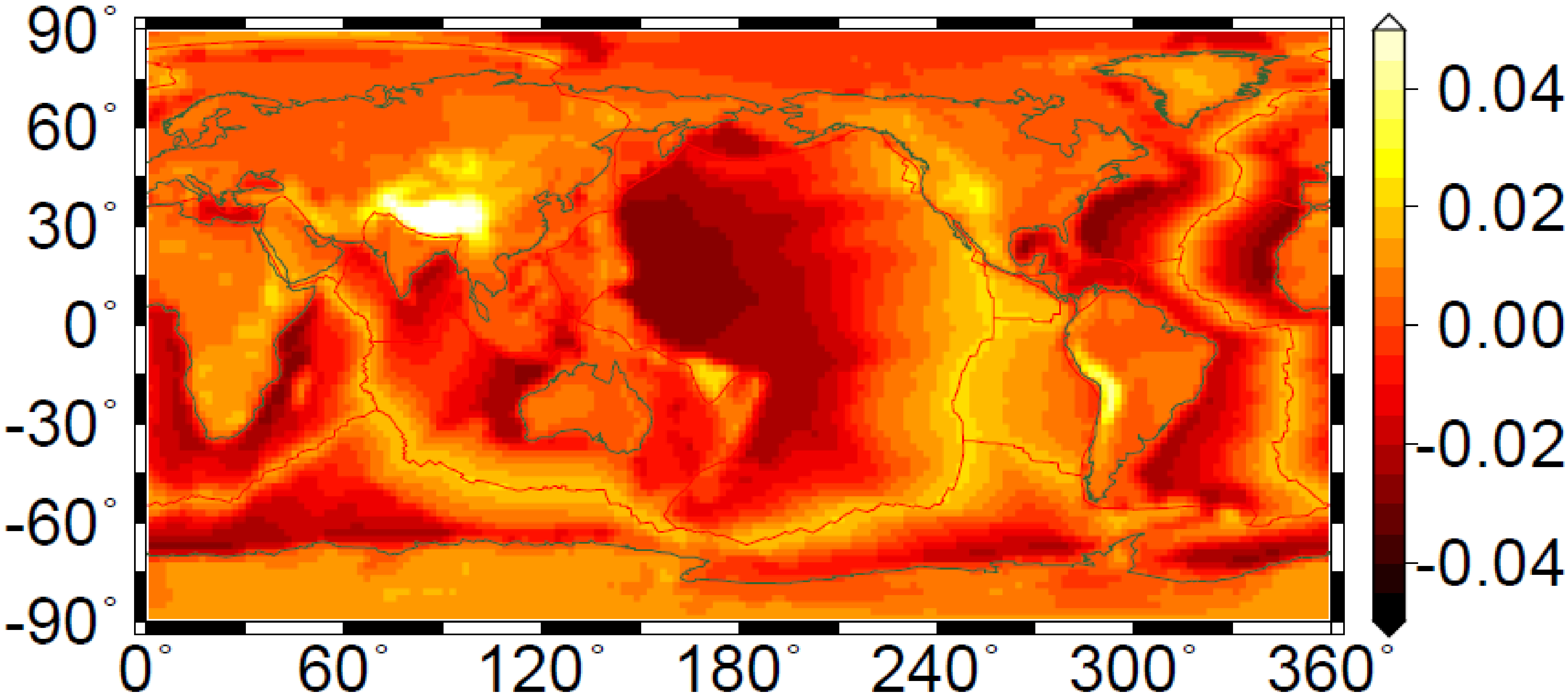

Figure 3. Differential potential energy $\Delta U = U - \overline{U}$ ($\overline{U} = 2.616 \times 10^{14}$ Jm^{-2}) of our $2^\circ \times 2^\circ$ model in units of 10^{14} Jm^{-2}. Min/mean/max values of ΔU for oceanic and continental lithosphere are $-0.03/-0.004/0.023$ and $-0.013/0.007/0.078$, respectively.

Becker and O'Connell (2001)

GPE torques

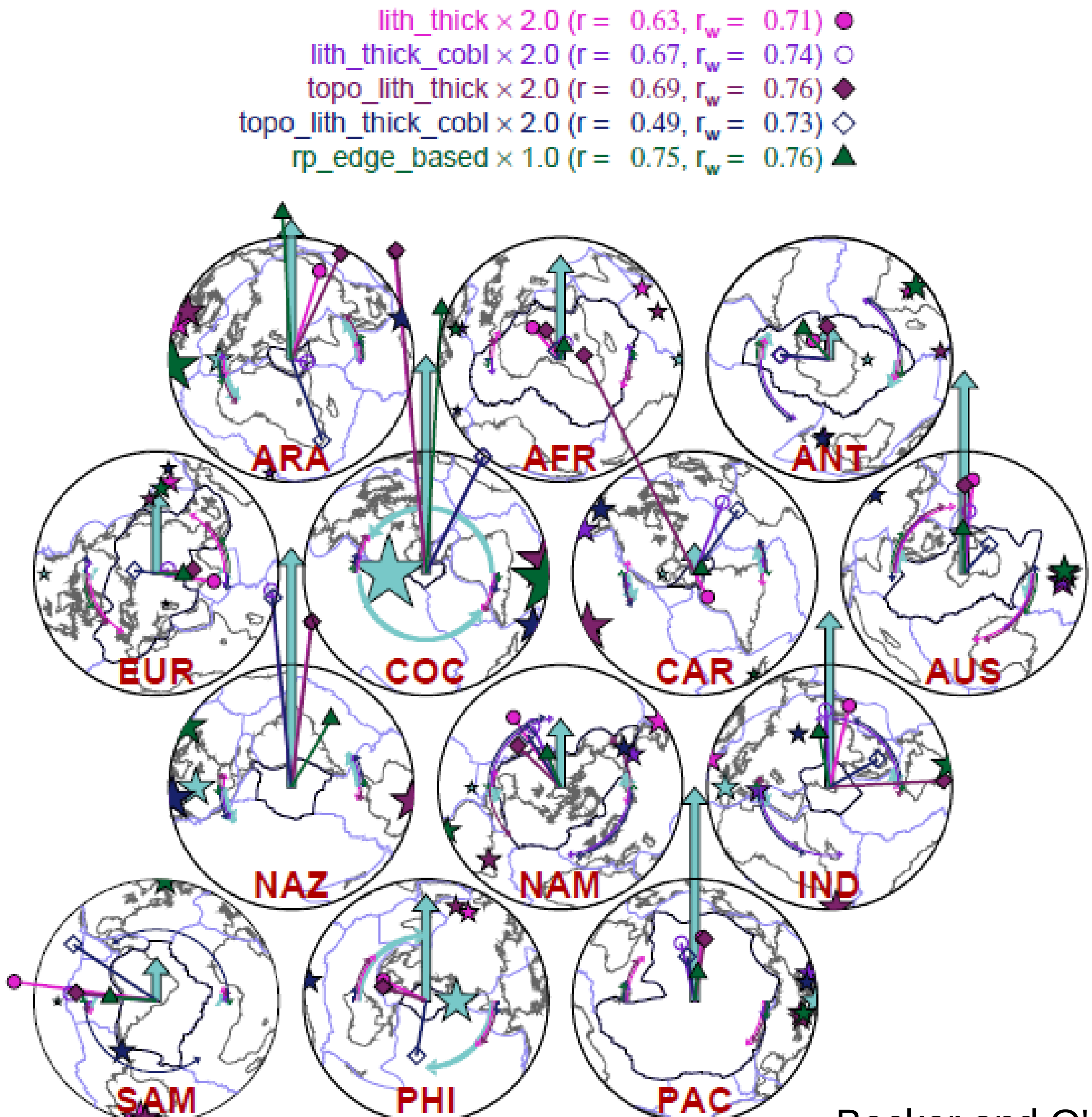

Becker and O'Connell (2001)

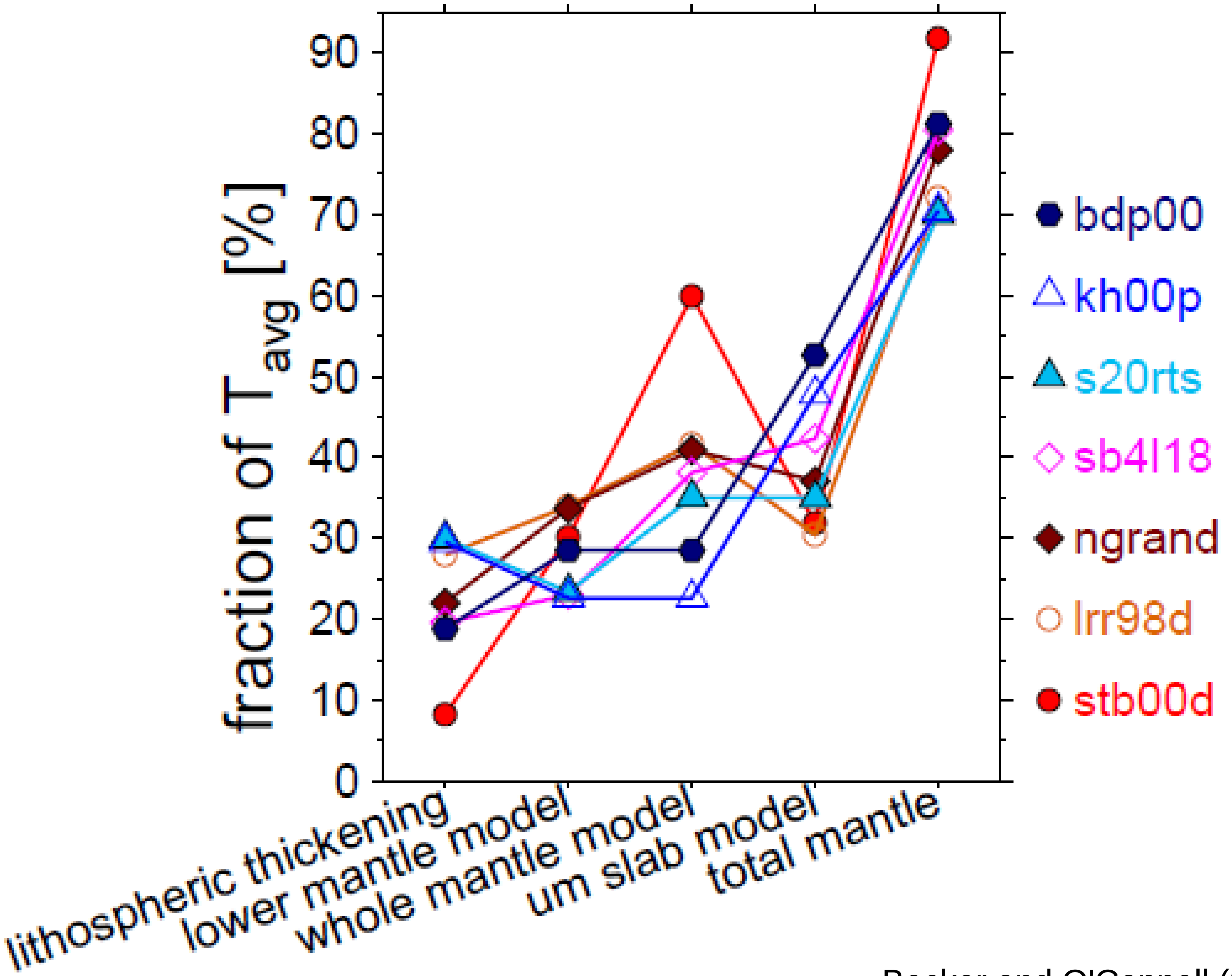

Becker and O'Connell (2001)